

# **A Study of Variable Thrust, Variable Specific Impulse Trajectories for Solar System Exploration**

A Thesis  
Presented to  
The Academic Faculty

by

**Tadashi Sakai**

In Partial Fulfillment  
of the Requirements for the Degree  
Doctor of Philosophy

School of Aerospace Engineering  
Georgia Institute of Technology  
December 2004

# **A Study of Variable Thrust, Variable Specific Impulse Trajectories for Solar System Exploration**

Approved by:

John R. Olds, Advisor  
School of Aerospace Engineering

Robert D. Braun  
School of Aerospace Engineering

Eric N. Johnson  
School of Aerospace Engineering

Amy R. Pritchett  
School of Industrial and Systems Engineering

David W. Way  
National Aeronautics and Space Administration

Date Approved: November 2004

*To Naomi*

## ACKNOWLEDGEMENTS

There are many people whom I would like to thank. First, I would like to express my sincere gratitude and thanks to my graduate advisor Dr. John Olds. It has been a privilege to work with you. Without your guidance, wisdom, encouragement, and patience, this research would have not been possible.

I would also like to thank the other members of my committee, Dr. Robert Braun, Dr. Eric Johnson, Dr. Amy Pritchett, and Dr. David Way. Your advice and insight has proved invaluable. I would also like to thank Dr. Panagiotis Tsiotras for his advice.

Thank you also to my friends and coworkers in the Space Systems Design Lab. I really had a great time working with you. Especially I would like to thank Tim Kokan, David Young, Jimmy Young, and Kristina Alemany for their proofreading of this thesis. Reading and correcting my English must have been tough work. Other than the members of SSDL, Yoko Watanabe's knowledge and comments were really helpful. I hope their research will be fruitful and successful.

I would like to thank my family in Japan. My father Toshio, mother Takae, elder brother Hiroshi, and younger sister Maki; they have all supported me so much. I can not thank you enough.

Finally, I must thank my wife, Naomi, who has provided endless encouragement and support during the most difficult times of my work. Having you in my life to share my dreams and experiences makes them all the more special.

# TABLE OF CONTENTS

<b>ACKNOWLEDGEMENTS</b>	<b>iv</b>
<b>LIST OF TABLES</b>	<b>viii</b>
<b>LIST OF FIGURES</b>	<b>x</b>
<b>LIST OF SYMBOLS AND ABBREVIATIONS</b>	<b>xv</b>
<b>SUMMARY</b>	<b>xvii</b>
<b>I INTRODUCTION</b>	<b>1</b>
1.1 Problems of Variable Thrust, Variable $I_{sp}$ Trajectory Optimization . . . . .	1
1.2 Motivation for Research . . . . .	3
1.3 Research Goals and Objectives . . . . .	5
1.4 Approach . . . . .	6
1.5 Organization of the Thesis . . . . .	7
<b>II EXHAUST-MODULATED PLASMA PROPULSION</b>	<b>9</b>
2.1 Overview . . . . .	9
2.2 Mechanism . . . . .	10
2.3 Choosing the Power Level . . . . .	13
2.4 Literature Review . . . . .	16
<b>III PRELIMINARY STUDY: SIMPLE TRAJECTORIES</b>	<b>20</b>
3.1 Problem Formulation . . . . .	20
3.2 Results . . . . .	23
<b>IV INTRODUCTION TO OPTIMIZATION PROBLEMS</b>	<b>29</b>
4.1 Solution Methods for Optimization Problems . . . . .	29
4.2 Indirect Methods – Calculus of Variations . . . . .	30
4.2.1 Problems without Terminal Constraints, Fixed Terminal Time . . .	30
4.2.2 Some State Variables Specified at a Fixed Terminal Time . . . . .	32
4.2.3 Inequality Constraints on the Control Variables . . . . .	34
4.2.4 Bang-off-bang Control . . . . .	35

<b>V</b>	<b>OPTIMIZATION OF INTERPLANETARY TRAJECTORY</b>	<b>37</b>
5.1	Assumptions . . . . .	37
5.2	Equations of Motion for Low Thrust Trajectories . . . . .	42
5.2.1	VSI – No Constraints on $I_{sp}$ . . . . .	42
5.2.2	VSI – Inequality Constraints on $I_{sp}$ . . . . .	43
5.2.3	CSI – Continuous Thrust . . . . .	44
5.2.4	CSI – Bang-Off-Bang Control . . . . .	45
5.3	Solving the High Thrust Trajectory . . . . .	46
5.4	Problems with Swing-by . . . . .	49
5.4.1	Mechanism . . . . .	49
5.4.2	Equations of Motion . . . . .	50
5.4.3	Powered Swing-by . . . . .	54
<b>VI</b>	<b>DEVELOPMENT OF THE APPLICATION “<i>SAMURAI</i>”</b>	<b>56</b>
6.1	Overview . . . . .	56
6.1.1	Capabilities . . . . .	56
6.1.2	Performance Index for Each Engine . . . . .	59
6.2	C++ Classes . . . . .	60
6.3	Flow and Schemes . . . . .	64
6.3.1	<i>SAMURAI</i> Flowchart . . . . .	64
6.3.2	VSI Constrained $I_{sp}$ . . . . .	66
6.3.3	CSI Continuous Thrust . . . . .	67
6.3.4	CSI Bang-Off-Bang . . . . .	67
6.4	Examples of Input and Output . . . . .	69
6.5	Validation and Verification . . . . .	74
6.5.1	Validation of High Thrust with IPREP . . . . .	74
6.5.2	Validation of CSI with ChebyTOP . . . . .	74
<b>VII</b>	<b>PRELIMINARY RESULTS: PROOF OF CONCEPT</b>	<b>79</b>
7.1	Problem Description . . . . .	79
7.2	Numerical Accuracy . . . . .	82
7.3	Results and Discussion . . . . .	84

7.4	Relationship among Fuel Consumption, Jet Power, and Travel Distance . .	93
<b>VIII</b>	<b>NUMERICAL EXAMPLES: “REAL WORLD” PROBLEMS</b>	<b>99</b>
8.1	Scientific Mission to Venus . . . . .	100
8.1.1	Venus Exploration . . . . .	100
8.1.2	Problem Description . . . . .	100
8.1.3	Results . . . . .	100
8.2	Human Mission to Mars: Round Trip . . . . .	108
8.2.1	Mars Exploration . . . . .	108
8.2.2	Problem Description . . . . .	109
8.2.3	Results . . . . .	109
8.3	JIMO: Jupiter Icy Moons Orbiter . . . . .	120
8.3.1	JIMO Overview . . . . .	120
8.3.2	Problem Description . . . . .	121
8.3.3	Results . . . . .	121
8.4	Uranus and beyond . . . . .	125
8.5	Swing-by Trajectories with Mars . . . . .	128
<b>IX</b>	<b>CONCLUSIONS AND FUTURE WORK</b>	<b>137</b>
9.1	Conclusions and Observations . . . . .	138
9.2	Research Accomplishments . . . . .	141
9.3	Recommended Future Work . . . . .	142
<b>APPENDIX A</b>	<b>— RESULTS FROM PRELIMINARY STUDY</b>	<b>144</b>
<b>APPENDIX B</b>	<b>— EQUATIONS USED IN THE PROGRAM <i>SAMURAI</i></b>	<b>155</b>
<b>APPENDIX C</b>	<b>— NUMERICAL TECHNIQUES</b>	<b>159</b>
<b>APPENDIX D</b>	<b>— “<i>SAMURAI</i>” CODE MANUAL</b>	<b>177</b>
<b>REFERENCES</b>		<b>180</b>
<b>VITA</b>		<b>186</b>

# LIST OF TABLES

1-1	Examples of Spacecraft Propulsion Systems[4][42]. . . . .	1
3-1	Trip Time Savings(Comparison by Distance): $(VSI - CSI)/CSI \times 100$ (%) .	28
3-2	Trip Time Savings(Comparison by Initial Mass): $(VSI - CSI)/CSI \times 100$ (%)	28
7-1	Orbital Data[37]. . . . .	80
7-2	Transfer Orbit to Venus with 10MW Jet Power. . . . .	85
7-3	Transfer Orbit to Saturn with 30MW Jet Power. . . . .	86
7-4	Time Until Spacecraft Mass ( $m_0 = 100MT$ ) Becomes Zero (in TU <sub>Sun</sub> ). . .	86
7-5	Fuel Consumption for VSI type II and CSI type I (kg). . . . .	89
8-1	Earth – Mars Round Trip Fuel Consumption for VSI type I. . . . .	111
8-2	Earth – Mars Round Trip Fuel Consumption. . . . .	113
8-3	Comparison of High Thrust $\Delta V$ for Earth – Jupiter: With and Without Mars Swing-by . . . . .	129
8-4	Comparison of High Thrust $\Delta V$ for Earth – Saturn: With and Without Mars Swing-by . . . . .	130
8-5	Comparison of Fuel Consumption for VSI type I: from Earth to Jupiter With and Without Mars Swing-by. . . . .	132
8-6	Comparison of Fuel Consumption for VSI type I: from Earth to Saturn With and Without Mars Swing-by. . . . .	132
8-7	Comparison of Fuel Consumption for VSI type II: from Earth to Jupiter With and Without Mars Swing-by. . . . .	134
8-8	Comparison of Fuel Consumption for VSI type II: from Earth to Saturn With and Without Mars Swing-by. . . . .	134
8-9	Comparison of Fuel Consumption for CSI type II: from Earth to Jupiter With and Without Mars Swing-by. . . . .	135
8-10	Comparison of Fuel Consumption for CSI type II: from Earth to Saturn With and Without Mars Swing-by. . . . .	135
A-1	Transfer Orbit to Venus with 20MW Jet Power. . . . .	144
A-2	Transfer Orbit to Venus with 30MW Jet Power. . . . .	145
A-3	Transfer Orbit to Mars with 10MW Jet Power. . . . .	146
A-4	Transfer Orbit to Mars with 20MW Jet Power. . . . .	147
A-5	Transfer Orbit to Mars with 30MW Jet Power. . . . .	148
A-6	Transfer Orbit to Asteroids with 10MW Jet Power. . . . .	149



A-7	Transfer Orbit to Asteroids with 20MW Jet Power. . . . .	150
A-8	Transfer Orbit to Asteroids with 30MW Jet Power. . . . .	151
A-9	Transfer Orbit to Jupiter with 10MW Jet Power. . . . .	152
A-10	Transfer Orbit to Jupiter with 20MW Jet Power. . . . .	152
A-11	Transfer Orbit to Jupiter with 30MW Jet Power. . . . .	153
A-12	Transfer Orbit to Saturn with 10MW Jet Power. . . . .	153
A-13	Transfer Orbit to Saturn with 20MW Jet Power. . . . .	154

# LIST OF FIGURES

1-1	Future Interplanetary Flight with VASIMR[5]. . . . .	3
1-2	Transfer Trajectory from Earth to Mars with Thrust Direction. . . . .	4
2-1	VX-10 Experiment at Johnson Space Center[45]. . . . .	10
2-2	Synoptic View of the VASIMR Engine[22]. . . . .	12
2-3	Power Partitioning and Relationship between Thrust and $I_{sp}$ . . . . .	13
2-4	Thrust vs. Mass Flow Rate for a CSI Engine. . . . .	15
2-5	Thrust vs. Mass Flow Rate for a VSI Engine. . . . .	15
2-6	Thrust vs. Mass Flow Rate for a VSI Engine with Limitations. . . . .	16
3-1	Trajectories for Preliminary Study. . . . .	20
3-2	Preliminary Study: $I_{sp}$ and Fuel Consumptions for VSI and CSI. . . . .	21
3-3	Results: $R = 100$ DU, $m_0 = 20$ MT, $P_J = 500$ kW. . . . .	23
3-4	$I_{sp}$ histories for VSI and CSI when CSI $I_{sp}$ is 3,000 sec: $R = 100$ DU, $m_0 = 20$ MT, $P_J = 500$ kW. . . . .	24
3-5	Results: $R = 500$ DU, $m_0 = 20$ MT, $P_J = 500$ kW. . . . .	25
3-6	Results $R = 1,000$ DU, $m_0 = 20$ MT, $P_J = 500$ kW. . . . .	26
3-7	Results: $R = 100$ DU, $m_0 = 5$ MT, $P_J = 500$ kW. . . . .	27
3-8	Results: $R = 100$ DU, $m_0 = 10$ MT, $P_J = 500$ kW. . . . .	27
4-1	Bang-off-bang Control: Choosing Control to Minimize $q_i$ . . . . .	36
5-1	Sphere of Influence of $m_2$ with respect to $m_1$ . . . . .	38
5-2	In-plane Thrust Angle $\theta$ and Out-of-plane Thrust Angle $\phi$ in Inertial Frame. . . . .	45
5-3	Switching Function and Switching Times for Bang-Off-Bang. . . . .	46
5-4	Gauss Problem: Direction of Motion for the Same Vectors and the Same Time of Flight. . . . .	47
5-5	Schematic Diagram of Forming of Gravity Assist Maneuver. . . . .	51
5-6	Swing-by: Inside the SOI. . . . .	52
5-7	Geometry of a Powered Swing-by Maneuver. . . . .	54
6-1	Examples of Thrust Histories. . . . .	58
6-2	<i>SAMURAI</i> Flowchart. . . . .	63
6-3	Input $C_3$ and $\Delta V$ requirements. . . . .	65

6-4	$\alpha$ (in-plane thrust angle) and $\beta$ (out-of-plane thrust angle) in the Spacecraft-centered Coordinates. . . . .	70
6-5	Results with <i>SAMURAI</i> and IPREP: $\Delta V$ Requirements for High Thrust Venus Transfer. . . . .	75
6-6	Results with <i>SAMURAI</i> and IPREP: $\Delta V$ Requirements for High Thrust Mars Transfer. . . . .	75
6-7	Results with <i>SAMURAI</i> and IPREP: $\Delta V$ Requirements for High Thrust Jupiter Transfer. . . . .	76
6-8	Results with <i>SAMURAI</i> and ChebyTOP: Trajectory Comparison for CSI type I Mars Transfer. . . . .	77
6-9	Results with <i>SAMURAI</i> and ChebyTOP: Trajectory Comparison for CSI type II Mars Transfer. . . . .	78
7-1	2D Trajectories for Proof-of-Concept Problems. . . . .	80
7-2	Tolerance vs. CPU Time for Different Number of Time Steps. . . . .	83
7-3	Tolerance vs. Fuel Consumption for Different Number of Time Steps. . . .	83
7-4	A Trajectory with More Than One Revolution - CSI type I engine. . . . .	87
7-5	A Trajectory with Long Time of Flight - VSI type I engine. . . . .	88
7-6	VSI type II: Thrust History for Different Levels of $I_{sp}$ Limit. . . . .	90
7-7	VSI type II: $I_{sp}$ History for Different Levels of $I_{sp}$ Limit. . . . .	90
7-8	VSI type II: Fuel Consumption for Different Levels of $I_{sp}$ Limit. . . . .	91
7-9	CSI type II: Thrust History for Different Levels of $I_{sp}$ Limit. . . . .	92
7-10	CSI type II: $I_{sp}$ History for Different Levels of $I_{sp}$ Limit. . . . .	92
7-11	CSI type II: Fuel Consumption for Different Levels of $I_{sp}$ . . . . .	93
7-12	Relative Fuel Consumption of VSI with respect to CSI: Comparison by Jet Power. . . . .	95
7-13	Relative Fuel Consumption of VSI with respect to CSI: Comparison by Distance from the Sun (The Best $I_{sp}$ is Chosen for Each CSI Mission). . . . .	96
7-14	Relative Fuel Consumption of VSI with respect to CSI: Comparison by Distance from the Sun ( $I_{sp}$ for CSI is the Same for All Missions). . . . .	96
7-15	Fuel Consumption between VSI and CSI: When $I_{sp}$ for CSI Differs for Each Mission. . . . .	97
7-16	Fuel Consumption between VSI and CSI: When $I_{sp}$ for All CSI Cases Are the Same. . . . .	98
8-1	Fuel Consumption for VSI type II: Earth – Venus. . . . .	101
8-2	Trajectory from Earth to Venus with 160-day Time of Flight. . . . .	102

8-3	Fuel Consumption for VSI type II: Earth – Venus. . . . .	102
8-4	VSI type II Trajectory from Earth to Venus with 90-day Time of Flight. . .	103
8-5	Thrust Steering Angle for VSI type II: Earth to Venus, 90-day Time of Flight.	104
8-6	Thrust Magnitude and $I_{sp}$ for VSI type II: Earth to Venus, 90-day Time of Flight. . . . .	104
8-7	Fuel Consumption for CSI type I: Earth – Venus. . . . .	105
8-8	CSI Type I Trajectory from Earth to Venus with 90-day Time of Flight. . .	105
8-9	Thrust Steering Angle for CSI type I: Earth – Venus, Day 250, 90 day TOF.	106
8-10	Thrust Magnitude and $I_{sp}$ for CSI type I: Earth – Venus, Day 250, 90 day TOF. . . . .	106
8-11	CSI Type II Trajectory from Earth to Venus with 90-day Time of Flight. . .	106
8-12	Thrust Steering Angle for CSI type II: Earth – Venus, Day 260, 90 day TOF.	107
8-13	Thrust Magnitude and $I_{sp}$ for CSI type II: Earth – Venus, Day 260, 90 day TOF. . . . .	107
8-14	Fuel Consumption for High Thrust: Earth – Venus. . . . .	107
8-15	Fuel Consumption for VSI type I, 10 MW Jet Power: Earth – Mars Outbound.	110
8-16	Fuel Consumption for VSI type I, 10MW Jet Power: Earth – Mars Inbound.	110
8-17	Fuel Consumption for VSI type II: Earth – Mars Outbound. . . . .	111
8-18	Fuel Consumption for VSI type II: Mars – Earth Inbound. . . . .	111
8-19	Fuel Consumption for CSI type I: Earth – Mars Outbound. . . . .	112
8-20	Fuel Consumption for CSI type I: Earth – Mars Inbound. . . . .	112
8-21	Fuel Consumption for CSI type II: Earth – Mars Outbound. . . . .	112
8-22	Fuel Consumption for CSI type II: Mars – Earth Inbound. . . . .	112
8-23	Fuel Consumption for High Thrust: Earth – Mars Outbound. . . . .	113
8-24	Fuel Consumption for High Thrust: Earth – Mars Inbound. . . . .	113
8-25	VSI Type II Trajectory from Earth to Mars with 120-day Time of Flight. . .	114
8-26	Thrust Steering Angle for VSI type II: Earth – Mars Outbound. . . . .	115
8-27	Thrust Magnitude and $I_{sp}$ for VSI type II: Earth – Mars Outbound. . . . .	115
8-28	Thrust Steering Angle for VSI type II: Mars – Earth Inbound. . . . .	115
8-29	Thrust Magnitude and $I_{sp}$ for VSI type II: Mars – Earth Inbound. . . . .	115
8-30	CSI Type I Trajectory from Earth to Mars with 120-day Time of Flight. . .	116
8-31	CSI Type II Trajectory from Earth to Mars with 120-day Time of Flight. . .	117

8-32 Thrust Steering Angle for CSI type II: Mars – Earth Outbound. . . . .	118
8-33 Thrust Magnitude and $I_{sp}$ for CSI type II: Mars – Earth Outbound. . . . .	118
8-34 Thrust Steering Angle for CSI type II: Mars – Earth Inbound. . . . .	118
8-35 Thrust Magnitude and $I_{sp}$ for CSI type II: Mars – Earth Inbound. . . . .	118
8-36 JIMO: Jupiter Icy Moons Orbiter [3]. . . . .	120
8-37 Fuel Consumption for VSI type I: Earth – Jupiter. . . . .	121
8-38 Fuel Consumption for VSI type II: Earth – Jupiter. . . . .	122
8-39 Fuel Consumption for CSI type I: Earth – Jupiter. . . . .	123
8-40 Transfer Trajectory for VSI type II: Earth – Jupiter. . . . .	124
8-41 Thrust Steering Angle for VSI type II: Earth – Jupiter, 365-day TOF. . . .	124
8-42 Thrust Magnitude and $I_{sp}$ for VSI type II: Earth – Jupiter, 365-day TOF. .	124
8-43 Transfer Trajectory for CSI type I: Earth – Jupiter. . . . .	124
8-44 Thrust Steering Angle for CSI type I: Earth – Jupiter, 365-day TOF. . . .	125
8-45 Thrust Magnitude and $I_{sp}$ for CSI type I: Earth – Jupiter, 365-day TOF. .	125
8-46 Transfer Trajectory for CSI type II: Earth – Jupiter. . . . .	125
8-47 Thrust Steering Angle for CSI type II: Earth – Jupiter, 365-day TOF. . . .	126
8-48 Thrust Magnitude and $I_{sp}$ for CSI type II: Earth – Jupiter, 365-day TOF. .	126
8-49 Transfer Trajectory for VSI type II: Earth – Uranus. . . . .	127
8-50 Departure Phase of Transfer Trajectory for VSI type II: Earth – Uranus. . .	127
8-51 Transfer Trajectory for CSI type I: Earth – Uranus. . . . .	127
8-52 Departure Phase of Transfer Trajectory for CSI type I: Earth – Uranus. . .	127
8-53 Transfer Trajectory for CSI type II: Earth – Uranus. . . . .	128
8-54 Departure Phase of Transfer Trajectory for CSI type II: Earth – Uranus. . .	128
8-55 Transfer Trajectory for High Thrust: Earth to Saturn without Swing-by. . .	130
8-56 Transfer Trajectory for High Thrust: Earth to Saturn with Mars Swing-by. .	130
8-57 Transfer Trajectory for VSI type I: Earth to Jupiter without Swing-by. . . .	131
8-58 Transfer Trajectory for VSI type I: Earth to Jupiter with Mars Swing-by. .	131
8-59 Transfer Trajectory for VSI type I: Earth to Saturn without Swing-by. . . .	131
8-60 Transfer Trajectory for VSI type I: Earth to Saturn with Mars Swing-by. .	131
8-61 Transfer Trajectory for VSI type II: Earth to Jupiter without Swing-by. . .	132
8-62 Transfer Trajectory for VSI type II: Earth to Jupiter with Mars Swing-by. .	132

8-63	Transfer Trajectory for VSI type II: Earth to Saturn without Swing-by. . .	133
8-64	Transfer Trajectory for VSI type II: Earth to Saturn with Mars Swing-by. .	133
8-65	Transfer Trajectory for CSI type II: Earth to Jupiter without Swing-by. . .	133
8-66	Transfer Trajectory for CSI type II: Earth to Jupiter with Mars Swing-by. .	133
8-67	Transfer Trajectory for CSI type II: Earth to Saturn without Swing-by. . .	133
8-68	Transfer Trajectory for CSI type II: Earth to Saturn with Mars Swing-by. .	133
8-69	Specific Energy for Swing-by Trajectory: Earth – Mars – Jupiter. . . . .	135
8-70	Specific Energy for Swing-by Trajectory: Earth – Mars – Saturn. . . . .	136
9-1	Example of Fuel vs. Time of Flight for VSI type I. . . . .	139
C-1	Flowchart of Powell’s method[78]. . . . .	164
C-2	Example of Exterior Penalty Function [78]. . . . .	170
C-3	Example of Interior Penalty Function [78]. . . . .	171
C-4	Example of Extended Penalty Function [78]. . . . .	172
C-5	VRML Example – Simple House. . . . .	174

# LIST OF SYMBOLS AND ABBREVIATIONS

$\alpha$	In-plane thrust angle in the spacecraft-centered coordinates.
$\beta$	Out-of-plane thrust angle in the spacecraft-centered coordinates.
$c$	Exhaust velocity relative to the spacecraft (m/s).
$C_3$	$V_\infty^2$ (twice of the kinetic energy of the spacecraft per unit mass at the edge of the SOI).
$\Delta V$	Delta V.
$\dot{m}$	Rate of propellant flow (kg/s).
$g_0$	Acceleration of gravity at sea level (9.806 m/s <sup>2</sup> ).
$H$	The Hamiltonian.
$I_{sp}$	Specific Impulse.
$J$	Performance index.
$L$	The Lagrangian.
$\lambda$	The Lagrange multiplier.
$m_0$	Initial mass of the spacecraft.
$\phi$	Out-of-plane thrust angle in the Cartesian coordinates.
$P_J$	Jet power of the engine (W).
$R$	Distance between two point masses for the preliminary study.
$S$	Switching function (used for bang-off-bang control).
$T$	Thrust(Newton, kg·m/s <sup>2</sup> ).
$\mathbf{V}_{HT_{fin}}$	Final velocity for high thrust.
$\mathbf{V}_{HT_{ini}}$	Initial velocity for high thrust.
$\mathbf{V}_{pl}$	Velocity of planet. $V_{pl_{ini}}$ and $V_{pl_{fin}}$ are $V_{pl}$ of departure planet and arrival planet, respectively.
<b>AU</b>	Astronomical Unit (1 AU = 1.4959965E+08 km).
<b>ChebyTOP</b>	Chebyshev Trajectory Optimization Program.
<b>CSI</b>	Constant Specific Impulse.
<b>DU</b>	Distance Unit.
<b>IPREP</b>	Interplanetary PREProcessor.

<b>MT</b>	Metric ton (1,000 kg).
<b>NASA</b>	National Aeronautics and Space Administration.
<b>SAMURAI</b>	Simulation and Animation Model Used for Rockets with Adjustable $I_{sp}$ .
<b>SOI</b>	Sphere of Influence.
<b>TOF</b>	Time of Flight.
<b>TU</b>	Time Unit.
<b>VASIMR</b>	VARIABLE Specific Impulse Magnetoplasma Rocket.
<b>VRML</b>	Virtual Reality Modeling Language.
<b>VSI</b>	Variable Specific Impulse.
$\theta$	In-plane thrust angle in the Cartesian coordinates.
$V_\infty$	$V$ infinity. $V_{\infty\_ini}$ and $V_{\infty\_fin}$ are $V_\infty$ at departure and arrival, respectively.
$\zeta_p$	Propellant mass fraction ( $m_{propellant}/m_{initial}$ ).



## SUMMARY

A study has been performed to determine the advantages and disadvantages of variable thrust and variable  $I_{sp}$  trajectories for solar system exploration. Relative to traditional high thrust/low  $I_{sp}$  or even low thrust/high  $I_{sp}$  trajectories, these variable thrust missions have a potential to positively impact trip times and propellant requirements for solar system exploration.

There have been several numerical research efforts for variable thrust, variable  $I_{sp}$ , power-limited trajectory optimization problems. All of these results conclude that variable thrust, variable  $I_{sp}$  (variable specific impulse, or VSI) engines are superior to constant thrust, constant  $I_{sp}$  (constant specific impulse, or CSI) engines. That means VSI engines can achieve a mission with a smaller amount of propellant mass than CSI engines. However, most of these research efforts assume a mission from Earth to Mars, and some of them further assume that these planets are circular and coplanar. Hence they still lack the generality.

This research has been conducted to answer the following questions:

- Is a VSI engine always better than a CSI engine or a high thrust engine for any mission to any planet with any time of flight considering lower propellant mass as the sole criterion?
- If a planetary swing-by is used for a VSI trajectory, how much fuel can be saved? Is the fuel savings of a VSI swing-by trajectory better than that of a CSI swing-by or high thrust swing-by trajectory?

To support this research, an unique, new computer-based interplanetary trajectory calculation program has been created based on a survey of approaches documented in available

literature. This program utilizes a calculus of variations algorithm to perform overall optimization of thrust,  $I_{sp}$ , and thrust vector direction along a trajectory that minimizes fuel consumption for interplanetary travel between two planets. It is assumed that the propulsion system is power-limited, and thus the compromise between thrust and  $I_{sp}$  is a variable to be optimized along the flight path. This program is capable of optimizing not only variable thrust trajectories but also constant thrust trajectories in 3-D space using a planetary ephemeris database. It is also capable of conducting planetary swing-bys.

Using this program, various Earth-originating trajectories have been investigated and the optimized results have been compared to traditional CSI and high thrust trajectory solutions. Results show that VSI rocket engines reduce fuel requirements for any mission compared to CSI rocket engines. Fuel can be saved by applying swing-by maneuvers for VSI engines, but the effects of swing-bys due to VSI engines are smaller than that of CSI or high thrust engines.

# CHAPTER I

## INTRODUCTION

### *1.1 Problems of Variable Thrust, Variable $I_{sp}$ Trajectory Optimization*

Conventional propulsion systems are roughly classified into two types: high thrust rockets, and low thrust rockets. Table 1-1 shows examples of spacecraft propulsion systems. For a launch vehicle, high thrust rockets such as solid rockets or bipropellant liquid rockets must be used at the present time. This is because the thrust-to-weight ratio must be greater than one to vertically launch the vehicle from the ground. If a high thrust rocket is used for an interplanetary mission, the rocket is initially fired for a short period of time to accelerate the vehicle to the proper speed to reach the destination. If the spacecraft is to be placed in the desired parking orbit without an aerocapture maneuver, a second firing of the engine is used near the destination to decelerate the vehicle. Most of the fuel is consumed by these two burns. During the rest of the transfer time the engine is turned off and the vehicle coasts around the Sun without any propulsive energy added.

**Table 1-1:** Examples of Spacecraft Propulsion Systems[4][42].

Method	$I_{sp}$ (sec)	Thrust (N)	Duration
<b>Chemical</b>		$0.1 - 1.2 \times 10^7$	minutes
Liquid			
Monopropellant	140 – 235		
Bipropellant	320 – 460		
Solid	260 – 300		
Hybrid	290 – 350		
<b>Electric</b>		0.0001 – 20	months – years
Electrothermal	500 – 1,000		
Electromagnetic	1,000 – 7,000		
Electrostatic	2,000 – 10,000		
Nuclear thermal	800 – 1,100	up to $1.2 \times 10^7$	minutes
VASIMR	1,000 – 30,000	40 – 1,200	days – months

VASIMR – VArIable Specific Impulse Magnetoplasma Rocket.

On the other hand, low thrust rockets cannot be used for a launch vehicle because the thrust-to-weight ratio of the engine alone is less than one. Low thrust rockets do provide an advantage for interplanetary missions. Low thrust engines typically have higher specific impulse than higher thrust engines. This higher specific impulse results in less fuel being consumed when compared to high thrust rockets. Due to the low thrust level, trip times are typically longer for low thrust rockets when compared to the high thrust engines. This is especially true if the spacecraft has to leave the gravity well of the Earth or if it has to conduct an orbital insertion at the destination planet using its engines.

The comparison between low thrust systems and high thrust systems can be thought of in the same way as the comparison between a car driving in low gear and a car driving in high gear. A car starting from rest or climbing up a hill requires high thrust, and a driver chooses low gear to exert high thrust at the expense of high fuel consumption. In contrast, a car cruising on a highway needs high fuel efficiency rather than high thrust, so a car cruising with high speed uses its top gear to save fuel.

A conventional propulsion system cannot modulate its specific impulse. So, depending on the purpose of the mission, a mission designer must select the rocket type.

The concept of modulating thrust and specific impulse has been theoretically evaluated since the early 1950's[9][25]. Fig. 1-1 shows an artist's concept of future interplanetary travel with a rocket that can modulate its specific impulse. Currently there are several projects ongoing worldwide relevant to rocket engines that can modulate their thrust and  $I_{sp}$ . This research includes mechanical tests at ground facilities as well as trajectory simulations with computers. However, a question emerges: "What are the advantages of having a propulsion system that can modulate its specific impulse depending on the operational condition?"

The study of trajectory optimization problems is very important for space development. If a trajectory can be optimized by either minimizing fuel consumption or finding the best launch opportunity that minimizes time from Earth to another planetary body, that trajectory will save operational costs as well as increase the probability of success of a mission.

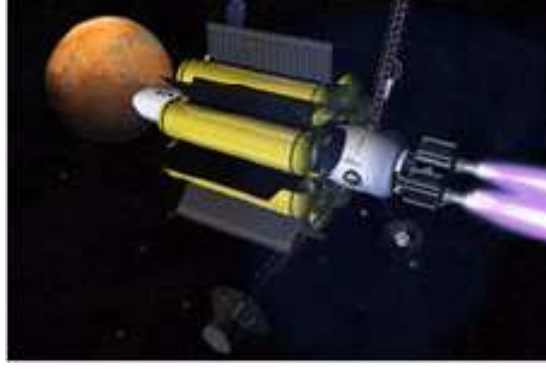


**Figure 1-1:** Future Interplanetary Flight with VASIMR[5].

For high thrust engines, the interplanetary trajectory is nearly a conic section that is determined only by the time of flight and the positions of departure planet and arrival planet. Therefore only the times of departure and arrival are optimized. Because there are two orbits passing through the departure planet to the arrival planet with the prescribed time of flight, the orbit that requires less fuel is normally chosen.

For trajectories with CSI engines, the thrust direction should be controlled so that the spacecraft reaches the target planet with the prescribed time of flight. Therefore finding an optimal trajectory for CSI engines is the same as finding a history of the best thrust direction. If the engine has a capability of turning the engine on and off, switching times (on  $\rightarrow$  off or off  $\rightarrow$  on) should be appropriately determined.

For trajectories with VSI engines, because the thrust level and  $I_{sp}$  are variable, finding an optimal trajectory for this type of rocket means finding a history of the best thrust direction and a history of the best thrust level (possibly including zero thrust) that minimizes the fuel consumption for entire mission. The trajectory is calculated from initial conditions (initial mass, initial position and velocity), final conditions (final position and velocity), time of flight, and the vehicle's available power level. Fig. 1-2 shows an example trajectory for a VSI engine.

## ***1.2 Motivation for Research***

For interplanetary missions, finding a trajectory that minimizes the fuel consumption is important. Reducing the fuel consumption not only saves cost for fuel but also cost for

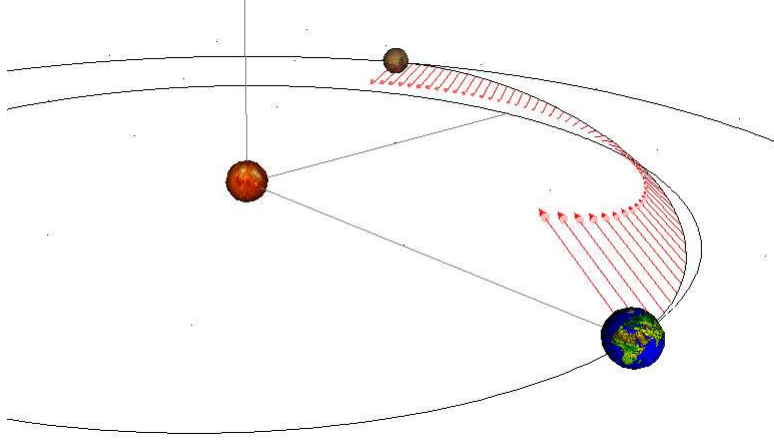


**Figure 1-2:** Transfer Trajectory from Earth to Mars with Thrust Direction.

launch from the ground, and therefore the cost for the entire mission decreases.

Selecting a suitable engine type for a mission is also important. So far, high thrust engines and constant  $I_{sp}$  low thrust engines have been used for interplanetary missions. If a variable  $I_{sp}$  engine, which is under development, could be used for a mission, it may reduce the mission cost. Analyzing trajectories with variable  $I_{sp}$  engines and comparing them to trajectories with constant  $I_{sp}$  engines or high thrust engines should help in selecting the engine type.

There have been several numerical research efforts for variable thrust, variable  $I_{sp}$  (variable specific impulse, or VSI), limited-power trajectory optimization problems [25][49][20][69][61][72]. Both indirect methods and direct methods have been used to evaluate this problem. Most of the research efforts assume a human mission to Mars, and all of these results conclude that VSI engines are superior to constant thrust, constant  $I_{sp}$  (or CSI) engines. That means VSI engines require less amount of propellant than CSI engines for a mission.

This research started with the following questions:

- Does a VSI engine always require less fuel than a CSI engine or a high thrust engine for any mission to any planet with any time of flight?
  - If the answer is yes, is it possible to find a qualitative relationship between fuel

consumption and other parameters such as power level, time of flight, or semi-major axis of the transfer orbit?

- If the answer is no, in what situations are CSI or high thrust better than VSI?
- If a planetary swing-by is used for a VSI trajectory, how much fuel can be saved relative to the non swing-by case? Is the fuel saving of the VSI swing-by trajectory better than that of a CSI swing-by trajectory or a high thrust swing-by trajectory?

To answer the above questions, a study of a variable thrust, variable  $I_{sp}$  rocket engine, particularly focusing on the optimization of interplanetary trajectories with this type of rocket engine, is conducted in this research. A number of interplanetary trajectories with different combinations of departure date, time of flight, and target planet are simulated numerically and the fuel requirements for VSI, CSI, and high thrust engines are compared.

### ***1.3 Research Goals and Objectives***

The primary goal of this research is to demonstrate the advantages and disadvantages of VSI engines over conventional engines such as CSI engines and high thrust engines that are currently used for interplanetary missions when considering fuel consumption as the only criterion. If the merits and demerits of using a VSI engine over a CSI engine and a high thrust engine are parameterized, this data can be used to determine the engine type for a particular mission. Therefore, the goal of this research is to establish a generalized rule that:

1. Qualitatively states the advantages and disadvantages of a VSI engine.
2. Quantitatively determines the fuel savings by using a VSI engine over a CSI or a high thrust engine.

For example, goal 1 may be written as, “to travel from Earth to Mars, VSI is always better than other types of engines, but as the trip time increases the merit of using a VSI engine gradually decreases.” Similarly, goal 2 may be written as, “going from Earth to

Jupiter in 3 years with a VSI engine saves about 20% of the total fuel over a CSI engine and 33% over a high thrust engine.”

To support the goal described above, numerical analyses should be conducted. As far as the author knows, there are currently no programs available that can calculate interplanetary trajectories with all of VSI, CSI, and high thrust engines. Therefore, an additional goal is to create an interplanetary trajectory optimization program that can calculate the trajectories to conduct this research.

The program should have the capability of calculating transfer trajectories from one planet to another, and it should be used for any type of engine including VSI, CSI, and high thrust. The program also should be able to calculate swing-by trajectories with those same types of engines. The program should be robust, accurate, and fast.

## ***1.4 Approach***

To achieve the above research objectives, several steps were taken in this research.

At first, to become familiar with interplanetary optimization problems, a literature review was conducted. This work included finding and studying a proper method to solve this kind of problem, understanding orbital mechanics and methods of solving optimization problems, and addressing the contribution of this research to the field of interplanetary trajectory optimization problems.

Next, proof-of-concept study was conducted that was designed to be simple, yet still representative of the problems. A simple two-dimensional trajectory was used to compare fuel consumption of VSI, CSI, and high thrust engines by integrating equations of motion.

Then an interplanetary trajectory optimization software application was created using a method learned during the literature review. The application was developed to be easy to use, run quickly, and produce accurate results.

Using this application, a preliminary study was conducted to confirm the implementation of the application. Assuming that the orbits of planets around the Sun are circular and coplanar, two-dimensional trajectories from Earth to other planets were calculated. With



this research, a large database was obtained regarding fuel requirements. A rule of thumb for the relationship between fuel requirements and the distance from Earth to target planets as well as the relationship between fuel requirements and time of flight for each type of engine was established.

Finally, “real world” examples were considered to check if the relationships obtained in the previous step can be applied to the actual three-dimensional interplanetary trajectories. Planet positions and velocities are given as functions of time that are obtained from actual observations. Using the position and velocity data for planets, simulations for transfer trajectories were conducted.

## ***1.5 Organization of the Thesis***

This thesis is organized into nine chapters and four appendices:

- Chapter 2 briefly describes an engine that is capable of modulating thrust and specific impulse. In this chapter, as an example of a VSI engine, the mechanism of the VASIMR engine that is currently under development at NASA Johnson Space Center is presented. Then this chapter provides a mathematical way of finding the best power level to be operated throughout the mission. Several research efforts for low thrust trajectories that have been done by other researchers are also introduced from the literature review.
- Chapter 3 presents the preliminary, proof-of-concept study with simple trajectories. Using two-dimensional simple spiral trajectories, the fuel requirements of high thrust, low thrust with constant  $I_{sp}$ , and low thrust with variable  $I_{sp}$  are compared.
- Chapter 4 is an overview of optimization problems. Examples of methods to solve general trajectory optimization problems are presented. At first, several optimization methods are introduced. The method of calculus of variations that is then applied to different types of optimization problems is presented.
- Chapter 5 describes general interplanetary trajectory optimization problems. The assumptions made to conduct this research are first defined, and then the required

equations of motion to solve the optimization problems are determined.

- Chapter 6 explains the development of the software application *SAMURAI* in detail. Capabilities of this application, C++ classes and schemes, and example inputs and outputs are shown. A brief explanation of VRML that displays the trajectory on the web browser is also described.
- Chapter 7 shows the preliminary results from *SAMURAI*. Two-dimensional transfer trajectories between two planets are calculated. Planets are assumed to be orbiting around the Sun with zero eccentricity and zero inclination. A large database of fuel requirements is generated and the characteristics of VSI engines are discussed.
- Chapter 8 shows the “real world” numerical examples. Using three-dimensional actual ephemeris data of planets, transfer trajectories from Earth to other planets with and without swing-bys are computed.
- Chapter 9 closes the thesis with conclusions and recommendations for future work.
- There are four appendices: Appendix A shows the additional results for the preliminary study obtained in Chapter 7, Appendix B provides the additional equations used in the application. Chapter C introduces all the programming techniques required to solve the problems proposed in this research. The examples of techniques introduced in this section are optimal control programming, line search, Powell’s method, and penalty functions. Appendix D is the users’ manual for the application *SAMURAI*.

## CHAPTER II

### EXHAUST-MODULATED PLASMA PROPULSION

This chapter contains a brief description of an engine that is capable of modulating thrust and specific impulse at constant power.

There are several types of exhaust modulated engines under experiment such as VASIMR (Variable Specific Impulse Magnetoplasma Rocket), currently studied at the Advanced Space Propulsion Laboratory at NASA's Johnson Space Center in Houston (Fig. 2-1), or EICR (Electron and Ion Cyclotron Resonance) Plasma Propulsion Systems at Kyushu University, Japan[2].

Because these systems are similar, the mechanism of the VASIMR engine is presented in this section.

#### **2.1 Overview**

The concept of exhaust modulation has been known theoretically since the early 1950's[9][25], but the technology to construct these systems had remained elusive until the late 1960's.

The electric propulsion systems such as ion engines and the Hall thrusters accelerate ions present in plasmas by applying electric fields externally or by charging axially. These ion acceleration features, in turn, result in accelerated exhaust beams that must be neutralized by electron sources located at the outlets before the exhaust streams leave the engine.

A MPD (Magnetoplasmadynamic thruster) plasma injector includes a cathode in contact with the plasma. This cathode becomes eroded and the plasma becomes contaminated with cathode material. This erosion and contamination limit the lifetime of the thruster and degrade efficiency[23].

The design of the VASIMR avoids those limiting features as VASIMR has an electrodeless design (a fact that enables the VASIMR to operate at much greater power densities). Instead of heating (or accelerating) the ions with electrodes, VASIMR heats the ions by the

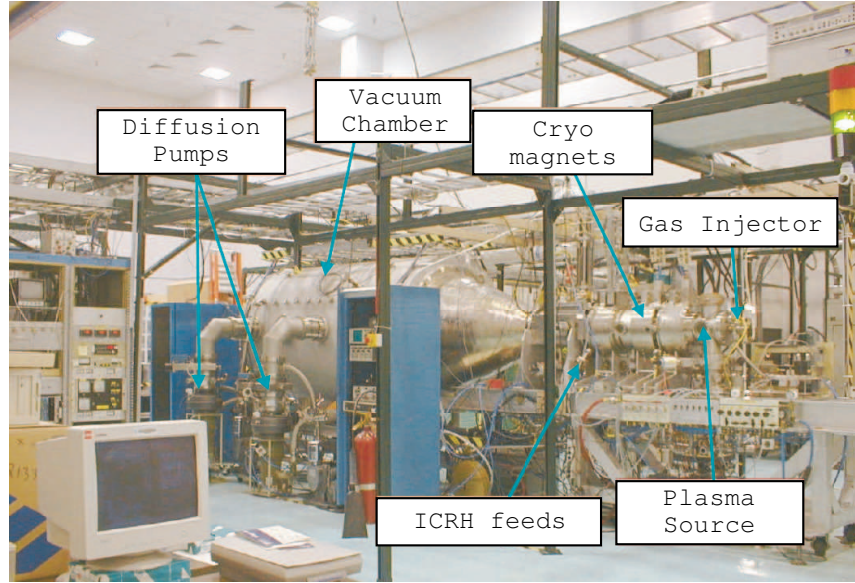


**Figure 2-1:** VX-10 Experiment at Johnson Space Center[45].

action of electromagnetic waves, similar to a microwave oven. Therefore, contamination is virtually eliminated and premature failures of components are unlikely. A magnetic field is used to trap these high temperature particles.

With its long lifetime and reliability, the VASIMR engine is expected to be used for many purposes including:

- Boosting satellites to higher orbits.
- Retrieving and servicing spacecraft in high Earth orbits.
- Course correction and drag make-up for space station.
- Human and robotic missions to other planets.

A more precise explanation of the mechanics of the VASIMR engine is introduced in the next section.

## 2.2 *Mechanism*

Rocket thrust,  $T$ , is measured in Newtons ( $\text{kg}\cdot\text{m}/\text{s}^2$ ) and is the product of the exhaust velocity relative to the spacecraft,  $c(\text{m}/\text{s})$ , and the rate of propellant flow,  $\dot{m}(\text{kg}/\text{s})$ .

$$T = -\dot{m}c. \quad (2-1)$$

The negative sign shows that the direction of the thrust is opposite to the direction of the exhaust velocity. The same thrust is obtained by ejecting either more material at low velocity or less material at high velocity. The latter saves fuel but generally entails high exhaust temperatures.

The rocket performance is measured by its specific impulse, or  $I_{sp}$ , which is the exhaust velocity divided by the acceleration of gravity at sea level,  $g_0(9.806\text{m/s}^2)$ , as

$$I_{sp} = \frac{c}{g_0}. \quad (2-2)$$

The specific impulse is a rough measure of how fast the propellant is ejected out of the back of the rocket. A rocket with a high specific impulse does not need as much fuel as a rocket with a low specific impulse to achieve the same  $\Delta V$ . Although thrust is directly proportional to  $I_{sp}$  (because  $T = -\dot{m}c$  and  $c = g_0 I_{sp}$ ), the power needed to produce it is proportional to the square of the  $I_{sp}$ . Therefore the power required for a given thrust increases linearly with  $I_{sp}$ . These relationships can be expressed in the following equation:

$$P_J = \frac{T c}{2} = -\frac{1}{2} g_0 I_{sp} T = -\frac{1}{2} \dot{m} g_0^2 I_{sp}^2 \quad \text{where } P_J \text{ is the jet power.} \quad (2-3)$$

Chemical rockets obtain this power through the exothermic reaction of fuel and oxidizer. In other propulsion systems, the power must be imparted to the exhaust by a propellant heater or accelerator. Solar panels or nuclear reactors may be used to generate this power.

The greatest advantage of the VASIMR engine is that it can change its thrust level and specific impulse at a constant power level by changing the amount and the velocity of the exhaust ions. This is how VASIMR modulates its thrust and  $I_{sp}$ .

VASIMR uses charged particles called plasma as a source of thrust. The temperature of the plasma ranges from 10,000 K to more than 10 million K. At these temperatures, the ions move at a velocity of 300,000 m/s. This is 60 times faster than the particles in the best chemical rockets whose temperature is only about a few thousand K.

For a given jet power  $P_J$ , the relationship between thrust  $T$  and  $I_{sp}$  is expressed as  $P_J = \frac{1}{2} T I_{sp} g_0$ . When the power is set constant, thrust and  $I_{sp}$  are inversely related. Increasing one always comes at the expense of the other.

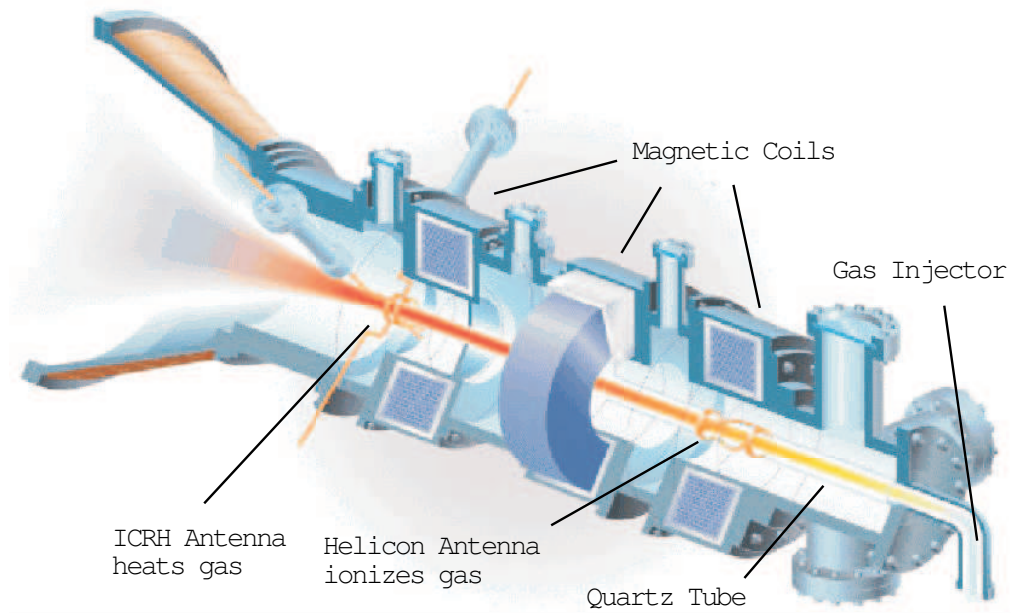


**Figure 2-2:** Synoptic View of the VASIMR Engine[22].

As shown in Fig. 2-2[22], the VASIMR rocket system consists of three major magnetic cells called “forward,” “central,” and “aft.” First, a neutral gas, typically hydrogen, is injected from the injector to the forward cell and ionized by the helicon antenna[5].

Second, this charged gas is heated to reach the desired density in the engine’s central cell. This heating process is done by the action of electromagnetic waves, which is similar to what happens in a microwave oven. The plasma is trapped by the magnetic field that is generated by the magnetic coils so that it can be heated to 10 million K.

Third, heated plasma enters the nozzle at the aft cell, where the plasma detaches from the magnetic field and is exhausted to provide thrust.

VASIMR can change its thrust and  $I_{sp}$  by changing the fraction of power sent to the Helicon antenna vs. the ICRH antenna (See Fig. 2-3). The helicon antenna is used to ionize gas injected from the gas injector. The ICRH (ion cyclotron resonance heating) antenna heats the gas and accelerate the particle before these particles are exhausted to space. When more power is sent to Helicon antenna, more gases are ionized, which means more ions are ejected. But because the total system power level is constant, power sent to ICRH antenna decreases, which means these ions exit with a lower velocity. These low speed, large quantity

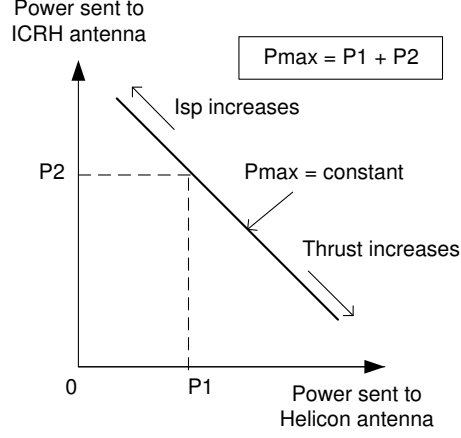


**Figure 2-3:** Power Partitioning and Relationship between Thrust and  $I_{sp}$ .

of ions act as a source of a high thrust, low  $I_{sp}$  engine. On the other hand, when less power is sent to the Helicon antenna and more power is sent to the ICRH antenna, small amount of gases are ionized and they are accelerated to a higher exit velocity. These high speed ions act as a source of a low thrust, high  $I_{sp}$  rocket engine.

In the absence of any constraints on the time required to perform a given orbital transfer, it is always optimal to operate the engine at its highest possible specific impulse value. However, if time is important, then it may be beneficial to trade some of the specific impulse in return for high thrust[72].

As mentioned in Chap. 1, the choice of the combination of the thrust and  $I_{sp}$  could be considered in a similar way to an automobile transmission. Initially the spacecraft needs high thrust so that it gets enough speed to begin the transfer. This is similar to a car starting with low gear from rest. As the spacecraft's speed increases,  $I_{sp}$  is allowed to gradually increase and therefore thrust decreases for higher fuel efficiency, just as a car shifts up its gear as its speed increases.

### 2.3 Choosing the Power Level

In the last section, the operational power level is assumed to be maximum (therefore constant). As explained so far, a VSI spacecraft needs high thrust near the departure planet and target planet, but low fuel consumption is desirable for the rest of the path. VASIMR

has two options to lower fuel consumption: either by increasing  $I_{sp}$  while the power is kept constant or by decreasing the power level while  $I_{sp}$  is kept constant.

In this section, fuel consumption at a power level other than the maximum is investigated mathematically[49]. Then the reason the maximum power level should be always chosen to achieve the least fuel consumption is presented.

The equation of motion of a spacecraft in a vacuum is given by

$$m\ddot{\vec{r}} = \dot{m}\vec{c} + m\vec{g} \quad (2-4)$$

where  $\vec{r}$  is the position of spacecraft,  $\vec{g}$  is the acceleration of gravity,  $\vec{c}$  is the exhaust velocity, and  $\dot{m}$  is the mass flow rate. The acceleration vector  $\vec{a}$  due to the thrust  $\vec{T}(= \dot{m}\vec{c})$  is expressed as

$$\vec{a} = \frac{\vec{T}}{m} = \ddot{\vec{r}} - \vec{g}. \quad (2-5)$$

For an electric-powered ion thruster, the jet power,  $P_J$ , can be expressed as, using thrust,  $T$ , and exhaust velocity,  $c$ ,

$$P_J = \frac{Tc}{2}. \quad (2-6)$$

Since  $T = -\dot{m}c$ ,

$$P_J = -\frac{T^2}{2\dot{m}}. \quad (2-7)$$

Then for a given jet power, the thrust versus mass flow rate curve of an ion rocket is written as

$$T = \sqrt{-2\dot{m}P_J}. \quad (2-8)$$

This behavior is very different from that of a conventional constant exhaust velocity rocket, because for these rockets the thrust versus mass flow rate curve is

$$T = -\dot{m}c \quad (2-9)$$

as introduced in the last section. Figs. 2-4 and 2-5 show the trend of thrust with respect to mass flow rate for CSI and VSI, respectively.



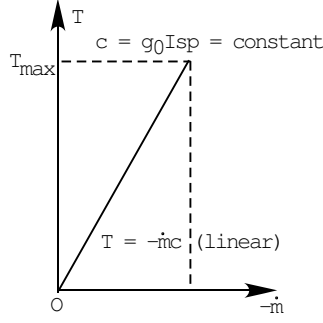


**Figure 2-4:** Thrust vs. Mass Flow Rate for a CSI Engine.

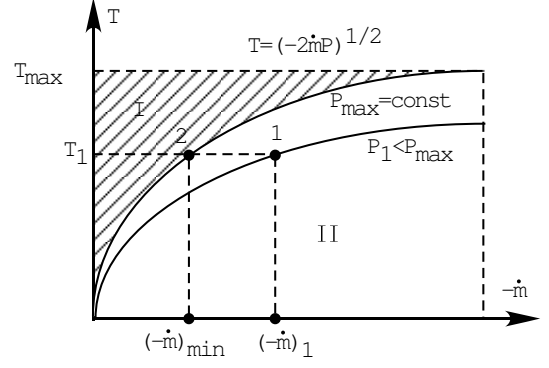


**Figure 2-5:** Thrust vs. Mass Flow Rate for a VSI Engine.

The mass flow rate, on the other hand, is expressed as:

$$\dot{m} = -\frac{T}{c} \quad \text{for CSI} \quad (2-10)$$

$$\dot{m} = -\frac{T^2}{2P_J} \quad \text{for VSI} \quad (2-11)$$

Therefore, it is advantageous to have high exhaust velocity for CSI or high power for VSI in order to minimize propellant consumption. Although the same level of thrust can be achieved by different combinations of  $\dot{m}$  and  $P_J$  from Eqn. 2-8, it is the best to choose  $P_J$  at its maximum. This is because  $\dot{m}$  is at a minimum if  $P_J$  is chosen at its maximum in Eqn. 2-11.

As is shown in Fig. 2-4, for a rocket with constant exhaust velocity, the thruster operates at maximum thrust only because  $c$  cannot be varied. Fig. 2-5 corresponds to the variable  $c$  case for a given power. The thruster can operate in Region II, and cannot operate in Region I, since it corresponds to the power greater than the maximum power  $P_{max}$  that the thruster can exert. Note that it is not optimal to operate at a power level less than  $P_{max}$ . For the same thrust  $T_1$ , the operation at  $P_{max}$  depicted by point 2 results in the minimum mass flow rate.

For a practical engine, because of the physical restrictions, there is an upper limit for the exhaust velocity an engine can achieve, and this limit set an upper limit on  $I_{sp}$ . As shown in Fig. 2-6, Region I that is unreachable by an engine is extended by the inclusion of the boundary  $OB$ . This line is defined by the physical constraints of an engine and it

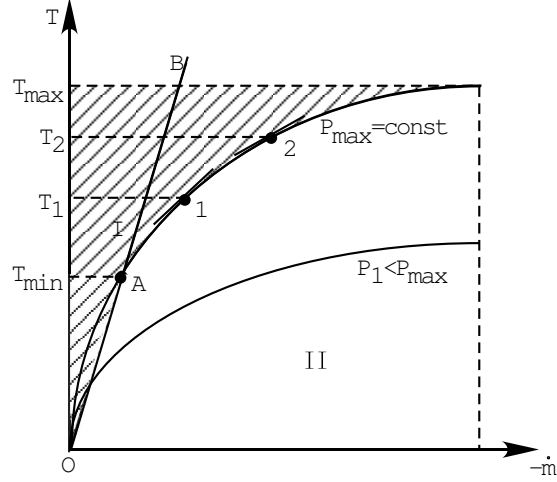


**Figure 2-6:** Thrust vs. Mass Flow Rate for a VSI Engine with Limitations.

corresponds to the equation  $T = -\dot{m}c_{max}$ , where  $c_{max}$  is the maximum exhaust velocity the rocket can achieve. Hence, line  $OB$  represents the maximum  $I_{sp}$ . This boundary is necessary to prevent  $I_{sp}$  from growing to very large values as the thrust is decreased towards its minimum value. The minimum thrust magnitude the engine can have for  $P_{max}$  is defined at point  $A$ .

## 2.4 Literature Review

There have been a number of studies on low thrust trajectories for both CSI and VSI engines. One of the earliest and most notable applications of the calculus of variations to the orbit transfer problem was done by Lawden in 1963[54]. Lawden set the foundations for the functional optimization of space trajectories. He showed that the thrust direction vector is expressed by the Lagrange multipliers, and the vector is referred to as the primer vector.

A book by Marec[59] published in 1979, covered a study of optimal space trajectories comprehensively, including both high thrust and low thrust propulsion systems. He applied the Contensou-Pontryagin Maximum Principle to obtain equations of optimal trajectories.

In addition to the study of general optimal trajectory problems introduced above, a number of low thrust trajectory optimization problems have been studied for decades. Most of the problems deal with trajectories with CSI engines. There are also several studies

on variable thrust, variable  $I_{sp}$  trajectories, and in the next few pages these studies are introduced.

In the paper published in 1995, Chang-Diaz, Hsu, Braden, Johnson, and Yang [25] studied human-crewed fast trajectories with a VSI engine to and from Mars. Their study does not include planetocentric phases at departure and arrival, but only heliocentric phase is considered. In addition to completing a nominal round trip scenario (a 101-day outbound trip, a 30-day stay, and a 104-day return), their work shows that a VSI engine has the ability to abort a mission when something goes wrong during the outbound phase. Chang-Diaz, an advocator of VASIMR(VARiable Specific Impulse Magnetoplasma Rocket), and his colleagues have not only simulated the trajectory analysis but also have conducted a number of hardware experiments with a VSI engine[65][74][43][66][30][44].

Kechichian(1995)[49] described the method of optimizing a VSI low thrust trajectory from LEO to GEO using a set of non-singular equinoctial orbital elements. His paper includes all the equations required to perform the calculus of variations to find the set of control variables ( $I_{sp}$  and thrust direction) for a constant power, variable  $I_{sp}$  trajectory. The upper and lower bounds for the  $I_{sp}$  are set to simulate the physical constraints of the engine. This study is only for the orbit around the Earth and the equations cannot be used for the escape trajectory as the equinoctial orbital elements are only valid for a trajectory with an eccentricity of less than one.

Casalino, Colasurdo, and Pastrone(1999)[20] analyzed the optimal 2-dimensional heliocentric trajectory with a VSI engine. Using the shooting method, they studied trajectories with and without swing-bys to escape from the solar system. Their main concern was to obtain the best history of thrust and pitch angle to maximize the specific energy of the spacecraft at the end of calculation which does not have a planetary capture at the end. The conclusion of this research was that a trajectory with swing-bys can get more escape energy than a trajectory without swing-bys.

The research of VSI trajectories done by Nah and Vadali(2001)[61] includes the gravitational effects of the Sun, the departure planet (Earth), and the arrival planet throughout an entire trajectory. Mars is chosen as the arrival planet, and the actual ephemeris for

Earth and Mars is used. A shooting method was used to obtain the control variables that maximize the final mass of the spacecraft at Mars arrival. The upper limit for  $I_{sp}$  is set as a constraint.

Seywald, Roithmayr, and Troutman(2003)[72] studied a circular-to-circular low thrust orbit transfer with a prescribed transfer time. They solved the optimal control problem analytically and studied the thrust history that minimizes the fuel consumption for a transfer orbit between two circular orbits with prescribed time of flight. Their work concludes that, if the thrust magnitude is always low enough such that it qualifies as “low thrust”, the optimal thrust magnitude is always proportional to the vehicle mass. They also investigated how much fuel is saved if a VSI engine, instead of a CSI engine, is used, and concluded that the percentage of fuel savings depends strongly on the boundary conditions such as flight time and initial and final values of the semi-major axis.

The work done by Ranieri and Ocampo(2003)[69] is specialized for human missions to Mars. Using the nonlinear programming boundary value solver, they studied a round trip to Mars using VASIMR. This trajectory includes a heliocentric outbound trajectory from Earth to Mars, a several month stay at Mars, then a heliocentric inbound trajectory from Mars to Earth. Planetary bodies are assumed to be point masses (zero sphere of influence). The objective is either to minimize the initial mass with a given final mass or to maximize the final mass with a given initial mass for an unbounded  $I_{sp}$  engine and a CSI engine. A CSI engine can turn its power on and off, resulting in a bang-off-bang thrust profile. In this paper, the fuel requirements for a round trip with VSI and a trajectory with CSI are compared. The results show that the fuel consumption with VSI is more than the CSI for the outbound trajectory, but it is less than CSI for the inbound trajectory. The result is that VSI requires less fuel than CSI for an overall round trip.

Each of these papers gives interesting features of VSI engines. No paper compares VSI engines with high thrust engines, and only two papers (by Seywald[72] and by Ranieri[69]) compare a VSI engine with a CSI engine. The paper by Ranieri studied Earth to Mars and Mars to Earth trajectories, and the paper by Seywald studied circular-to-circular geocentric

transfer orbits. That means there still remains ambiguity of the advantages of a VSI engine over a CSI engine in general. A swing-by trajectory was studied in Casalino's paper[20], but he does not include planetary capture at the end of the mission.

Therefore, it is still ambiguous if using VSI engines is more beneficial than using CSI engines for any interplanetary missions. Also, the effects of planetary swing-bys for transfer orbits between two planets are unknown.

Hence, research questions still remain: Is VSI always better than CSI or high thrust for any trajectory? Or if we apply swing-bys and simulate a planetary capture at the end of mission, what characteristics does the trajectory have?

## CHAPTER III

### PRELIMINARY STUDY: SIMPLE TRAJECTORIES

Before proceeding to the actual interplanetary trajectory optimization problems, it is good to start by checking the advantages and disadvantages of a VSI engine over a CSI engine or a high thrust engine with simple examples.

#### 3.1 *Problem Formulation*

The problem in this chapter is defined as follows: How much fuel is required and how long does it take for a spacecraft on a circular orbit around a planet to reach the point  $P$  whose distance from the planet's center is  $R$ ?

Fig 3-1 shows examples of the trajectories. To conduct this study, forces other than the propulsive force from the spacecraft and the gravity forces from the planet are neglected. By doing this, the problem can be simplified such that the fuel consumption and transfer time depend only on the engine type. The equations of motion and mass of the spacecraft are defined as differential equations. By integrating these equations, the time of flight and required propellant mass to reach the target are calculated. The types of engines considered in this study are high thrust, VSI, and CSI. For each of the thrust types, trip time and propellant mass required to reach the point  $P$  are compared. A shorter trip time and a smaller amount of the propellant mass are desired.

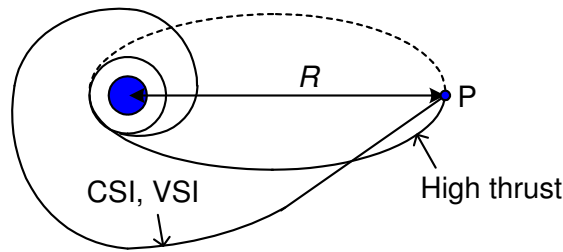


**Figure 3-1:** Trajectories for Preliminary Study.

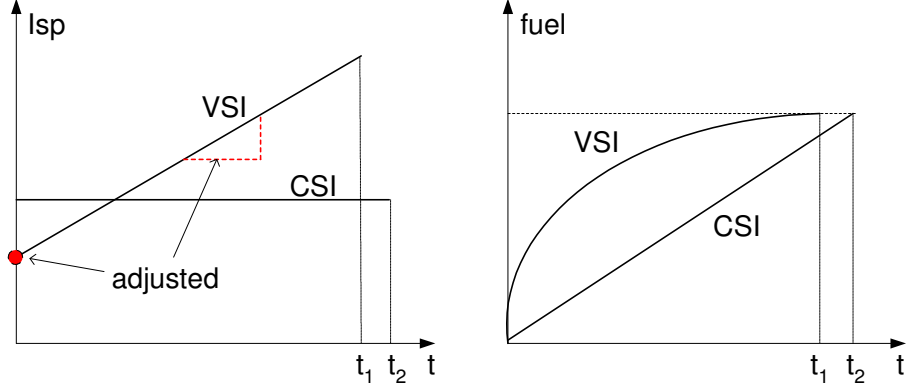


**Figure 3-2:** Preliminary Study:  $I_{sp}$  and Fuel Consumptions for VSI and CSI.

For high thrust, two-body orbital mechanics is applied. In this case, the spacecraft does not follow the spiral trajectory but the trajectory follows either an ellipse, a parabola, or a hyperbola. The least energy required (but the longest trip time required) trajectory for high thrust is an ellipse with its apoapsis (farthest point from the planet) located at  $P$  as shown in Fig. 3-1. It is assumed that the spacecraft fires an instantaneous burn at the periapsis (closest point from a mass) and follows the half-ellipse toward the apoapsis.  $\Delta V$  at the departure is used to calculate the required propellant mass in the following way: with  $I_{sp}$  specified,  $m_p = m_0(A - 1)/A$ , where  $A = \exp(\Delta V/(g_0 \cdot I_{sp}))$ .

For low thrust with constant  $I_{sp}$  (CSI),  $I_{sp}$  values of 3,000, 5,000, and 8,000 seconds are considered. The trip time required to reach the point  $P$  is obtained by propagating the equations of motion. From the trip time, propellant mass consumed is calculated as  $m_p = 2t \cdot P_J/(g_0 \cdot I_{sp})$ , where  $t$  is the trip time,  $P_J$  is jet power of the thrust, and  $g_0$  is  $9.806\text{m/s}^2$ .

For low thrust with variable  $I_{sp}$  (VSI), it is assumed that the thrust is allowed to change linearly with time as shown in Fig. 3-2. The starting  $I_{sp}$  and the slope of  $I_{sp}$  with respect to time are adjusted so that the spacecraft reaches the point  $P$  with the least trip time. Also, the starting  $I_{sp}$  and the  $I_{sp}$  slope are set so that the required propellant mass is constrained to be the same amount as the CSI cases. Hence, there are three VSI cases that are corresponding 3,000, 5,000, and 8,000 sec of CSI cases. The fuel consumption for each VSI case is the same as the fuel consumption for each CSI case.

The thrust vector is assumed to be tangential to the path for both of VSI and CSI engines.

At first a CSI with certain  $I_{sp}$  case is calculated and the propellant mass is computed. Then a VSI case is computed by adjusting the slope and the initial  $I_{sp}$  so that the required propellant mass equals the CSI case with an  $I_{sp}$  of 3,000 sec. By doing this, only trip times should be compared when comparing CSI and VSI, with the shorter trip time case considered to be better than the longer trip time case.

The following cases are considered: the distance between two point masses,  $R$ , is set to 100 DU, 500 DU, and 1,000 DU. “DU”, or Distance Unit, is defined as the radius of the planet. Initial masses of 5 MT, 10 MT, and 20 MT are considered. The jet power is set to 500 kW for VSI and CSI engines. The values of time of flight for VSI, CSI, and high thrust are compared and the amount of fuel saved (or increased) is calculated when a VSI engine was used. Time of flight is measured in TU, or Time Unit. TU is defined such that the speed of the spacecraft in the hypothetical reference circular orbit (whose radius is 1 DU) is 1 DU/TU. Then the value of the gravitational parameter,  $\mu$ , will turn out to be 1 DU<sup>3</sup>/TU<sup>3</sup>. TU and DU are called canonical units[12].

Because only two-dimensional cases are considered, the equations of motion of the spacecraft in Cartesian Coordinates are

$$\dot{x} = u \tag{3-1}$$

$$\dot{y} = v \tag{3-2}$$

$$\dot{u} = -\frac{\mu x}{r^3} + \frac{T_x}{m} \tag{3-3}$$

$$\dot{v} = -\frac{\mu y}{r^3} + \frac{T_y}{m} \tag{3-4}$$

$$\tag{3-5}$$

where  $\mu$  is the gravitational constant (1 DU<sup>3</sup>/TU<sup>3</sup>), and  $r = (x^2 + y^2)^{1/2}$ ;  $T_x$ , and  $T_y$  are the  $x$  and  $y$  components of the thrust;  $m$  is the mass of the spacecraft.



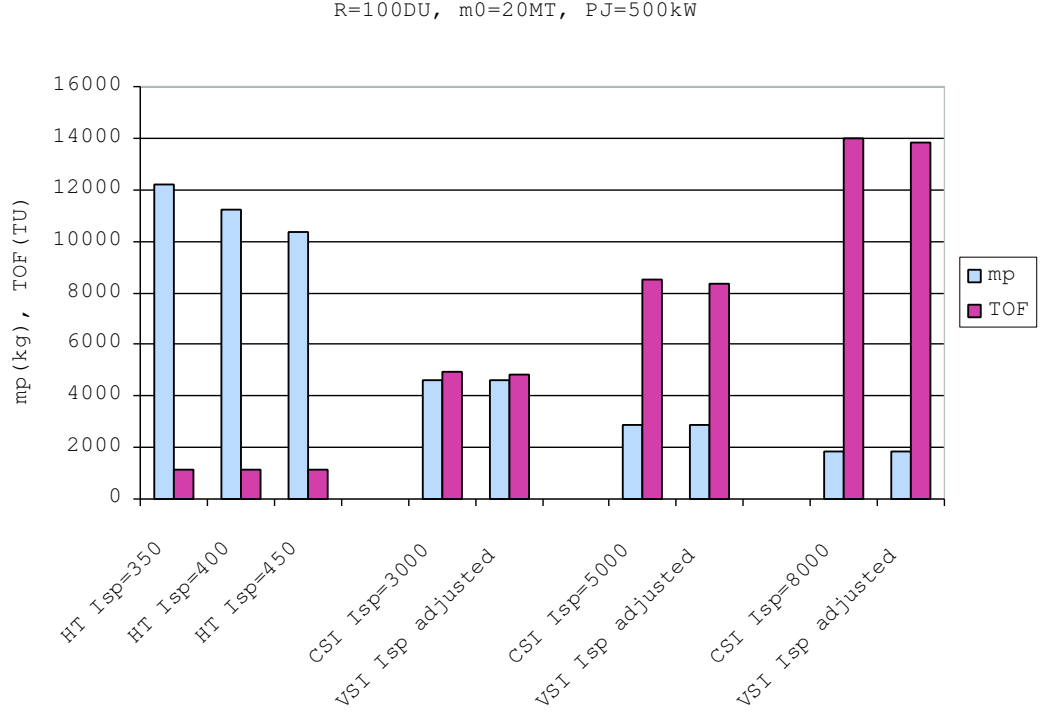


**Figure 3-3:** Results:  $R = 100 \text{ DU}$ ,  $m_0 = 20 \text{ MT}$ ,  $P_J = 500 \text{ kW}$ .

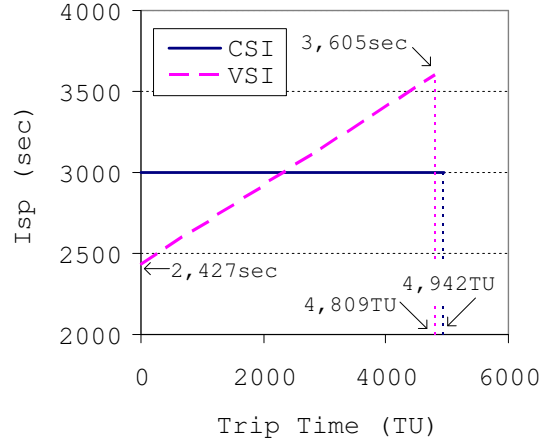
### 3.2 Results

Fig. 3-3 shows the comparison of propellant mass and time of flight for high thrust, CSI, and VSI when  $R$  is 100 TU, initial mass is 20 MT, and jet power is 500 kW. For high thrust, three different realistic  $I_{sp}$  cases are computed, resulting in a decrease of the required propellant mass as  $I_{sp}$  increases.

For low thrust cases, CSI cases are first computed. Then, as explained above, VSI cases are computed so that fuel consumption becomes the same amount of that of CSI cases. The slope and the initial  $I_{sp}$  of the linearly increasing  $I_{sp}$  are adjusted so that the spacecraft reaches the point  $P$  with the shortest trip time.

Fig. 3-4 shows the  $I_{sp}$  histories of VSI and CSI when  $I_{sp}$  for CSI is 3,000 sec.  $I_{sp}$  for VSI starts at 2,427 sec and ends at 3,605 sec. This figure shows that time of flight for VSI is 133 TU shorter than CSI.

As can be seen from Fig. 3-3, the high thrust trip time is the smallest, and the trip



**Figure 3-4:**  $I_{sp}$  histories for VSI and CSI when CSI  $I_{sp}$  is 3,000 sec:  $R = 100$  DU,  $m_0 = 20$  MT,  $P_J = 500$  kW.

time for 8,000 sec constant  $I_{sp}$  is the longest. When  $I_{sp}$  is high, thrust is low. So it was expected that 8,000 sec of  $I_{sp}$  takes longer to reach the point  $P$  than both 3,000 sec and 5,000 sec  $I_{sp}$  cases. But because 8,000 sec  $I_{sp}$  is more efficient than others, it requires the least propellant. When the thrust (therefore  $I_{sp}$ ) is modulated, as shown in the figure, the trip time decreases. From this result, it is possible to say that higher thrust is desirable in the vicinity of the attracting body while most of the power should be used to escape from the gravity well of the attracting body. Higher  $I_{sp}$  is desirable when the spacecraft is far from the attracting body and higher fuel efficiency is needed rather than higher thrust.

Fig. 3-5 and Fig. 3-6 are the results for  $R = 500$  and 1,000 DU, respectively, with a 20 MT initial mass and 500 kW jet power. For both cases there is a similar tendency to the  $R = 100$  DU Case. When  $R$  becomes very large, trip time for the high thrust becomes very large too, and high thrust becomes worse for both propellant consumption and trip time. This is because, when  $R$  becomes large, the high thrust trajectory with the minimum propellant mass becomes close to a parabola. The velocity near apoapsis becomes very slow, and therefore it takes quite a long time to get to the target.

The above examples are calculated by equating the propellant mass for CSI and VSI. If trip time, instead of propellant mass, is equated and the results are compared, it is easily guessed that propellant mass for VSI becomes smaller than that for CSI. That means that by

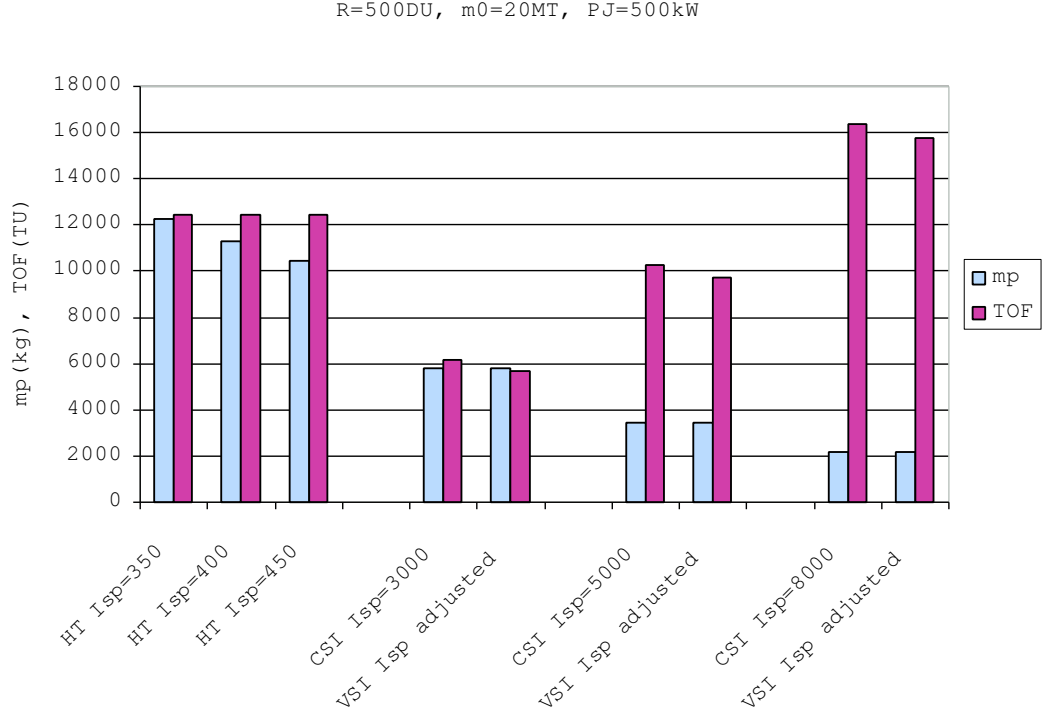


**Figure 3-5:** Results:  $R = 500$  DU,  $m_0 = 20$  MT,  $P_J = 500$  kW.

adjusting trip time and propellant mass, it is possible to make both trip time and propellant mass of VSI shorter and smaller than those of CSI. Therefore, it is concluded that, for this simplified example, modulating thrust and specific impulse lowers either propellant mass or trip time, or possibly both.

Table 3-1 shows the comparison of trip time for low thrust with a different  $I_{sp}$  and a different distance between two attracting bodies,  $R$ . The maximum trip time decrease is about 11% if  $I_{sp}$  is modulated. It is interesting to note that as  $R$  increases the benefit of modulating thrust increases. Considering the trip from Earth to Mars, the closest distance between Earth and Mars is about 0.5AU, or 11,728 DU. According to these results, the benefit of variable thrust should therefore be significant.

Next, instead of comparing by the travel distance, fuel requirements for different values of the initial mass are compared. Fig. 3-7 shows the results for an initial mass of 5 MT,  $R$  of 100 DU, and  $P_J$  of 500 kW, and Fig. 3-8 shows the results for initial mass of 10 MT,  $R$  of 100 DU, and  $P_J$  of 500 kW. These figures show that for all cases, VSI is better than

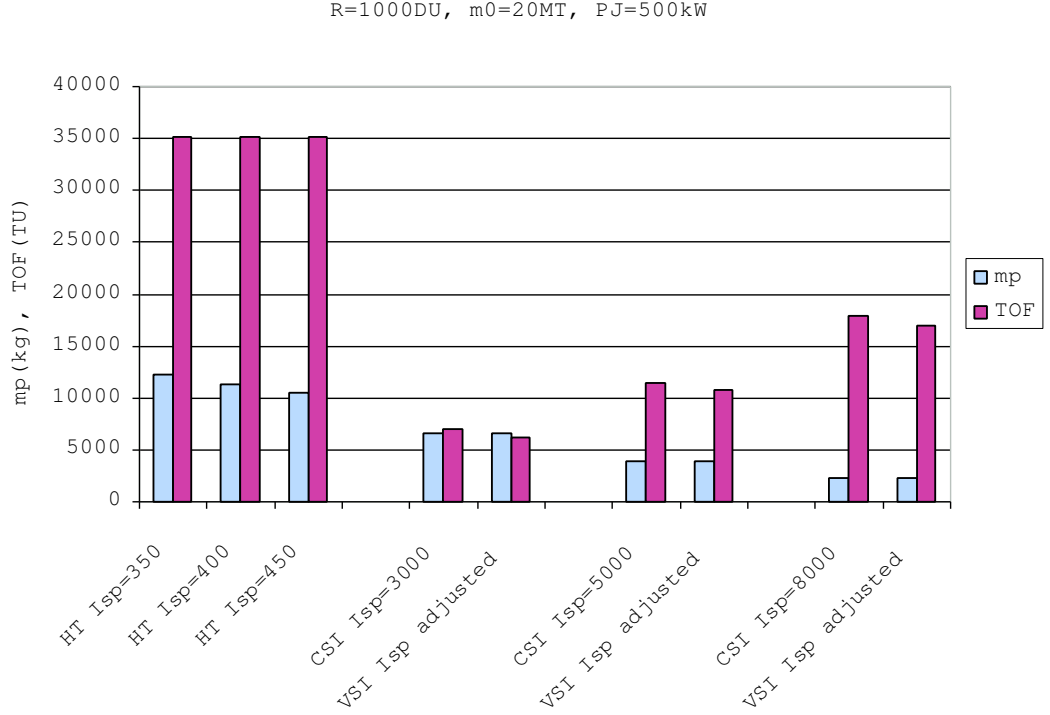


**Figure 3-6:** Results  $R = 1,000$  DU,  $m_0 = 20$  MT,  $P_J = 500$  kW.

CSI. Table 3-2 presents the summary of the trip time savings for each initial mass and each  $I_{sp}$ . As the initial mass decreases, the effect of using VSI over CSI increases. Therefore, in order to use a VSI engine efficiently, having a lighter spacecraft is desirable.

These calculations were based on the equations of motion (Eqn. 2-4) introduced in Sec. 2.3. The magnitude of acceleration is calculated as  $a = T/m$  from Eqn. 2-5, and the relationship between thrust and jet power is  $T = \sqrt{-2\dot{m}P_J}$  (Eqn. 2-8). Hence, halving the mass of the spacecraft doubles the magnitude of acceleration, and quadrupling the jet power also doubles the acceleration. That means that decreasing the spacecraft mass has the same effect as increasing the jet power.

To deal with the effects of the spacecraft mass and the power level on fuel consumption, a parameter  $P/m$ , the power to mass ratio, is introduced. For the same power, smaller mass makes  $P/m$  higher. For the same mass, higher power makes  $P/m$  higher. Therefore, from the above discussions, having a spacecraft with high  $P/m$  is beneficial in reducing the fuel consumption.

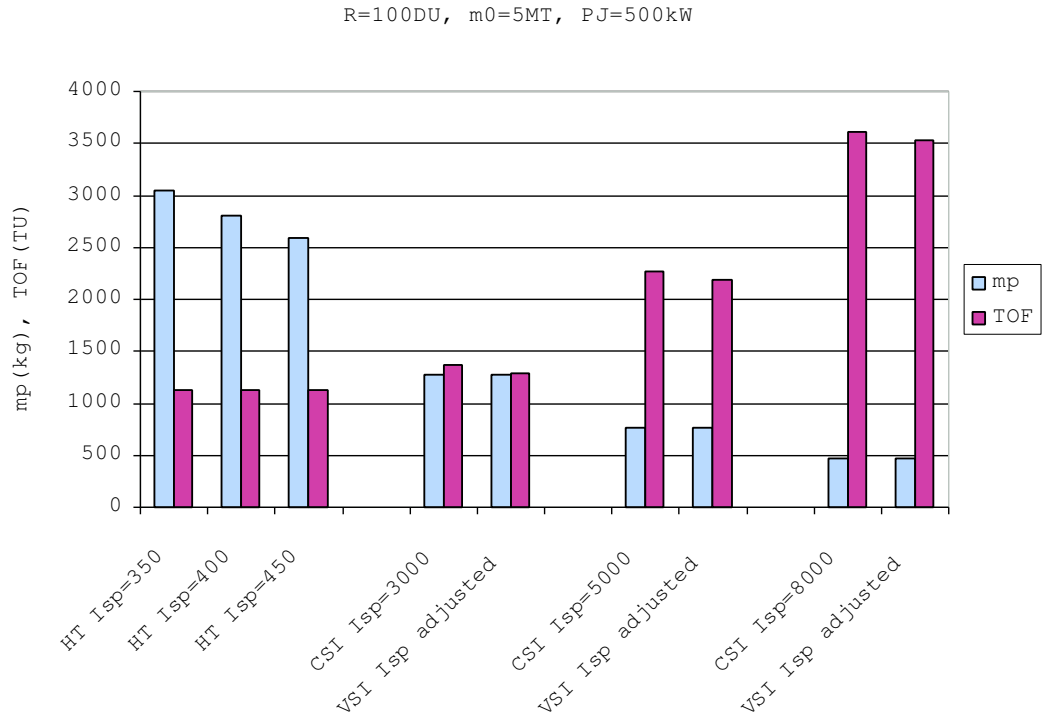


**Figure 3-7:** Results:  $R = 100$  DU,  $m_0 = 5$  MT,  $P_J = 500$  kW.

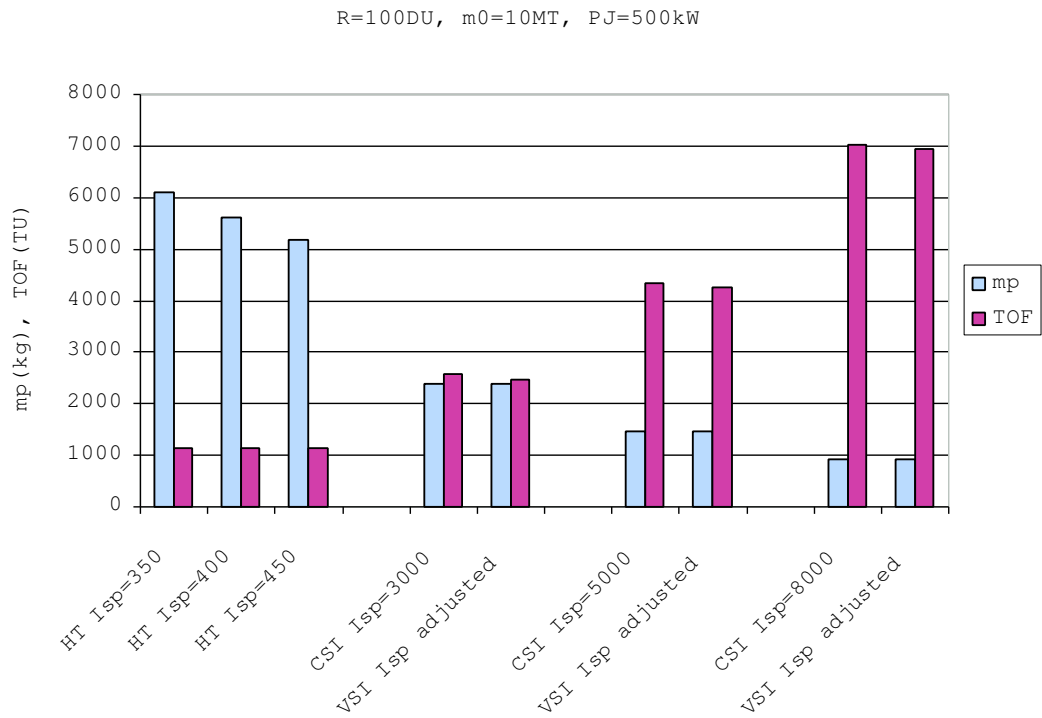


**Figure 3-8:** Results:  $R = 100$  DU,  $m_0 = 10$  MT,  $P_J = 500$  kW.

**Table 3-1:** Trip Time Savings(Comparison by Distance):  $(VSI - CSI)/CSI \times 100$  (%)

	$I_{sp}(\text{sec})$		
R(DU)	3,000	5,000	8,000
100	-2.69	-1.55	-1.20
500	-8.26	-5.08	-3.41
1,000	-11.29	-5.89	-5.25

**Table 3-2:** Trip Time Savings(Comparison by Initial Mass):  $(VSI - CSI)/CSI \times 100$  (%)

	$I_{sp}(\text{sec})$		
$m_0(\text{MT})$	3,000	5,000	8,000
5.0	-5.71	-3.44	-1.94
10.0	-3.74	-2.19	-1.23
20.0	-2.69	-1.55	-1.20

In summary, from the preliminary study conducted in this chapter, these conclusions have been obtained:

- The merit of using a VSI engine increases as the travel distance increases.
- Increasing the power to mass ratio  $P/m$  positively affects using a VSI engine over a CSI engine or a high thrust engine.

In the following chapters, actual interplanetary trajectories are studied and the fuel requirements are investigated. If the above conclusions can be applied to the actual trajectories, using a VSI engine for a transfer from Earth to Jupiter is more effective than from Earth to Mars. Further conclusions are that a lighter, higher-powered spacecraft (higher power to mass ratio) is relatively more desirable for a VSI propulsion system compared to a CSI propulsion system.

## CHAPTER IV

### INTRODUCTION TO OPTIMIZATION PROBLEMS

#### *4.1 Solution Methods for Optimization Problems*

Solution methods for trajectory optimization problems are typically identified as either direct methods or indirect methods. In this section the characteristics of these methods are presented.

Direct methods discretize the optimization problem through events and phases, and the subsequent problem is solved using nonlinear programming techniques[55]. These techniques include shooting, multiple shooting, and transcription or collocation methods. In the shooting method, the control history is discretized as a polynomial, with the trajectory variables as functions of the integrated equations of motion. In the collocation method, the trajectory is discretized over an entire trajectory as a set of polynomials for both state variables and control variables[55]. Solutions obtained with these direct methods are generally considered sub-optimal due to the discretization of either the state or controls, or both[69].

Indirect methods use calculus of variations techniques to characterize the optimization problem as a two-point boundary value problem. The optimal control scheme is an indirect method. The optimal control uses a first variation technique to determine necessary conditions for an optimum, and second variation techniques are used to determine whether the point is the minimum, the maximum, or a saddle point[17]. This method involves applying calculus of variations principles and solving the corresponding two point boundary value problem[51]. Initial estimates of the Lagrange multipliers must be provided, but since they do not have physical meanings, guessing the initial values of the Lagrange multiplier is difficult and may lead to problems with convergence.

There also exist hybrid methods that numerically integrate the Euler-Lagrange equations (and control the spacecraft based on the primer vector). These methods solve a nonlinear

programming problem where the Lagrange multipliers of the indirect method and the relevant mission parameters form part of the parameter vector while extremizing a general scalar cost function[69].

Each of the above methods have pros and cons: indirect methods are difficult to formulate, whereas with direct methods, mathematical suboptimal solutions are obtained. In this research, an indirect method is selected since they calculate an optimal solution rather than a suboptimal solution. The equations of motion used in this research are not very complicated and can be implemented into the application without difficulties. Also, there are several excellent literature available for programming with indirect methods[17][49][69][41][57].

## ***4.2 Indirect Methods – Calculus of Variations***

The calculus of variations is concerned with the problem of minimizing or maximizing functionals, a functional being a quantity whose value depends upon the sets of values taken by certain associated functions over domains of their variables for which they are defined[54]. In this section, some methods to solve different types of optimization problems are described.

### **4.2.1 Problems without Terminal Constraints, Fixed Terminal Time**

Consider the dynamic system is described by the following nonlinear differential equations:

$$\dot{x} = f[x(t), u(t), t], \quad x(t_0) \text{ given}, \quad t_0 \leq t \leq t_f, \quad (4-1)$$

where  $x(t)$ , an  $n$ -vector function, is determined by  $u(t)$ , an  $m$ -vector function. Suppose we wish to choose the history of control variables  $u(t)$  to minimize the performance index  $J$  (scalar) of the form

$$J = \phi[x(t_f), t_f] + \int_{t_0}^{t_f} L[x(t), u(t), t] dt \quad (4-2)$$

where  $\phi[x(t_f), t_f]$  is a scalar function that will be minimized, and  $L[x(t), u(t), t]$  is the Lagrangian. By adjoining the system differential equations Eqn. 4-1 to  $J$  with multiplier



functions  $\lambda(t)$  and modifying it, we get the following equation:

$$\begin{aligned}
\bar{J} &= \phi[x(t_f), t_f] + \int_{t_0}^{t_f} [L[x(t), u(t), t] + \lambda^T(t)f[x(t), u(t), t] - \dot{x}]dt \\
&= \phi[x(t_f), t_f] + \int_{t_0}^{t_f} [L[x(t), u(t), t] + \lambda^T(t)f[x(t), u(t), t]]dt - \int_{t_0}^{t_f} \lambda^T \dot{x}dt \\
&= \phi[x(t_f), t_f] + \int_{t_0}^{t_f} H[x(t), u(t), t]dt - \int_{t_0}^{t_f} \lambda^T \dot{x}dt \\
&= \phi[x(t_f), t_f] + \int_{t_0}^{t_f} H[x(t), u(t), t]dt - [\lambda^T x]_{t_0}^{t_f} + \int_{t_0}^{t_f} \dot{\lambda}^T xdt \\
&= \phi[x(t_f), t_f] + \int_{t_0}^{t_f} \{H[x(t), u(t), t] + \dot{\lambda}^T x\}dt + \lambda^T(t_0)x(t_0) - \lambda^T(t_f)x(t_f) \quad (4-3)
\end{aligned}$$

where  $H$  is the Hamiltonian

$$H[x(t), u(t), t] = L[x(t), u(t), t] + \lambda^T(t)f[x(t), u(t), t]. \quad (4-4)$$

Now consider the variation in  $\bar{J}$  due to variations in  $u(t)$  for fixed times  $t_0$  and  $t_f$ ,

$$\delta\bar{J} = \left[ \left( \frac{\partial\phi}{\partial x} - \lambda^T \right) \delta x \right]_{t=t_f} + [\lambda^T \delta x]_{t=t_0} + \int_{t_0}^{t_f} \left[ \left( \frac{\partial H}{\partial x} + \dot{\lambda}^T \right) \delta x + \frac{\partial H}{\partial u} \delta u \right] dt. \quad (4-5)$$

At a stationary point  $\delta\bar{J} = 0$ , so we should choose multipliers and variables of this equation so that  $\delta\bar{J}$  becomes zero. If the multiplier  $\lambda(t)$  is chosen

$$\lambda^T(t_f) = \frac{\partial\phi}{\partial x(t_f)} \quad (4-6)$$

$$\dot{\lambda}^T(t) = -\frac{\partial H}{\partial x} = -\frac{\partial L}{\partial x} - \lambda^T \frac{\partial f}{\partial x}, \quad (4-7)$$

Eqn. 4-5 becomes

$$\delta\bar{J} = \lambda^T(t_0)\delta x(t_0) + \int_{t_0}^{t_f} \frac{\partial H}{\partial u} \delta u dt. \quad (4-8)$$

When  $x(t_0)$  is given,  $\delta x(t_0) = 0$ . Therefore for an extremum,  $\delta\bar{J}$  must be zero for arbitrary  $\delta u(t)$ , and this can only happen if

$$\frac{\partial H}{\partial u} = \frac{\partial L}{\partial u} + \lambda^T \frac{\partial f}{\partial u} = 0, \quad t_0 \leq t \leq t_f. \quad (4-9)$$

Therefore, to find a control variables  $u(t)$  that produces the stationary value of  $J$ , differential equations 4-1 and 4-7 should be solved with boundary conditions 4-6 with  $x(t_0)$  given, then  $u(t)$  is determined by Eqn. 4-9. Note that for any state  $x$ , the associate costate  $\lambda_x$

evaluated at time  $t$  represents the sensitivity of the optimum  $J$  (denoted  $J^*$ ) with respect to perturbations in the state  $x$  at time  $t$ , i.e.

$$\lambda_x = \frac{\partial J^*}{\partial x(t)} \quad (4-10)$$

#### 4.2.2 Some State Variables Specified at a Fixed Terminal Time

If  $x_i$ , the  $i$ -th component of the state vector  $x$ , is prescribed at terminal time  $t_f$ ,  $\delta x_i$  at  $t_f$  is zero. Then the first term of Eqn. 4-5 vanishes. Also, if all of  $n$  components of  $x$  are given at initial time  $t_i$ , then the second term of this equation also vanishes because  $\delta x_i(t_i) = 0$ . Suppose that  $q$  components of  $x$  are prescribed at  $t_f$ , then  $\phi = \phi[x_{q+1}, \dots, x_n]_{t_f}$ . Then using a  $n$ -component vector  $p$ , Eqn. 4-8 becomes

$$\delta J = \int_{t_0}^{t_f} \left[ \frac{\partial L}{\partial u} + p^T \frac{\partial f}{\partial u} \right] \delta u dt \quad (4-11)$$

where

$$\dot{p} = - \left( \frac{\partial f}{\partial x} \right)^T p - \left( \frac{\partial L}{\partial x} \right)^T \quad (4-12)$$

$$p_j(t_f) = \begin{cases} 0, & j = 1, \dots, q \\ (\partial \phi / \partial x_j)|_{t=t_f}, & j = q+1, \dots, n. \end{cases} \quad (4-13)$$

These equations determine the influence functions  $p$  for the performance index.

Next, suppose a performance index  $J = x_i(t_f)$ , the  $i$ -th component of the state vector at the final time. This will make influence functions for  $x_i(t_f)$  by substituting  $\phi = x_i(t_f)$  and  $L = 0$  in Eqn. 4-11. Then by expressing the influence functions in the  $n \times q$  matrix form  $R$ , Eqns. 4-11, 4-12, and 4-13 become

$$\delta x_i(t_f) = \int_{t_0}^{t_f} R_i^T \frac{\partial f}{\partial u} \delta u dt, \quad i = 1, \dots, q \quad (4-14)$$

where

$$\dot{R}_i = - \left( \frac{\partial f}{\partial x} \right)^T R_i \quad (4-15)$$

$$R_{ij}(t_f) = \begin{cases} 0, & i \neq j \\ 1, & i = j, \quad j = 1, \dots, n, \end{cases} \quad (4-16)$$

where  $R_i$  are components of  $i$ -th column of matrix  $R$ .

Now, we can construct a  $\delta u(t)$  history that decreases  $J$ .  $\delta u(t)$  should be made so that it produces  $\delta J < 0$  and satisfies the  $q$  terminal constraints  $\delta x_i(t_f) = 0$ . To do this, adjoint  $q$  equations of Eqn. 4-14 and Eqn. 4-11 using an constant  $\nu_i$ .

$$\delta J + \sum_{i=1}^q \nu_i \delta x_i(t_f) = \int_{t_0}^{t_f} \left\{ \frac{\partial L}{\partial u} + [p + \nu R]^T \frac{\partial f}{\partial u} \right\} \delta u dt. \quad (4-17)$$

If we choose, with a positive scalar constant  $k$ ,

$$\delta u = -k \left\{ \frac{\partial L}{\partial u} + [p + \nu_i R_i]^T \frac{\partial f}{\partial u} \right\} \quad (4-18)$$

and substitute this into Eqn. 4-17,

$$\delta J + \nu_i \delta x_i(t_f) = -k \int_{t_0}^{t_f} \left\| \frac{\partial L}{\partial u} + [p + \nu_i R_i]^T \frac{\partial f}{\partial u} \right\|^2 dt < 0, \quad (4-19)$$

which is negative unless the integrand vanishes. Therefore, if we can determine  $\nu_i$  so that it satisfies the terminal constraints ( $\delta x_i(t_f) = 0$ ), the performance index decreases with  $\delta u$  of Eqn. 4-18. Substituting Eqn. 4-18 into Eqn. 4-14,

$$0 = \delta x(t_f) = -k \int_{t_0}^{t_f} R^T \frac{\partial f}{\partial u} \left[ \left( \frac{\partial f}{\partial u} \right)^T [p + \nu R] + \left( \frac{\partial L}{\partial u} \right)^T \right] dt \quad (4-20)$$

$$0 = \int_{t_0}^{t_f} R^T \frac{\partial f}{\partial u} \left[ \left( \frac{\partial f}{\partial u} \right)^T p + \left( \frac{\partial L}{\partial u} \right)^T \right] dt + \nu \int_{t_0}^{t_f} R^T \left( \frac{\partial f}{\partial u} \right) \left( \frac{\partial f}{\partial u} \right)^T R dt, \quad (4-21)$$

from which the appropriate choice of the  $\nu_i$ 's is

$$\nu = -Q^{-1}g, \quad (4-22)$$

where  $Q$  is a  $(q \times q)$  matrix and  $g$  is a  $q$ -component vector:

$$Q_{ij} = \int_{t_0}^{t_f} R^T \left( \frac{\partial f}{\partial u} \right) \left( \frac{\partial f}{\partial u} \right)^T R dt, \quad i, j = 1, \dots, q, \quad (4-23)$$

$$g_i = \int_{t_0}^{t_f} R^T \frac{\partial f}{\partial u} \left[ \left( \frac{\partial f}{\partial u} \right)^T p + \left( \frac{\partial L}{\partial u} \right)^T \right] dt, \quad i = 1, \dots, q. \quad (4-24)$$

Thus, a  $\delta u(t)$  history that minimizes the performance index has been constructed.

If the terminal state is prescribed as a form of functions

$$\psi[x(t_f), t_f] = 0 \quad q \text{ equations}, \quad (4-25)$$

the performance index can be written with a multiplier vector  $\nu$  (a  $q$  vector) as follows.

$$J = \phi[x(t_f), t_f] + \nu^T \psi[x(t_f), t_f] + \int_{t_0}^{t_f} L[x(t), u(t), t] dt. \quad (4-26)$$

If we define a scalar function  $\Phi = \phi + \nu^T \psi$ , the development above can be applied without change. Then necessary conditions for  $J$  to have a stationary value are

$$\dot{x} = f(x(t), u(t), t) \quad (4-27)$$

$$\dot{\lambda} = -\frac{\partial f^T}{\partial x} \lambda - \frac{\partial L^T}{\partial x} \quad (4-28)$$

$$\frac{\partial H^T}{\partial u} = \frac{\partial f^T}{\partial u} \lambda + \frac{\partial L^T}{\partial u} = 0 \quad (4-29)$$

$$\lambda^T(t_f) = \left( \frac{\partial \phi}{\partial x} + \nu^T \frac{\partial \psi}{\partial x} \right)_{t=t_f} \quad (4-30)$$

$$\psi[x(t_f), t_f] = 0 \quad (4-31)$$

$$x(t_0) \quad \text{given.} \quad (4-32)$$

### 4.2.3 Inequality Constraints on the Control Variables

Suppose that we have an inequality constraint on the system:

$$C(u(t), t) \leq 0. \quad (4-33)$$

where  $u(t)$  is the  $m$ -component control vector,  $m \geq 2$ , and  $C$  is a scalar function. For example, when we would like to limit the  $I_{sp}$  level less than or equal to 30,000m/s,  $C$  is expressed as  $C = I_{sp} - 30,000 \leq 0$ .

If we define the Hamiltonian with a Lagrange multiplier  $\mu(t)$

$$H = \lambda^T f + L + \mu^T C, \quad (4-34)$$

the necessary condition on  $H$  is

$$H_u = \lambda^T f_u + L_u + \mu^T C_u = 0 \quad (4-35)$$

$$\text{and } \mu \begin{cases} \geq 0, & C = 0, \\ = 0, & C < 0. \end{cases} \quad (4-36)$$

The positivity of the multiplier  $\mu$  when  $C = 0$  is interpreted as the requirement that the gradient of original Hamiltonian ( $\lambda^T f_u + L_u$ ) be such that improvement can only come by violating the constraints.

The differential equations for costate vectors are

$$\dot{\lambda}^T(t) = -\frac{\partial H}{\partial x} = -\frac{\partial L}{\partial x} - \lambda^T \frac{\partial f}{\partial x} - \mu^T C_x = -\frac{\partial L}{\partial x} - \lambda^T \frac{\partial f}{\partial x}. \quad (4-37)$$

Therefore to calculate costate vectors we can use Eqn. 4-7 because  $C$  is not a function of  $x$ . Boundary conditions should be chosen so that the initial and terminal constraints for state variables are satisfied.

#### 4.2.4 Bang-off-bang Control

This type of control is applied to the fixed-time, minimum-fuel problem with constrained input magnitude. For example, a CSI rocket that can turn its engine on/off as needed would obey this control law.

Consider the problem with the following linear system[57].

$$\dot{x} = Ax + Bu \quad (4-38)$$

Assume that the fuel used in each component of the input is proportional to the magnitude of that component. Then the cost function to be minimized is

$$J(t_0) = \int_{t_i}^{t_f} \sum_{i=1}^m c_i |u_i(t)| dt, \quad (4-39)$$

where  $c_i$  is a component of a  $m$  vector  $C = [c_1 \ c_2 \ \cdots \ c_m]^T$  and  $u_i(t)$  is a component of a  $m$  vector  $|u(t)| = [|u_1| \ |u_2| \ \cdots \ |u_m|]^T$ .

Suppose that the control is constrained as

$$|u(t)| \leq 1 \quad t_i \leq t \leq t_f. \quad (4-40)$$

The Hamiltonian is

$$H = C^T |u| + \lambda^T (Ax + Bu) \quad (4-41)$$

and according to the Pontryagin's minimum principle, the optimal control must satisfy

$$C^T |u^*| + (\lambda^*)^T (Ax^* + Bu^*) \leq C^T |u| + (\lambda^*)^T (Ax^* + Bu) \quad (4-42)$$

for all admissible  $u(t)$ .  $(*)$  denotes optimal quantities. This equation can be reduced to

$$C^T |u^*| + (\lambda^*)^T Bu^* \leq C^T |u| + (\lambda^*)^T Bu \quad (4-43)$$

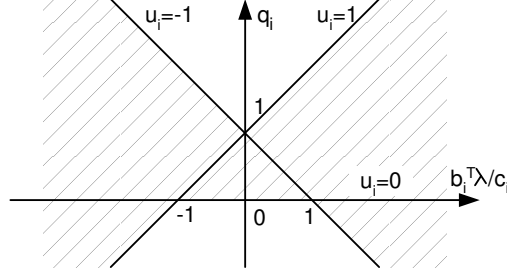


**Figure 4-1:** Bang-off-bang Control: Choosing Control to Minimize  $q_i$ .

If we assume that all of the  $m$  components of the control variables are independent,

$$|u_i^*| + \frac{(\lambda^*)^T b_i u_i^*}{c_i} \leq |u_i| + \frac{(\lambda^*)^T b_i u_i}{c_i}, \quad (4-44)$$

where  $b_i$  are the columns of  $B$ . Since

$$|u_i| = \begin{cases} u_i, & u_i \geq 0 \\ -u_i, & u_i \leq 0 \end{cases} \quad (4-45)$$

we can write the quantity we are trying to minimize by selection of  $u_i(t)$  as

$$q_i(t) = |u_i| + \frac{b_i^T \lambda u_i}{c_i} = \begin{cases} (1 + b_i^T \lambda / c_i) |u_i|, & u_i \geq 0 \\ (1 - b_i^T \lambda / c_i) |u_i|, & u_i \leq 0 \end{cases} \quad (4-46)$$

Fig.4-1 shows the relationship between  $q_i$  and  $b_i^T \lambda u_i$  for  $u_i = 1, u_i = 0$ , and  $u_i = -1$ , and when  $-1 < u_i(t) < 1$ ,  $q_i(t)$  takes on values inside the shaded area. Therefore, if we neglect the singular points ( $b_i^T \lambda / c_i = 1$  or  $-1$ ), the control can be expressed as

$$u_i(t) = \begin{cases} 1, & b_i^T \lambda / c_i < -1 \\ 0, & -1 < b_i^T \lambda / c_i < 1 \\ -1, & 1 < b_i^T \lambda / c_i. \end{cases} \quad (4-47)$$

This is called a bang-off-bang control law.

## CHAPTER V

### OPTIMIZATION OF INTERPLANETARY TRAJECTORY

#### *5.1 Assumptions*

Consider a spacecraft travelling from one planet to another. The spacecraft, leaving from the departure planet, must control its thrust direction to reach the target planet. In addition to the thrust direction, a VSI engine should control its thrust magnitude, and a CSI engine that is capable of turning the engine on/off should control the switching times.

Normally, a spacecraft launched from the ground with a launch vehicle takes either one of the following steps.

- If the launch vehicle is not powerful enough or the spacecraft needs docking or other on-orbit operations, the spacecraft is placed in Earth orbit at first, and then it boosts to escape the Earth's gravity well.
- If the launch vehicle has enough power to send the spacecraft out of the Earth's gravity well, the spacecraft flies directly to the target.

In either case, at first the spacecraft's motion is affected by the Earth's gravitational force. Then as the spacecraft goes farther away from Earth, the gravitational force from the Earth becomes smaller and the force from the Sun becomes dominant.

In actual missions, while the spacecraft is travelling from one planet to another, it is subject to various forces including its own thrust, a gravitational force from the Sun, and gravitational forces from all the planets and satellites, and other planetary bodies. However, most of those forces are very small compared to the forces from the Sun or nearby planets, and therefore most of the forces can be neglected. For example, a gravitational force from Pluto affecting a spacecraft travelling from Earth to Mars is too small and it can be neglected.

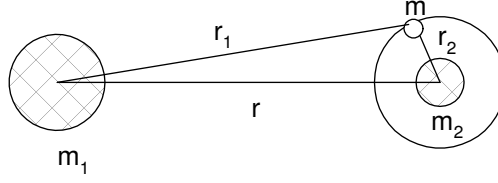


**Figure 5-1:** Sphere of Influence of  $m_2$  with respect to  $m_1$ .

When analyzing a low-thrust interplanetary trajectory, an approximation technique similar to the patched conic concept[37] for high-thrust trajectory is often used. An entire trajectory is divided into several phases and they are analyzed separately so that a spacecraft is only subject to one gravitational force from one attracting body. The endpoint conditions of each part of trajectory come from the endpoint conditions of other parts, and after completing the calculation of each part, the results are combined together. This is to avoid solving complex multi-body problems. For example, with a Mars mission the first phase will be a geocentric trajectory as the spacecraft escapes from the Earth's gravitational attraction. The second phase will be a heliocentric trajectory for the transfer from Earth's orbit to Mars, and the third phase will be an approach trajectory with Mars as the attracting force. In this case there will be two patches and at each patch the velocity is calculated with the concept of the “*sphere of influence*[37].”

**The Sphere of Influence** Suppose a spacecraft with mass  $m$  is travelling in a gravitational field formed by a larger body (usually the Sun) with mass  $m_1$  and a smaller body (a planet) with mass  $m_2$  as shown in Fig. 5-1. The force exerted by  $m_2$  on  $m$  is

$$F_{m,m_2} = \frac{-G m m_2}{r_2^2} \quad (5-1)$$

where  $r_2$  is the distance between the spacecraft and the mass  $m_2$ . Similarly the force exerted by  $m_1$  on  $m$  is

$$F_{m,m_1} = \frac{-G m m_1}{r_1^2} \quad (5-2)$$

where  $r_1$  is the distance between the spacecraft and the mass  $m_1$ . Then the ratio of the forces is

$$\frac{F_{m_2}}{F_{m_1}} = \left( \frac{r_1}{r_2} \right)^2 \frac{m_2}{m_1} \quad (5-3)$$



The sphere of influence (or SOI) is defined as the region in which the force exerted by the smaller mass,  $m_2$ , is much greater than that exerted on  $m$  by  $m_1$ , we can think of the edge of the SOI at  $r_2$  as being established when the ratio of the forces is approximately a tenth ( $F_{m_1}/F_{m_2} \cong 0.1$ ). The approximate expression for the radius of the SOI is then

$$r_2 \approx r \left( \frac{10m_2}{m_1} \right)^{0.5} \quad (5-4)$$

where  $r$  is the distance between mass  $m_1$  and mass  $m_2$ . Usually the radius of the SOI is expressed in the following empirical manner:

$$r_{SOI} = r \left( \frac{m_2}{m_1} \right)^{0.4} \quad (5-5)$$

For example, the radius of the SOI for the Earth with respect to the Sun can be calculated as 0.00618 AU or 924,500 km using Eqn. 5-5.

Suppose that, a spacecraft is launched and when it reaches the edge of the SOI and it has a velocity  $\mathbf{V}_{sc}^E$  with respect to Earth, whose velocity is  $\mathbf{V}_E^{Sun}$  with respect to the Sun. Then the spacecraft's velocity with respect to the Sun at this moment is

$$\mathbf{V}_{sc}^{Sun} = \mathbf{V}_E^{Sun} + R[E \rightarrow Sun] \mathbf{V}_{sc}^E \quad (5-6)$$

where  $R[E \rightarrow Sun]$  is a transformation matrix from the Earth-centered coordinates to the heliocentric coordinates. The spacecraft velocity with respect to Earth at the SOI,  $\mathbf{V}_{sc}^E$ , is often written as  $\mathbf{V}_\infty$ .

In this research, instead of calculating  $\mathbf{V}_\infty$  by integrating the equations of motions inside the sphere of influence, the planet's gravity is ignored, and a parameter  $C_3$  is used. This is the square of  $V_\infty$  ( $\sqrt{C_3} = V_\infty$ ) and expresses the twice of the kinetic energy of the spacecraft per unit mass ( $\text{km}^2/\text{s}^2$ ) at the edge of the SOI. This  $C_3$  value is often given as a launch vehicle parameter, and  $\mathbf{V}_\infty$  is calculated with this value. Then the initial velocity of the spacecraft with respect to the Sun is calculated with Eqn. 5-6. And even if the magnitude of  $C_3$  is the same for two missions, the velocity of the spacecraft with respect to the Sun may be different because the direction of the motion of the spacecraft at the edge of the SOI may be different.

As for the position of the spacecraft with respect to the Sun when it is the edge of the Earth's SOI, another approximation is usually taken by assuming that the spacecraft is at the center of the Earth. As shown above, the radius of the SOI for the Earth is 0.00618AU, the error induced by this approximation is considered to be small enough to be neglected.

The same discussion is applied to the arrival planet. Final velocity at the arrival planet is calculated by the predetermined  $C_3$  value. The final position is set to be the center of the arrival planet at the moment. Of course in real life the spacecraft may circularize around the planet and/or land on the ground after complicated operations, but these schemes are not dealt with this research.

Therefore, in this research, the planetocentric phases are neglected and only interplanetary trajectories are considered. That means that the spacecraft is first placed in the position where the Earth's center exists, and its velocity is calculated by the  $C_3$  and the velocity of the Earth. The spacecraft departs from the Earth's position without gravitational pull from Earth as if there is no Earth.

We should be careful when neglecting planetocentric phases. When using low thrust propulsion systems, it may take a long time and require some amount of fuel to escape from the departure planet's gravity well. Time and fuel may also be required for orbital insertion at the arrival planet. The time of flight in this research does not include these times of flight for spiral-in and spiral-out phases. The fuel requirements are also neglected for these phases.

The spacecraft controls in-plane thrust angle and the out-of-plane thrust angle to reach the target planet. For a VSI engine, thrust magnitude is also a control variable in addition to thrust direction. At the end of the mission, the target position is the center of the planet, and the final velocity is calculated from  $C_3$  at the target planet and the velocity of the target planet with respect to the Sun.

Another approximation used in this research is that the spacecraft is assumed to be a point mass ejecting fuel from it to gain thrust. There is no attitude control problem, and the thrust direction is assumed to be able to turn instantaneously.

With those approximations and assumptions stated above, for a given time of flight, the fuel consumption is calculated for each type of engine and for each mission.

To express the state of the spacecraft,  $x$ ,  $y$ ,  $z$  components of position and velocity vectors in the Cartesian coordinates are used.

$$\dot{x} = u \quad (5-7)$$

$$\dot{y} = v \quad (5-8)$$

$$\dot{z} = w \quad (5-9)$$

$$\dot{u} = -\frac{\mu x}{r^3} + \frac{T_x}{m} \quad (5-10)$$

$$\dot{v} = -\frac{\mu y}{r^3} + \frac{T_y}{m} \quad (5-11)$$

$$\dot{w} = -\frac{\mu z}{r^3} + \frac{T_z}{m} \quad (5-12)$$

where  $\mu$  is the gravitational constant,  $r = (x^2 + y^2 + z^2)^{1/2}$ ;  $T_x$ ,  $T_y$ , and  $T_z$  are the components of the thrust;  $m$  is the mass of the spacecraft at the moment.

The merit of using this set of state variables are that these can be used for any type of trajectory (elliptic, parabolic, or hyperbolic).

There are some other sets of variables that express the state of the spacecraft such as the six classical orbital elements (the semi-major axis  $a$ , the eccentricity  $e$ , the inclination  $i$ , the longitude of ascending node  $\Omega$ , the argument of periapsis  $\omega$ , and the mean anomaly  $M$ ) or equinoctial orbital elements ( $a = a$ ,  $h = e \sin(\omega + \Omega)$ ,  $k = e \cos(\omega + \Omega)$ ,  $p = \tan(i/2) \sin \Omega$ ,  $q = \tan(i/2) \cos \Omega$ , and  $L = \nu + \omega + \Omega$ )[13]. The equations of motion with the classical orbital elements can not be used for a trajectory if the inclination is zero or 180 degrees. The equations with the equinoctial orbital elements can be used only when the eccentricity is less than one.

In this research, a trajectory with its inclination of zero or 180 degrees may be met with, so the six classical orbital elements are not desirable. Also, because there is a possibility for a trajectory to become hyperbolic, equinoctial orbital elements cannot be used. Therefore in this research, position and velocity vectors in the Cartesian coordinates are used to express the equations of motion of the spacecraft.

## 5.2 Equations of Motion for Low Thrust Trajectories

From rocket propulsion fundamentals and using Newton's law for a variable mass body, the equation of motion of a spacecraft is

$$m\ddot{\vec{r}} = \dot{m}\vec{c} + m\vec{g} \quad (5-13)$$

where  $\vec{r}$  is the vehicle position vector,  $\vec{g}$  is the acceleration of gravity,  $\vec{c}$  is the exhaust velocity, and  $\dot{m}$  is mass flow rate.

This equation of motion is expressed by a set of differential equations for a position vector  $\vec{r} = [x \ y \ z]^T$  and a velocity vector  $\vec{V} = [u \ v \ w]^T$ . The spacecraft's mass is also obtained by a differential equation for mass  $m$ .

$$f = \begin{bmatrix} \dot{\vec{r}} \\ \dot{\vec{V}} \\ \dot{m} \end{bmatrix} = \begin{bmatrix} \vec{V} \\ -\mu\vec{r}/r^3 + \vec{T}/m \\ -T^2/2P_J \end{bmatrix} \quad (5-14)$$

In this research, the expression for the thrust vector  $\vec{T} = [T_x \ T_y \ T_z]^T$  differs depending on the problem so that each problem is solved most effectively.

### 5.2.1 VSI – No Constraints on $I_{sp}$

For this problem, control variables are the same as the components of the thrust vector.

$$\vec{u} = \begin{bmatrix} u_0 \\ u_1 \\ u_2 \end{bmatrix} = \begin{bmatrix} T_x \\ T_y \\ T_z \end{bmatrix} \quad (5-15)$$

Then the equations of motion are

$$f = \begin{bmatrix} \dot{x} \\ \dot{y} \\ \dot{z} \\ \dot{u} \\ \dot{v} \\ \dot{w} \\ \dot{m} \end{bmatrix} = \begin{bmatrix} u \\ v \\ w \\ -\mu x/r^3 + T_x/m \\ -\mu y/r^3 + T_y/m \\ -\mu z/r^3 + T_z/m \\ -(T_x^2 + T_y^2 + T_z^2)/2P_J \end{bmatrix} \quad (5-16)$$

This type of problem can be solved with the method explained in 4.2.2.

### 5.2.2 VSI – Inequality Constraints on $I_{sp}$

For this type of problem, we use the following control variables:

$$\vec{u} = \begin{bmatrix} u_0 \\ u_1 \\ u_2 \\ u_3 \end{bmatrix} = \begin{bmatrix} l_x \\ l_y \\ l_z \\ T \end{bmatrix} \quad (5-17)$$

where  $T$  is the magnitude of thrust,  $l_x, l_y, l_z$  are the direction cosines of the direction of thrust in the inertial frame, and are subject to  $l_x^2 + l_y^2 + l_z^2 = 1$ . Then the equations of motion are

$$f = \begin{bmatrix} \dot{\vec{r}} \\ \dot{\vec{V}} \\ \dot{m} \end{bmatrix} = \begin{bmatrix} \vec{V} \\ -\mu\vec{r}/r^3 + \vec{l}T/m \\ -T^2/2P_J \end{bmatrix} \quad (5-18)$$

The Hamiltonian of this system is

$$\begin{aligned} H &= \vec{\lambda}_r \cdot \vec{V} - \frac{\mu}{r^3} \vec{\lambda}_V \cdot \vec{r} + \vec{l} \cdot \vec{\lambda}_V T/m - \lambda_m T^2/2P_J \\ &= \vec{\lambda}_r \cdot \vec{V} - \frac{\mu}{r^3} \vec{\lambda}_V \cdot \vec{r} - \frac{\lambda_m}{2P_J} \left( T - \frac{\vec{l} \cdot \vec{\lambda}_V P_J}{m\lambda_m} \right)^2 + \frac{(\vec{l} \cdot \vec{\lambda}_V)^2 P_J}{2m^2 \lambda_m}. \end{aligned} \quad (5-19)$$

According to the Pontryagin's maximum principle, the thrust vector must be selected in such a manner so as to maximize  $H$  at each instant of time. Therefore, we choose  $\vec{l}$  parallel to  $\vec{\lambda}_V$ . Then  $\vec{l}$  and  $T$  are expressed as

$$\vec{l} = \begin{bmatrix} l_x & l_y & l_z \end{bmatrix}^T = \vec{\lambda}_V / \lambda_V, \quad \vec{\lambda}_V = \begin{bmatrix} \lambda_u & \lambda_v & \lambda_w \end{bmatrix}^T \quad (5-20)$$

$$T = \frac{P_J \lambda_V}{m \lambda_m} \quad (5-21)$$

The vector  $\vec{l}$  is called the primer vector [54]. The equations of motion and the control

vector are

$$f = \begin{bmatrix} \dot{x} \\ \dot{y} \\ \dot{z} \\ \dot{u} \\ \dot{v} \\ \dot{w} \\ \dot{m} \end{bmatrix} = \begin{bmatrix} u \\ v \\ w \\ -\mu x/r^3 + l_x T/m \\ -\mu y/r^3 + l_y T/m \\ -\mu z/r^3 + l_z T/m \\ -T^2/2P_J \end{bmatrix}, \quad \vec{u} = \begin{bmatrix} u_0 \\ u_1 \\ u_2 \\ u_3 \end{bmatrix} = \begin{bmatrix} l_x \\ l_y \\ l_z \\ T \end{bmatrix}. \quad (5-22)$$

Therefore, solving this type of problem is the same as finding the Lagrange multipliers.

### 5.2.3 CSI – Continuous Thrust

For continuous thrust, the propellant mass is proportional to the time of flight. That means that for a fixed time of flight the propellant mass does not change. The problems dealt in this research are fixed time problems, so the propellant mass cannot be used as the performance index. For this type of problem, the following performance index is used:

$$J = [u(t_f) - u_{target}]^2 + [v(t_f) - v_{target}]^2 + [w(t_f) - w_{target}]^2 \quad (5-23)$$

and the terminal constraints are

$$\psi = \begin{bmatrix} x(t_f) - x_{target} \\ y(t_f) - y_{target} \\ z(t_f) - z_{target} \end{bmatrix} = 0. \quad (5-24)$$

Because the thrust magnitude is fixed, there are two control variables.

$$\vec{u} = \begin{bmatrix} u_0 \\ u_1 \end{bmatrix} = \begin{bmatrix} \theta \\ \phi \end{bmatrix} \quad (5-25)$$

where  $\theta$  and  $\phi$  are in-plane thrust angle and out-of-plane thrust angle in the inertial frame as shown in Fig. 5-2.

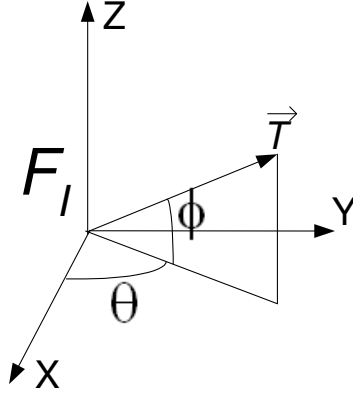


**Figure 5-2:** In-plane Thrust Angle  $\theta$  and Out-of-plane Thrust Angle  $\phi$  in Inertial Frame.

Then the equations of motion are

$$f = \begin{bmatrix} \dot{x} \\ \dot{y} \\ \dot{z} \\ \dot{u} \\ \dot{v} \\ \dot{w} \\ \dot{m} \end{bmatrix} = \begin{bmatrix} u \\ v \\ w \\ -\mu x/r^3 + T \cos \theta \cos \phi/m \\ -\mu y/r^3 + T \sin \theta \cos \phi/m \\ -\mu z/r^3 + T \sin \phi/m \\ -T^2/2P_J \end{bmatrix}. \quad (5-26)$$

#### 5.2.4 CSI – Bang-Off-Bang Control

For this type of problem, the thrust level is restricted so that it can take either the maximum value( $T_{max}$ ) or the minimum value(0).

Because  $T = 2P_J/c$ , the Hamiltonian can be expressed as follows using the primer vector.

$$\begin{aligned} H &= \vec{\lambda}_r \cdot \vec{V} - \frac{\mu}{r^3} \vec{\lambda}_V \cdot \vec{r} + T \left( \vec{l} \cdot \vec{\lambda}_V/m - \lambda_m/c \right) \\ &= \vec{\lambda}_r \cdot \vec{V} - \frac{\mu}{r^3} \vec{\lambda}_V \cdot \vec{r} + T S \end{aligned} \quad (5-27)$$

where  $S$  is the switching function

$$S = \vec{l} \cdot \vec{\lambda}_V/m - \lambda_m/c \quad (5-28)$$

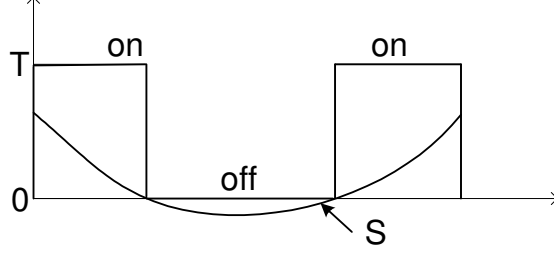


**Figure 5-3:** Switching Function and Switching Times for Bang-Off-Bang.

To maximize the Hamiltonian, we choose the thrust level according to the switching function.

$$\begin{cases} \text{when } S > 0, T = T_{max} \\ \text{when } S < 0, T = 0 \end{cases} \quad (5-29)$$

The equations of motion and the control vector are the same as the VSI constrained case.

$$f = \begin{bmatrix} \dot{x} \\ \dot{y} \\ \dot{z} \\ \dot{u} \\ \dot{v} \\ \dot{w} \\ \dot{m} \end{bmatrix} = \begin{bmatrix} u \\ v \\ w \\ -\mu x/r^3 + l_x T/m \\ -\mu y/r^3 + l_y T/m \\ -\mu z/r^3 + l_z T/m \\ -T^2/2P_J \end{bmatrix}, \quad \vec{u} = \begin{bmatrix} u_0 \\ u_1 \\ u_2 \\ u_3 \end{bmatrix} = \begin{bmatrix} l_x \\ l_y \\ l_z \\ T \end{bmatrix} \quad (5-30)$$

### 5.3 Solving the High Thrust Trajectory

When a high thrust propulsion system (mostly chemical) is used, usually burn time is very short compared to the entire mission duration. At the beginning of the mission the spacecraft fires an engine to accelerate to gain enough velocity to reach the target planet, and once it reaches near the target planet, it burns again for such as an orbital insertion or a landing. This burn process can be simulated with two instantaneous burns at the beginning and at the ending, and the rest of the time the spacecraft is assumed to obey Newton's law. Therefore a high thrust trajectory can be solved without integrating the equations of motion once we know the positions of departure and arrival planets. Gauss



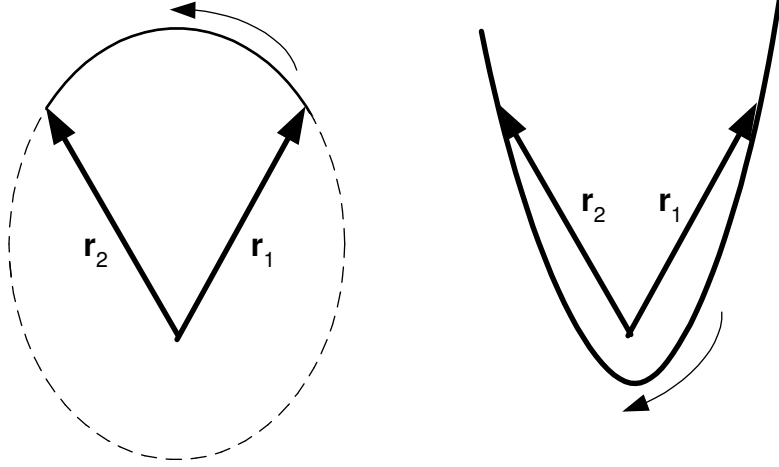


**Figure 5-4:** Gauss Problem: Direction of Motion for the Same Vectors and the Same Time of Flight.

problem (or Lambert's problem) solves such a trajectory.

**Gauss Problem[12]** The Gauss problem (or Lambert's problem) is defined as follows: Find  $\vec{v}_1$  and  $\vec{v}_2$  from given  $\vec{r}_1$ ,  $\vec{r}_2$ , the time of flight  $t$  from  $\vec{r}_1$  and  $\vec{r}_2$ , and the direction of motion.

Although there are an infinite number of orbits passing through  $\vec{r}_1$  and  $\vec{r}_2$ , there are only two which have the specified time of flight. The two vectors  $\vec{r}_1$  and  $\vec{r}_2$  uniquely define the plane of the transfer orbit unless they are collinear and in opposite directions ( $\Delta\nu = \pi$ ,  $\Delta\nu$  is the angle between  $\vec{r}_1$  and  $\vec{r}_2$ ), and the relationship between four vectors  $\vec{r}_1$ ,  $\vec{r}_2$ ,  $\vec{v}_1$ , and  $\vec{v}_2$  are expressed by two scalar functions  $f$ ,  $g$ , and their time derivatives as follows:

$$\vec{r}_2 = f\vec{r}_1 + g\vec{v}_1 \quad (5-31)$$

$$\vec{v}_1 = \frac{\vec{r}_2 - f\vec{r}_1}{g} \quad (5-32)$$

$$\vec{v}_2 = \dot{f}\vec{r}_1 + \dot{g}\vec{v}_1 \quad (5-33)$$

where

$$f = 1 - \frac{r_2}{p}(1 - \cos \Delta\nu) = 1 - \frac{a}{r_1}(1 - \cos \Delta E) \quad (5-34)$$

$$g = \frac{r_1 r_2 \sin \Delta\nu}{\sqrt{\mu p}} = t - \sqrt{\frac{a^3}{\mu}}(\Delta E - \sin \Delta E) \quad (5-35)$$

$$\dot{f} = \sqrt{\frac{\mu}{p}} \tan \frac{\Delta\nu}{2} \left( \frac{1 - \cos \Delta\nu}{p} - \frac{1}{r_1} - \frac{1}{r_2} \right) = \frac{-\sqrt{\mu a}}{r_1 r_2} \sin \Delta E \quad (5-36)$$

$$\dot{g} = 1 - \frac{r_1}{p}(1 - \cos \Delta\nu) = 1 - \frac{a}{r_2}(1 - \cos \Delta E). \quad (5-37)$$

Here  $a$  is semi-major axis,  $p$  is semi-latus rectum, and  $\Delta E$  is difference of the eccentric anomaly that corresponds to  $\Delta\nu$ .

The above expression is not for any conic section but only for ellipse because the eccentric anomaly  $E$  is defined only when the eccentricity is less than one.

To solve trajectories with any eccentricity, another expression is required. For this research “Solution via universal variables” is used.

**Solution via Universal Variables[12]** Using universal variables  $x$  and  $z$ , Eqn. 5-34 to 5-37 are expressed as follows:

$$f = 1 - \frac{r_2}{p}(1 - \cos \Delta\nu) = 1 - \frac{x^2}{r_1}C \quad (5-38)$$

$$g = \frac{r_1 r_2 \sin \Delta\nu}{\sqrt{\mu p}} = t - \frac{x^3}{\sqrt{\mu}}S \quad (5-39)$$

$$\dot{f} = \sqrt{\frac{\mu}{p}} \frac{(1 - \cos \Delta\nu)}{\sin \Delta\nu} \left( \frac{1 - \cos \Delta\nu}{p} - \frac{1}{r_1} - \frac{1}{r_2} \right) = -\frac{\sqrt{\mu}}{r_1 r_2} x(1 - zS) \quad (5-40)$$

$$\dot{g} = 1 - \frac{r_1}{p}(1 - \cos \Delta\nu) = 1 - \frac{x^2}{r_2}C. \quad (5-41)$$

Solving for  $x$  from Eqn. 5-38, we get

$$x = \sqrt{\frac{r_1 r_2 (1 - \cos \Delta\nu)}{p C}}. \quad (5-42)$$

Substituting for  $x$  in Eqn. 5-40 and cancelling  $\sqrt{\mu/p}$  from both sides, yields,

$$\frac{1 - \cos \Delta\nu}{\sin \Delta\nu} \left( \frac{1 - \cos \Delta\nu}{p} - \frac{1}{r_1} - \frac{1}{r_2} \right) = -\sqrt{\frac{1 - \cos \Delta\nu}{r_1 r_2}} \frac{(1 - zS)}{\sqrt{C}}. \quad (5-43)$$

If we multiply both sides by  $r_1 r_2$  and rearrange, the following expression is obtained:

$$\frac{r_1 r_2 (1 - \cos \Delta\nu)}{p} = r_1 + r_2 - \frac{\sqrt{r_1 r_2} \sin \Delta\nu}{\sqrt{1 - \cos \Delta\nu}} \frac{(1 - zS)}{\sqrt{C}}. \quad (5-44)$$

If we define parameters  $A$  and  $y$  as

$$A = \frac{\sqrt{r_1 r_2} \sin \Delta\nu}{\sqrt{1 - \cos \Delta\nu}} \quad (5-45)$$

$$y = \frac{r_1 r_2 (1 - \cos \Delta\nu)}{p} = r_1 + r_2 - A \frac{(1 - zS)}{\sqrt{C}}, \quad (5-46)$$

$x$  is expressed as

$$x = \sqrt{\frac{y}{C}} \quad (5-47)$$

and Eqn. 5-39 becomes

$$\sqrt{\mu} t = x^3 S + \frac{r_1 r_2 \sin \Delta\nu}{\sqrt{p}} = x^3 S + A\sqrt{y}. \quad (5-48)$$

Then equations 5-38, 5-39, and 5-41 become

$$f = 1 - \frac{y}{r_1} \quad (5-49)$$

$$g = A\sqrt{\frac{y}{\mu}} \quad (5-50)$$

$$\dot{g} = 1 - \frac{y}{r_2} \quad (5-51)$$

Since  $\vec{r}_2 = f\vec{r}_1 + g\vec{v}_1$ ,  $\vec{v}_1$  and  $\vec{v}_2$  can be computed as

$$\vec{v}_1 = \frac{\vec{r}_2 - f\vec{r}_1}{g} \quad (5-52)$$

$$\vec{v}_2 = \dot{f}\vec{r}_1 + \dot{g}\vec{v}_1 = \frac{\dot{g}\vec{r}_2 - \dot{r}_1}{g}. \quad (5-53)$$

The numerical method of computing the Gauss problem is explained in Appendix C.

## 5.4 Problems with Swing-by

### 5.4.1 Mechanism

The use of swing-by is a technique that is referred to as “gravity assist”[37]. Studies of interplanetary flight with gravity assist maneuvers are known to deal with cases where the spacecraft on its way from one celestial body to another approaches a third attracting body, which brings about a significant change in the spacecraft trajectory[53]. The use of swing-by may reduce the propulsive velocity budget, and the mechanism is explained in the following manner.

Assume a spacecraft entering an SOI of a planet with incoming velocity  $\mathbf{V}_{\infty_i}$ , a velocity vector with respect to the planet.  $\mathbf{V}_{\infty_i}$  can be expressed as  $\mathbf{V}_{\infty_i} = \mathbf{V}_i^H - \mathbf{V}_{pl}^H$ , where  $\mathbf{V}_i^H$  is the heliocentric velocity of the spacecraft and  $\mathbf{V}_{pl}^H$  is the heliocentric velocity of the planet. If no propulsive force is added, the energy of the swing-by trajectory with respect to the swing-by planet remains constant, so the magnitude of the outgoing velocity magnitude  $V_{\infty_o}$  is equal to the incoming velocity magnitude  $V_{\infty_i} (= |\mathbf{V}_{\infty_i}|)$  but the direction has been changed. Therefore, the outgoing “heliocentric” velocity  $\mathbf{V}_o^H (= \mathbf{V}_{\infty_o} + \mathbf{V}_{pl}^H)$  is not equal to  $\mathbf{V}_i^H$ , in both magnitude and direction. That means the spacecraft either increases or decreases its energy with a planetary swing-by. Using the equation of the conservation of the energy:

$$m_{sc}\Delta\mathcal{E}_{sc} + m_{pl}\Delta\mathcal{E}_{pl} = 0 \quad (5-54)$$

where  $m_{sc}$  and  $m_{pl}$  are the mass of spacecraft and planet, and  $\Delta\mathcal{E}_{pl}$  and  $\Delta\mathcal{E}_{sc}$  are the energy change due to the swing-by for spacecraft and planet, respectively, then the energy the spacecraft gained is

$$\Delta\mathcal{E}_{sc} = -\frac{m_{pl}}{m_{sc}}\Delta\mathcal{E}_{pl}. \quad (5-55)$$

A Mercury swing-by produces the largest energy change because of its highest heliocentric velocity among all planets, and a Jupiter swing-by gives the largest trajectory deflection for a given  $V_{\infty}$  because of its largest mass.

Next, general expressions for the planetary swing-by are developed.

#### 5.4.2 Equations of Motion

Suppose that the position and velocity of the spacecraft in the heliocentric coordinate system ( $\vec{r}_{sc1}^h$  and  $\vec{V}_{sc1}^h$ ) are known at the moment (time  $t_1$ ). It enters the sphere of influence of a swing-by body whose position in the heliocentric coordinates is  $\vec{r}_{pl1}^h = \vec{r}_{pl}(t_1)$  and velocity is  $\vec{V}_{pl1}^h = \vec{V}_{pl}(t_1)$  (see Fig. 5-5)[53].

The coordinates are transferred from heliocentric coordinates to planetocentric coordinates and the position and velocity vector of the spacecraft with respect to the swing-by

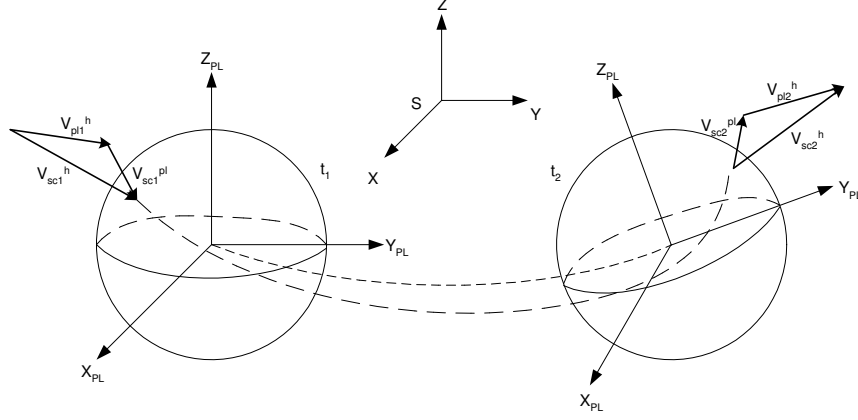


**Figure 5-5:** Schematic Diagram of Forming of Gravity Assist Maneuver.

planet( $\vec{r}_{sc1}^{pl}$  and  $\vec{V}_{sc1}^{pl}$ ) are obtained.

$$\vec{r}_{sc1}^{pl} = [x_1 \ y_1 \ z_1]^T = R[h \rightarrow pl](\vec{r}_{rc1}^h - \vec{r}_{pl1}^h), \quad |\vec{r}_{sc1}^{pl}| = r_{SOI} \quad (5-56)$$

$$\vec{V}_{sc1}^{pl} = [u_1 \ v_1 \ w_1]^T = R[h \rightarrow pl](\vec{V}_{rc1}^h - \vec{V}_{pl1}^h) \quad (5-57)$$

Here  $r_{SOI}$  is the radius of the planetary sphere of influence and  $R[h \rightarrow pl]$  is the transformation matrix from heliocentric coordinates to planetocentric coordinates at this moment.

The specific energy of spacecraft  $\mathcal{E}$ , specific angular momentum  $H$ , eccentricity  $\epsilon$ , and semi-major axis  $a$  of the hyperbolic trajectory are expressed as

$$\mathcal{E} = V_{sc1}^{pl2}/2 - \mu_{pl}/r_{SOI} \approx V_{sc1}^{pl2}/2 \quad (5-58)$$

$$H = \beta V_{sc1}^{pl} \quad (5-59)$$

$$\epsilon = \sqrt{1 + \frac{2\mathcal{E}H^2}{\mu_{pl}^2}} \quad (5-60)$$

$$a = -\mu_{pl}/2\mathcal{E} \quad (5-61)$$

where  $\beta = \sqrt{r_1^2 v_1^2 - (\vec{r}_1 \cdot \vec{v}_1)^2}/v_1$  is the impact parameter( $v_1 = |\vec{V}_{sc1}^{pl}|$ ), that is the aiming point distance of the spacecraft swing-by from the center of the planet. Then the closest approach distance between the spacecraft and the center of the swing-by planet,  $r_p$ , is

$$r_p = a(1 - \epsilon). \quad (5-62)$$

The gravity assist maneuver results in a rotation of the spacecraft velocity vector after

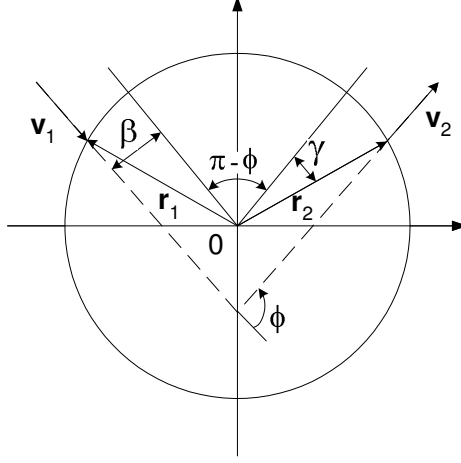


**Figure 5-6:** Swing-by: Inside the SOI.

hyperbolic flyby of the planet. The angle of rotation of the spacecraft velocity is

$$\phi = 2 \arctan \frac{\mu_{pl}}{\beta v_{\infty}^2}. \quad (5-63)$$

To determine the coordinates of the spacecraft “exit” point on the sphere of influence, the following relationships are used:

$$\phi^* = -\pi + \phi - 2\gamma; \quad \gamma = \arcsin \frac{\beta}{r_{SOI}}. \quad (5-64)$$

Here  $\mu_{pl}$  is the gravitational parameter of the swing-by planet,  $v_{\infty} = (v_1^2 - 2\mu_{pl}/r_1)^{1/2}$  is the hyperbolic excess velocity of the spacecraft at the swing-by planet. Because there is no propulsive energy added to the spacecraft inside the SOI,  $v_{\infty} = |\vec{V}_{sc1}^{pl}| = |\vec{V}_{sc2}^{pl}|$ . Note that the following restriction may be imposed on  $\beta$ :

$$\beta \geq \beta_{min} = r_{pmin} \sqrt{1 + \frac{2\mu_{pl}}{r_{pmin} v_{\infty}^2}}, \quad (5-65)$$

where  $r_{pmin}$  is the minimum admissible distance in the periapsis of the swing-by parabola and is determined by

$$r_{pmin} = r_{pl} + h_{atm} \quad (5-66)$$

where  $r_{pl}$  is the radius of the planet and  $h_{atm}$  is the height of the atmosphere if one exists.

With above expressions for  $\phi$  and  $\phi^*$ , coordinates of the spacecraft exit point from the sphere of influence,  $\vec{r}_{sc2}^{pl} = [x_2 \ y_2 \ z_2]^T$ , and the coordinates of the spacecraft velocity in the

planetocentric coordinate system,  $\vec{V}_{sc2}^{pl} = [u_2 \ v_2 \ w_2]^T$ , can be written as:

$$\vec{r}_{sc2}^{pl} = \begin{bmatrix} x_2 \\ y_2 \\ z_2 \end{bmatrix} = \Omega(\phi^*) \vec{r}_{sc1}^{pl} = \Omega(\phi^*) \begin{bmatrix} x_1 \\ y_1 \\ z_1 \end{bmatrix} \quad (5-67)$$

$$\vec{V}_{sc2}^{pl} = \begin{bmatrix} u_2 \\ v_2 \\ w_2 \end{bmatrix} = \Omega(\phi) \vec{V}_{sc1}^{pl} = \Omega(\phi) \begin{bmatrix} u_1 \\ v_1 \\ w_1 \end{bmatrix} \quad (5-68)$$

The transformation matrix  $\Omega$  is written as

$$\Omega = \begin{bmatrix} h_x h_x (1 - \cos \phi) + \cos \phi & h_x h_y (1 - \cos \phi) - h_z \sin \phi & h_z h_x (1 - \cos \phi) + h_y \sin \phi \\ h_x h_y (1 - \cos \phi) + h_z \sin \phi & h_y h_y (1 - \cos \phi) + \cos \phi & h_y h_z (1 - \cos \phi) - h_x \sin \phi \\ h_z h_x (1 - \cos \phi) - h_y \sin \phi & h_y h_z (1 - \cos \phi) + h_x \sin \phi & h_z h_z (1 - \cos \phi) + \cos \phi \end{bmatrix} \quad (5-69)$$

where  $[h_x \ h_y \ h_z]^T$  is the unit vector of angular momentum ( $\vec{r}_{sc1}^{pl} \times \vec{V}_{sc1}^{pl} / |\vec{r}_{sc1}^{pl} \times \vec{V}_{sc1}^{pl}|$ ).

The duration of the spacecraft motion in the swing-by planet's sphere of influence can be derived from

$$\Delta t = 2 \sqrt{\frac{a^3}{\mu_{pl}}} \left( \csc \frac{\phi}{2} \sinh H - H \right) \quad (5-70)$$

$$\cosh H = \left( 1 + \frac{r_{SOI}}{a} \right) \sin \frac{\phi}{2} \quad (5-71)$$

$$a = \left( \frac{v_1^2}{\mu_{pl}} - \frac{2}{r_{SOI}} \right)^{-1} \quad (5-72)$$

Therefore, the spacecraft, entering the sphere of influence at time  $t_1$  with position  $r_{sc1}^h$  and velocity  $V_{sc1}^h$  in the heliocentric coordinates, leaves the sphere of influence of the swing-by planet at time  $t_2 = t_1 + \Delta t$  whose position is  $\vec{r}_{pl2}^h = \vec{r}_{pl}(t_2)$  and velocity is  $\vec{V}_{pl2}^h = \vec{V}_{pl}(t_2)$ . The spacecraft position  $r_{sc2}^h$  and velocity  $V_{sc2}^h$  at this moment (time  $t_1$ ) is expressed as

$$r_{sc2}^h = \vec{r}_{pl2}^h + R[pl \rightarrow h] \vec{r}_{sc2}^{pl} \quad (5-73)$$

$$V_{sc2}^h = \vec{V}_{pl2}^h + R[pl \rightarrow h] \vec{V}_{sc2}^{pl} \quad (5-74)$$

where  $R[pl \rightarrow h]$  is the transformation matrix from planetocentric coordinates to heliocentric coordinates at this moment.

Usually the duration the spacecraft is inside the SOI,  $\Delta t$ , is assumed to be zero for an approximation. This is possible because normally  $\Delta t$  is small compared to the entire mission duration.

### 5.4.3 Powered Swing-by

A swing-by trajectory for a high thrust engine consists of a series of conic sections. The endpoint velocity requirements for each leg are determined by the Gauss method. The time of flight and position vectors of two planets for each leg are required to conduct the Gauss method. As explained in the last section, for a swing-by trajectory the initial velocity for the next leg is calculated from the final velocity of previous leg. In order to obtain the required initial velocity for the next leg, the impact parameter and the inclination of the hyperbolic trajectory inside the SOI are adjusted. However, sometimes the required initial velocity cannot be achieved if the final velocity of previous leg is too fast or too slow. Then an additional  $\Delta V$  should be added during the swing-by maneuver.

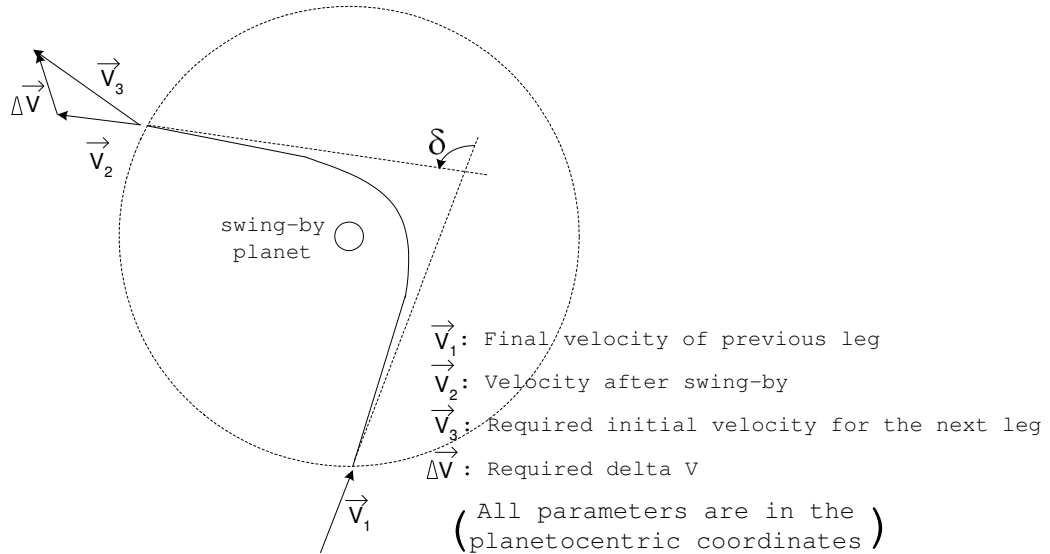


**Figure 5-7:** Geometry of a Powered Swing-by Maneuver.

Suppose that the final velocity of previous leg in the Heliocentric coordinates is  $\vec{V}_1$ , and after a swing-by maneuver the exit velocity at the exit point from the SOI is obtained as  $\vec{V}_2$  in the Heliocentric coordinates (see Fig. 5-7). If the initial velocity for the next leg is calculated as  $\vec{V}_3$  with the Gauss method, an additional burn is required, and it is calculated



as  $\Delta\vec{V} = \vec{V}_3 - \vec{V}_2$ .

The only way to adjust  $\Delta V$  is to adjust the entry point at the SOI because the final velocity of previous leg cannot be adjusted. Therefore, finding the minimum  $\Delta V$  for a high thrust swing-by trajectory is equivalent to finding the proper entry point at the SOI.

## CHAPTER VI

### DEVELOPMENT OF THE APPLICATION “*SAMURAI*”

Using all of the techniques introduced through the last chapter and in the Appendix C, a numerical analysis software application “*SAMURAI*” – Simulation and Animation Model Used for Rockets with Adjustable  $I_{sp}$  – has been developed in C++. *SAMURAI* simulates interplanetary trajectories with different types of propulsion systems. In this chapter, capabilities of *SAMURAI*, classes implemented in *SAMURAI*, and the flow of calculation are introduced. A full description of input data is in Appendix D.

#### 6.1 Overview

##### 6.1.1 Capabilities

*SAMURAI* is an interplanetary trajectory optimization application that calculates the thrust history (thrust magnitude and direction) for a prescribed condition (initial position and velocity, target position and velocity, and time of flight). Several types of engines can be analyzed. *SAMURAI* utilizes a calculus of variations algorithm to evaluate the control history that minimizes the fuel consumption for a transfer trajectory from one planet to another. A trajectory with a planetary swing-by can also be calculated.

Normally, low thrust applications employ perturbation techniques that require the thrust level to be very small. *SAMURAI* directly integrates the equations of motion for a spacecraft to determine the spacecraft’s path. Because *SAMURAI* does not use any perturbation techniques, it can calculate trajectories with any thrust level.

The engine types *SAMURAI* can deal with are the following:

- VSI engine type I (variable thrust and variable  $I_{sp}$ , no limit for  $I_{sp}$ )
- VSI engine type II (variable thrust and variable  $I_{sp}$ , with an upper limit for  $I_{sp}$ )
- CSI engine type I (constant thrust and constant  $I_{sp}$ , continuous burn)

- CSI engine type II (constant thrust and constant  $I_{sp}$ , bang-off-bang control)
- High thrust engine (idealized instantaneous burn)

Fig. 6-1 shows examples of thrust histories for these engines. A VSI engine type I can modulate its thrust and  $I_{sp}$  without limit. Without an upper limit, the  $I_{sp}$  for this type of engine may sometimes reach very high value, such as several hundred thousand seconds, which is impossible to achieve. In reality, there are some physical constraints on an engine.

For a VSI type II engine users can specify an upper limit for  $I_{sp}$  in order to simulate such a constraint. For both VSI engine types, the power is fixed at its maximum level. Note that imposing an upper limit on  $I_{sp}$  is the same as imposing a lower limit on the thrust.

A CSI type I engine operates with a given thrust magnitude throughout the mission, so total fuel consumption is proportional to the time of flight. *SAMURAI* calculates the minimum thrust level while satisfying the target conditions.

A CSI type II engine can turn its power on and off to avoid unnecessary fuel consumption, resulting in a bang-off-bang control. Users need to input the thrust level of the engine so that the switching times will be calculated.

The high thrust engine modeled in this research is a representative engine that fires for infinitesimally small amounts of time at departure and arrival. Users need to specify the value of  $I_{sp}$ .

For these different types of engines, *SAMURAI* calculates a control history (thrust direction and magnitude) that minimizes the fuel consumption for a given time of flight and given endpoint conditions (position and velocity vectors). Users can specify the endpoint conditions with the following options:

- If users would like to use the actual ephemeris data of the planets, the departure date, time of flight, ID number of the departure planet, and ID number of the arrival planet should be input. From the departure date and time of flight, planets' positions and velocities are calculated using the ephemeris data.
- If users would like to create their own planets, positions and velocities of departure and arrival points and time of flight are required. These values are directly used as

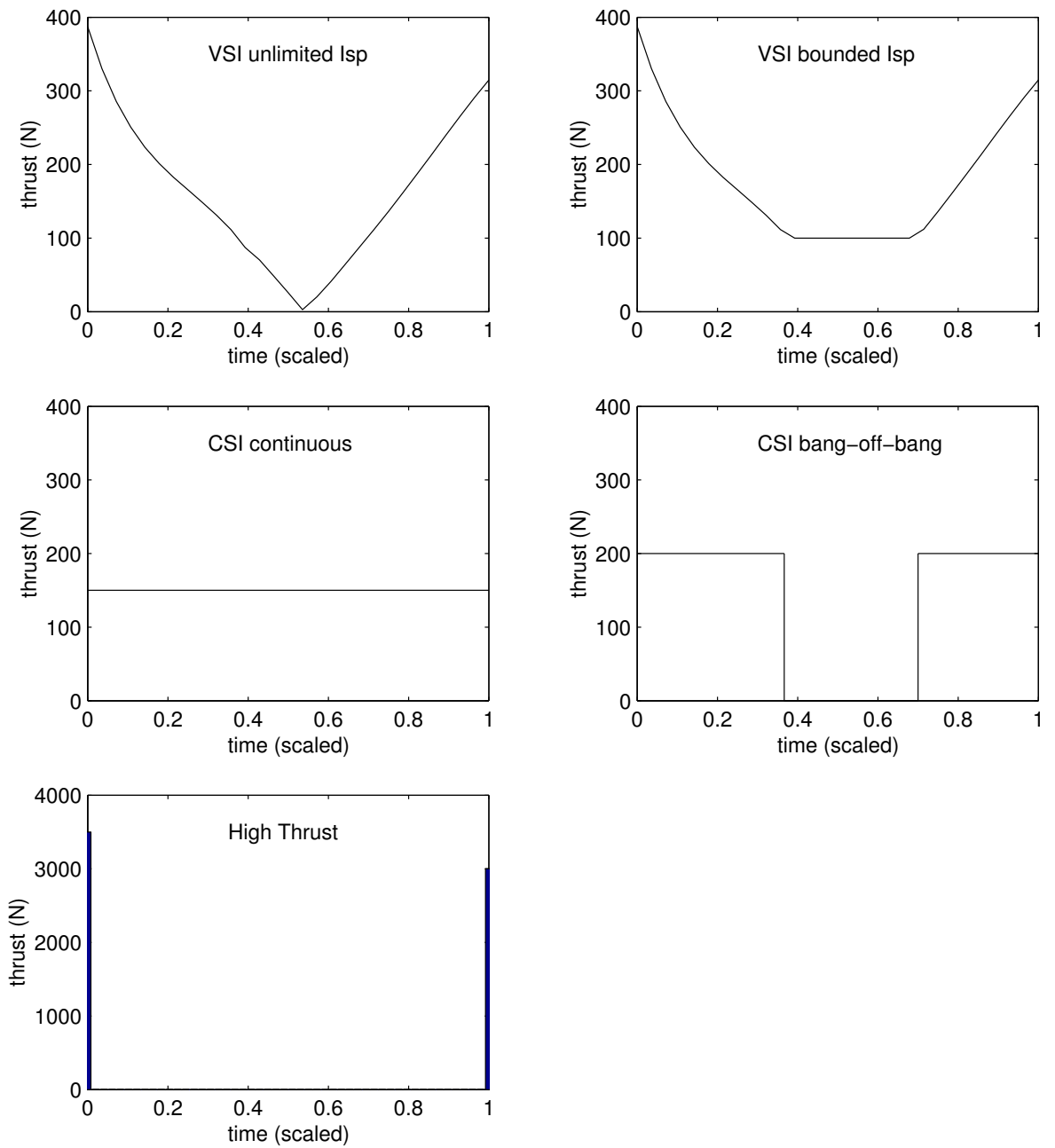


**Figure 6-1:** Examples of Thrust Histories.

the endpoint conditions.

In addition to calculating the trajectory for one value of the departure date and time of flight, *SAMURAI* has the capability to conduct a grid search with these two parameters by specifying the range of each parameter. Then *SAMURAI* finds the best launch date and time of flight for the given initial and final conditions.

Other input data required are jet power (W), initial mass (kg), and  $C_3$  values at departure and arrival which are introduced in Sec. 5.1. Optional data may be input such as the maximum number of iterations or the tolerance for the convergence criteria to avoid a long computation time and suboptimal results.

### 6.1.2 Performance Index for Each Engine

Since the target for VSI engines is to minimize fuel consumption, we would like to maximize the mass at  $t_f$ . Therefore, the performance index is expressed as the negative value of the mass of spacecraft:

$$J = -m(t_f) \quad (\phi = -m(t_f) \quad \text{and} \quad L = 0), \quad (6-1)$$

subject to the endpoint constraints:

$$\begin{bmatrix} x(t_i) \\ y(t_i) \\ z(t_i) \\ u(t_i) \\ v(t_i) \\ w(t_i) \end{bmatrix} \text{ are given, } \psi = X(t_f) - X_{target} = \begin{bmatrix} x(t_f) - x_{target} \\ y(t_f) - y_{target} \\ z(t_f) - z_{target} \\ u(t_f) - u_{target} \\ v(t_f) - v_{target} \\ w(t_f) - w_{target} \end{bmatrix} = 0 \quad (6-2)$$

$x(t_i)$ ,  $y(t_i)$ , and  $z(t_i)$  are position components of the departure planet, and  $x_{target}$ ,  $y_{target}$ , and  $z_{target}$  are position components of the arrival planet. If both  $C_3$ 's at departure and arrival are zero,  $X_{target}$  is the position and velocity of the arrival planet. If either one of  $C_3$ 's or both  $C_3$ 's are nonzero, then the best thrust direction at the endpoints is calculated so that it minimizes the fuel consumption. In such a case,  $u(t_i)$ ,  $v(t_i)$ ,  $w(t_i)$ , and  $u_{target}$ ,

$v_{target}$ ,  $w_{target}$  are not the velocity components of the planets, but the sum of the planet's velocity and the velocity of the spacecraft with respect to the planet ( $\mathbf{V}_\infty$ ).

For CSI cases, because the fuel consumption is proportional to the flight time ( $t_f - t_i$ ), the spacecraft mass cannot be used as the performance index. Instead, the performance index and constraints are defined as follows:

$$\text{Minimize } J = \frac{1}{2} [(u(t_f) - u_{target})^2 + (v(t_f) - v_{target})^2 + (w(t_f) - w_{target})^2] \quad (6-3)$$

subject to

$$\psi = \begin{bmatrix} x(t_f) - x_{target} \\ y(t_f) - y_{target} \\ z(t_f) - z_{target} \end{bmatrix} = 0. \quad (6-4)$$

Because the thrust magnitude is fixed for CSI, the control variables are just two angles (in-plane thrust angle and out-of-plane thrust angle) as explained in Chap. 5.

For CSI type I, the minimum thrust level is obtained through an iterative process. If the target conditions are not satisfied with a trial thrust level, a new optimization is performed with a new, slightly bigger thrust level. If the constraints are satisfied, then a calculation with a lower thrust level is performed. This process is iterated until the minimum thrust level that satisfies the constraints is found.

For CSI type II, a bang-off-bang thrust profile is created with the switching function introduced in Sec. 5.2. Switching times (on  $\rightarrow$  off and off  $\rightarrow$  on) that satisfy Eqns. 6-1 and 6-2 are calculated.

For high thrust, the Gauss problem is solved to obtain the endpoint velocities for the input time of flight. No optimization process is required unless the two endpoint vectors are collinear. When the two endpoint vectors are collinear or almost collinear, endpoint velocity vectors are computed using Powell's method so that total  $\Delta V$  is minimized.

## 6.2 C++ Classes

*SAMURAI* contains 20 classes. The important classes are introduced here.

- *Appli* class controls all of the classes. This class creates all the classes, initializes them,

and then starts calculation. After the minimum-fuel trajectory is obtained, *Vrml* class is called and a VRML file is created.

- *Inp* class reads input data. All of the input parameters are checked and if an inappropriate parameter is found, it ends the program. In this class, all the input data is converted into canonical units: km  $\rightarrow$  DU, day or second  $\rightarrow$  TU, kg  $\rightarrow$  non-dimensional etc.
- *Calc* class controls the grid search procedure and calculates the overall minimum-fuel trajectory for an input range of departure date and time of flight. Departure date and time of flight are set in this class, and they are sent to *Mission* class in which the optimal trajectory for a given departure date and time of flight is calculated.
- *Mission* class controls the calculation of the minimum-fuel trajectory for the time interval that is sent from *Calc* class. At first the planets' positions and velocities are calculated with *Planet* class. Then the spacecraft velocity at the initial point and final point are calculated. These endpoint conditions are used as the initial condition and the target condition of the optimization problem. An iterative procedure is required until the minimum-fuel trajectory for the time interval is found.
- *Phase* class calculates the minimum-fuel trajectory for a given initial condition, final condition, and time of flight sent from *Mission* class. This class is implemented for each phase (trajectory from one planet to another). Therefore, for a swing-by trajectory calculation, this class is called twice from *Mission* class.
- *Powell* class conducts Powell's method. This class is used for several optimization schemes as explained in Chap. C.
- *Line* class conducts a line search, using three-point quadratic approximations.
- *Opt* class handles optimal control processes with the first-order gradient algorithm. From initial state variables and an initial guess of the control history, an optimal control history that minimizes the cost function is calculated.

- *Ode* class solves ordinary differential equations with the Runge-Kutta method. With state variables at initial time and histories of the control variables throughout the propagation period, a history of state variables are calculated by integrating the differential equations.
- *Func* class contains required functions. Differential equations for spacecraft's equations of motion, the derivatives of these equations with respect to the state variables and control variables, and other equations to conduct the optimization process are stored in this class.
- *HighThrust* class calculates a high thrust trajectory using the Gauss method. From two position vectors of planets and time of flight, velocity vectors at the initial and final points are calculated. If the two position vectors are collinear, Powell's method is used to minimize the fuel requirement as explained in Chap. C.
- *Planet* class calculates a planet's position and velocity. With the input Julian date, the position and velocity at that instant are calculated using the functions stored in this class.
- *Swingby* class controls the swing-by process. With the incoming velocity vector obtained from phase 1 and a guessed value of the impact parameter, the outgoing velocity vector is calculated. This velocity is used as the initial velocity of the transfer orbit for phase 2. Powell's method is used to find a set of the best incoming velocity vectors and the entry point at the sphere of influence that minimizes the overall fuel consumption.
- *Vrml* class creates a VRML file that draws an animation of the resulting optimal trajectory on the web browser. This class converts the state variables and control variables to the VRML format, and prints them out to a file.



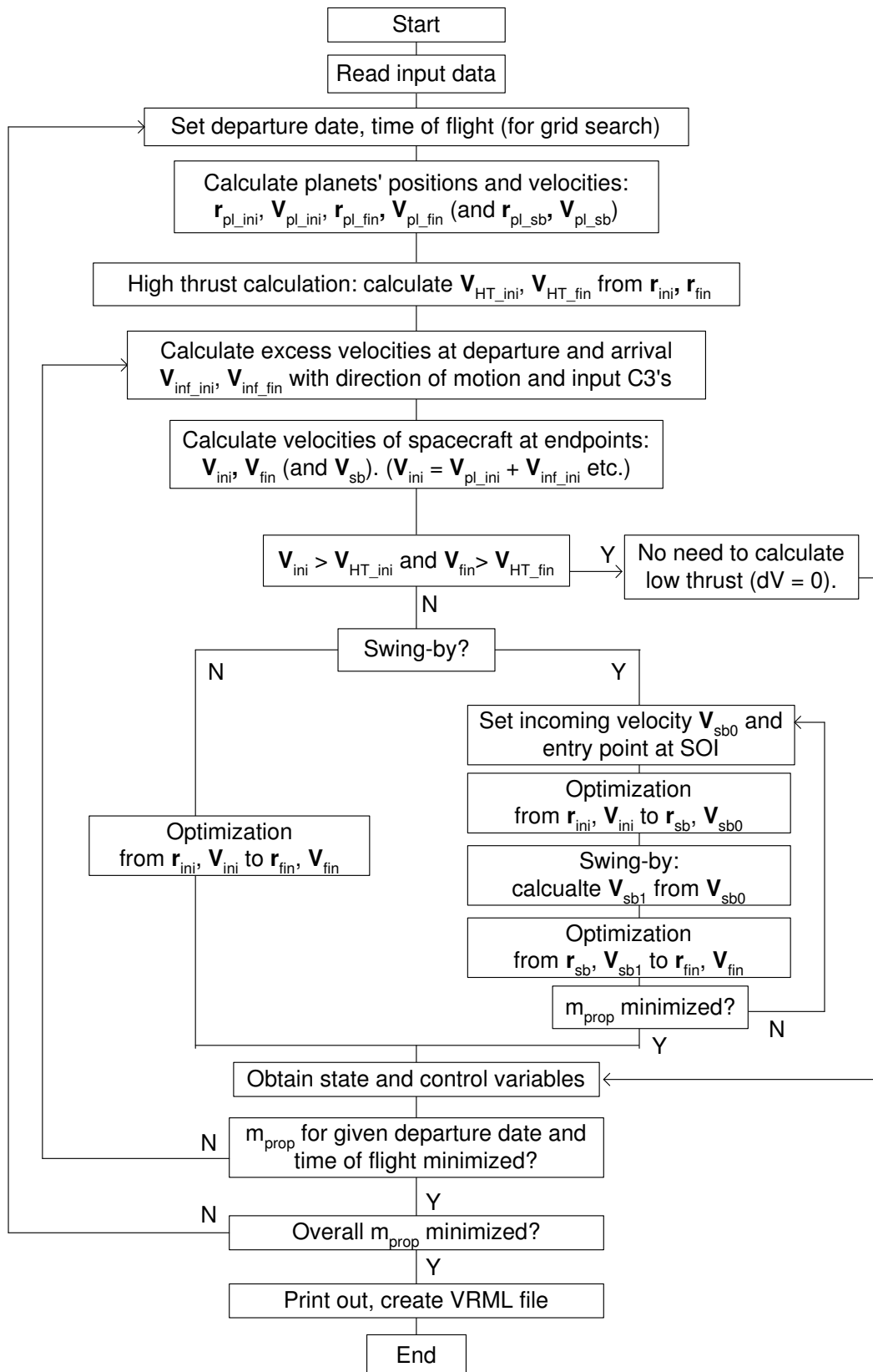


**Figure 6-2:** *SAMURAI* Flowchart.

## 6.3 Flow and Schemes

### 6.3.1 SAMURAI Flowchart

Fig. 6-2 shows the flow chart of *SAMURAI*. At first the input data is read from an input file. Input parameters such as the number of time steps, jet power, initial mass, and upper limit for  $I_{sp}$  are read and fixed.

In “*calc*” class, the departure date and the arrival date are set and the planets’ positions are calculated from them.

Once the positions of the departure and arrival planets are set, the high thrust trajectory calculation is performed using the Gauss method. With this calculation, velocities at both endpoints  $\mathbf{V}_{HT_{ini}}$  and  $\mathbf{V}_{HT_{fin}}$  are obtained. These values can be interpreted as the velocities required to travel between these two planets without any additional propulsive force.

Users can input the maximum  $C_3$ ’s at departure and arrival to simulate the excess velocity  $V_\infty$  at each planet. As stated previously,  $\sqrt{C_3} = V_\infty$ , and the spacecraft’s possible maximum velocities at two endpoints are calculated with this value and the planets’ velocities ( $\mathbf{V}_{pl}$ ):  $\mathbf{V}_{ini} = \mathbf{V}_{pl_{ini}} + \mathbf{V}_{\infty_{ini}}$  and  $\mathbf{V}_{fin} = \mathbf{V}_{pl_{fin}} + \mathbf{V}_{\infty_{fin}}$ .

If the maximum  $\mathbf{V}_{ini} \geq \mathbf{V}_{HT_{ini}}$  at departure and the maximum  $\mathbf{V}_{fin} \geq \mathbf{V}_{HT_{fin}}$  at arrival, we do not need to calculate low thrust trajectories because the spacecraft reaches the target without any propulsive force. The results from the Gauss problem will be the answer in this case (See Fig. 6-3).

If  $\mathbf{V}_{ini} < \mathbf{V}_{HT_{ini}}$  or  $\mathbf{V}_{fin} < \mathbf{V}_{HT_{fin}}$  or both, then the computation of a low thrust trajectory is required. With the input value of  $C_3$  and the direction of motion of the spacecraft,  $\mathbf{V}_{ini}$  and  $\mathbf{V}_{fin}$  are calculated and are used as endpoint conditions for optimization.

When the trajectory does not do a swing-by maneuver, class “*Opt*” calculates the thrust history that minimizes the fuel consumption. Whereas for an optimization with a swing-by, a more complicated process is required as shown in Fig. 6-2.

The first phase of the trajectory from the departure planet to the swing-by planet is calculated with a guessed value of the final velocity at the swing-by planet.

At the SOI, the swing-by planet’s velocity is subtracted from the final velocity at the swing-by planet in the Heliocentric coordinates and then converted into the planetocentric

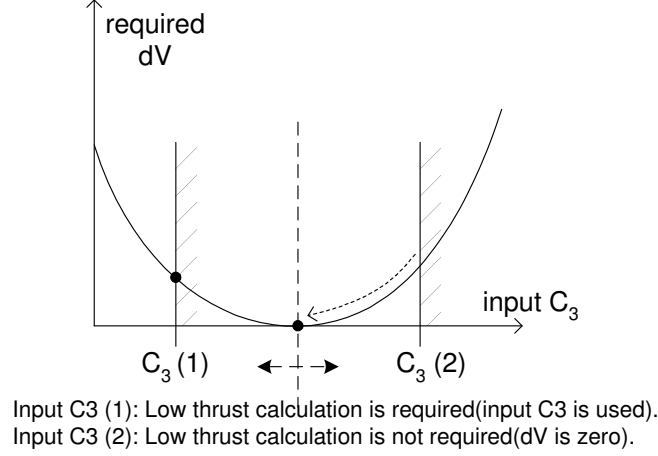


**Figure 6-3:** Input  $C_3$  and  $\Delta V$  requirements.

incoming velocity.

This incoming velocity is used as the initial velocity of the hyperbolic trajectory inside the SOI. The calculation of the trajectory inside the SOI is executed to compute the outgoing planetocentric velocity.

This outgoing velocity is then converted back into the Heliocentric velocity and the swing-by planet's velocity is added.  $\Delta V$  is calculated if needed and is added to the spacecraft velocity. Using this velocity as the initial velocity of the second phase, an optimization is executed with the “*Opt*” class from the swing-by planet to the target planet. The overall fuel consumption for the swing-by trajectory is minimized by adjusting the incoming velocity and the entry point at the swing-by planet. Therefore, an iterative process is required until the minimum-fuel trajectory is obtained.

With the above process, the minimum-fuel trajectory for a given time of flight starting with  $\mathbf{V}_{ini}$  and ending with  $\mathbf{V}_{fin}$  is obtained. But we may improve this trajectory by adjusting these endpoint velocities while keeping the time of flight fixed. This is done by adjusting the direction of motion of the spacecraft with respect to the planet. Therefore the above process is iterated by adjusting the directions of motion of the spacecraft at the departure and arrival planets until the fuel consumption is minimized.

When the actual ephemeris of planets is used, a grid search may be conducted to find the best launch opportunity and the time of flight that minimizes the fuel consumption over

a range of departure dates and times of flight.

After all of the above process are finished, a VRML file that draws a 3D animation is created.

### 6.3.2 VSI Constrained $I_{sp}$

Finding an optimal solution for a VSI unconstrained  $I_{sp}$  problem is relatively simple. The 1st-order gradient algorithm introduced in the previous chapter is suitable for this kind of problem.

However, constrained cases are complicated and require more calculations than unconstrained cases. To solve VSI type II problems, the initial guess for the Lagrange multiplier  $\lambda(t_i)$  is required in order to estimate the control vector at initial time.

For VSI type II calculations, the results from VSI type I are used. This is because the thrust histories are similar to each other for unconstrained arcs, and the Lagrange multipliers obtained in VSI type I calculations should be used as an initial guess for VSI type II calculation.

The following steps are taken to obtain the results for VSI type II.

1. Calculate a trajectory for VSI type I.
2. Obtain the Lagrange multipliers  $\vec{\lambda}$  at initial time  $t_i$  from the previous step.
3. From  $\vec{x}$  and  $\vec{\lambda}$ , calculate the control variables:

$$\vec{l} = [l_x \ l_y \ l_z]^T = \vec{\lambda}_V / \lambda_V, \quad T = \frac{P_J \lambda_V}{m \lambda_m}. \quad (6-5)$$

4. Integrate  $\dot{x}$  and  $\dot{\lambda}$  forward from  $t_i$  to final time  $t_f$  with the control variables obtained in the step 3:

$$\int_{t_i}^{t_f} \dot{x} dt, \quad \int_{t_i}^{t_f} \dot{\lambda} dt \quad (6-6)$$

5. Check if the resulting  $x(t_f)$  satisfies the terminal constraints  $\psi(t_f) = 0$ .
6. If not, return to step 3 with the new values of  $\lambda(t_i)$ .  $\lambda(t_i)$  should be chosen so that it satisfies  $\psi(t_f) = 0$  AND minimizes the performance index  $J$ . Powell's method is used to estimate the next  $\lambda(t_i)$ .

7. Iterate until  $J$  is minimized and  $\psi(t_f) = 0$  is satisfied with the desired degree of accuracy.

### 6.3.3 CSI Continuous Thrust

The CSI type I problem (continuous thrust) is not a constrained problem. The control variables are now only two (in-plane thrust angle and out-of-plane thrust angle), hence it is simpler to optimize than VSI type I problem that have three control variables (thrust magnitude in addition to two angles).

For constant thrust problems, sometimes the optimizer cannot find the answer because the thrust magnitude is not sufficient to reach the target. For example, if we would like to find a trajectory from Earth to Pluto with a time of flight of 1 year and  $I_{sp}$  of 100,000 sec and 1 kW of jet power, then the optimizer cannot find the answer because the thrust level is too low. On the other hand, if we would like to find a trajectory from Earth to Mars with a 300-day time of flight, we do not need 3,000 sec of  $I_{sp}$  and 50 MW of jet power because it is too much.

*SAMURAI* finds the minimum thrust level while satisfying the terminal conditions using an iterative process. If the thrust level is not enough to reach the target, the thrust level of the next step is made a little bit larger than the previous step. On the other hand, if starting with too much thrust, the thrust level of the next step is a little bit smaller than the previous step. The process is iterated until the minimum thrust level is found.

### 6.3.4 CSI Bang-Off-Bang

Finding the solution for CSI type II (bang-off-bang) requires finding the switching times, and the switching times are determined by the sign of the switching function. As shown in Sec. 5.2.4, the switching function is a function of the Lagrange multipliers. Therefore, for CSI type II problems, an initial guess for the Lagrange multipliers is required to start the calculation. This is similar to the VSI type II case.

The following steps are taken.

1. Calculate a trajectory for VSI type I.

2. Obtain the Lagrange multipliers  $\vec{\lambda}$  at initial time  $t_i$  from the previous step.
3. From  $\lambda(\vec{t}_0)$ , calculate the control variables  $u(t_0)$  at initial time:

$$u = [u_0 \ u_1 \ u_2 \ u_3]^T = [l_x \ l_y \ l_z \ T]^T, l = [l_x \ l_y \ l_z]^T = \vec{\lambda}_V / \lambda_V \quad (6-7)$$

$T$  is determined by the sign of the switching function.

$$S = \vec{l} \cdot \vec{\lambda}_V / m = \lambda_m / c \quad (6-8)$$

If  $S$  is positive,  $T$  is the prescribed value, and if  $S$  is negative,  $T = 0$ .

4. Integrate  $\dot{x}$  and  $\dot{\lambda}$  forward from  $t_i$  to final time  $t_f$ . Control variables need to be calculated as the time step proceeds. Control variables for the next step can be calculated by the equations in the previous step.
5. Check if the resulting  $x(t_f)$  satisfies the terminal constraints  $\psi(t_f) = 0$ .
6. If not, return to step 3 with the new values of  $\lambda(t_i)$ .  $\lambda(t_i)$  should be chosen so that it satisfies  $\psi(t_f) = 0$  AND minimizes the performance index  $J$ . Powell's method is used to estimate the next  $\lambda(t_i)$ .
7. Iterate until  $J$  is minimized and  $\psi(t_f) = 0$  is satisfied with the desired degree of accuracy.

The switching function method described above only estimates the solution, and the terminal constraints are not usually satisfactorily met. More computation is required by increasing the burn time step by step. For example, suppose that the total time step is 300 steps, and the switching function estimates switching times as the 50th and 250th steps. If the terminal condition is not satisfactory, that means more burn time is needed. The first switching time should be greater than 50, and the second switching time should be smaller than 250. Therefore, using steps 50 and 250 as initial guesses for the switching times, the burn time is increased one by one until the terminal constraints are satisfied.

## 6.4 Examples of Input and Output

*SAMURAI* calculates a transfer trajectory between two planets with or without a swing-by. As stated previously, in addition to the trajectory for the actual planets, users can make up their own planetary bodies and calculate the transfer trajectory for these planets. The mandatory input data is as follows:

- Option ID number (1 for VSI type I, 4 for CSI type II, etc.)
- Planet's position and velocity
  - Coordinates of positions and velocities of planets in the Cartesian coordinates.
  - ID number for planets (3 for Earth, 4 for Mars, etc.)
- Departure date (yyyy/mm/dd)
- Time of flight (day)
- Jet power (W)
- Initial mass (kg)
- Maximum allowable  $I_{sp}$  for constrained case
- $I_{sp}$  for CSI type II and high thrust

In addition to theis input data, users can also specify other parameters such as the maximum number of iterations and the tolerance for terminal conditions.

Output from *SAMURAI* is the following:

- History of state variables ( $x, y, z, u, v, w, m$ )
- History of control variables (thrust magnitude and direction)
- VRML file

Thrust direction is expressed by two angles in the spacecraft-centered coordinates.  $\alpha$  is the in-plane thrust angle and  $\beta$  is the out-of-plane thrust angle (see Fig. 6-4).  $x, y$ , and  $z$  axes of the spacecraft-centered coordinates are defined as follows:

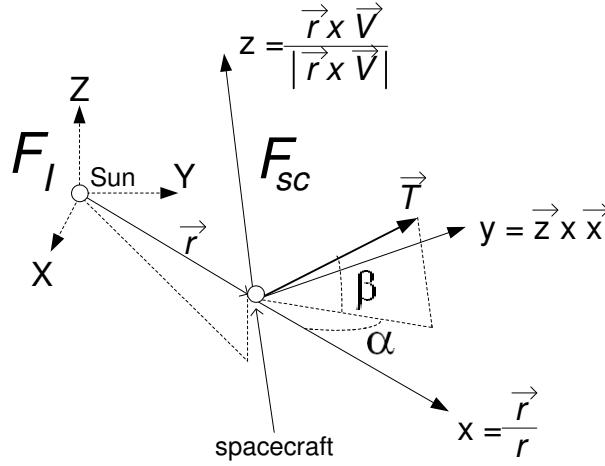


**Figure 6-4:**  $\alpha$  (in-plane thrust angle) and  $\beta$  (out-of-plane thrust angle) in the Spacecraft-centered Coordinates.

$$\vec{x} = \vec{r}/|\vec{r}| \quad (6-9)$$

$$\vec{z} = \vec{r} \times \vec{V}/|\vec{r} \times \vec{V}| \quad (6-10)$$

$$\vec{y} = \vec{z} \times \vec{x} \quad (6-11)$$

where  $\vec{r}$  and  $\vec{V}$  are position and velocity vectors of spacecraft.

A few example input files and corresponding output files are introduced.

The following input data is used to calculate a trajectory with a VSI type I engine. The spacecraft departs from a planet whose position is (1, 0, 0) and velocity is (0, 1, 0) to a planet whose position is (-1.5, 0, 0) and velocity is (0, -0.8165, 0). This is to simulate an Earth to Mars, two-dimensional, coplanar trajectory. The time of flight is 180 days, and the number of time steps is 30; therefore, the variables are evaluated once every 6 days. Jet power is 1.0E+07 W or 10 MW, initial mass is 1.0E+05 kg or 100 MT, and the C3 values are zero for both departure and arrival. A line starting with “//” is a comment line.

```
//
// VSI, no constraints, no swing-by
//
option      1           // VSI no constraints
timeSteps   100         // Number of time steps
initial     1.0  0.0  0.0  0.0  1.0   0.0 // DU, DU/TU
target      -1.5  0.0  0.0  0.0 -0.8165 0.0 // DU, DU/TU
tof         180.0       // Time of Flight (day)
```



```

Pj      1.0e+07    // Jet Power (W)
m0      1.0E+05    // Initial mass (kg)
C3dep   0.0        // C3 at departure (km^2/s^2)
C3arr   0.0        // C3 at arrival (km^2/s^2)
$end

```

The output for this input data is as follows:

```

=====
==          S A M U R A I          ==
==          Simulation and Animation Model          ==
==          Used for                          ==
==          Rockets with Adjustable Isp            ==
=====

Option = 1
Variable Isp, unconstrained Isp

Number of steps      30
Initial condition
1.00000              0.00000              0.00000              1.00000              0.00000              1.00000
Target condition
-1.50000             0.00000             0.00000             -0.81650             0.00000             0.00000
Time of Flight
180.00 (day)        3.09636 (TU_Sun)

Jet Power      1.000e+07 (W)      1.000e+04 (kW)      10.000 (MW)
Initial mass   1.000e+05 (kg)     100.000 (MT)

maximum C3 at departure planet      0.00000 (km2/s2)
maximum C3 at arrival planet        0.00000 (km2/s2)

a      e      i(deg)      0(deg)      o(deg)      L(deg)      M(deg)
1.00000 0.00000 0.00000 0.00000 0.00000 NaN NaN
a      e      i(deg)      0(deg)      o(deg)      L(deg)      M(deg)
1.50001 0.00001 0.00000 0.00000 0.00000 0.00000 0.00000

Optimal State and Control Variables
i      TU      day      x[ 0]      x[ 1]      x[ 2]      x[ 3]      x[ 4]      x[ 5]      x[ 6]      u[ 0]      u[ 1]      u[ 2]      u[ 3]
0  0.00  0.0  0.00000  0.00000  0.00000  0.00000  1.00000  0.00000  1.00000  -0.99463  -0.10345  0.00000  0.56289
1  0.10  6.0  0.99169  0.10290  0.00000  -0.15693  0.99018  0.00000  0.97491  -0.99813  -0.06108  0.00000  0.48333
2  0.21  12.0  0.96753  0.20439  0.00000  -0.30770  0.97239  0.00000  0.95619  -0.99997  -0.00825  0.00000  0.42092
3  0.31  18.0  0.92810  0.30360  0.00000  -0.45311  0.94584  0.00000  0.94181  -0.99870  0.05097  0.00000  0.37203
4  0.41  24.0  0.87392  0.39960  0.00000  -0.59341  0.90930  0.00000  0.93043  -0.99383  0.11087  0.00000  0.33352
5  0.52  30.0  0.80553  0.49126  0.00000  -0.72814  0.86128  0.00000  0.92120  -0.98623  0.16536  0.00000  0.30237
6  0.62  36.0  0.72354  0.57733  0.00000  -0.85602  0.80027  0.00000  0.91356  -0.97782  0.20946  0.00000  0.27570
7  0.72  42.0  0.62876  0.65638  0.00000  -0.97485  0.72509  0.00000  0.90723  -0.97067  0.24040  0.00000  0.25094
8  0.83  48.0  0.52226  0.72692  0.00000  -1.08156  0.63533  0.00000  0.90203  -0.96620  0.25781  0.00000  0.22603
9  0.93  54.0  0.40546  0.78744  0.00000  -1.17251  0.53186  0.00000  0.89789  -0.96470  0.26334  0.00000  0.19957
10 1.03  60.0  0.28019  0.83661  0.00000  -1.24410  0.41710  0.00000  0.89474  -0.96558  0.26009  0.00000  0.17089
11 1.14  66.0  0.14863  0.87343  0.00000  -1.29351  0.29502  0.00000  0.89252  -0.96769  0.25216  0.00000  0.13993
12 1.24  72.0  0.01318  0.89741  0.00000  -1.31945  0.17063  0.00000  0.89110  -0.96966  0.24445  0.00000  0.10713
13 1.34  78.0  -0.12372  0.90856  0.00000  -1.32245  0.04912  0.00000  0.89034  -0.96985  0.24371  0.00000  0.07317
14 1.44  84.0  -0.25979  0.90746  0.00000  -1.30478  -0.06506  0.00000  0.89002  -0.96349  0.26776  0.00000  0.03871
15 1.55  90.0  -0.39303  0.89506  0.00000  -1.26979  -0.16883  0.00000  0.88996  -0.96423  0.71976  0.00000  0.00487
16 1.65  96.0  -0.52187  0.87255  0.00000  -1.22118  -0.26066  0.00000  0.88991  0.99440  -0.10570  0.00000  0.03067
17 1.75  102.0  -0.64508  0.84121  0.00000  -1.16240  -0.34040  0.00000  0.88967  0.98710  -0.16008  0.00000  0.06517
18 1.86  108.0  -0.76179  0.80225  0.00000  -1.09626  -0.40882  0.00000  0.88903  0.98270  -0.18518  0.00000  0.10003
19 1.96  114.0  -0.87135  0.75679  0.00000  -1.02481  -0.46729  0.00000  0.88773  0.97871  -0.20524  0.00000  0.13555
20 2.06  120.0  -0.97331  0.70577  0.00000  -0.94940  -0.51735  0.00000  0.88555  0.97468  -0.22358  0.00000  0.17204
21 2.17  126.0  -1.06730  0.64998  0.00000  -0.87081  -0.56056  0.00000  0.88219  0.97063  -0.24056  0.00000  0.20975
22 2.27  132.0  -1.15304  0.59004  0.00000  -0.78935  -0.59835  0.00000  0.87737  0.96669  -0.25594  0.00000  0.24877
23 2.37  138.0  -1.23022  0.52645  0.00000  -0.70503  -0.63198  0.00000  0.87074  0.96302  -0.26943  0.00000  0.28907
24 2.48  144.0  -1.29855  0.45958  0.00000  -0.61761  -0.66250  0.00000  0.86195  0.95976  -0.28081  0.00000  0.33042
25 2.58  150.0  -1.35769  0.38969  0.00000  -0.52671  -0.69076  0.00000  0.85066  0.95703  -0.28998  0.00000  0.37244
26 2.68  156.0  -1.40726  0.31698  0.00000  -0.43181  -0.71744  0.00000  0.83650  0.95490  -0.29691  0.00000  0.41461
27 2.79  162.0  -1.44681  0.24159  0.00000  -0.33236  -0.74307  0.00000  0.81918  0.95342  -0.30164  0.00000  0.45623
28 2.89  168.0  -1.47584  0.16359  0.00000  -0.22770  -0.76800  0.00000  0.79846  0.95261  -0.30420  0.00000  0.49651
29 2.99  174.0  -1.49379  0.08305  0.00000  -0.11716  -0.79246  0.00000  0.77420  0.95247  -0.30465  0.00000  0.53459
30 3.10  180.0  -1.50000  0.00001  0.00000  -0.00001  -0.81650  0.00000  0.74640  0.95310  -0.30267  0.00000  0.56937

target -1.50000  0.00000  0.00000  0.00000  -0.81650  0.00000

Control variables and Isp:
m0 1.000e+05 (kg) Pj 1.000e+07 (W)
i      alpha      beta      --      thrust(N)      Isp(s)
0      -95.94      0.00      0.00      333.800      6110.15
1      -84.50      0.00      0.00      286.619      7115.94
2      -72.91      0.00      0.00      249.607      8171.11
3      -61.48      0.00      0.00      220.617      9244.82
4      -50.51      0.00      0.00      197.779      10312.34
5      -40.27      0.00      0.00      179.307      11374.74
6      -30.98      0.00      0.00      163.492      12475.01
7      -22.73      0.00      0.00      148.809      13705.90
8      -15.49      0.00      0.00      134.037      15216.42
9      -9.13      0.00      0.00      118.348      17233.59
10     -3.46      0.00      0.00      101.336      20126.69
11      1.76      0.00      0.00      82.978      24579.66
12      6.78      0.00      0.00      63.530      32103.80
13     11.98      0.00      0.00      43.390      47005.09
14     18.39      0.00      0.00      22.953      88860.33
15     53.61      0.00      0.00      2.890      705635.43
16    -161.88      0.00      0.00      18.185      112155.37
17    -154.47      0.00      0.00      38.647      52774.28
18    -148.88      0.00      0.00      59.318      34383.82
19    -143.64      0.00      0.00      80.380      25374.15
20    -138.49      0.00      0.00      102.022      19991.54
21    -133.31      0.00      0.00      124.382      16397.60
22    -128.01      0.00      0.00      147.524      13825.33
23    -122.50      0.00      0.00      171.418      11898.18
24    -116.68      0.00      0.00      195.939      10409.19
25    -110.47      0.00      0.00      220.861      9234.62
26    -103.77      0.00      0.00      245.865      8295.48

```

27	-96.54	0.00	0.00	270.547	7538.67
28	-88.80	0.00	0.00	294.436	6927.03
29	-80.67	0.00	0.00	317.015	6433.67
30	-72.38	0.00	0.00	337.641	6040.64

FinalMass= 74639.88461 (kg)  
 FuelConsumed= 25360.11539 (kg)  
 Wall time 0.000 (sec), CPU time 0.125 (sec)

Another example is a grid search for a trajectory from Earth to Jupiter with a VSI type II engine. The actual planets' positions and velocities are used for the initial condition and target condition. The range of the departure date is between 100 days after Sep. 1, 2010, and 300 days after Sep. 1, 2010, with 20-day increments. Times of flight ranges from 300 days to 500 days with 50-day increments. Therefore  $11 \times 5 = 55$  cases are calculated. Jet power is 10MW, initial mass is 100MT, and maximum allowable  $I_{sp}$  is 30,000 sec.

```
//
// VSI, constrained Isp, no swing-by
//
option 2
timeSteps 50
depPlanet 3 // Earth
arrPlanet 5 //Jupiter
date 2010 9 1 0 0 0 // yyyy mm dd hr min sec
depRange 100 300 20 // initial final increment
tofRange 300 500 50 // initial final increment
jetPower 1.000E+07 // (W)
initialMass 100000 // (kg)
maxIsp 30000.0 // (sec)
maxC3dep 0.0 // km^2/s^2
maxC3arr 0.0 // km^2/s^2
$end
```

The output for this input data is as follows:

```
=====
==          S A M U R A I          ==
==          Simulation and Animation Model          ==
==          Used for          ==
==          Rockets with Adjustable Isp          ==
=====

Option = 2
Variable Isp, constrained Isp

Number of steps 50
Departure planet 3 Earth
Arrival planet 5 Jupiter

Calendar Date 9/ 1/2010 0: 0: 0
Julian Date 2455440.50000

Departure Date: from 100.00 to 300.00 with 20.00 increment(day)
                  from 1.72020 to 5.16060 with 0.34404 increment(TU_Sun)
Time of Flight: from 300.00 to 500.00 with 50.00 increment(day)
                  from 5.16060 to 8.60099 with 0.86010 increment(TU_Sun)

Jet Power 1.000e+07 (W) 1.000e+04 (kW) 10.000 (MW)
Initial mass 1.000e+05 (kg) 100.000 (MT)

Maximum Isp 30000.00 (sec)
maximum C3 at departure planet 0.00000 (km2/s2)
maximum C3 at arrival planet 0.00000 (km2/s2)
mininum T 67.986 (N)

..... (omitted) .....

Optimal State and Control Variables

Departure date: 2011/ 6/ 8 0: 0: 0 (2455720.50000 Julian date)
Arrival date: 2012/10/20 0: 0: 0 (2456220.50000 Julian date)

i TU day x[ 0] x[ 1] x[ 2] x[ 3] x[ 4] x[ 5] x[ 6] u[ 0] u[ 1] u[ 2] u[ 3]
```

0	0.00	0.0	-0.24488	-0.98482	0.00000	0.95432	-0.24514	-0.00000	1.00000	0.95694	-0.29012	-0.00972	0.24428
1	0.17	10.0	-0.07379	-1.01410	-0.00004	1.02152	-0.09302	-0.00048	0.99106	0.98467	-0.17392	-0.01327	0.24097
2	0.34	20.0	0.10651	-1.01645	-0.00017	1.06070	0.06501	-0.00108	0.98249	0.99820	-0.05783	-0.01600	0.23394
3	0.52	30.0	0.29101	-0.99138	-0.00040	1.07055	0.22235	-0.00173	0.97453	0.99835	0.05423	-0.01880	0.22363
4	0.69	40.0	0.47466	-0.93965	-0.00076	1.05223	0.37157	-0.00243	0.96736	0.98706	0.15886	-0.02161	0.21068
5	0.86	50.0	0.65282	-0.86331	-0.00124	1.00962	0.50578	-0.00313	0.96107	0.96717	0.25297	-0.02442	0.19589
6	1.03	60.0	0.82180	-0.76547	-0.00184	0.94881	0.62001	-0.00381	0.95569	0.94202	0.33444	-0.02724	0.18011
7	1.20	70.0	0.97905	-0.64989	-0.00255	0.87686	0.71193	-0.00446	0.95118	0.91496	0.40243	-0.03005	0.16416
8	1.38	80.0	1.12330	-0.52047	-0.00337	0.80043	0.78192	-0.00506	0.94746	0.88871	0.45730	-0.03282	0.14865
9	1.55	90.0	1.25430	-0.38084	-0.00429	0.72477	0.83226	-0.00563	0.94441	0.86513	0.50029	-0.03553	0.13396
10	1.72	100.0	1.37255	-0.23412	-0.00530	0.65343	0.86623	-0.00615	0.94195	0.84519	0.53310	-0.03815	0.12028
11	1.89	110.0	1.47902	-0.08282	-0.00641	0.58887	0.88762	-0.00666	0.93986	0.82916	0.55753	-0.04067	0.11465
12	2.06	120.0	1.57509	0.07125	-0.00760	0.53268	0.90019	-0.00721	0.93786	0.81682	0.57529	-0.04308	0.11465
13	2.24	130.0	1.66225	0.22687	-0.00889	0.48509	0.90678	-0.00781	0.93586	0.80770	0.58784	-0.04540	0.11465
14	2.41	140.0	1.74195	0.38321	-0.01028	0.44549	0.90937	-0.00848	0.93387	0.80127	0.59640	-0.04766	0.11465
15	2.58	150.0	1.81550	0.53972	-0.01180	0.41306	0.90943	-0.00921	0.93187	0.79698	0.60194	-0.04994	0.11465
16	2.75	160.0	1.88405	0.69608	-0.01345	0.38699	0.90802	-0.01000	0.92987	0.79436	0.60519	-0.05231	0.11465
17	2.92	170.0	1.94863	0.85211	-0.01524	0.36645	0.90590	-0.01086	0.92787	0.79306	0.60666	-0.05493	0.11465
18	3.10	180.0	2.01012	1.00774	-0.01719	0.35071	0.90358	-0.01180	0.92588	0.79283	0.60667	-0.05804	0.11465
19	3.27	190.0	2.06928	1.16298	-0.01930	0.33912	0.90141	-0.01282	0.92388	0.79356	0.60532	-0.06203	0.11465
20	3.44	200.0	2.12679	1.31786	-0.02160	0.33112	0.89961	-0.01397	0.92188	0.79537	0.60233	-0.06774	0.11465
21	3.61	210.0	2.18320	1.47248	-0.02411	0.32624	0.89828	-0.01529	0.91989	0.79800	0.59663	-0.07712	0.11465
22	3.78	220.0	2.23903	1.62691	-0.02686	0.32409	0.89742	-0.01693	0.91789	0.80576	0.58437	-0.09628	0.11465
23	3.96	230.0	2.29470	1.78122	-0.02993	0.32450	0.89670	-0.01944	0.91589	0.82447	0.54354	-0.15754	0.11465
24	4.13	240.0	2.35067	1.93541	-0.03355	0.31763	0.87990	-0.01855	0.91390	-0.04890	0.57405	-0.22100	0.11465
25	4.30	250.0	2.40398	2.08394	-0.03631	0.29566	0.85057	-0.01672	0.91190	-0.07285	-0.68121	-0.06988	0.11465
26	4.47	260.0	2.45238	2.22803	-0.03930	0.26734	0.82533	-0.01738	0.90990	-0.07969	-0.65023	-0.00879	0.11465
27	4.64	270.0	2.49596	2.36789	-0.04229	0.23971	0.80108	-0.01719	0.90791	-0.07682	-0.64007	0.00930	0.11465
28	4.82	280.0	2.53485	2.50363	-0.04522	0.21287	0.77746	-0.01672	0.90591	-0.07728	-0.63503	0.01800	0.11465
29	4.99	290.0	2.56919	2.63537	-0.04804	0.18677	0.75436	-0.01611	0.90391	-0.07745	-0.63211	0.02310	0.11465
30	5.16	300.0	2.59911	2.76316	-0.05076	0.16132	0.73168	-0.01540	0.90192	-0.07751	-0.63029	0.02642	0.11465
31	5.33	310.0	2.62469	2.88709	-0.05334	0.13644	0.70937	-0.01464	0.89992	-0.07767	-0.62914	0.02875	0.11465
32	5.50	320.0	2.64605	3.00721	-0.05579	0.11206	0.68738	-0.01384	0.89792	-0.07772	-0.62843	0.03046	0.11465
33	5.68	330.0	2.66325	3.12358	-0.05810	0.08812	0.66566	-0.01301	0.89593	-0.07773	-0.62804	0.03176	0.11465
34	5.85	340.0	2.67636	3.23623	-0.06027	0.06457	0.64419	-0.01216	0.89393	-0.07761	-0.62789	0.03276	0.11465
35	6.02	350.0	2.68546	3.34520	-0.06229	0.04137	0.62293	-0.01129	0.89193	-0.07754	-0.62794	0.03356	0.11465
36	6.19	360.0	2.69059	3.45054	-0.06415	0.01848	0.60184	-0.01040	0.88994	-0.07735	-0.62814	0.03420	0.11465
37	6.36	370.0	2.69182	3.55226	-0.06586	-0.00455	0.58058	-0.00949	0.88784	-0.07705	-0.62848	0.03472	0.12013
38	6.54	380.0	2.68903	3.65028	-0.06742	-0.02814	0.55881	-0.00853	0.88555	-0.07666	-0.62894	0.03515	0.12522
39	6.71	390.0	2.68214	3.74451	-0.06880	-0.05252	0.53631	-0.00752	0.88301	-0.07619	-0.62950	0.03550	0.13358
40	6.88	400.0	2.67096	3.83479	-0.07000	-0.07798	0.51286	-0.00644	0.88012	-0.07564	-0.63016	0.03579	0.14190
41	7.05	410.0	2.65531	3.92095	-0.07102	-0.10455	0.48843	-0.00530	0.87688	-0.07503	-0.63090	0.03602	0.15016
42	7.22	420.0	2.63499	4.00283	-0.07183	-0.13224	0.46299	-0.00409	0.87326	-0.07435	-0.63172	0.03621	0.15834
43	7.40	430.0	2.60981	4.08024	-0.07242	-0.16109	0.43651	-0.00281	0.86925	-0.07360	-0.63262	0.03637	0.16643
44	7.57	440.0	2.57957	4.15300	-0.07279	-0.19110	0.40897	-0.00147	0.86484	-0.07280	-0.63360	0.03650	0.17441
45	7.74	450.0	2.54406	4.22094	-0.07293	-0.22230	0.38032	-0.00007	0.86001	-0.07194	-0.63464	0.03659	0.18227
46	7.91	460.0	2.50309	4.28385	-0.07282	-0.25469	0.35056	0.00140	0.85474	-0.07102	-0.63575	0.03667	0.18997
47	8.08	470.0	2.45643	4.34154	-0.07245	-0.28630	0.31965	0.00294	0.84904	-0.07004	-0.63693	0.03673	0.19751
48	8.26	480.0	2.40390	4.39382	-0.07181	-0.32312	0.28756	0.00454	0.84288	-0.06901	-0.63818	0.03676	0.20484
49	8.43	490.0	2.34527	4.44047	-0.07088	-0.35917	0.25427	0.00621	0.83628	-0.06791	-0.63950	0.03679	0.21194
50	8.60	500.0	2.28033	4.48130	-0.06967	-0.39644	0.21975	0.00794	0.82924	-0.06676	-0.64088	0.03679	0.21876
target			2.28033	4.48130	-0.06967	-0.39644	0.21975	0.00794					

Control variables and Isp:

m0	1.000e+05 (kg)	Pj	1.000e+07 (W)			
i	alpha	beta	--	thrust(N)	Isp(s)	
0	2.46	-0.56	0.00	144.859	14079.67	
1	4.81	-0.73	0.00	142.900	14272.74	
2	6.82	-0.86	0.00	138.730	14701.66	
3	8.62	-0.99	0.00	132.616	15379.54	
4	10.31	-1.11	0.00	124.934	16325.12	
5	11.95	-1.24	0.00	116.162	17558.38	
6	13.62	-1.36	0.00	106.809	19095.38	
7	15.33	-1.49	0.00	97.350	20950.97	
8	17.10	-1.61	0.00	88.148	23138.02	
9	18.91	-1.73	0.00	79.438	25674.95	
10	20.73	-1.85	0.00	71.330	28593.47	
11	22.52	-1.97	0.00	67.986	30000.00	
12	24.22	-2.08	0.00	67.986	30000.00	
13	25.80	-2.18	0.00	67.986	30000.00	
14	27.23	-2.29	0.00	67.986	30000.00	
15	28.50	-2.39	0.00	67.986	30000.00	
16	29.60	-2.50	0.00	67.986	30000.00	
17	30.54	-2.63	0.00	67.986	30000.00	
18	31.34	-2.79	0.00	67.986	30000.00	
19	32.02	-3.00	0.00	67.986	30000.00	
20	32.62	-3.32	0.00	67.986	30000.00	
21	33.23	-3.85	0.00	67.986	30000.00	
22	34.11	-4.95	0.00	67.986	30000.00	
23	36.52	-8.48	0.00	67.986	30000.00	
24	162.96	11.26	0.00	67.986	30000.00	
25	-152.16	-4.68	0.00	67.986	30000.00	
26	-148.49	-1.15	0.00	67.986	30000.00	
27	-146.46	-0.10	0.00	67.986	30000.00	
28	-144.75	0.41	0.00	67.986	30000.00	
29	-143.14	0.70	0.00	67.986	30000.00	
30	-141.54	0.89	0.00	67.986	30000.00	
31	-139.91	1.02	0.00	67.986	30000.00	
32	-138.24	1.11	0.00	67.986	30000.00	
33	-136.49	1.17	0.00	67.986	30000.00	
34	-134.67	1.21	0.00	67.986	30000.00	
35	-132.74	1.24	0.00	67.986	30000.00	
36	-130.72	1.26	0.00	67.986	30000.00	
37	-128.54	1.27	0.00	71.240	28629.58	
38	-126.14	1.28	0.00	74.257	27466.19	
39	-123.47	1.27	0.00	79.215	25747.16	
40	-120.46	1.26	0.00	84.147	24238.10	
41	-117.08	1.25	0.00	89.044	22905.11	
42	-113.27	1.23	0.00	93.897	21721.37	
43	-109.02	1.20	0.00	98.695	20665.35	
44	-104.30	1.18	0.00	103.428	19719.60	
45	-99.11	1.15	0.00	108.086	18869.88	
46	-93.50	1.11	0.00	112.655	18104.49	
47	-87.53	1.08	0.00	117.123	17413.90	
48	-81.34	1.05	0.00	121.472	16790.45	
49	-75.06	1.01	0.00	125.681	16228.18	
50	-68.87	0.97	0.00	129.727	15722.01	

FinalMass= 82923.72159 (kg)  
FuelConsumed= 17076.27841 (kg)

Wall time 3117.000 (sec), CPU time 2998.078 (sec)

The precise explanation of input data is in Appendix D.

## **6.5 Validation and Verification**

When a new computer application is created, validation is necessary to check if the application works properly and the results are accurate. In order to validate *SAMURAI*, several analyses have been performed and the results with *SAMURAI* are compared to the results with other existing reliable interplanetary trajectory calculation programs.

There are no applications to calculate general VSI trajectories. Therefore, validation for CSI engines and high thrust engines are performed. IPREP is used to compare the results for high thrust, and ChebyTOP is used for CSI trajectories.

### **6.5.1 Validation of High Thrust with IPREP**

IPREP (Interplanetary PREProcessor) is a rapid grid-search optimizer on launch and arrival windows, minimum  $\Delta V$  or mass optimization created by Martin Marietta Astronautics. IPREP is widely used to estimate  $\Delta V$  for high thrust trajectories.

To compare the results with *SAMURAI* and the results with IPREP, transfer trajectories are calculated from Earth to Venus, Mars, and Jupiter. Time of flight is set to 200 days for Venus transfer, 180 days for Mars transfer, and 500 days for Jupiter transfer. Twelve departure dates are considered: the first day of each month in the year 2000.

Figs. 6-5 to 6-7 show the  $\Delta V$  requirements (at departure and arrival, and total) calculated with *SAMURAI* and IPREP. They show that the results obtained by *SAMURAI* match well with the results obtained by IPREP.

### **6.5.2 Validation of CSI with ChebyTOP**

ChebyTOP (Chebyshev Trajectory Optimization Program) is an analysis tool that enables the user to conduct rapidly the parametric analysis and optimization of interplanetary missions employing electrically propelled spacecraft. This program was developed by Boeing.

To compare the results with *SAMURAI* and the results with ChebyTOP, transfer trajectories from Earth to Mars are analyzed for CSI type I and type II engines. The following

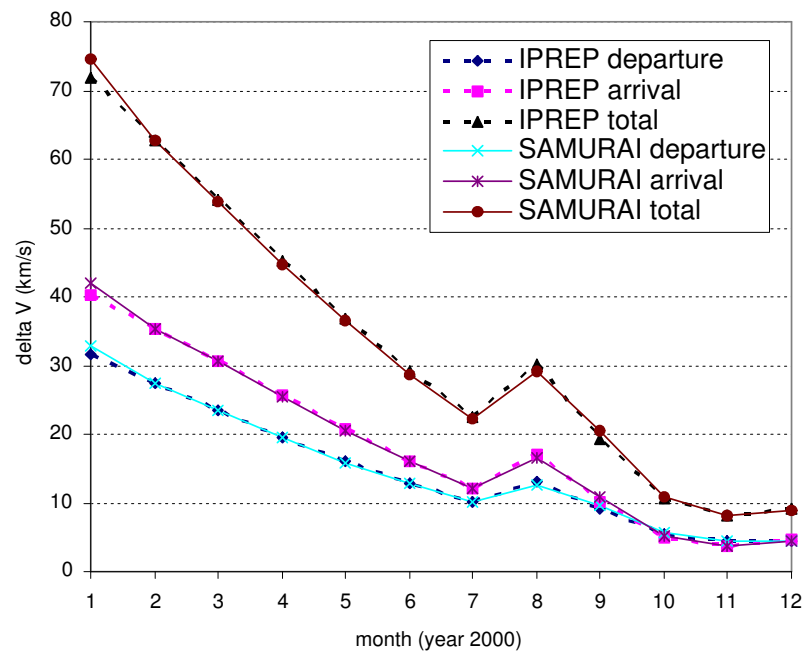


**Figure 6-5:** Results with *SAMURAI* and IPREP:  $\Delta V$  Requirements for High Thrust Venus Transfer.

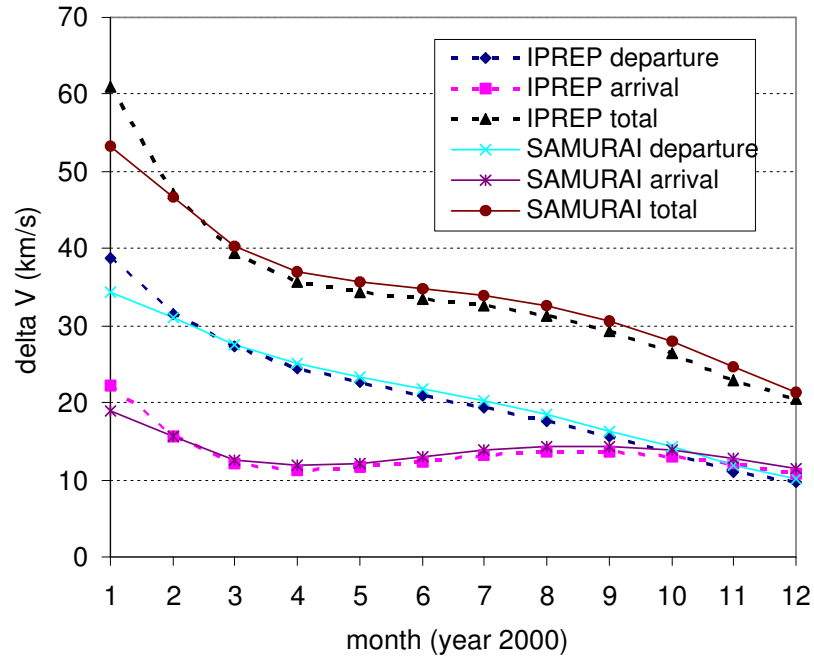


**Figure 6-6:** Results with *SAMURAI* and IPREP:  $\Delta V$  Requirements for High Thrust Mars Transfer.

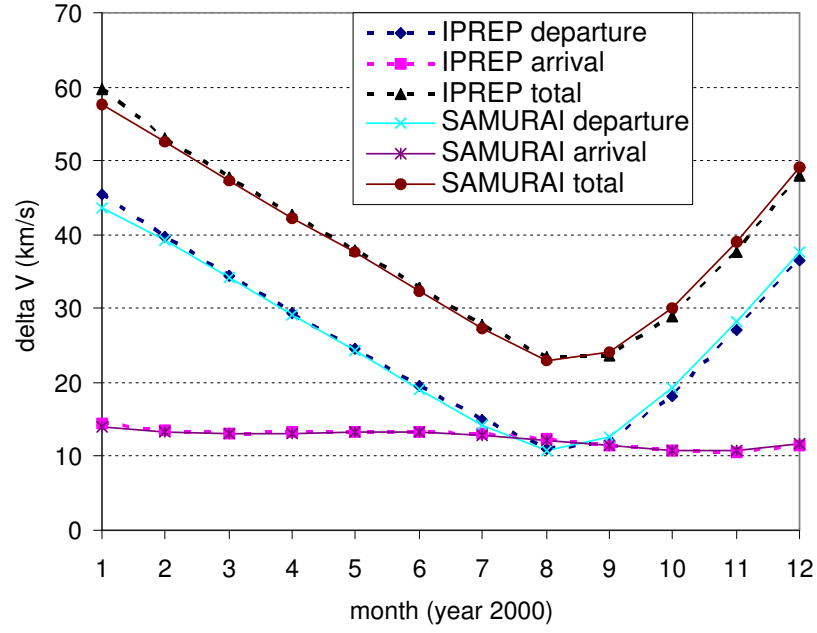


**Figure 6-7:** Results with *SAMURAI* and IPREP:  $\Delta V$  Requirements for High Thrust Jupiter Transfer.

assumptions are considered: 1,000 kg initial mass, departure date of June 1, 2018, and 120-days TOF for both CSI type I and type II engines.

**CSI type I** The result obtained with *SAMURAI* was the following: the maximum  $I_{sp}$  that satisfies the target conditions was 11,372 sec when the jet power is 100 kW, and the resulting propellant mass fraction  $\zeta_p (= m_{propellant}/m_{initial})$  was 0.16675.

Then the same trajectory was calculated using ChebyTOP with input  $I_{sp}$  of 11,372 sec. The resulting jet power requirement was 99.434 kW, and  $\zeta_p$  was calculated as 0.16579.

Trajectory is shown in Fig. 6-8. Although ChebyTOP does not output the history of the thrust direction, this figure shows that the path obtained with *SAMURAI* is very close to the path obtained with ChebyTOP.

**CSI type II** For a trajectory with a CSI type II engine,  $I_{sp}$  is set to 5,000 sec in this section. The following are some important values.

For *SAMURAI*, jet power was 91.23 kW, the first switching time ( $t_1$ ) was 14.4 day, and the second switching time ( $t_2$ ) was 103.2 day. The resulting  $\zeta_p$  was 0.2125. For ChebyTOP,

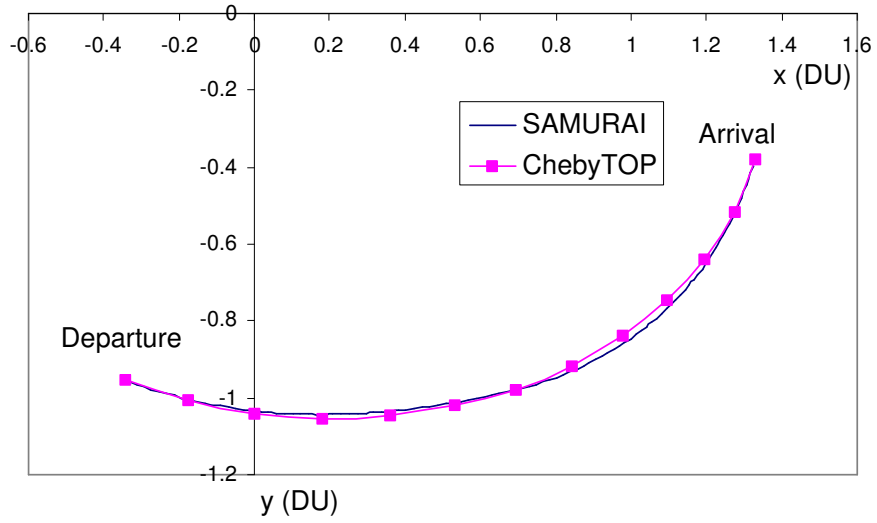


**Figure 6-8:** Results with *SAMURAI* and ChebyTOP: Trajectory Comparison for CSI type I Mars Transfer.

jet power was 91.23 kW,  $t_1$  was 13.3 day and  $t_2$  was 102.0 day. The resulting  $\zeta_p$  was 0.2051.

Trajectory is shown in Fig. 6-9. Again, the trajectories with *SAMURAI* and ChebyTOP are similar.

The validation conducted in this section shows that *SAMURAI* is reliable to conduct general trajectory calculations for CSI engines and high thrust engines. In the following two chapters, *SAMURAI* is used to analyze various interplanetary trajectories.

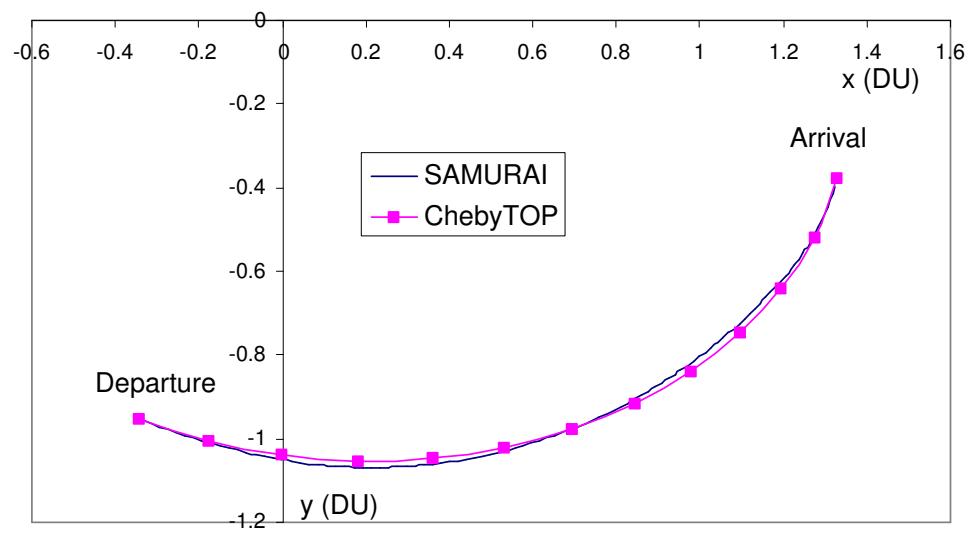


**Figure 6-9:** Results with *SAMURAI* and ChebyTOP: Trajectory Comparison for CSI type II Mars Transfer.



## CHAPTER VII

### PRELIMINARY RESULTS: PROOF OF CONCEPT

One of the objectives of this research is to compare different types of engines and discuss their advantages and disadvantages. In this research comparison is performed by calculating the fuel consumption of each engine for the same trajectory. The trajectories should have the same initial condition, the same target condition, and the same time of flight. The problem should be made as simple as possible so that the comparison of these engines clearly states the advantages or disadvantages of each engine.

In this chapter, a large database is generated using *SAMURAI*. Transfer orbits from Earth to other planets are calculated for five different engines (VSI type I and II, CSI type I and II, and high thrust). The fuel consumption for each engine is calculated and compared against the breadth of results obtained. Given the large number of analyses required to populate the comparative database, two simplifying assumptions are made in this chapter. First, the departure and arrival orbits are assumed to be circular and coplanar. Second, the planetary alignment between departure and arrival is represented by a range of lead angles, therefore eliminating departure date as an explicit variable.

#### ***7.1 Problem Description***

The minimum fuel transfer trajectory for each of five engines is calculated. As stated above, the planets are assumed to be orbiting around the Sun in a circular orbit (zero eccentricity), and these orbits are further assumed to be coplanar (zero inclination). This allows for a two-dimensional transfer orbit to be assumed.

Table 7-1 shows some orbital data for planets. The eccentricity is less than 0.1 and the inclination is less than a few percent for planets except Mercury and Pluto. The inclination and the eccentricity of Earth and the four destination planets considered in this chapter are small enough and the orbits of these planets can be approximated by circular and coplanar

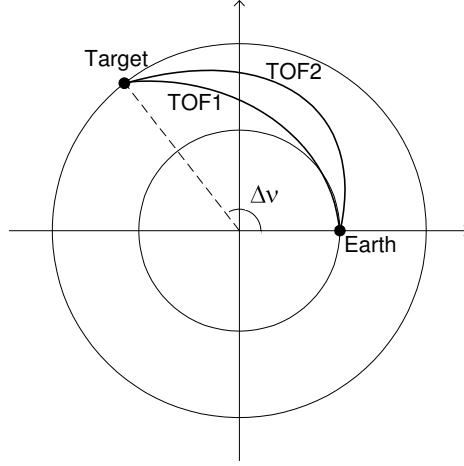


**Figure 7-1:** 2D Trajectories for Proof-of-Concept Problems.

orbits.

**Table 7-1:** Orbital Data[37].

Planet	Semi-major axis (AU)	Period (day)	Eccentricity $\epsilon$	Inclination (deg)
Mercury	0.3871	87.97	0.2056	7.004
Venus	0.7233	224.7	0.0068	3.394
Earth	1.000	365.2	0.0167	0.000
Mars	1.524	687.0	0.0934	1.850
Jupiter	5.203	4,332	0.0482	1.306
Saturn	9.539	10,760	0.0539	2.489
Uranus	19.18	30,690	0.0471	0.773
Neptune	30.07	60,190	0.0050	1.773
Pluto	39.44	90,460	0.2583	17.14

The spacecraft is assumed to depart from Earth at a position of  $(x, y) = (1.0, 0.0)$  and a velocity of  $(u, v) = (0.0, 1.0)$ .  $C_3$ 's at departure and arrival are assumed to be zero for all cases. The unit of position is in AU (1 AU = 1.4959965E+08km), and the unit of velocity is in AU/TU (1 TU = 58.132821 day = 5.0226757E+06 sec, 1 AU/TU = 29.78495 km/s). The target position and velocity are calculated with the semi-major axis of the arrival planet and the true anomaly difference between Earth and the target planet,  $\Delta\nu$ , as shown in Fig. 7-1.

Simplified representations of the orbits of four planets (Venus, Mars, Jupiter, and Saturn) and an asteroid in the asteroid belt are considered as destinations in this chapter. Semi-major axes for these destinations are set to 0.7 AU (Venus), 1.5 AU (Mars), 3.0 AU (asteroid), 5.0 AU (Jupiter), and 10.0 AU (Saturn). Three to five  $\Delta\nu$ 's are considered:  $60^\circ$ ,  $90^\circ$ ,  $120^\circ$ ,  $150^\circ$ ,  $180^\circ$  for Venus, Mars, and the asteroid,  $90^\circ$ ,  $120^\circ$ ,  $150^\circ$ ,  $180^\circ$  for Jupiter, and  $120^\circ$ ,  $150^\circ$ ,  $180^\circ$  for Saturn.

The velocity of a spacecraft on a circular orbit with radius  $r$  is expressed as  $\sqrt{\mu/r}$  where the gravitational parameter  $\mu$  in the canonical units is  $1 \text{ AU}^3/\text{TU}^2$ . Hence, if Mars is chosen as the target planet and  $\Delta\nu = 120^\circ$  is used, the target condition is

$$\begin{aligned} \text{position} \quad (x, y) &= (1.5 \cos 120^\circ, 1.5 \sin 120^\circ) = (-0.750, 1.299), \\ \text{velocity} \quad (u, v) &= \left(-\sqrt{\frac{1}{1.5}} \sin 120^\circ, \sqrt{\frac{1}{1.5}} \cos 120^\circ\right) = (-0.707, -0.408). \end{aligned}$$

Three levels of the jet power (10, 20, and 30MW) are considered for all destinations, and the initial mass is set to  $1.0\text{E}+05 \text{ kg}$  (100MT) for all cases.

For each target condition and jet power, the trajectory for several values of time of flight are calculated. The range for the time of flight for each destination is selected so that it includes the time of flight that minimizes the fuel consumption for high thrust. For example, the time of flight for a Hohmann transfer from Earth to Mars is 4.454 TU, so the range of time of flight for Earth  $\rightarrow$  Mars trajectories with  $\Delta\nu = 180^\circ$  is chosen several values between 3.0 TU and 5.0 TU.

For VSI type II (bounded  $I_{sp}$  case), the maximum allowable  $I_{sp}$  is set to 30,000 seconds. The  $I_{sp}$  is determined by the exhaust velocity of the engine, and an  $I_{sp}$  of 30,000 seconds is appropriate with current or near-future technology [22].

For CSI type I, the minimum required thrust level that enables the spacecraft to reach the target is calculated. For example, higher thrust (and hence lower  $I_{sp}$ ) is required for fast transfer and therefore higher fuel consumption is expected for this case. On the other hand, when the transfer time is very long, less thrust (and higher  $I_{sp}$ ) is required and therefore small amount of fuel may be needed.

For CSI type II (bang-off-bang case) the  $I_{sp}$  level is set to 5,000 seconds, and the  $I_{sp}$  for

high thrust is set to 450 seconds.

## 7.2 Numerical Accuracy

Before calculating the transfer trajectories, the numerical accuracy is investigated to determine the tolerance and number of time steps required. Input values for these parameters for the remaining sections of this paper are determined based on the discussion in this section.

In *SAMURAI*, users can specify a tolerance for the convergence criteria. *SAMURAI* terminates the calculation when it finds a trajectory whose final conditions match the target condition within this tolerance:

$$|x_i(t_f) - x_{i_{target}}| \leq \epsilon, \quad i = 0 - 5 \quad \text{or} \quad x, y, z, u, v, \text{ and } w \quad (7-1)$$

where  $\epsilon$  is the input convergence criteria. The smaller this value becomes, the longer the computation takes.

Users can also specify the number of time steps along the trajectory. When the time of flight is 300 days and the number of the time steps that user specified is 300 steps, *SAMURAI* evaluates the state and control variables once a day. The larger the number of time steps becomes, the more accurate the results become, but a larger number of time steps requires more computation time.

To determine the appropriate values for these two inputs, 2D trajectories for VSI type I engine simulating transfer trajectories from Earth to Mars with 150-day time of flight are calculated for different tolerances and number of time steps. Fig. 7-2 shows the CPU time for different tolerance and number of time steps.

The CPU (Pentium 1.90 GHz, 512 MB RAM) time requirements increase as the tolerance decreases, and as the number of time steps increase. We should choose a sufficiently small tolerance and a sufficiently large number of time steps to give an accurate result, but at the same time not requiring a large computational commitment. Fig. 7-3 shows the fuel consumption for different tolerance and number of time steps. As can be seen in this figure, the results for tolerances smaller than 1.0E-05 are almost the same for any number of time steps, and the results for the time steps larger than 300 are almost the same. That

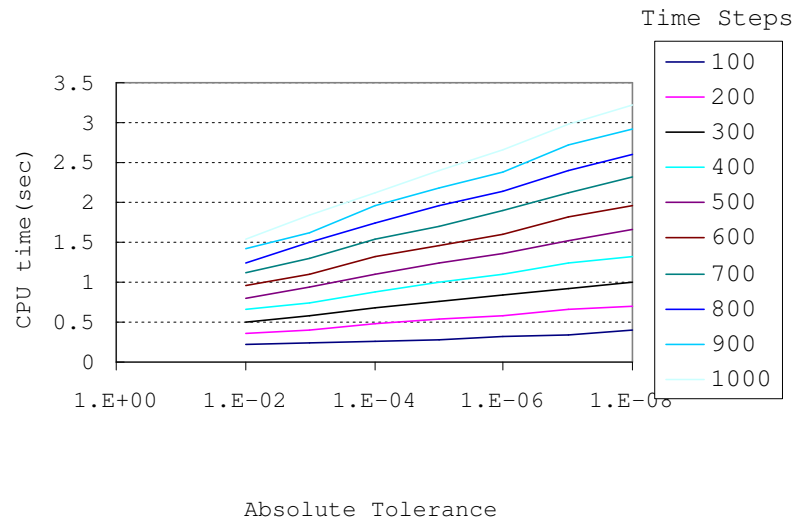


**Figure 7-2:** Tolerance vs. CPU Time for Different Number of Time Steps.

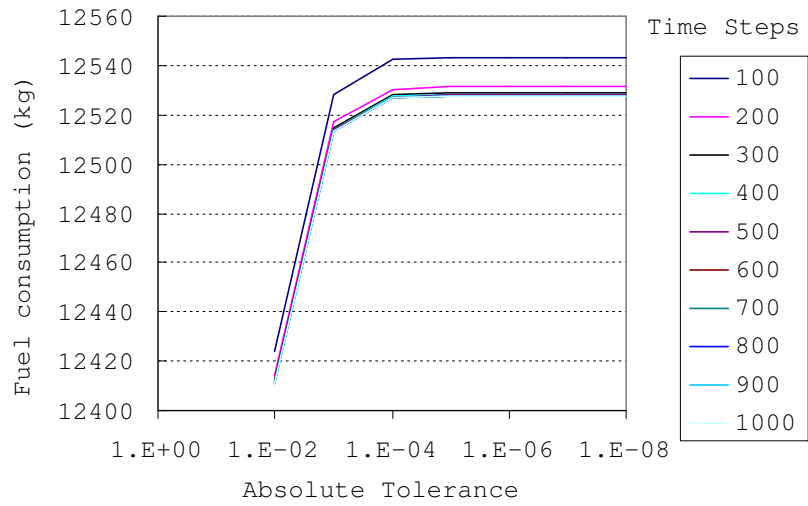


**Figure 7-3:** Tolerance vs. Fuel Consumption for Different Number of Time Steps.

means the tolerance of 1.0E-05 and the number of time steps of 300 are enough to obtain the accurate results.

Similar calculations have been performed for other planets, and the following numbers are used: 300 time steps for Venus, Mars, and the asteroids, and 500 time steps for Jupiter and Saturn. Absolute convergence tolerance of 1.0E-05 is used for the computation for all the planets.

### 7.3 *Results and Discussion*

Table 7-2 shows an example of fuel consumption. This table shows the fuel requirements for an Earth to Venus transfer with 10 MW jet power. For example, the first cell of Table 7-2 (86011.9) shows the fuel requirement in kg for an Earth to Venus transfer when  $\Delta\nu$  is  $60^\circ$  for a VSI type I engine with 10 MW of jet power. Earth's position is (1, 0) and velocity is (0, 1), and because the  $\Delta\nu$  between Earth and Venus is  $60^\circ$ , Venus' position and velocity are (0.3750, 0.6495) and (-1.0, 0.5774), respectively.

Table 7-3 shows the fuel requirements for an Earth to Saturn transfer with 30 MW jet power.

The reminder of the database over (2,000 simulations) is displayed in Appendix A. Tables in Appendix A show the fuel requirements (kg) for the different terminal conditions (position and velocity calculated from the semi-major axis of the orbit of the target planet and  $\Delta\nu$ ), the different jet power settings (MW), and the different engine types.

In these tables, if a result is 100,000.0, that means the calculation does not converge or the spacecraft consumes all of its mass before it reaches the target because of the  $I_{sp}$  restrictions imposed. For example, in Table 7-2 when  $\Delta\nu$  is  $60^\circ$ , a spacecraft with a CSI type II engine whose  $I_{sp}$  is 5,000 sec cannot reach Venus because of an insufficient thrust level.

There is also a time of flight restriction on VSI type II engine, where the maximum allowable  $I_{sp}$  is 30,000 sec. Table 7-4 shows the time until mass becomes zero for a spacecraft whose initial mass is 1.0E+05kg (100MT). For example, if the jet power is 30 MW the burn time should be shorter than 28.717 TU. In Table 7-3, for VSI type II, all of the spacecraft

**Table 7-2:** Transfer Orbit to Venus with 10MW Jet Power.

Venus	Fuel	Consumed (kg)										
Pj	10.000	(MW)	nju	60.000 (deg)	r	0.3750	0.6495	V	-1.0000	0.5774		
TOF (TU_Sun)	0.600	0.700	0.800	0.900	1.000	1.100	1.200	1.300	1.400	1.500	1.600	
VSI type I	86011.9	71244.5	54950.4	47872.8	50044.1	55170.0	60021.5	63884.6	66829.7	69064.3	70772.0	
VSI typeII	86027.7	71256.0	54952.2	47874.5	50057.8	55174.9	60022.2	63884.6	66829.7	69064.3	70772.0	
CSI type I	99590.9	88666.7	67897.1	55612.1	56315.9	60781.0	65222.9	68922.1	71862.4	74177.9	76002.0	
CSI typeII	100000.0	100000.0	100000.0	100000.0	100000.0	100000.0	100000.0	100000.0	100000.0	100000.0	100000.0	
highThrust	99962.2	99517.3	98209.7	97435.0	98007.0	98951.2	99520.5	99780.0	99893.8	99945.5	99970.3	
Pj	10.000	(MW)	nju	90.000 (deg)	r	-0.0000	0.7500	V	-1.1547	-0.0000		
TOF (TU_Sun)	1.000	1.100	1.200	1.300	1.400	1.500	1.600	1.700	1.800	1.900	2.000	
VSI type I	58840.7	39928.5	25648.1	20916.9	23775.7	29842.8	36301.7	42049.9	46845.6	50756.4	53930.5	
VSI typeII	58850.0	39968.9	25671.1	20930.4	23820.7	29886.9	36318.7	42055.9	46847.5	50757.2	53930.8	
CSI type I	76443.8	54149.2	34152.9	26268.7	29689.5	36000.3	42244.3	47745.0	52392.1	56258.0	59459.7	
CSI typeII	100000.0	100000.0	29585.2	28248.0	28080.9	33220.7	40784.1	45464.3	50395.1	53988.8	57666.1	
highThrust	99199.9	96601.8	92196.7	90080.6	91669.9	94920.9	97316.9	98602.2	99248.9	99578.9	99753.5	
Pj	10.000	(MW)	nju	120.000 (deg)	r	-0.3750	0.6495	V	-1.0000	-0.5774		
TOF (TU_Sun)	1.000	1.200	1.400	1.600	1.800	2.000	2.200	2.400	2.600	2.800	3.000	
VSI type I	85656.1	65896.8	35273.8	12312.3	10614.9	19564.8	29331.5	37193.5	43092.3	47475.3	50757.3	
VSI typeII	85658.2	65903.1	35314.8	12433.6	10756.3	19673.3	29388.0	37230.0	43121.1	47501.0	50781.9	
CSI type I	98677.9	82543.3	48405.4	17491.5	14841.7	25317.4	35453.9	43510.4	49605.9	54187.6	57652.0	
CSI typeII	100000.0	100000.0	45046.4	21395.0	17299.8	25907.9	35853.3	43124.2	48890.8	54991.7	58919.7	
highThrust	99995.2	99784.6	96844.2	83979.1	81463.7	91996.8	97086.1	98835.5	99480.0	99743.9	99863.0	
Pj	10.000	(MW)	nju	150.000 (deg)	r	-0.6495	0.3750	V	-0.5773	-1.0000		
TOF (TU_Sun)	1.400	1.600	1.800	2.000	2.200	2.400	2.600	2.800	3.000	3.200	3.400	
VSI type I	67583.6	44162.1	20318.1	6555.6	4886.2	9900.6	16778.1	23327.5	28903.9	33467.7	37157.2	
VSI typeII	67608.2	44212.3	20441.7	6849.5	5279.3	10180.5	16981.4	23491.8	29048.2	33601.4	37285.4	
CSI type I	83326.0	58324.3	29148.9	9821.0	7436.9	14355.1	22374.0	29676.3	35782.2	40737.7	44725.6	
CSI typeII	100000.0	100000.0	28582.3	15043.3	13789.7	18052.0	29334.5	31591.0	38861.9	44127.1	48305.8	
highThrust	99879.8	98789.1	92977.7	76848.6	70563.1	83707.4	92446.6	96349.1	98107.2	98950.3	99382.1	
Pj	10.000	(MW)	nju	180.000 (deg)	r	-0.7500	-0.0000	V	0.0000	-1.1547		
TOF (TU_Sun)	2.000	2.200	2.400	2.600	2.800	3.000	3.200	3.400	3.600	3.800	4.000	
VSI type I	26936.8	11677.5	3827.5	2450.2	4937.8	9089.2	13622.2	17932.6	21793.6	25156.8	28048.0	
VSI typeII	27052.3	11913.8	4363.8	3346.2	5540.8	9510.2	13965.6	18238.6	22080.7	25434.0	28322.1	
CSI type I	37470.2	17397.3	5949.4	3886.6	7945.5	13411.3	19035.8	24217.4	28761.5	32659.0	35970.3	
CSI typeII	36772.6	21144.2	12034.7	15210.5	14040.4	21311.4	28080.9	29835.9	34599.6	38109.8	40115.5	
highThrust	96465.2	88436.0	73129.6	64867.6	75219.4	85622.9	91707.3	95046.0	96914.4	97999.5	98654.8	

mass (100MT) is consumed and therefore the spacecraft cannot reach the target when the time of flight exceeds 30 TU.

From these results (Appendix A), several facts were observed. For almost all the cases (any target condition, jet power, and time of flight), the VSI type I engine is the most effective. This is understandable because the VSI engine offers more degrees of freedom to the simulation. If other types of engines are more effective than the VSI type I engine, the optimizer would simply choose to match that thrust history within VSI. For example, if the constant  $I_{sp}$  engine is more effective than the variable  $I_{sp}$  engine, then the resulting control history for VSI type I should look like that of CSI type I.

There are some numerical exceptions in the database that must be explained. If the transfer time is considerably long, the spacecraft with a CSI type I engine sometimes revolves around the Sun more than once before reaching the target planet. This helps lowering the

**Table 7-3:** Transfer Orbit to Saturn with 30MW Jet Power.

Saturn	Fuel	Consumed (kg)										
Pj	30.000 (MW)	nju	120.000 (deg)	r	-5.0000	8.6603	V	-0.2739	-0.1581			
TOF (TU_Sun)	20.000	22.000	24.000	26.000	28.000	30.000	32.000	34.000	36.000	38.000	40.000	
VSI type I	6772.1	6242.3	5816.0	5455.4	5140.0	4857.7	4601.3	4365.9	4148.5	3946.7	3758.9	
VSI typeII	69645.0	76609.5	83574.0	90538.5	97503.0	100000.0	100000.0	100000.0	100000.0	100000.0	100000.0	
CSI type I	6516.6	5860.9	4089.3	3195.7	6127.5	2493.1	2419.5	3427.4	3845.5	1918.8	2588.0	
CSI typeII	50144.4	49643.0	48138.6	45631.4	49141.5	45130.0	48138.6	51147.3	54156.0	57164.6	100000.0	
highThrust	99698.5	99640.2	99600.0	99577.6	99570.8	99576.6	99591.8	99613.1	99637.9	99664.0	99689.9	
Pj	30.000 (MW)	nju	150.000 (deg)	r	-8.6603	5.0000	V	-0.1581	-0.2739			
TOF (TU_Sun)	20.000	22.000	24.000	26.000	28.000	30.000	32.000	34.000	36.000	38.000	40.000	
VSI type I	4617.4	4255.5	4002.6	3810.7	3654.4	3519.8	3399.1	3288.1	3184.1	3085.6	2991.8	
VSI typeII	69645.0	76609.5	83574.0	90538.5	97503.0	100000.0	100000.0	100000.0	100000.0	100000.0	100000.0	
CSI type I	9803.5	5256.5	4229.3	8277.0	3854.2	2294.1	2839.1	9729.8	2769.2	3574.4	1764.6	
CSI typeII	50144.4	66190.6	42121.3	45631.4	42121.3	57164.7	72208.0	51147.3	45130.0	57164.6	60173.3	
highThrust	99369.4	99086.7	98824.4	98611.2	98460.4	98373.1	98342.9	98358.7	98408.6	98480.9	98566.1	
Pj	30.000 (MW)	nju	180.000 (deg)	r	-10.0000	-0.0000	V	0.0000	-0.3162			
TOF (TU_Sun)	24.000	26.000	28.000	30.000	32.000	34.000	36.000	38.000	40.000	42.000	44.000	
VSI type I	2795.0	2652.5	2556.5	2487.1	2433.0	2387.5	2347.1	2309.4	2273.3	2237.9	2203.1	
VSI typeII	83574.0	90538.5	97503.0	100000.0	100000.0	100000.0	100000.0	100000.0	100000.0	100000.0	100000.0	
CSI type I	5923.3	4295.8	6359.6	4098.5	8041.8	5758.1	7503.3	2269.8	8679.2	2777.9	5029.6	
CSI typeII	42121.3	45631.4	42121.3	67695.0	48138.6	42622.8	54156.0	38109.8	50144.4	52651.6	66190.6	
highThrust	99108.2	98745.0	98372.4	98023.9	97725.5	97493.0	97331.2	97236.4	97199.5	97209.0	97253.4	

**Table 7-4:** Time Until Spacecraft Mass ( $m_0 = 100\text{MT}$ ) Becomes Zero (in TU\_Sun).

$I_{sp}$ (sec)	Jet Power (MW)		
	10	20	30
10,000	9.572	4.786	3.191
20,000	38.290	19.145	12.763
30,000	96.152	43.076	28.717

required thrust level drastically, and therefore the fuel requirements are less than that of VSI type I with less than one full revolution. For example, as seen in table A-12, if the target is Jupiter with a  $\Delta\nu = 90^\circ$  for a 10MW jet power and a time of flight more than 10 TU, CSI type I requires less fuel than VSI type I. Fig. 7-4 shows the VRML screen shot for this result when the time of flight is 14 TU. The spacecraft for these cases revolves around the Sun more than one time. This happens often when the target planets are far from the Sun (e.g. Jupiter and Saturn). Currently, *SAMURAI* does not always allow the VSI engine to choose a trajectory with more than one revolution. However, if the appropriate initial guess for control variables is chosen and a trajectory with more than one revolution could be obtained for VSI type I, VSI type I should require less propellant mass than CSI type I, or at least the same amount of the fuel should be required. This is due to the same reasons argued above that if the constant  $I_{sp}$  history is more effective than variable  $I_{sp}$ , the control



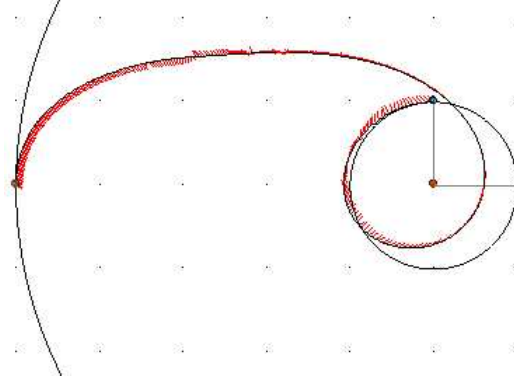


**Figure 7-4:** A Trajectory with More Than One Revolution - CSI type I engine.

history for variable  $I_{sp}$  should look like the one for constant  $I_{sp}$ .

The fact that VSI type I always requires less fuel than CSI type I was confirmed by manually choosing the initial guess of the control variables for several cases. When the initial guess of the control variables was adjusted for a VSI type I engine so that the spacecraft travels around the Sun more than one revolution, the fuel requirement becomes less than that of a CSI type I engine having more than one revolution.

As explained in Sec. 7.1, the range for the time of flight for each destination is selected so that it includes the time of flight that minimizes the fuel consumption for high thrust. It is interesting that when the destination is Venus or Mars, the time of flight that minimizes the fuel consumption is almost the same value for all of five types of engines. For example, the trajectories from Earth to Venus with a  $\Delta\nu = 120^\circ$  and a jet power of 10 MW, the fuel consumption is minimized for all of five engines at a time of flight of 1.8 TU. This also happens for trajectories from Earth to Mars with a  $\Delta\nu = 90^\circ$  and a jet power of 10 MW, where the time of flight to minimize the fuel consumption is 2.2 TU.

However, for the destinations far from the Sun (such as the asteroid, Jupiter, and Saturn), the above statement does not hold. For a trajectory from Earth to an asteroid with a  $\Delta\nu = 180^\circ$  and a jet power of 10 MW, the time of flight that minimizes fuel consumption for VSI type I is 8.0 TU, 7.0 TU for VSI type II, 7.5 TU for CSI type I, 7.0 TU for CSI type II, and 9.5 TU for high thrust. This can be explained in the following way: if the destination is near the Sun (and hence the trajectory is near the Sun), the gravitational force from the

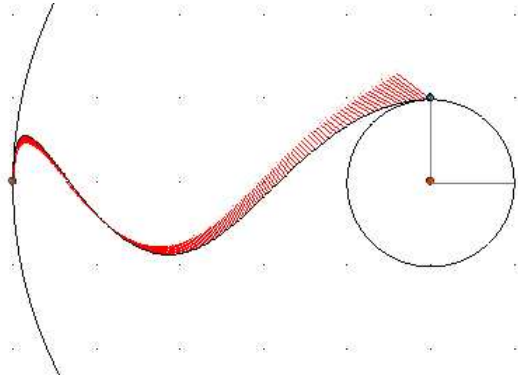


**Figure 7-5:** A Trajectory with Long Time of Flight - VSI type I engine.

Sun dominates the spacecraft's motion, and therefore the acceleration exerted by the engine is less effective than the acceleration due to the force from the Sun. The trajectories will then look similar for each of the engine types and therefore the flight times are similar for each. When the spacecraft is far from the Sun, the effect from the acceleration of the engine is larger than that of the Sun, and the spacecraft gets more freedom compared to the spacecraft near the Sun. The spacecraft can then choose the time of flight that is best for its engine type.

For many of the cases where the destination of the spacecraft is Jupiter or Saturn, the fuel consumption for the VSI type I becomes smaller and smaller as the time of flight becomes longer and longer (such as the case in Table A-9, Earth  $\rightarrow$  Jupiter with a  $\Delta\nu$  of  $90^\circ$  and a jet power of 10 MW). Hence for a VSI type I, it is desirable to have a very long flight time, assuming that there is no constraint on time of flight. It is shown in Fig. 7-5 that when the required time of flight is considerably long, the spacecraft wanders around between Earth and the target planet and just wastes time. This kind of movement is possible because the spacecraft is far from the Sun and the gravitational force from the Sun is relatively small.

The VSI type I engine is the fictitious engine that does not have any constraints on  $I_{sp}$ . Because VSI type II has a constraint on  $I_{sp}$ , it always requires more propellant than type I, or at least the same amount of the propellant as type I. When the time of flight is very short and the constraint on  $I_{sp}$  is always inactive, the control history becomes exactly the

same as type I, then the fuel consumption also becomes the same. On the other hand, as the time of flight increases, because a lower thrust will be used for a longer time of flight, the duration the constraint is active becomes longer. At a certain point when the time of flight is very long, the  $I_{sp}$  constraint becomes always active, then a VSI type II engine acts like a CSI type I engine (constant thrust and constant  $I_{sp}$ ).

**Table 7-5:** Fuel Consumption for VSI type II and CSI type I (kg).

TOF (TU_Sun)	9.0	10.0	11.0	12.0	13.0	14.0
VSI type II	28647.2	23229.7	31611.1	27858.0	30179.5	32501.0
CSI type I	24109.9	23215.0	25536.5	27858.0	30179.5	32501.0

Initial mass is 100,000 kg.

Maximum allowable  $I_{sp}$  for CSI type I is 30,000 sec.

Table 7-5 shows the fuel consumption for VSI type II and CSI type I for a trajectory from Earth to Jupiter with a  $\Delta\nu$  of  $90^\circ$  and a jet power of 10 MW. The  $I_{sp}$  for both engines is constrained at a maximum allowable  $I_{sp}$  of 30,000 sec. As seen in this table, when the time of flight exceeds 12 TU, the fuel consumption for both engines becomes the same. The thrust level for both engines is constant throughout the travel time with 30,000 sec  $I_{sp}$ . Using a VSI engine in this way is not recommended because the merit of using a VSI engine is that it can modulate its thrust and  $I_{sp}$ .

Figs. 7-6 and 7-7 show examples of the relationships among thrust,  $I_{sp}$ , and  $I_{sp}$  constraints for the VSI engine. It is shown in Fig. 7-6 that, as the constrained  $I_{sp}$  level decreases, the thrust level for unconstrained part decreases as well. This is because the spacecraft must spend unnecessary fuel during the constrained arcs, and therefore during the unconstrained arcs less thrust is enough. When the constrained  $I_{sp}$  level reaches 6,736 sec, the engine does not have to modulate its thrust and  $I_{sp}$  any more, and the thrust level is constant at 302.8 N throughout the trajectory. If the constrained  $I_{sp}$  level is less than 6,736 sec the spacecraft starts wasting the fuel because it has to exhaust more fuel than it needs to accomplish the mission.

From the discussions up to this point, the following statement could be derived: the fuel consumption for VSI type II engine with an  $I_{sp}$  limit of  $x$  seconds is always between that

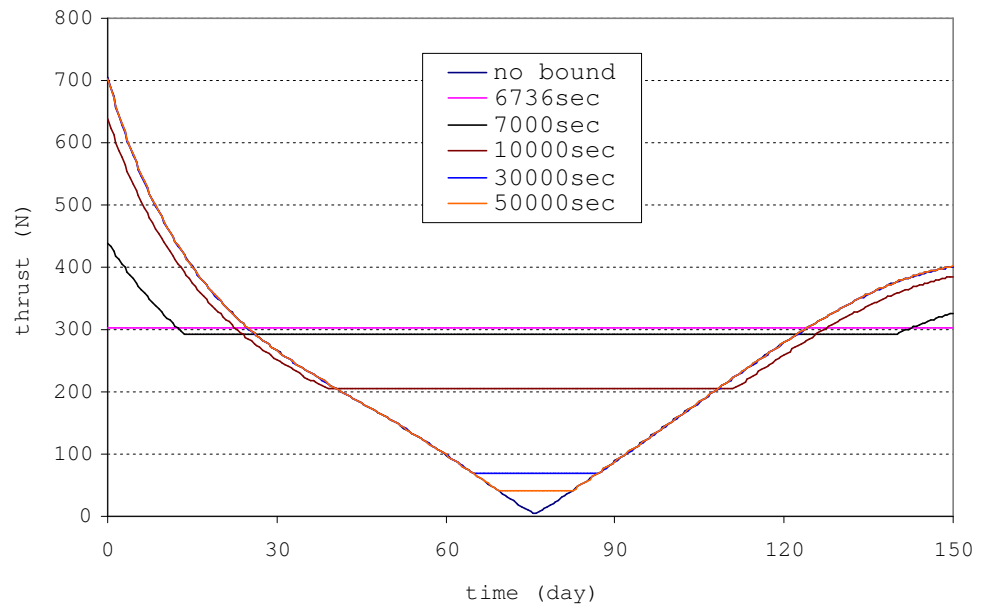


**Figure 7-6:** VSI type II: Thrust History for Different Levels of  $I_{sp}$  Limit.

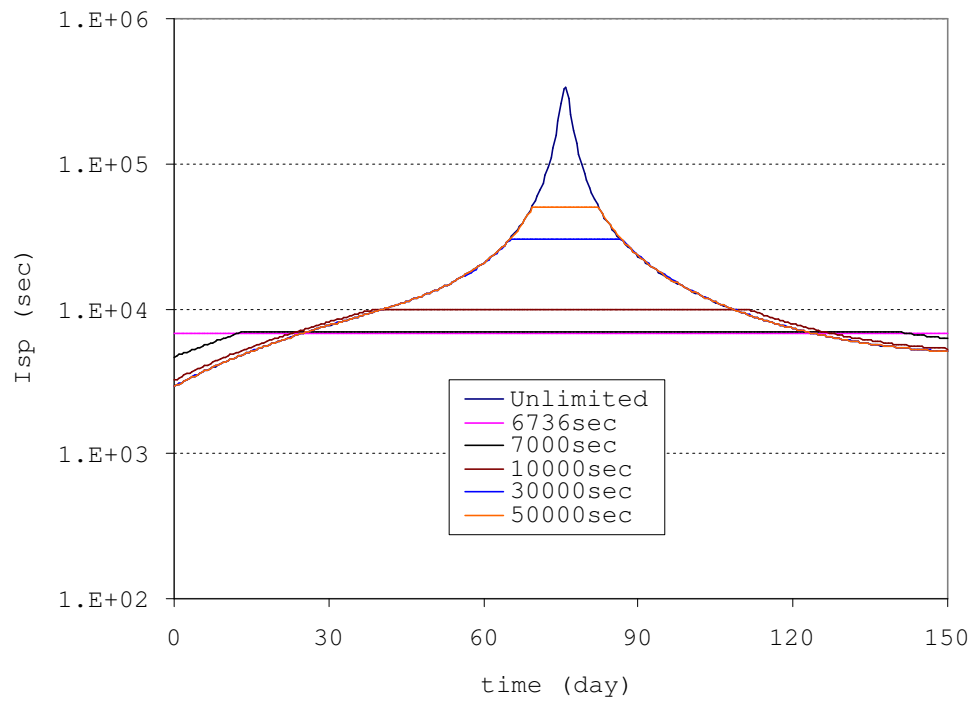


**Figure 7-7:** VSI type II:  $I_{sp}$  History for Different Levels of  $I_{sp}$  Limit.

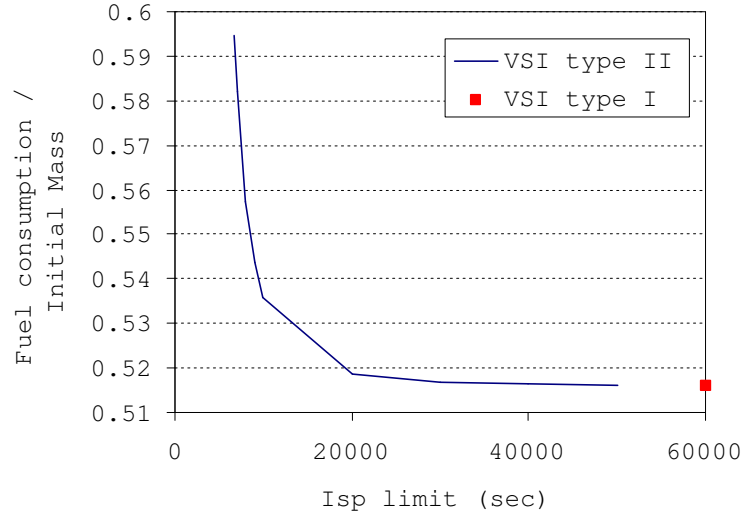


**Figure 7-8:** VSI type II: Fuel Consumption for Different Levels of  $I_{sp}$  Limit.

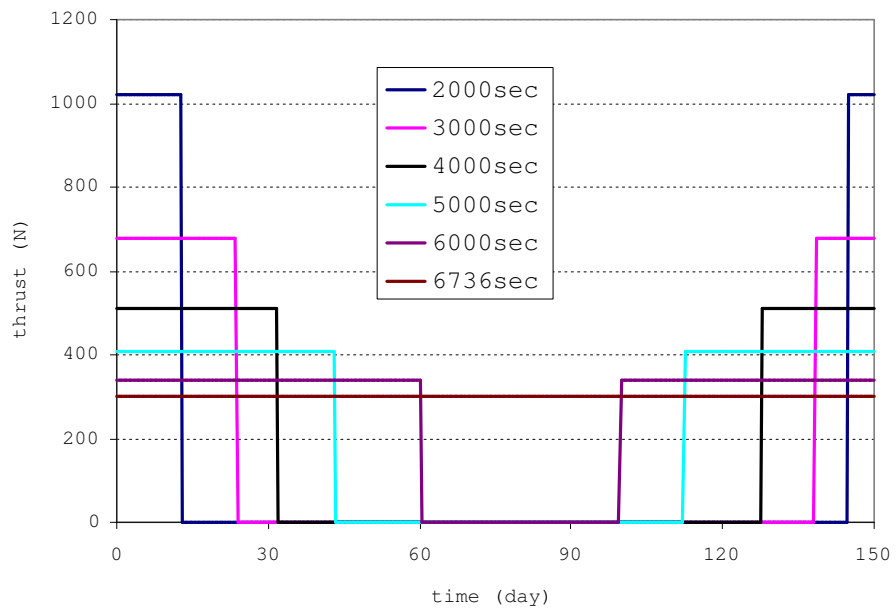
of the VSI type I and that of the CSI type I engine whose  $I_{sp}$  is  $x$  seconds.

Fig. 7-8 is the fuel consumption divided by the initial mass (100 MT) for different  $I_{sp}$  constraint levels. The value at an  $I_{sp}$  limit of 60,000 sec is the value for unconstrained case. It is easily seen that as the  $I_{sp}$  limit decreases, the thrust level and fuel consumption increase.

Figs. 7-9 and 7-10 show examples of the relationships among thrust,  $I_{sp}$ , and the  $I_{sp}$  constraints for the CSI type II engines. The initial and target conditions and time of flight are the same as the ones used for the VSI type II engines in the above discussion.

When the  $I_{sp}$  level is low, the thrust history looks like the one for a high thrust engine. Short burns are also required at the departure and at the arrival portions of the trajectory. As the  $I_{sp}$  level increases, more burn time will be required because the thrust level decreases, and when the  $I_{sp}$  reaches 6,736 sec, the engine with a thrust of 302.8 N has to be on in order for the spacecraft to reach the target.

Fig. 7-11 is the fuel consumption of the CSI type II engines for different  $I_{sp}$  levels. For reference, the fuel consumption for high thrust with 450 sec  $I_{sp}$  is shown in this figure. It is interesting that the fuel consumption for a 6,736 sec  $I_{sp}$  continuous thrust engine is more



**Figure 7-9:** CSI type II: Thrust History for Different Levels of  $I_{sp}$  Limit.

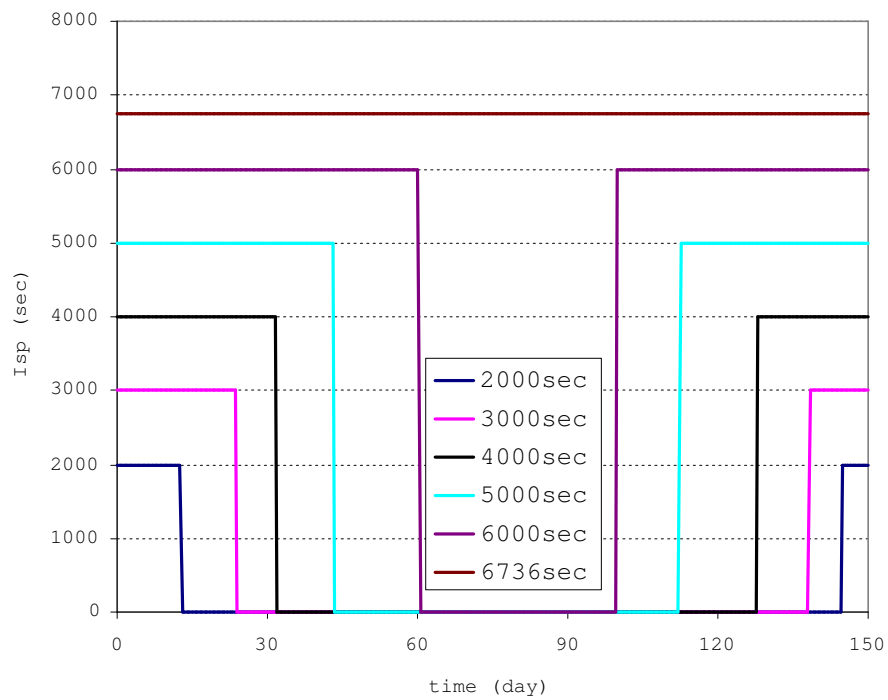


**Figure 7-10:** CSI type II:  $I_{sp}$  History for Different Levels of  $I_{sp}$  Limit.

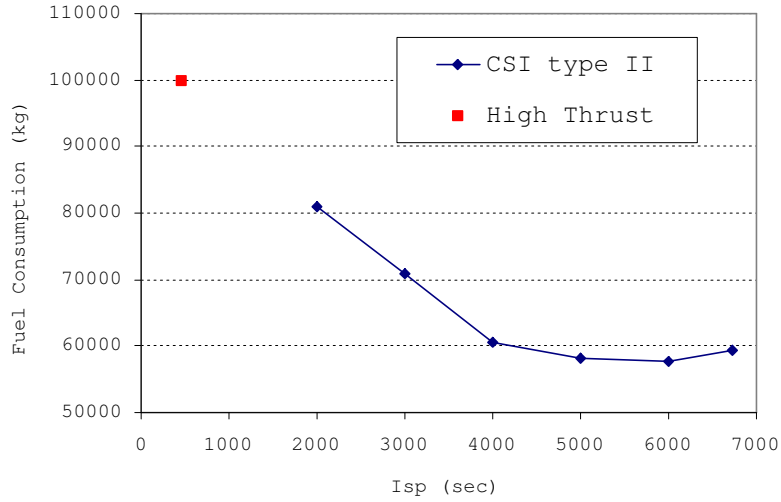


**Figure 7-11:** CSI type II: Fuel Consumption for Different Levels of  $I_{sp}$ .

than that of 6,000 sec or 5,000 sec bang-off-bang engine. That means the higher  $I_{sp}$  is not always effective for the CSI engine if the engine has the capability of switching on and off. In some cases, not firing the engine around the midpoint of the trajectory positively impacts the fuel consumption. This kind of result is often obtained (such as a trajectory from Earth to Venus with a  $\Delta\nu$  of  $90^\circ$ , a jet power of 10 MW, and a 1.4 to 2.0 TU time of flight as is shown in in Table 7-2) where the engine should only be fired at the departure and arrival segments of the trajectory in order to save fuel.

#### **7.4 Relationship among Fuel Consumption, Jet Power, and Travel Distance**

An additional calculation is performed in order to answer the following question: Is it possible to determine a relationship between the fuel consumption and the jet power, or between the fuel consumption and the distance between departure and arrival planets?

Several additional trajectories are calculated from Earth to Mercury, Venus, Mars, the asteroid, Jupiter, and Saturn whose  $\Delta\nu$ 's from Earth are  $180^\circ$ , and several values of time of flight are considered for each destination. Fuel consumption for the VSI type I and CSI type I engines are calculated and compared. The shorter time of flight was chosen for examples in this section. This is because a longer time of flight may result in a trajectory with more

than one revolution for the CSI type I engine, which may cause trouble in comparing fuel consumption.

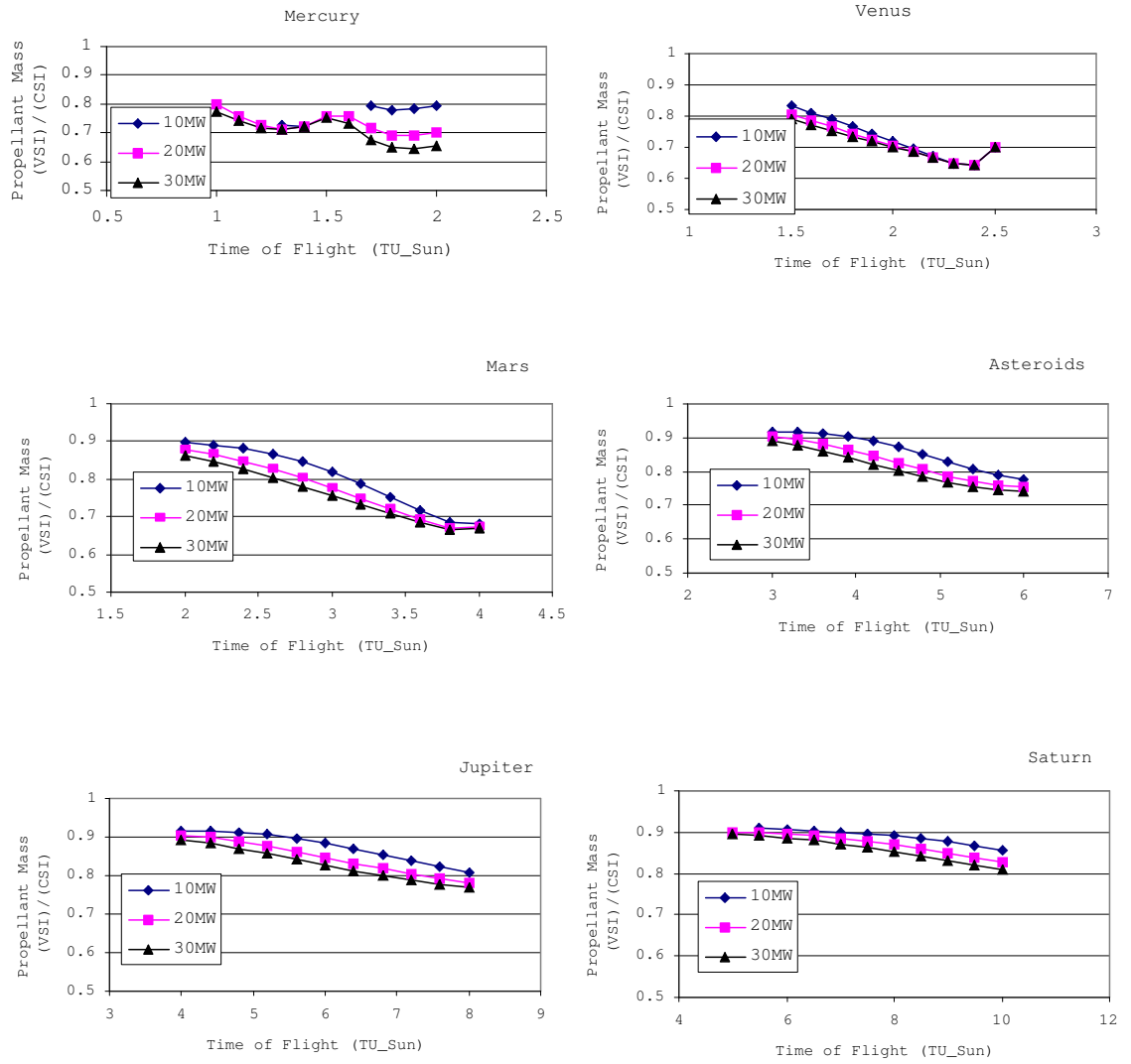
Fig. 7-12 shows the relative fuel consumption of the VSI type I with respect to CSI type I. The values shown in the figure are “fuel consumed with VSI” divided by “fuel consumed with CSI”. Therefore lower values mean that using a VSI type I engine needs less fuel than a CSI type I engine. This figure shows that a higher power to mass ratio ( $P/m$ ) is always better for the VSI engines. This result coincides with the result from the preliminary study of a simple trajectory outlined in Chap. 3.

Fig. 7-13 shows the relative fuel consumption as a function of distance between the Sun and the target planet.  $I_{sp}$  for CSI for each mission is maximized so that the fuel consumption is minimized for each case. From this figure, we may conclude that it is relatively more effective to use the VSI engine near the Sun. However, because these values are strongly affected by the time of flight and the jet power, the above conclusion may not hold for every case. If this conclusion is true, the result does not coincide with the result from Chap. 3 because in Chap. 3 we concluded that the merit of using a VSI engine increases as the travel distance increases.

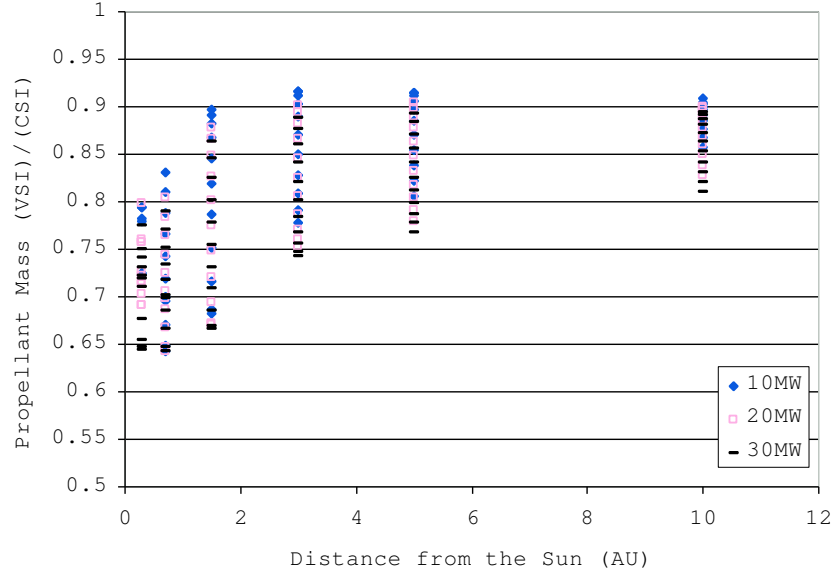
In Chap. 3, the  $I_{sp}$  values for the CSI engine (type I) are the same for all cases. Hence the fuel consumption is proportional to the time of flight. Whereas in this chapter the  $I_{sp}$  level for CSI in each case is different because *SAMURAI* calculates the minimum required thrust (and therefore maximum required  $I_{sp}$ ) that allows the spacecraft reach its target, given a limit on jet power. In such a case the fuel consumption is very likely to decrease as the time of flight increases. This is because as the time of flight increases, lower thrust level may be sufficient. Fig. 7-15 shows the fuel consumption for both the VSI and CSI engines where the  $I_{sp}$  for the CSI engine can be freely chosen. As shown in this figure,  $I_{sp}$  level for both CSI and VSI decreases as the time of flight increases because lesser thrust is sufficient for a longer time of flight.

Fig. 7-14 shows the relative fuel consumption as a function of distance between the Sun and the target planet. In this figure,  $I_{sp}$  for CSI is the same (30,000 sec) for all missions. This figure shows that as the travel distance increases using VSI engines is more efficient





**Figure 7-12:** Relative Fuel Consumption of VSI with respect to CSI: Comparison by Jet Power.



**Figure 7-13:** Relative Fuel Consumption of VSI with respect to CSI: Comparison by Distance from the Sun (The Best  $I_{sp}$  is Chosen for Each CSI Mission).

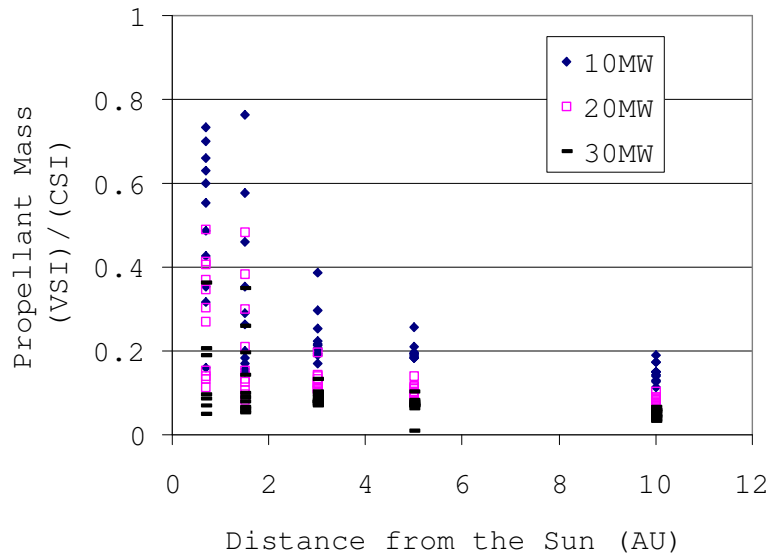


**Figure 7-14:** Relative Fuel Consumption of VSI with respect to CSI: Comparison by Distance from the Sun ( $I_{sp}$  for CSI is the Same for All Missions).

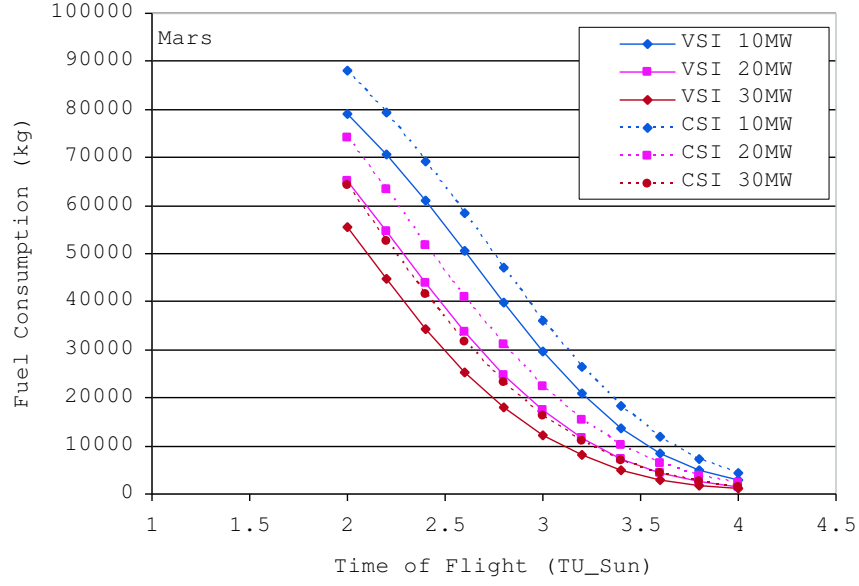


**Figure 7-15:** Fuel Consumption between VSI and CSI: When  $I_{sp}$  for CSI Differs for Each Mission.

than using CSI engines. These more constrained results coincide with the results from Chap. 3.

Fig. 7-16 shows the fuel consumption for both the VSI and CSI engines where the  $I_{sp}$  of the CSI is fixed to 15,000 sec for all cases. Some points for CSI are missing because at these points the  $I_{sp}$  of 15,000 sec is too high and therefore the thrust is too low to reach the target. When the  $I_{sp}$  is fixed, the fuel consumption for the CSI increases as time of flight increases because fuel consumption is proportional to the time of flight. It is apparent that when a fixed value of  $I_{sp}$  is used for the CSI engine, more fuel is required as the distance from the Sun and the target planet increases, because it usually takes more time to get there. This means that a VSI engine gets relatively more advantageous than a CSI engine as the distance between the Sun and the target planet increases.

In summary, these statements are obtained:

- The merit of using a VSI engine against a CSI engine increases as the power to mass ratio of the spacecraft increases.
- The merit of using a VSI engine over that of a CSI engine may increase or decrease

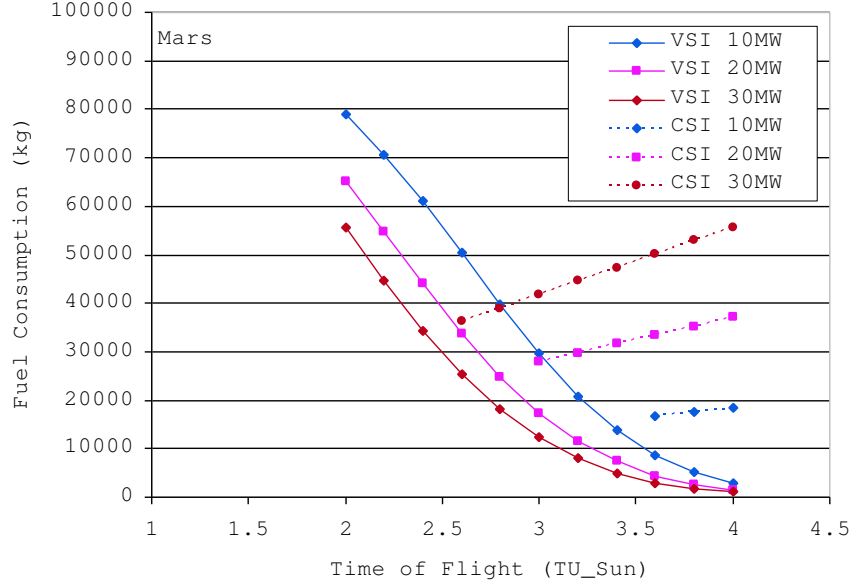


**Figure 7-16:** Fuel Consumption between VSI and CSI: When  $I_{sp}$  for All CSI Cases Are the Same.

as the travel distance increases depending on the problem settings.

- If the  $I_{sp}$  level of the CSI engine is fixed for any mission profile (any time of flight and any target conditions), the relative merit of using a VSI engine increases as the travel distance increases. Therefore, using a VSI engine for a transfer to Pluto is the most efficient.
- If the best  $I_{sp}$  level for the CSI engine is chosen for each mission depending on the mission profile (as done in a power-limited case), the merit of using a VSI engine decreases as the travel distance increases. Hence, using a VSI engine for a transfer to Mercury is the most efficient.

## CHAPTER VIII

### NUMERICAL EXAMPLES: “REAL WORLD” PROBLEMS

In this chapter, the real ephemeris of planets is used to calculate the transfer trajectories from Earth to various planets. Engines considered in this chapter are VSI type II (constrained  $I_{sp}$ ) with maximum allowable  $I_{sp}$  of 30,000 sec, CSI type I (continuous thrust), CSI type II (bang-off-bang) with 5,000 sec  $I_{sp}$ , and high thrust with 450 sec  $I_{sp}$ .

Although the results with VSI type I engines that have no constraints on  $I_{sp}$  (and therefore unrealistic) were not compared with the results of other types of engines, they were used to estimate the departure date and time of flight that minimize fuel consumption for other types of engines because computationally the VSI type I can be solved faster. As stated in the last chapter, the value of time of flight that minimizes the fuel consumption is sometimes the same for each engine type, and therefore the results with VSI type I engines are useful. Ten MW's of jet power is assumed for all cases.

Before going to the actual calculations, the concept of “synodic period” is introduced. A synodic period is defined as the time required for any phase angle between two planets to repeat itself [12]. This parameter is used to determine the launch opportunity. For two planets whose periods are  $p$  and  $q$ , the synodic period is expressed as  $1/(1/p - 1/q) = pq/(q - p)$ . If we miss a particular launch opportunity, we must wait until a desirable phase angle comes around again. For example, the synodic period of Earth and Mars is 780 days (2.14 years), and Earth and Venus is 584 days (1.6 years). So if we miss a launch opportunity to Mars, we have to wait until the next opportunity comes 2.14 years later. Usually transfer trajectory calculation for one synodic period is enough because fuel requirements show repetitive patterns for each synodic period.

## ***8.1 Scientific Mission to Venus***

### **8.1.1 Venus Exploration**

If Earth had a twin, it would be Venus. Venus is sometimes called Earth's "sister planet." The two planets are similar in size, mass, composition, and distance from the Sun. But there are also many differences. Venus has no oceans, and it is covered by thick, rapidly spinning clouds that trap surface heat. Therefore the surface temperature is over 450 °C, hotter than the surface of the planet Mercury. The high density of the atmosphere results in a surface pressure 90 times that of Earth. Because Venus reflects so much sunlight, it is usually the brightest planet in the sky.

Several probes have been sent to Venus so far. Two of them landed on the Venusian surface. The Magellan probe, launched in 1989, was the last spacecraft sent to Venus. This is partly because Venus seems less interesting than Mars and other outer planets. However, the ESA (European Space Agency) is planning to launch a Venus orbiter mission named "Venus Express (VEX)" in November 2005.

### **8.1.2 Problem Description**

Because the synodic period of Earth and Venus is 584 days, a grid search for launch date is performed for a 600-day range starting from Jan. 1, 2010. At first a wide range in time of flight is considered, then this range is narrowed down to an appropriate value, and the state and control variables for minimum fuel transfer for each engine type were analyzed. The initial mass of the spacecraft is set to 100 MT.

### **8.1.3 Results**

Fig. 8-1 shows the normalized fuel requirements for VSI type II with a 30,000 sec  $I_{sp}$  constraint. A 600-day range of launch dates starting from Jan. 1, 2010, with the time of flight between 100 and 300 days are calculated. A resulting value of 1.0 means either the program failed to calculate the results, or the mass becomes zero before reaching Venus. As shown in this figure, there is a region with very low values. For example, if the spacecraft leaves Earth on Aug. 1, 2010, and time of flight is 160 days, the fuel requirement is just 3,195

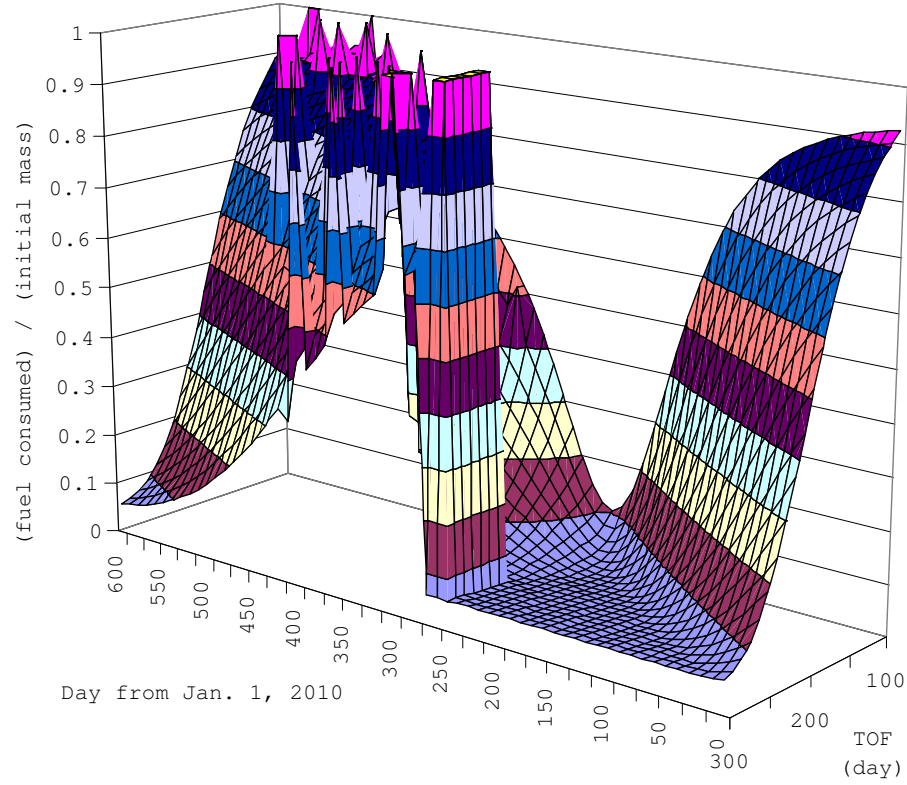


**Figure 8-1:** Fuel Consumption for VSI type II: Earth – Venus.

kg for a spacecraft with 100 MT initial mass. Fig. 8-2 shows the trajectory for this case drawn using VRML. The short red arrows along the trajectory shows the thrust directions. For this trajectory, the  $I_{sp}$  level is always 30,000 sec. In this case, if the time of flight is not restricted, the fuel consumption could be lowered by extending time of flight. However, using a VSI engine in this way is not desirable. As shown in Fig. 8-2, the thrust vectors are not aligned neatly around the midpoint. This is due to the fact that an engine that always operates at its maximum  $I_{sp}$  has to expel more fuel than required, because the spacecraft wastes fuel by thrusting in inappropriate directions. To avoid this from happening, we would rather shorten the time of flight.

The time of flight can be shortened at the expense of higher fuel cost. This would save mission operating cost and may mitigate the degradation of instruments due to the radiation from the Sun.

Fig. 8-3 shows the fuel requirements for the VSI type II for a 600-day range of departure

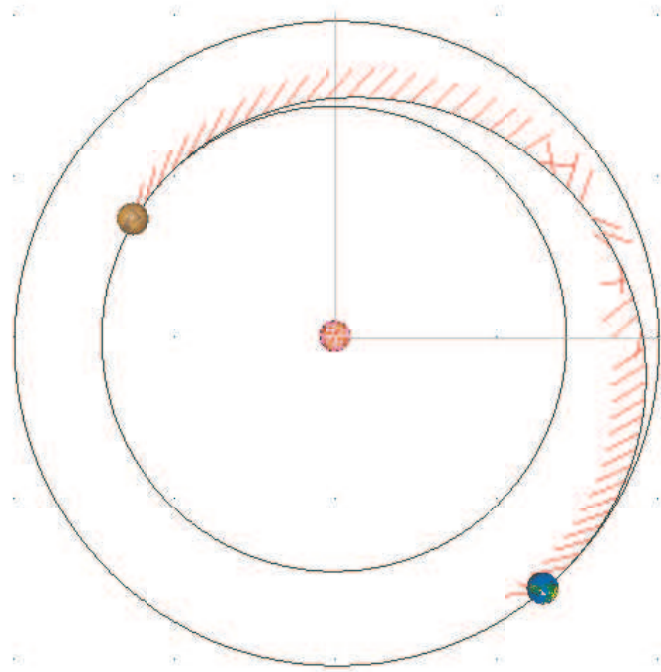


**Figure 8-2:** Trajectory from Earth to Venus with 160-day Time of Flight.

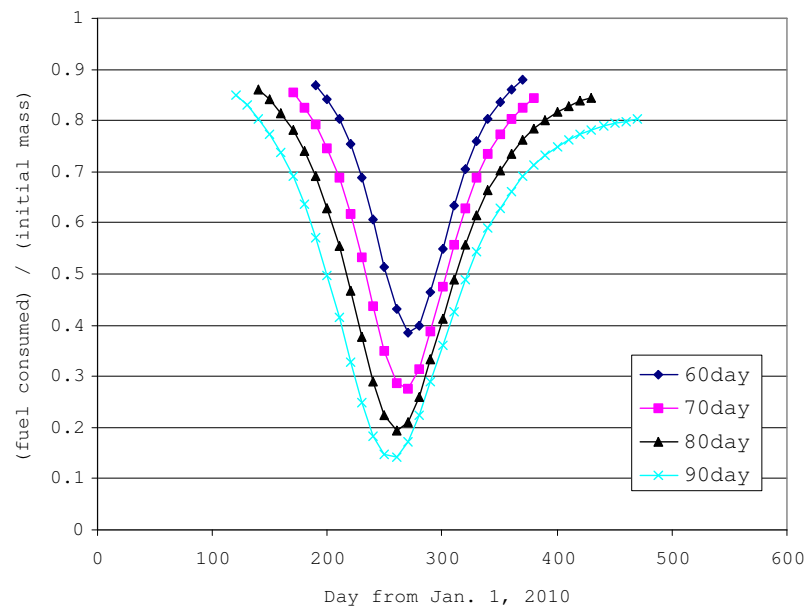


**Figure 8-3:** Fuel Consumption for VSI type II: Earth – Venus.



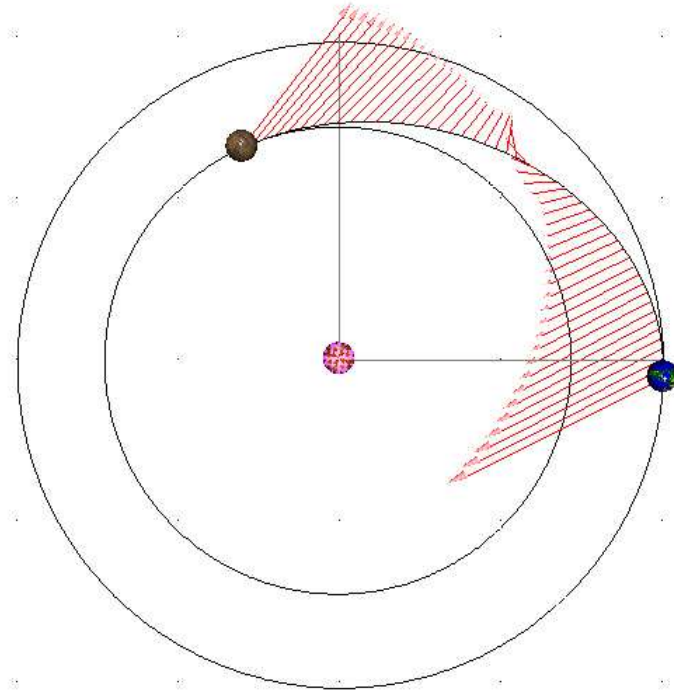


**Figure 8-4:** VSI type II Trajectory from Earth to Venus with 90-day Time of Flight.

dates with a time of flight between 60 and 90 days. If we choose Sep. 18, 2010, as the departure date with a 90-day time of flight, the minimum fuel consumption is achieved (14,302 kg). Fig. 8-4 shows the transfer trajectory, with thrust magnitude and direction displayed. Fig. 8-5 is the thrust steering angles and Fig. 8-6 shows the thrust magnitude and  $I_{sp}$ . Note that higher thrust is required at both departure and arrival. The thrust direction at departure is determined so that the spacecraft slows down and heads into a Venus' orbit which is inside the Earth's orbit. When the spacecraft nears Venus, the spacecraft further slows down to capture into Venus' orbit. Around the mid point of the trajectory, the  $I_{sp}$  constraint becomes active and the engine is operated with its maximum  $I_{sp}$  of 30,000 sec. This corresponds to a thrust level of 68 N when the jet power is 10 MW.

The same grid search is performed for CSI type I. The fuel requirements for a 600-day departure range with 60 to 90 day time of flight is shown in Fig. 8-7. The minimum fuel requirement for a 90-day time of flight is 18,865 kg. This occurs when the departure date is Sep. 8, 2010. Fig. 8-8 is a screen shot of the VRML for this trajectory. Similar to the

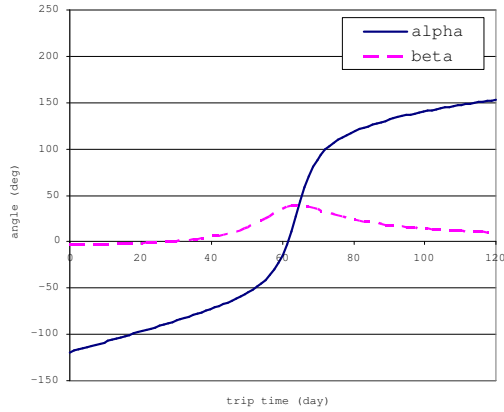


**Figure 8-5:** Thrust Steering Angle for VSI type II: Earth to Venus, 90-day Time of Flight.

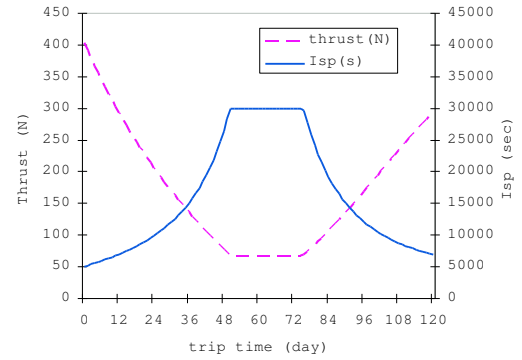


**Figure 8-6:** Thrust Magnitude and  $I_{sp}$  for VSI type II: Earth to Venus, 90-day Time of Flight.

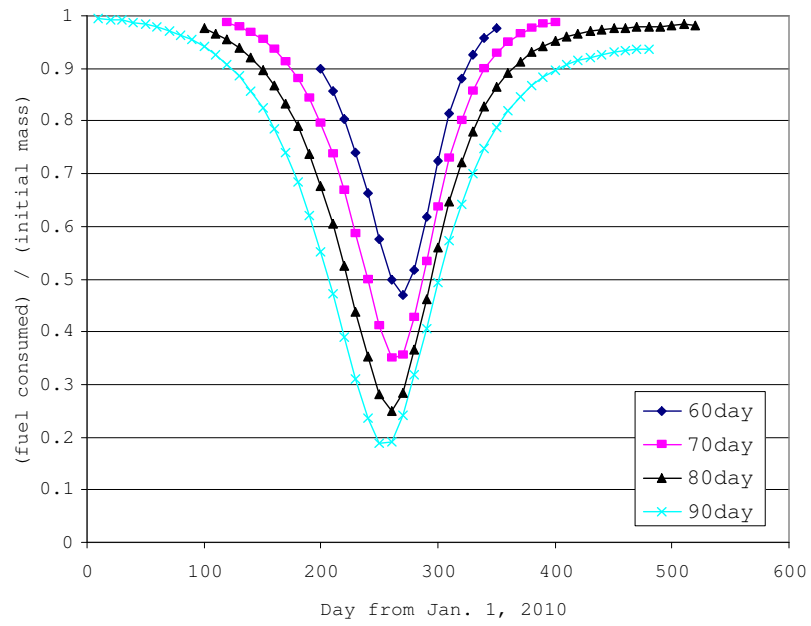
VSI type II, in order to reach the inner planet the spacecraft initially slows down its speed by expelling the fuel in the direction opposite to the velocity.

Fig. 8-9 shows the steering angle, and Fig. 8-10 is the thrust level and corresponding  $I_{sp}$  used throughout the CSI type I mission. *SAMURAI* calculated that, for 10 MW jet power, a thrust level of 220 N is required for this 90-day transfer. The  $I_{sp}$  corresponding to this thrust level is 9,270 sec.

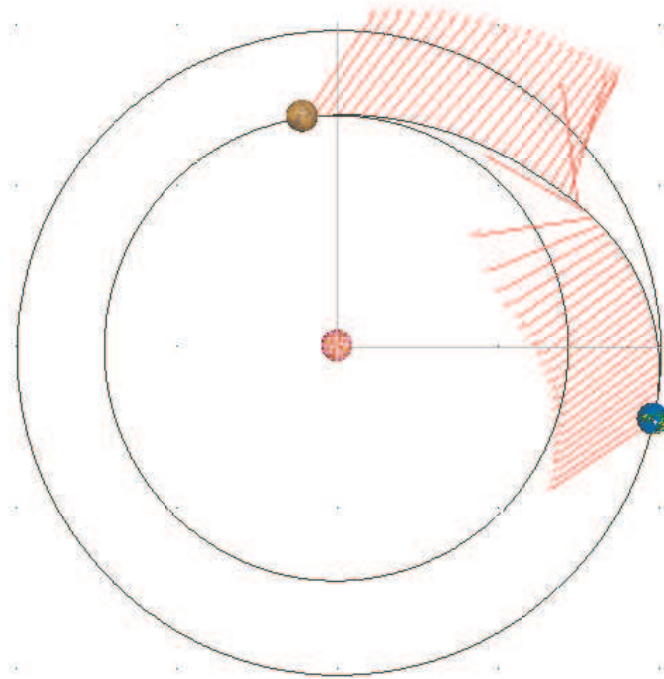
The trajectory for the CSI type II with a 5,000 sec  $I_{sp}$  limit looks similar to the one in Fig. 8-11, resulting in a bang-off-bang control. When the departure date is Sep. 18, 2010, the fuel consumption is minimized (20,702 kg) for the 90-day time of flight.

Fig. 8-12 shows thrust steering angle, and Fig. 8-13 shows thrust magnitude and  $I_{sp}$ . The engine is on for 13.5 days at the departure, and 14.4 days at the arrival. The thrust level corresponding to an  $I_{sp}$  of 5,000 sec is 408 N when the jet power is 10 MW.

Fig. 8-14 shows the fuel requirements for an Earth to Venus transfer orbit with high thrust. A 60 to 90-day time of flight is considered. When the time of flight is 90 days, the minimum fuel required departure date is Sep. 8, 2010. The required  $\Delta V$  at the departure is 4.116 km/s, and the  $\Delta V$  at the arrival is 5.051 km/s. With the assumed 450 sec of  $I_{sp}$ , the



**Figure 8-7:** Fuel Consumption for CSI type I: Earth – Venus.



**Figure 8-8:** CSI Type I Trajectory from Earth to Venus with 90-day Time of Flight.

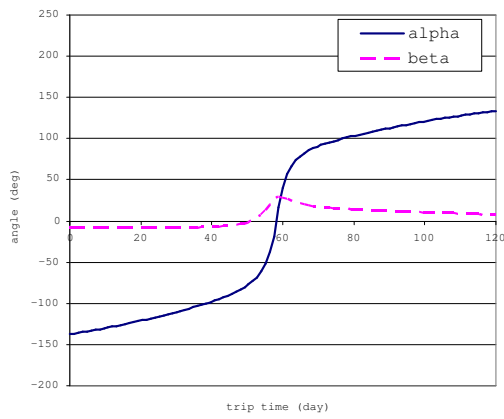


**Figure 8-9:** Thrust Steering Angle for CSI type I: Earth – Venus, Day 250, 90 day TOF.

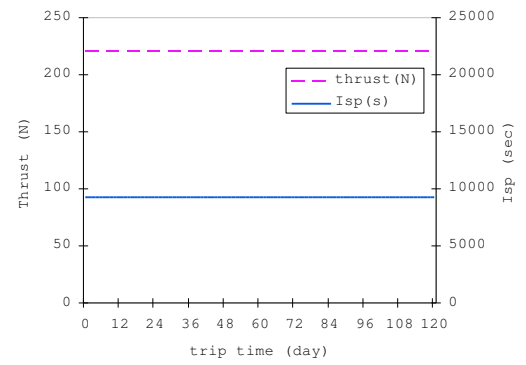


**Figure 8-10:** Thrust Magnitude and  $I_{sp}$  for CSI type I: Earth – Venus, Day 250, 90 day TOF.

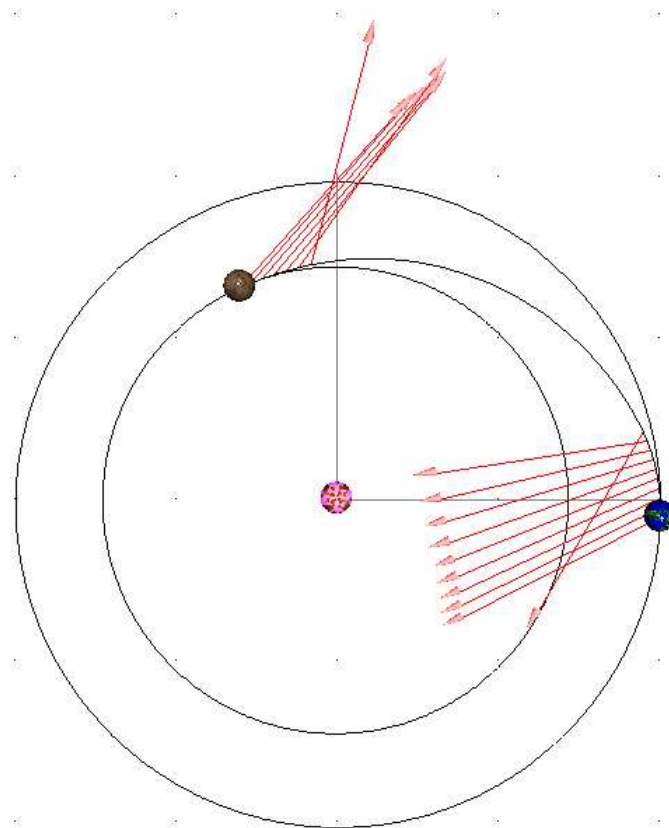


**Figure 8-11:** CSI Type II Trajectory from Earth to Venus with 90-day Time of Flight.

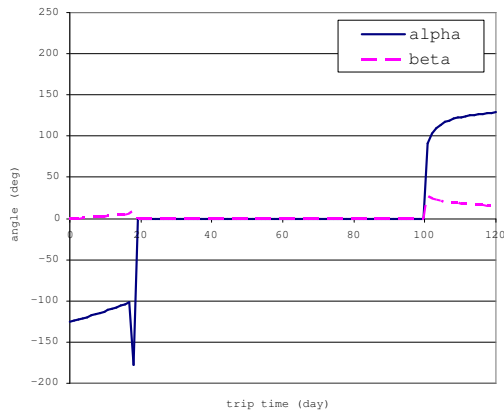


**Figure 8-12:** Thrust Steering Angle for CSI type II: Earth – Venus, Day 260, 90 day TOF.

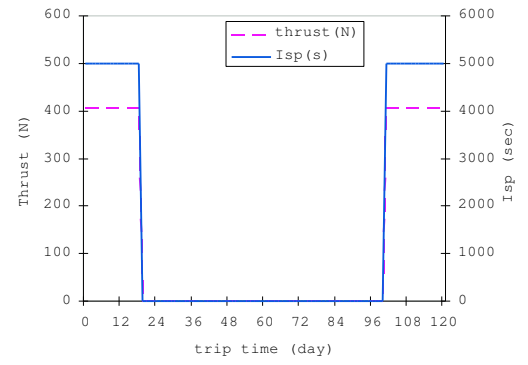


**Figure 8-13:** Thrust Magnitude and  $I_{sp}$  for CSI type II: Earth – Venus, Day 260, 90 day TOF.

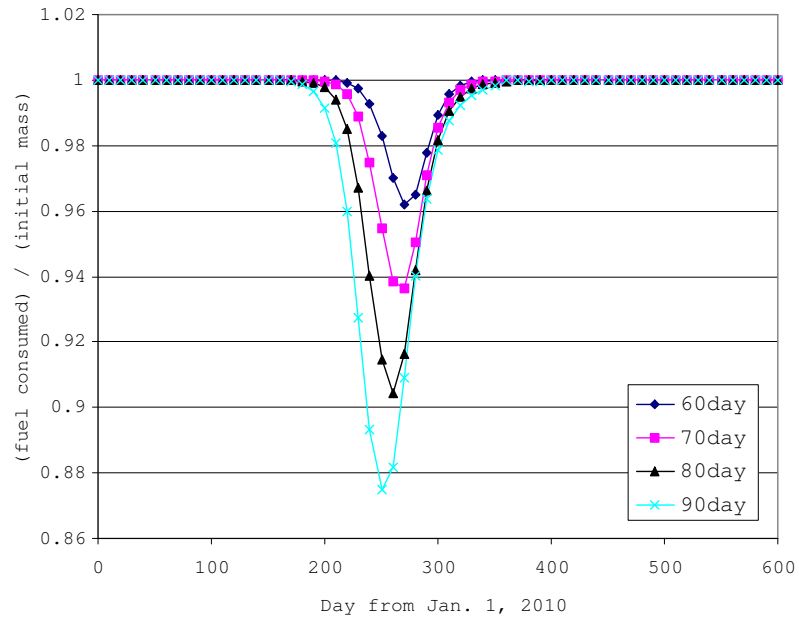


**Figure 8-14:** Fuel Consumption for High Thrust: Earth – Venus.

total fuel consumption is 87,475 kg. That means the weight of the probe may be restricted to less than a few percent of the initial mass unless non-zero  $C_3$ 's are assumed.

These results concluded that the VSI type II is most effective engine (least fuel required). As concluded in the last chapter, the departure date that minimizes the fuel requirements, is almost the same for all engine types.

## ***8.2 Human Mission to Mars: Round Trip***

### **8.2.1 Mars Exploration**

Outside of the Earth-Moon system, Mars is the most hospitable body in the solar system for humans and is currently the only real candidate for future human exploration and colonization [1].

In August of 1992, a “Why Mars” workshop was held in Houston, Texas. Six major elements behind the motivation for human Mars exploration were introduced by a consultant team consisting of 16 professionals from across the country.

- Human Evolution – Mars is the next logical step in the expansion of the human race into the stars.
- Comparative Planetology – by understanding Mars and its evolution as a planet, a better understanding of Earth will be achieved.
- International Cooperation – an international Mars exploration effort has the potential to bring about a sense of global unity as never seen before.
- Technological Advancement – the development of new and improved technologies for the Mars mission will enhance the lives of those on Earth while encouraging high-tech industry.
- Inspiration – the human Mars exploration mission will test our technological abilities to their maximum. The ingenuity of the mobilized populace will be tested and our accomplishments will serve to inspire future generations. A common focus will unite people from around the world as they expand the envelope of achievability.

- Investment – the cost of a crewed Mars exploration mission is reasonable when compared with the costs of other current societal expenditures.

### 8.2.2 Problem Description

Unlike unmanned missions whose time of flight is less important, the travel time for the human mission should be as short as possible in order to reduce crew exposure to zero gravity and cosmic radiation.

Therefore, in this section, the time of flight for each leg (outbound and inbound) is constrained between 90 days and 120 days. This range is much shorter than the planned missions by the chemical rockets whose time of flight is around 8 months. A grid search for departure date is conducted to find the best launch date that achieves the minimum fuel consumption. The range of departure dates for the outbound leg is 3,650 days from Jan. 1, 2010 with 10-day increments, and the range for inbound leg is 4,000 days from April. 1, 2010 with 10-day increments. Because the synodic period of Earth and Mars is about 2.14 years, there should exist about 4 to 5 minima in these search ranges. Time of flight was considered from 90 to 120 days with 10-day increments.

The initial outbound mass of the spacecraft is set to 100 MT. Although the actual initial mass for inbound leg may vary depending on the fuel consumption during the outbound leg, 80 MT is assumed. The  $I_{sp}$  constraint for VSI type II is 30,000 sec, and for CSI type II the  $I_{sp}$  is set to 5,000 sec.

### 8.2.3 Results

At first, a grid search for a VSI type I engine is performed. From this result, search ranges for VSI type II, CSI, and high thrust are determined. Fig. 8-15 and 8-16 show the fuel requirements for the outbound and inbound segments over a 10-year search range.

Table 8-1 shows the opportunities for an Earth – Mars round trip. It shows the departure date expressed as the number of days from Jan. 1, 2010, as well as the fuel requirements, the time of flight for outbound and inbound legs, the total fuel requirements, and the total trip time. It is shown in Table 8-1 that the launch opportunity for VSI type I which minimizes the fuel consumption occurs when the spacecraft leaves Earth on the 3,080th day from

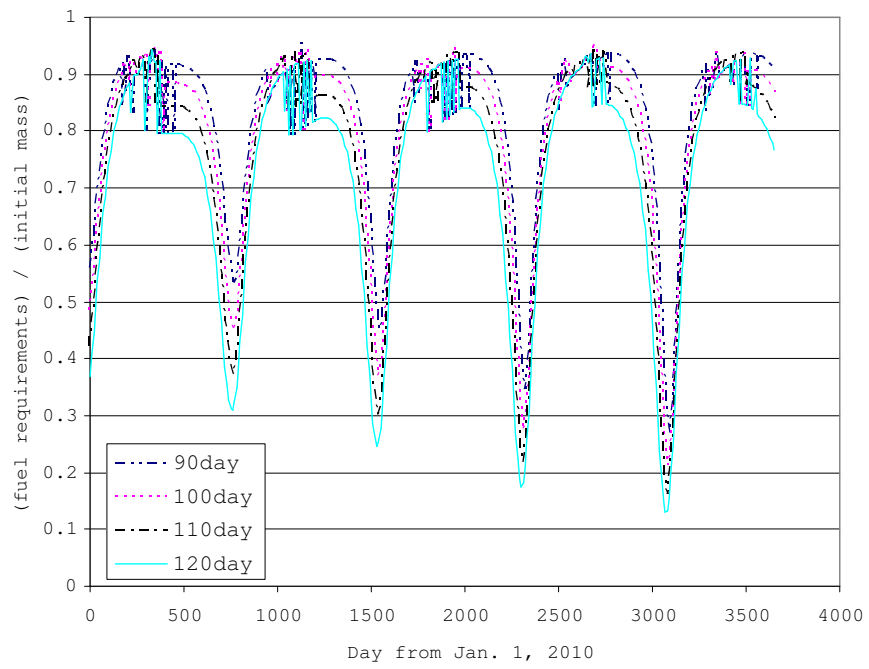


**Figure 8-15:** Fuel Consumption for VSI type I, 10 MW Jet Power: Earth – Mars Outbound.

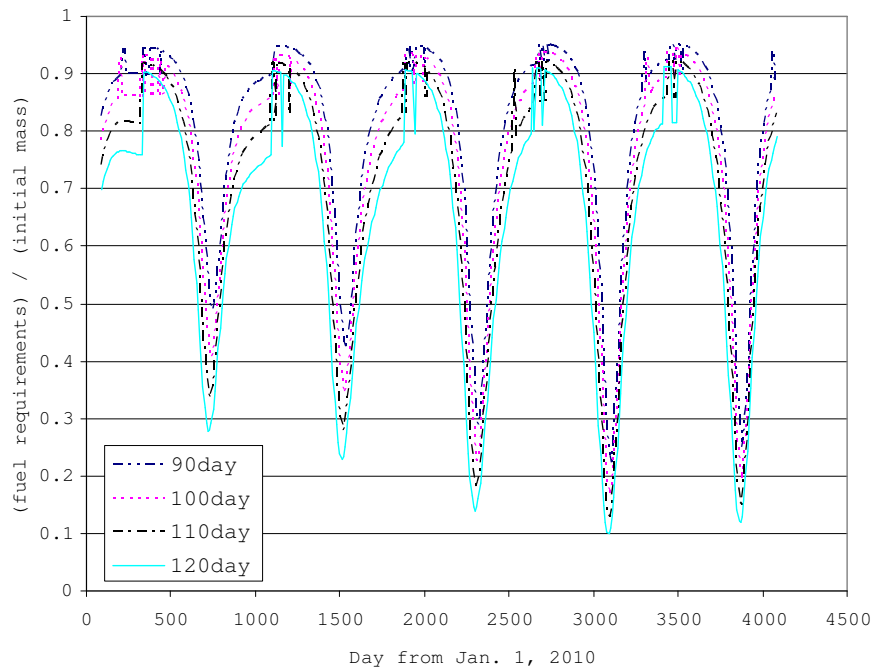


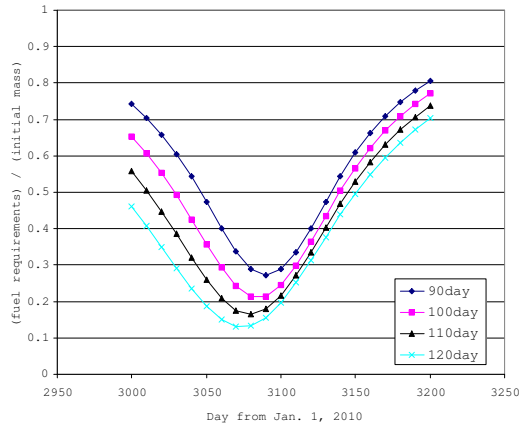
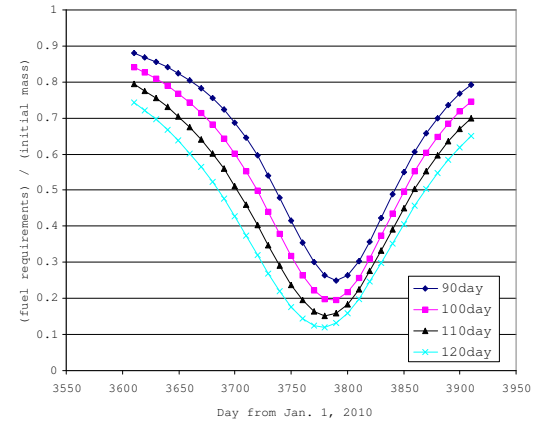
**Figure 8-16:** Fuel Consumption for VSI type I, 10MW Jet Power: Earth – Mars Inbound.



**Table 8-1:** Earth – Mars Round Trip Fuel Consumption for VSI type I.

No.	Outbound			Inbound			Total	
	Day	TOF	Fuel	Day	TOF	Fuel	Fuel	Time
1	760	120	31,055	1,520	120	27,870	58,925	1,640
2	1,530	120	24,573	2,310	120	14,502	39,075	2,430
3	2,310	120	18,149	3,090	120	9,888	28,037	3,210
4	3,080	120	13,182	3,870	120	11,807	24,989	3,990

Day: Day from Jan. 1, 2010, TOF (day), Fuel (kg), Time (day).

**Figure 8-17:** Fuel Consumption for VSI type II: Earth – Mars Outbound.**Figure 8-18:** Fuel Consumption for VSI type II: Mars – Earth Inbound.

Jan. 1, 2010, which is May 29, 2018, and leaves Mars on the 3,870th day, which is Aug. 6, 2020. Figs. 8-15 and 8-16 show that the best launch opportunity for the outbound trip may also exist between Day 3,000 and 3,200, and Day 3,700 to 4,000 for the inbound trip for other types of rockets. Based on these results, a finer grid search is performed around these departure dates for VSI type II, CSI type I and II, and high thrust. Figs. 8-17 and 8-18 show relative fuel requirements for a VSI type II engine for outbound trajectory and for inbound trajectory, respectively. Figs. 8-19 and 8-20 show the same quantities for a CSI type I engine, Figs. 8-21 and 8-22 are for a CSI type II engine, and Figs. 8-23 and 8-24 for a high thrust engine.

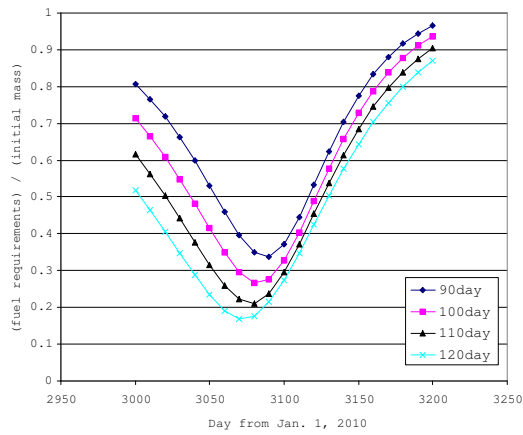


**Figure 8-19:** Fuel Consumption for CSI type I: Earth – Mars Outbound.

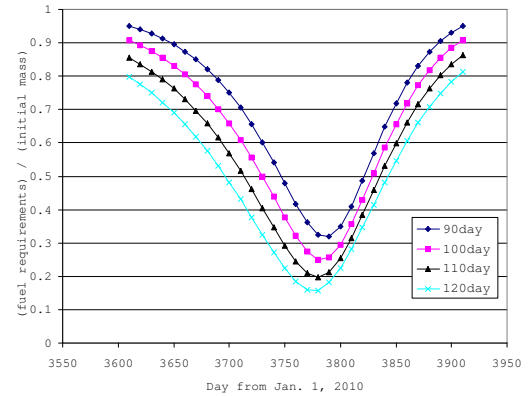


**Figure 8-20:** Fuel Consumption for CSI type I: Earth – Mars Inbound.

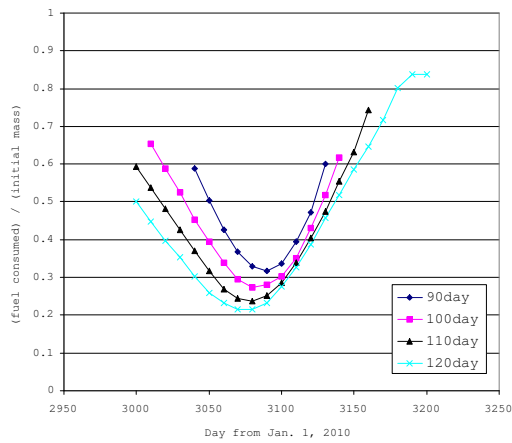


**Figure 8-21:** Fuel Consumption for CSI type II: Earth – Mars Outbound.

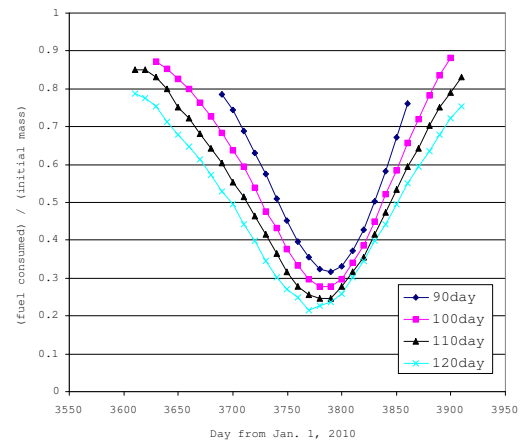


**Figure 8-22:** Fuel Consumption for CSI type II: Mars – Earth Inbound.

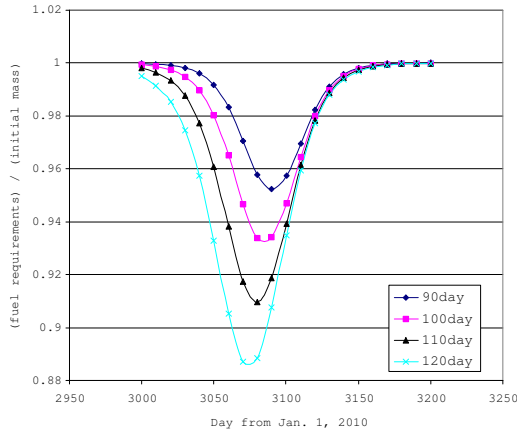


**Figure 8-23:** Fuel Consumption for High Thrust: Earth – Mars Outbound.

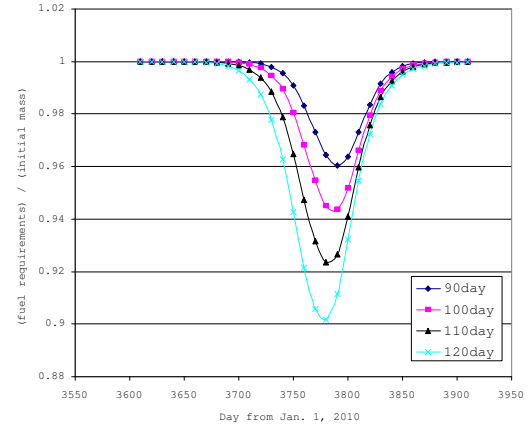


**Figure 8-24:** Fuel Consumption for High Thrust: Earth – Mars Inbound.

From these results, the minimum points for all cases exist around the 3,070th day for outbound and the 3,780th day for inbound. Further analyses with a finer grid are performed around these days. Table 8-2 shows the departure date, time of flight, and required fuel for the minimum fuel required cases for VSI type II, CSI type I, CSI type II, and high thrust. For high thrust,  $\Delta V$  is shown instead of fuel consumption.

**Table 8-2:** Earth – Mars Round Trip Fuel Consumption.

	Outbound			Inbound			Total	
	Departure	TOF	Fuel	Departure	TOF	Fuel	Fuel	Time
VSI type II	06/02/2018	120	12,959	08/03/2020	120	9,584	22,543	913
CSI type I	06/01/2018	120	16,716	08/02/2020	120	12,441	29,157	913
CSI type II	05/31/2018	120	20,702	07/27/2020	120	17,252	37,954	908
High Thrust	06/02/2018	120	(9.553)	08/04/2020	120	(10.225)	(19.778)	914

TOF (day), Fuel (kg), Time (day). For High Thrust  $\Delta V$  (km/s) is shown in parentheses.

Fig. 8-25 shows both outbound and inbound trajectories. The spacecraft leaves from Earth on June 2, 2018, and arrives at Mars on Sep. 30, 2018, with 12,959 kg of fuel consumption. The crew stay on Mars is 673 days. For the returning leg, the spacecraft departs Mars on Aug. 3, 2020, and arrives at Earth on Dec. 1, 2020, with 9,484 kg of fuel consumption. The total trip time is 913 days and total fuel consumption is 22,543 kg. As

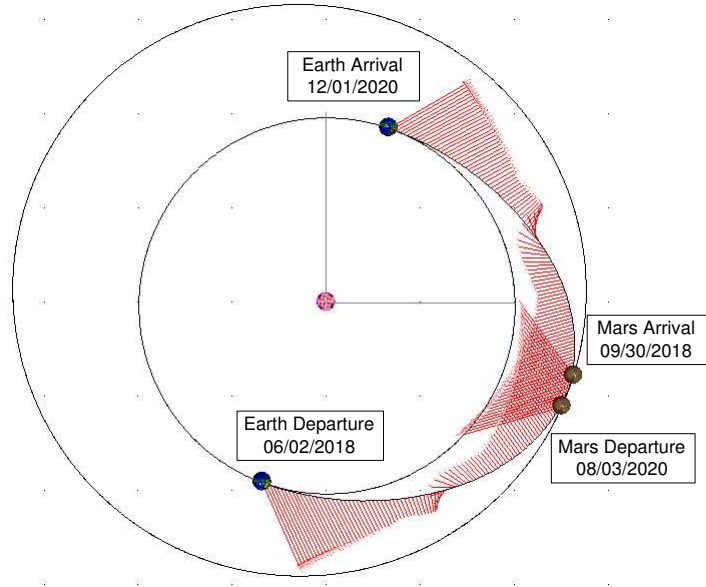


**Figure 8-25:** VSI Type II Trajectory from Earth to Mars with 120-day Time of Flight.

seen in this figure, a higher thrust is required at both departure and arrival phases of the trajectory. Fig. 8-26 is the steering angle and Fig. 8-27 is the thrust magnitude and  $I_{sp}$  for the outbound trajectory with a VSI type II engine. Fig. 8-28 and Fig. 8-29 are for the inbound trajectory.

The in-plane thrust angle for outbound and for inbound are completely different. The thrust direction for the first half of the outbound phase is directed outward so that the spacecraft reaches the Martian orbit which is outside the Earth orbit. Then around the midpoint where the thrust magnitude is now constrained and has its minimum value, the thrust direction flips from outward to inward so that the velocity of the spacecraft matches the velocity of Mars at the arrival date. For the inbound trajectory, the thrust direction for the first half is made so that the spacecraft decelerates and is sent back into Earth orbit. Around the midpoint the direction changes so that the spacecraft can satisfy the final position and velocity requirements. Because the inclination of Martian orbit is small ( $1.85^\circ$  to ecliptic plane), the out-of-plane thrust angle is small for both outbound and inbound.

Similar trajectories are drawn for CSI type I. Fig. 8-30 shows both outbound and inbound

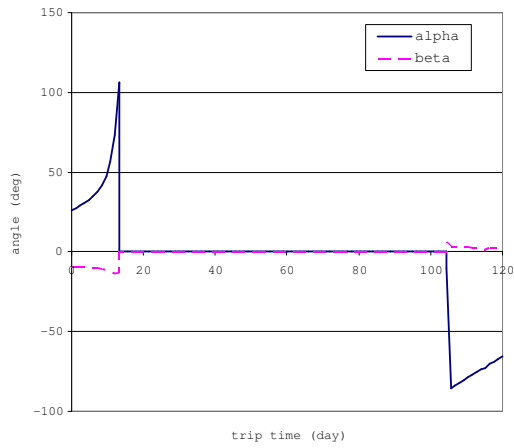


**Figure 8-26:** Thrust Steering Angle for VSI type II: Earth – Mars Outbound.

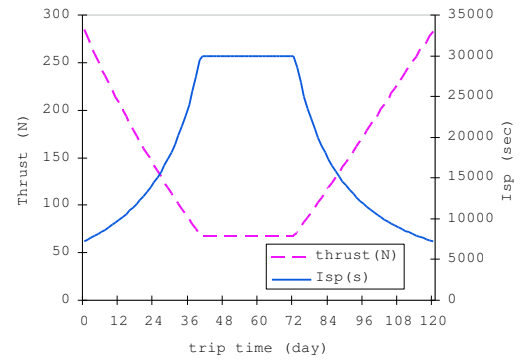


**Figure 8-27:** Thrust Magnitude and  $I_{sp}$  for VSI type II: Earth – Mars Outbound.

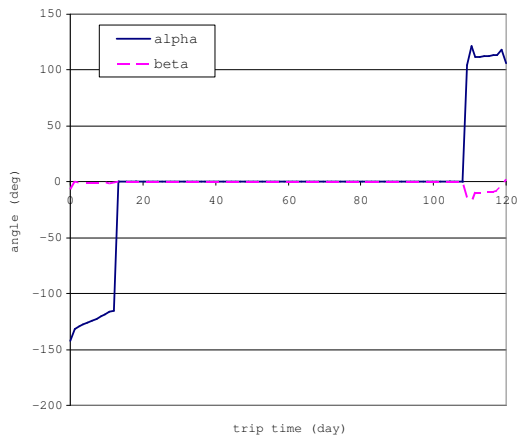


**Figure 8-28:** Thrust Steering Angle for VSI type II: Mars – Earth Inbound.

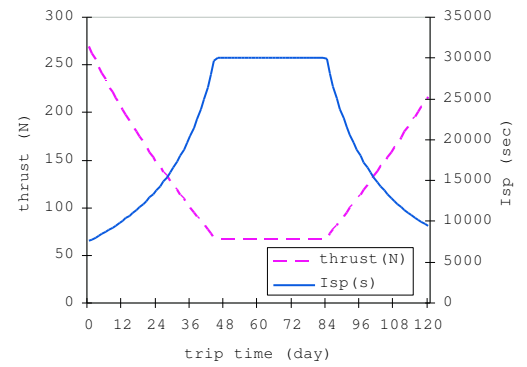


**Figure 8-29:** Thrust Magnitude and  $I_{sp}$  for VSI type II: Mars – Earth Inbound.

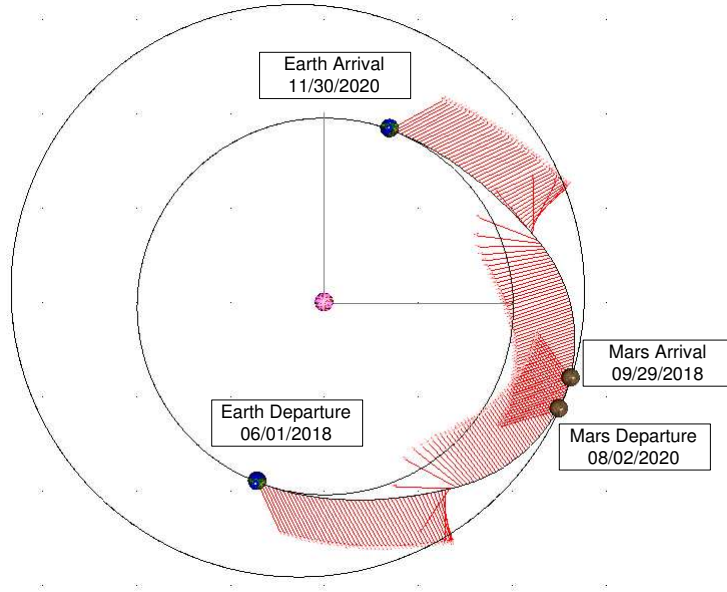


**Figure 8-30:** CSI Type I Trajectory from Earth to Mars with 120-day Time of Flight.

trajectories for round trip. The spacecraft leaves from Earth on June 1, 2018, and arrives at Mars on Sep. 29, 2018, with 16,716 kg of fuel consumption. Then the crew stays on the Mars surface for 673 days. For returning leg, the spacecraft departs Mars on Aug. 2, 2020, and arrives at Earth on Nov. 30, 2020, with 12,441 kg fuel consumption. Total trip time is 913 days and total fuel consumption is 29,157 kg.

Although the thrust level is fixed throughout the trajectory For CSI type I, the history of the thrust direction is similar to that of VSI type II. Around the midpoint, the direction completely changes for both the outbound and inbound trajectories.

Fig. 8-31 shows the transfer trajectories of both the outbound and inbound for CSI type II. The spacecraft leaves from Earth on May 31, 2018, and arrives at Mars on Sep. 28, 2018, with 20,702 kg of fuel consumption. The crew stays on the Mars surface is for 678 days. For the returning leg, the spacecraft departs Mars on July 27, 2020, and arrives at Earth on Nov. 24, 2020, with 17,252 kg fuel consumption. Total trip time is 908 days and total fuel consumption is 37,954 kg.

Fig. 8-32 is the steering angle, and Fig. 8-33 is the thrust magnitude and  $I_{sp}$  history for the outbound transfer of a CSI type II engine. The engine is on for 13.2 days at departure

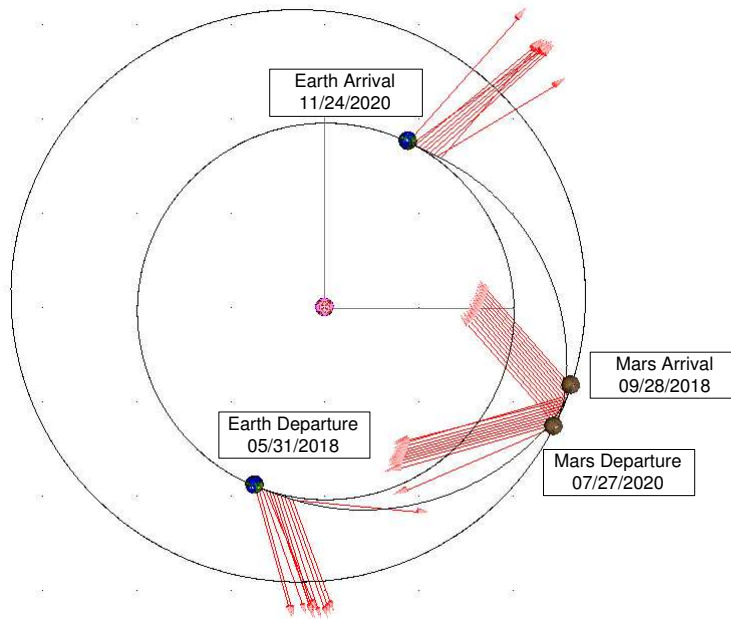


**Figure 8-31:** CSI Type II Trajectory from Earth to Mars with 120-day Time of Flight.

and 19.2 days at arrival. The first burn is made outward and boosts the spacecraft into the trans-Mars injection. As the spacecraft approaches Mars, an additional inward burn is made so that the spacecraft satisfies the target conditions. The histories of the same parameters for inbound transfer are shown in Figs. 8-34 and 8-35.

For high thrust, if the time of flight constraint is 120 days for both legs the  $\Delta V$  is 9.553 km/s for the outbound leg and 10.225 km/s for the inbound leg. Using these values, the fuel consumption for the outbound leg is 88,712 kg for an initial mass of 100 MT, assuming that the  $I_{sp}$  is 450 sec. Assuming no fuel consumption during the stay, the inbound initial mass is 11,288 kg. The required fuel for the inbound leg is 10,176 kg, and the final mass is 1,113 kg. These values seems unacceptable because the structural mass would likely be greater than 1,113 kg. To make the mission plan more realistic, the following option can be thought:

- Assume non-zero  $C_3$  at departure and at arrival.

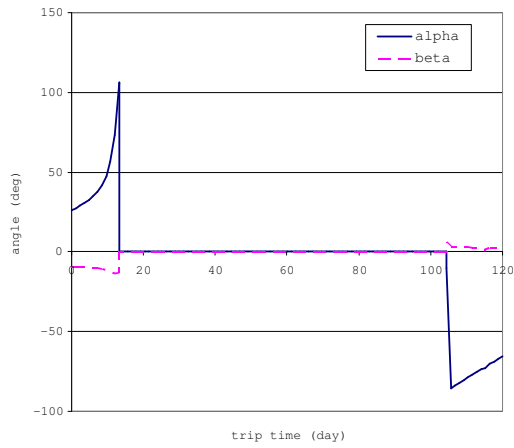


**Figure 8-32:** Thrust Steering Angle for CSI type II: Mars – Earth Outbound.

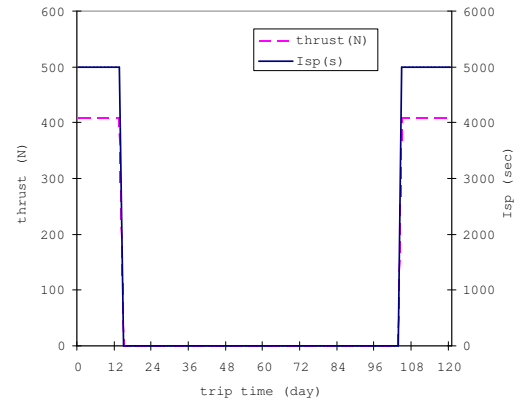


**Figure 8-33:** Thrust Magnitude and  $I_{sp}$  for CSI type II: Mars – Earth Outbound.

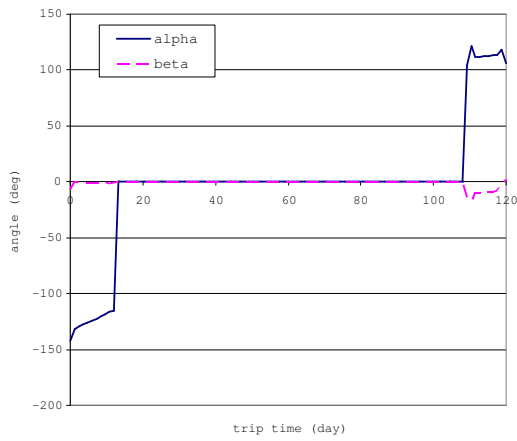


**Figure 8-34:** Thrust Steering Angle for CSI type II: Mars – Earth Inbound.

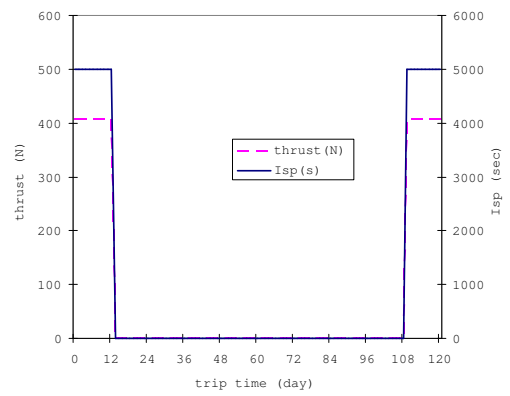


**Figure 8-35:** Thrust Magnitude and  $I_{sp}$  for CSI type II: Mars – Earth Inbound.



- Utilize in-situ resource production.
- Conduct aero-capture at Mars arrival and Earth arrival.
- Increase time of flight.

In reality the spacecraft usually has some non-zero value of  $C_3$ . If a spacecraft leaves LEO and heads to Mars it should have some velocity when it escapes from the Earth's sphere of influence.

In-situ resource utilization is the process of using the materials available in the environment. For a Mars mission, this typically refers to using atmospheric materials to make fuel. Mars has an atmosphere of 95% carbon dioxide, or  $\text{CO}_2$ , and can be reacted directly with the hydrogen brought from Earth as:  $3\text{CO}_2 + 6\text{H}_2 \rightarrow \text{CH}_4 + 2\text{CO} + 4\text{H}_2\text{O}$ . If the water obtained from this reaction is run through a simple electrolysis process, i.e.:  $2\text{H}_2\text{O} \rightarrow 2\text{H}_2 + \text{O}_2$ , the hydrogen trapped in the water as a result of the first equation can be brought back to product more and more methane, with a large amount of oxygen being produced that could serve as a backup to the life-supporting systems of the Mars habitat.

Aero-capture could also be used to capture into Earth and Mars orbit, this could help decrease the fuel requirements. The possibility of aero-capture is not analyzed in this research.

Finally, to explore the possibility of saving the fuel by increasing the time of flight, a broader range for time of flight is searched. The search range is now 100 to 400 days for both legs. The minimum fuel transfer is achieved when the spacecraft leaves Earth on May 1, 2018, and arrives at Mars on Nov. 17, 2018, and then leaves Mars on June 29, 2020, and arrives at Earth on Jan. 5, 2021. The time of flight is 200 days for the outbound leg and 190 days for the inbound leg. The  $\Delta V$  for the outbound leg is 6.013 km/sec, and 6.810 km/sec for the inbound leg. The fuel consumption for the outbound leg is 74,403 kg, and if no fuel is consumed during the stay, then the initial inbound mass is 25,597 kg. The inbound leg requires 20,127 kg of fuel, and gives a final mass of 5,470 kg. If other techniques introduced above are used, the fuel consumption could be lowered by allowing a longer time of flight.

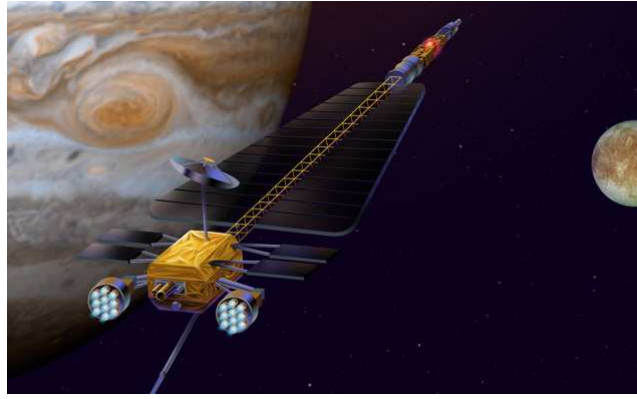


**Figure 8-36:** JIMO: Jupiter Icy Moons Orbiter [3].

## 8.3 *JIMO: Jupiter Icy Moons Orbiter*

### 8.3.1 JIMO Overview

NASA is currently in the preliminary definition phase for a “Jupiter Icy Moons Orbiter (JIMO)” probe, which will perform detailed observations of Ganymede, Callisto, and particularly Europa. They may harbor vast oceans beneath their icy surfaces. JIMO is expected to be powered by an advanced nuclear electric propulsion system [6] [3].

The JIMO mission has three major science goals:

1. Potential for Life: The mission would scout the potential for sustaining life on these moons.
2. Origins and Evolution: Another main science objective would be to investigate the origin and evolution of these moons.
3. Radiation Environments: The mission would also determine the radiation environments around these moons and the rates at which the moons are weathered by material hitting their surfaces.

Because the proposed JIMO requires the development and testing of many new technologies, the mission would not launch until 2011 or later.

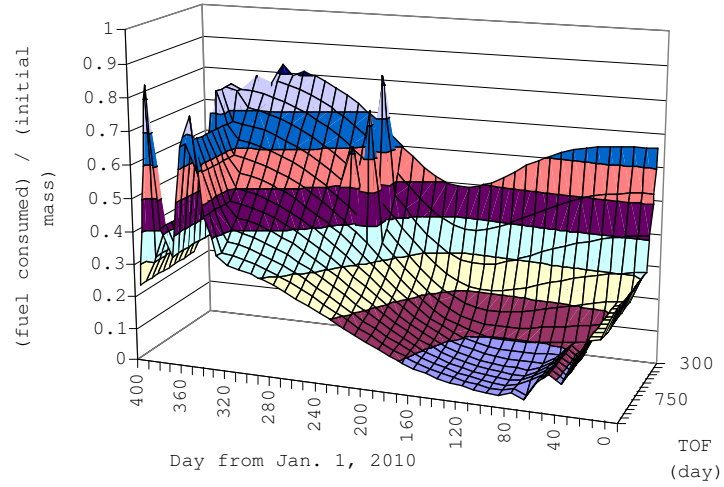


**Figure 8-37:** Fuel Consumption for VSI type I: Earth – Jupiter.

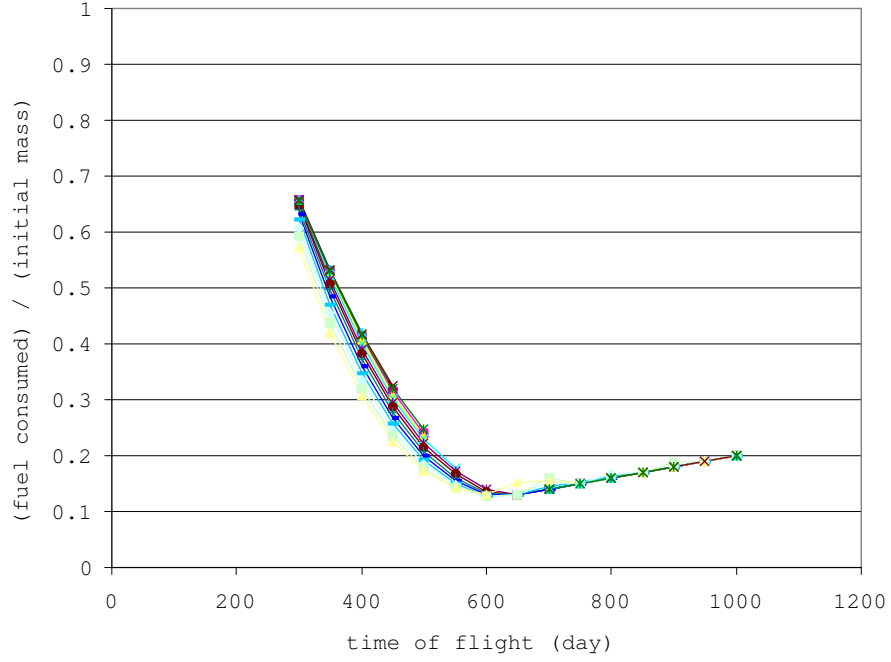
### 8.3.2 Problem Description

The synodic period of Earth and Jupiter is 398.9 days. The fuel requirements for a 400-day range of departure dates are searched starting from Jan. 1, 2010. Initially, a wide range of time of flight was considered, and then from the results, an appropriate value of time of flight was chosen and a more precise analyses could be conducted.

For this section, an upper  $I_{sp}$  limit for CSI type I is set to 30,000 sec. The  $I_{sp}$  limit for VSI type II is the same as the last sections (30,000 sec), and  $I_{sp}$  level for CSI type II is 5,000 sec.

### 8.3.3 Results

The trajectory for a VSI type I engine was analyzed to narrow the search range. Fig. 8-37 shows the fuel requirements for a transfer from Earth to Jupiter. The minimum-fuel transfer occurs when the spacecraft departs around 100 days after Jan. 1, 2010. A more precise analysis is performed around these days for VSI type II, CSI type I and II, and high thrust.



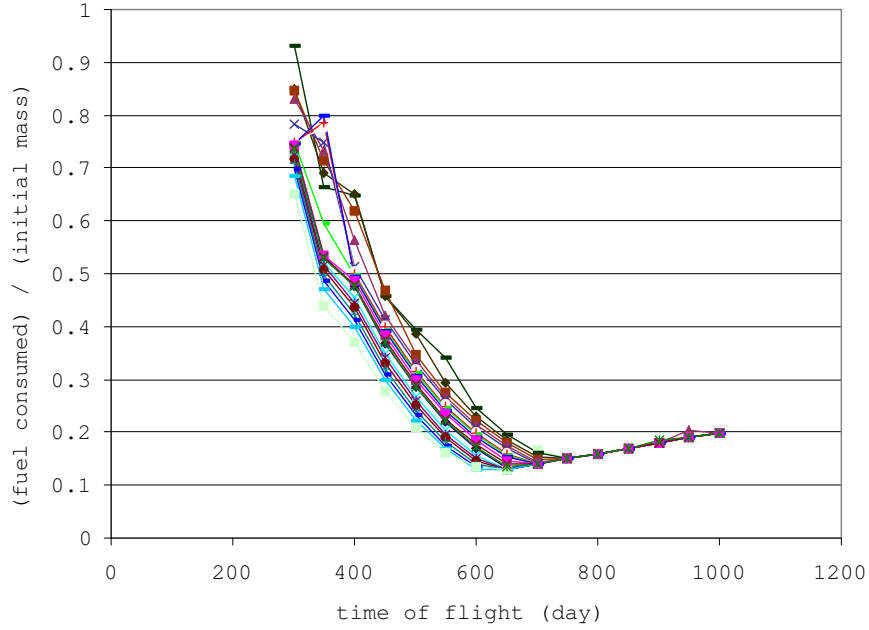
**Figure 8-38:** Fuel Consumption for VSI type II: Earth – Jupiter.

Fig. 8-38 shows the fuel requirements for an Earth to Jupiter transfer with VSI type II for several departure dates. When the time of flight is less than 600 days, the fuel requirements decrease as the time of flight increases. For a time of flight greater than 600 days, the fuel requirements increase as time of flight increases. When the time of flight exceeds about 600 days, the  $I_{sp}$  constraint (30,000 sec) becomes active throughout the trajectory, and the engine will operate like a CSI engine with  $I_{sp}$  level of 30,000 sec for the entire flight time. As stated in Sec. 8.1, this is not an appropriate way to operate a VSI engine.

Fig. 8-39 shows the relative fuel consumption for an Earth to Jupiter transfer with CSI type I for several departure dates. For CSI type I, similar tendency can be seen in the fuel consumption vs. time of flight as is seen for VSI type II. If the time of flight is less than 600 days, higher thrust is required, but when the time of flight exceeds 600 days, the  $I_{sp}$  is always on its constraint (30,000 sec) and the spacecraft starts to waste the fuel.

From the results above, a faster transfer is assumed, and the time of flight is fixed to 365 days. The departure date for all of the following calculation is set to April 1, 2010.

Fig. 8-40 shows the transfer trajectory for a 365-day time of flight. The trajectory goes

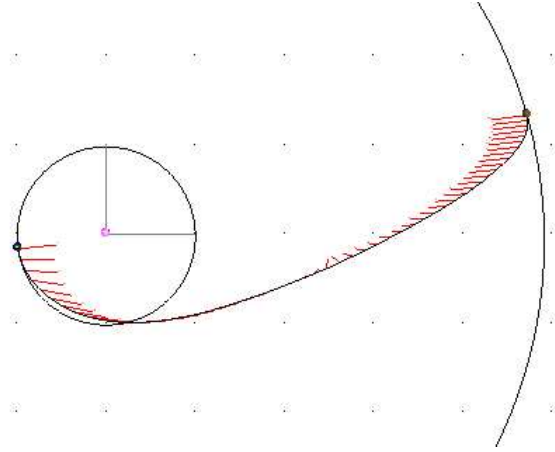


**Figure 8-39:** Fuel Consumption for CSI type I: Earth – Jupiter.

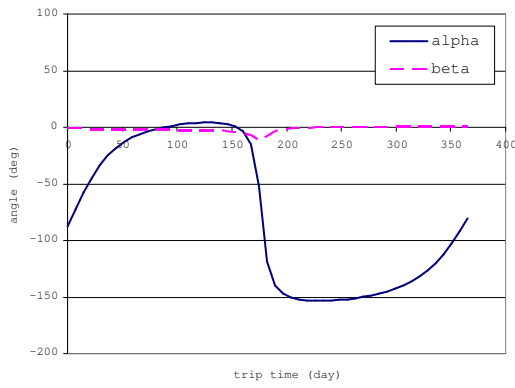
inside the Earth's orbit to achieve a fast transfer. Fig. 8-41 is the history of thrust steering angle, and Fig. 8-42 is the history of thrust and  $I_{sp}$  for VSI type II with a 365-day time of flight. With this flight 41,554.9 kg of fuel is consumed.

Fig. 8-43 is a screen shot of the VRML for Earth – Jupiter transfer with CSI type I departing April 1, 2010, and a 365-day time of flight. Fig. 8-44 is the history of thrust steering angle, and Fig. 8-45 is the histories of thrust and  $I_{sp}$  for CSI type I. The thrust direction is similar to that of VSI type II. For a 365-day mission, 173 N of thrust level is required. The corresponding  $I_{sp}$  is 11,816 sec with 46,979.5 kg of fuel consumed for this transfer.

Fig. 8-46 is the trajectory from Earth to Jupiter with CSI type II departing April 1, 2010, with a 365-day time of flight. Fig. 8-47 is the history of thrust steering angle, and Fig. 8-48 is the history of thrust and  $I_{sp}$  for CSI type II with a 365-day time of flight. The engine is on for 48.4 days at departure, and 69.7 days at arrival. Total fuel consumption is



**Figure 8-40:** Transfer Trajectory for VSI type II: Earth – Jupiter.



**Figure 8-41:** Thrust Steering Angle for VSI type II: Earth – Jupiter, 365-day TOF.

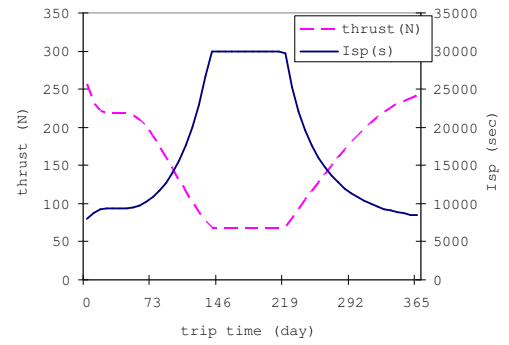


**Figure 8-42:** Thrust Magnitude and  $I_{sp}$  for VSI type II: Earth – Jupiter, 365-day TOF.

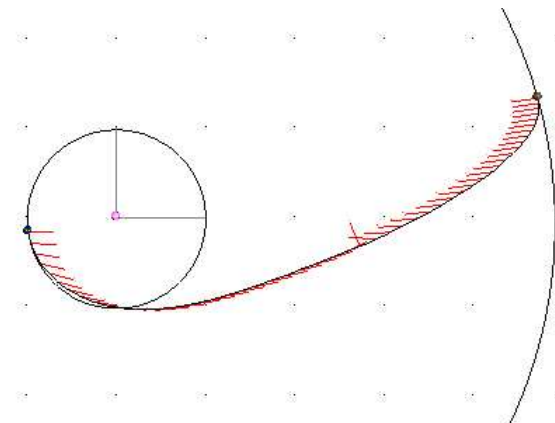


**Figure 8-43:** Transfer Trajectory for CSI type I: Earth – Jupiter.

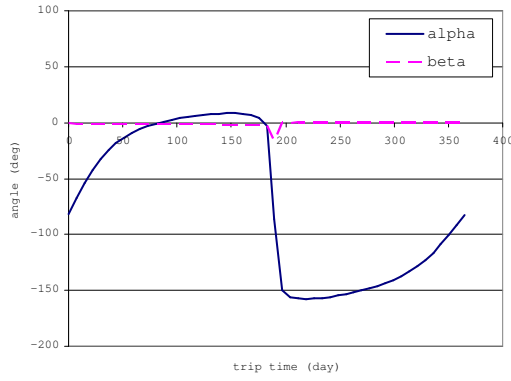


**Figure 8-44:** Thrust Steering Angle for CSI type I: Earth – Jupiter, 365-day TOF.

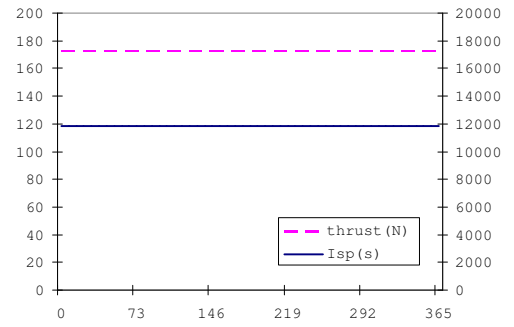


**Figure 8-45:** Thrust Magnitude and  $I_{sp}$  for CSI type I: Earth – Jupiter, 365-day TOF.

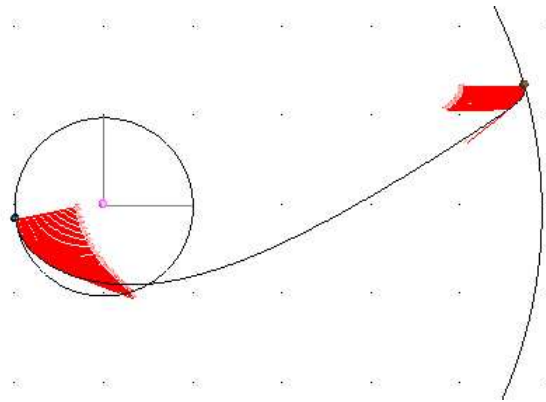


**Figure 8-46:** Transfer Trajectory for CSI type II: Earth – Jupiter.

60,344.9 kg.

## 8.4 *Uranus and beyond*

A transfer orbit to planets such as Uranus, Neptune, and Pluto, the launch opportunity comes about once a year because the synodic period for Earth and these planets is about one year. In this section a transfer trajectory from Earth to Uranus is analyzed. Transfer trajectories to other two planets should be similar.

One thing we should remember in computing a transfer trajectory to the planet far from the Sun is that as the transfer time gets longer, we need to think about the maximum allowable burn time. Consider a spacecraft with 100 MT ( $1.0\text{E}+05$  kg) of initial fuel and a

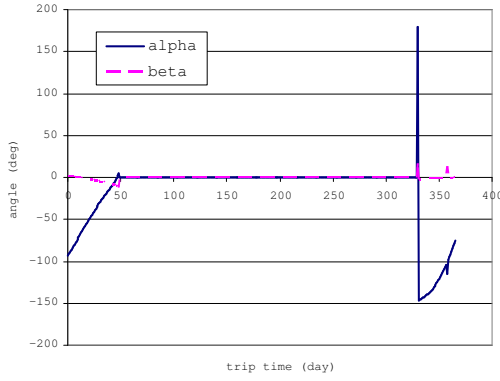


**Figure 8-47:** Thrust Steering Angle for CSI type II: Earth – Jupiter, 365-day TOF.

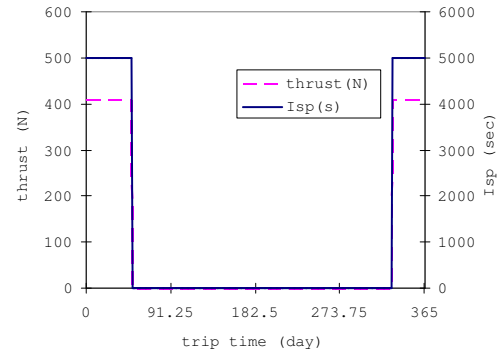


**Figure 8-48:** Thrust Magnitude and  $I_{sp}$  for CSI type II: Earth – Jupiter, 365-day TOF.

VSI type II engine with a 30,000 sec  $I_{sp}$  limit. If the jet power is 30 MW the propellant mass flow becomes  $\dot{m}_{prop} = 2P_J / (g_0 \cdot I_{sp})^2 = 6.933\text{E-}04$  kg/s. Then it takes  $1.0\text{E}+05 / 6.9334\text{E-}04 = 1.4424\text{E}+08$  sec = 1669.4 days = 4.57 years until the spacecraft mass becomes zero. For a jet power of 10 MW, 5008.2 days or 13.712 years is the time limit. We should reach the target planet at least by then. For a CSI type II engine with 10 MW jet power and 5,000 sec  $I_{sp}$ ,  $\dot{m}_{prop}$  is  $8.3197\text{E-}03$  kg/s, and the burn time should be less than 139.1 days.

A grid search for a 400-day range of departure date from Jan. 1, 2010, is conducted for VSI type I engine. The time of flight is fixed to 1,000 days. The minimum fuel trajectory is achieved when the spacecraft is launched on Aug. 28, 2010. Using this launch date and a 1,000-day time of flight, transfer trajectories for VSI type II, CSI type I, and CSI type II are calculated.

Figs. 8-49 to 8-54 show the transfer trajectories from Earth to Uranus with 1,000-day time of flight. 10MW of jet power is powerful enough to get the spacecraft to Uranus within the 1,000-day limit. For these types of engines, the trajectory is almost straight to Uranus. Fuel requirements are: 36,361.9 kg for VSI type II, 46,514.0 kg for CSI type I, 69006.7 kg for CSI type II. The thrust level for CSI type I is 103.8 N (corresponding  $I_{sp}$  is 19,656 sec), and burn time for CSI type II is 94 days (54 days at departure, 40 days at arrival).



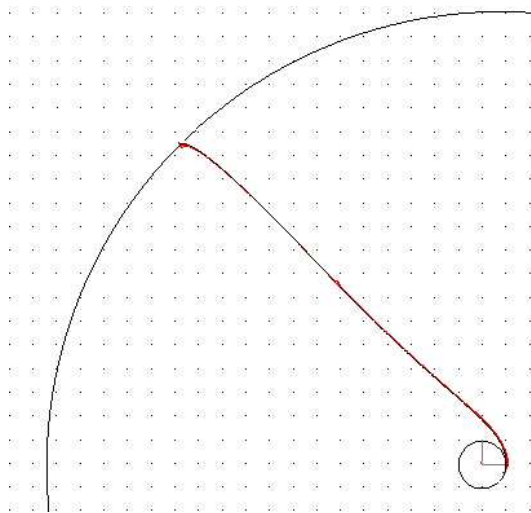


**Figure 8-49:** Transfer Trajectory for VSI type II: Earth – Uranus.

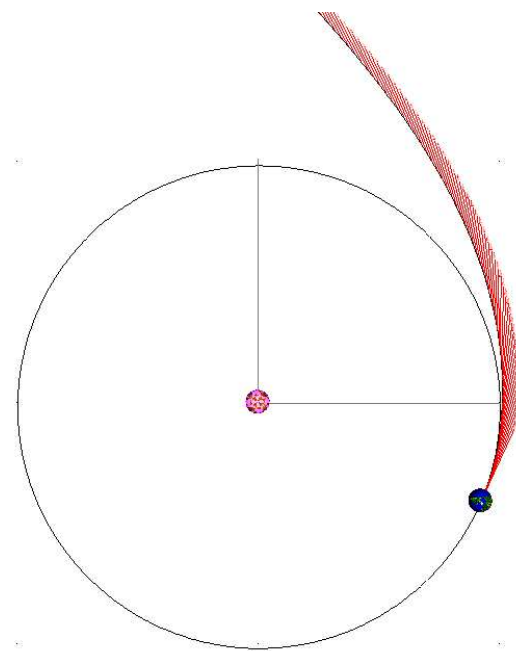


**Figure 8-50:** Departure Phase of Transfer Trajectory for VSI type II: Earth – Uranus.

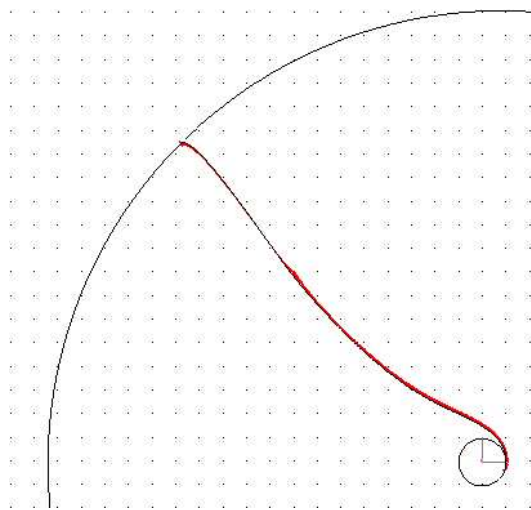


**Figure 8-51:** Transfer Trajectory for CSI type I: Earth – Uranus.

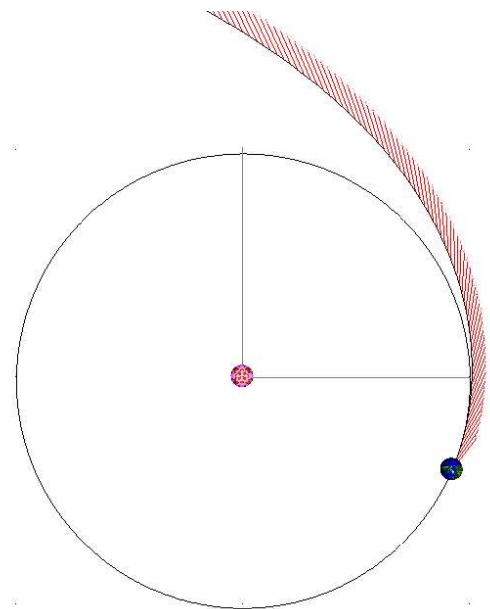


**Figure 8-52:** Departure Phase of Transfer Trajectory for CSI type I: Earth – Uranus.

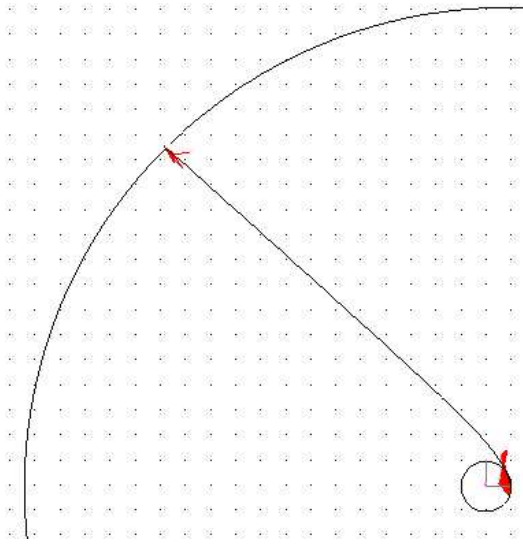


**Figure 8-53:** Transfer Trajectory for CSI type II: Earth – Uranus.

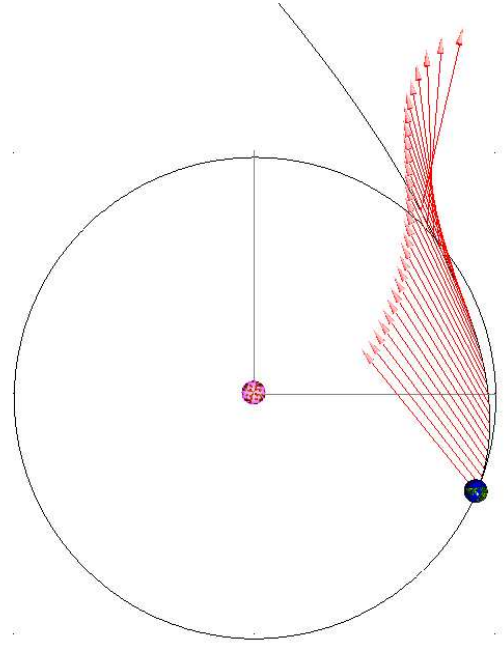


**Figure 8-54:** Departure Phase of Transfer Trajectory for CSI type II: Earth – Uranus.

## 8.5 *Swing-by Trajectories with Mars*

The final examples analyzed in this chapter are transfer trajectories utilizing a Mars swing-by. The spacecraft leaves Earth and conducts a swing-by at Mars en route to Jupiter or Saturn. A swing-by may save fuel consumption.

Instead of using actual ephemeris, the orbits of planets are assumed to be circular and coplanar as they are in the last chapter. Therefore the positions of the planets are expressed as the difference in the true anomaly ( $\Delta\nu$ ) with respect to Earth.

Swing-by trajectories with VSI type I, VSI type II, CSI type II, and high thrust are considered and their corresponding fuel consumptions are calculated. CSI type I is omitted for swing-by analysis.

For CSI type I, *SAMURAI* calculates the minimum constant thrust required to accomplish a mission, and the trajectory is simulated with this thrust level. For swing-by trajectories, the thrust level required for each phase is normally different. If the thrust

level required for the 1st phase is higher than that for the 2nd phase, redundant fuel is used throughout the 2nd phase because the engine will be operated with the thrust level required for 1st phase for an entire mission. Therefore using a CSI type I engine for a swing-by mission is not suitable.

The high thrust transfer orbits are calculated at first. A grid search is performed to find an appropriate configuration of planets to reduce the fuel consumption if the spacecraft utilizes a swing-by maneuver. The spacecraft is assumed to leave the Earth's position at (1.0, 0.0) with a velocity at (0.0, 1.0).  $\Delta\nu$  between Earth and these two planets is set to  $180^\circ$ , hence the spacecraft arrives at Jupiter whose position is (-5.0, 0.0) and velocity is (0.0, -0.4472), or at Saturn whose position is (-10.0, 0.0) and the velocity is (0.0, -0.3162). A time of flight of 6 to 16 TU is considered for Jupiter, and 10 to 20 TU of time of flight is considered for Saturn. The optimal Mars position and time of flight from Earth is searched in order to minimize the fuel consumption in each case.

Table 8-3 and 8-4 show the  $\Delta V$  requirements for high thrust with and without Mars swing-by for an Earth to Jupiter mission and an Earth to Saturn mission, respectively. It is shown that a maximum savings of 20 % can be achieved using a swing-by maneuver.

**Table 8-3:** Comparison of High Thrust  $\Delta V$  for Earth – Jupiter: With and Without Mars Swing-by

Total TOF (TU_Sun)	6	8	10	12	14	16
Without Swing-by	45.511	30.344	21.914	17.243	14.985	14.296
With Swing-by	43.768	25.402	18.120	14.717	13.695	13.789
Savings (%)	3.984	19.46	20.94	17.16	9.42	3.68

( $\Delta V$  in km/s)

Figs. 8-55 and 8-56 show the transfer trajectories from Earth to Saturn with and without swing-by at Mars. The total time of flight for these trajectories is 18 TU for both cases. For a swing-by case, the minimum fuel trajectory is obtained when the time of flight from Earth to Mars is 1.6 TU and the  $\Delta\nu$  between Earth and Mars is  $85^\circ$ . Impact parameter at Mars is 1.31515 Martian DU ( $\approx 4423$  km), and Turn angle is  $29.24^\circ$ . The Heliocentric

**Table 8-4:** Comparison of High Thrust  $\Delta V$  for Earth – Saturn: With and Without Mars Swing-by

Total TOF (TU_Sun)	10	12	14	16	18	20
Without Swing-by	57.905	46.420	38.624	32.908	28.611	25.322
With Swing-by	53.862	40.026	31.590	26.147	22.247	19.778
Savings (%)	6.982	13.77	18.21	20.55	22.24	21.89

( $\Delta V$  in km/s)

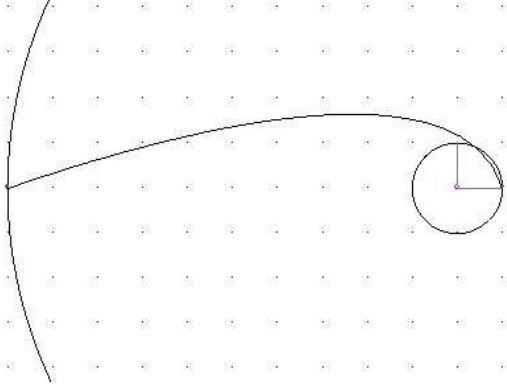


**Figure 8-55:** Transfer Trajectory for High Thrust: Earth to Saturn without Swing-by.

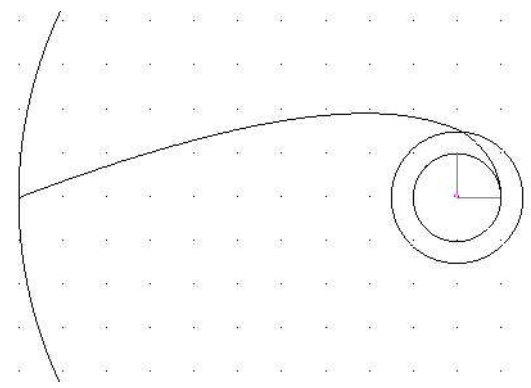


**Figure 8-56:** Transfer Trajectory for High Thrust: Earth to Saturn with Mars Swing-by.

velocity (AU/TU) changes as:

$$\text{Before Swing-by } (u, v, w) = (-0.79280, 0.52491, 0.00000), V = 0.950822$$

$$\text{After Swing-by } (u, v, w) = (-1.04188, 0.50742, 0.00000), V = 1.158874.$$

This energy increase makes the spacecraft with a swing-by maneuver possible to reach Saturn with less propellant than the spacecraft without a swing-by maneuver.

Next, a grid search for VSI type I is performed. Tables 8-5 and 8-6 show the fuel consumption with and without swing-bys. As shown in these tables, a swing-by maneuver can save fuel for VSI engines by several percent. Figs. 8-57 through 8-60 are the transfer trajectories with and without swing-by to Jupiter and Saturn.

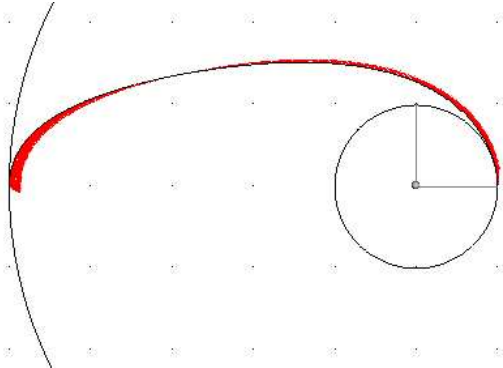


**Figure 8-57:** Transfer Trajectory for VSI type I: Earth to Jupiter without Swing-by.

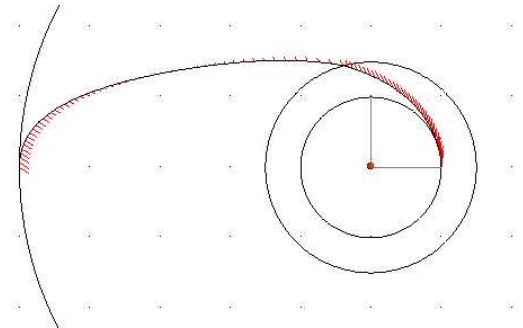


**Figure 8-58:** Transfer Trajectory for VSI type I: Earth to Jupiter with Mars Swing-by.

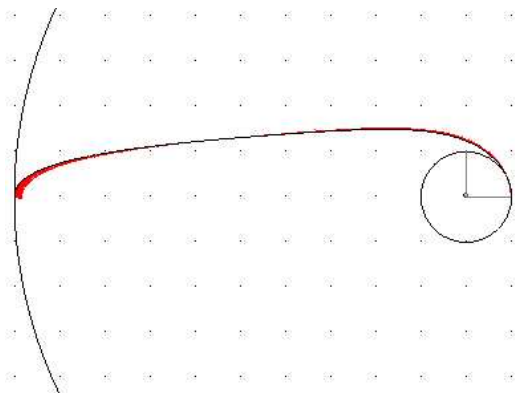


**Figure 8-59:** Transfer Trajectory for VSI type I: Earth to Saturn without Swing-by.

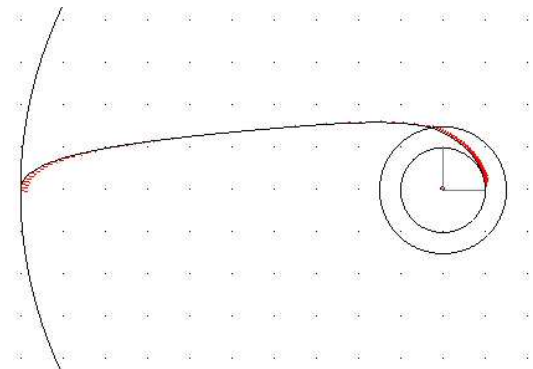


**Figure 8-60:** Transfer Trajectory for VSI type I: Earth to Saturn with Mars Swing-by.

**Table 8-5:** Comparison of Fuel Consumption for VSI type I: from Earth to Jupiter With and Without Mars Swing-by.

Total TOF (TU_Sun)	6	8	10	12	14	16
Without Swing-by	44764.1	20268.7	10675.1	7920.0	7466.6	7680.3
With Swing-by	45010.9	19625.1	10167.9	7874.3	7497.7	7731.9
Savings (%)	-0.548	3.279	4.988	0.580	-0.415	-0.667

(Fuel consumption in kg)

**Table 8-6:** Comparison of Fuel Consumption for VSI type I: from Earth to Saturn With and Without Mars Swing-by.

Total TOF (TU_Sun)	10	12	14	16	18	20
Without Swing-by	42157.6	27934.4	19061.1	13872.9	10867.5	9090.1
With Swing-by	40983.4	26735.4	17734.3	13365.3	10498.9	8977.8
Savings (%)	2.865	4.485	7.482	3.798	3.511	1.251

(Fuel consumption in kg)

The same grid search is performed for VSI type II and CSI type II. Tables 8-7 through 8-10 show the fuel consumption with and without swing-by. Figs. 8-61 through 8-68 are the transfer trajectories with and without swing-by for Jupiter and Saturn.

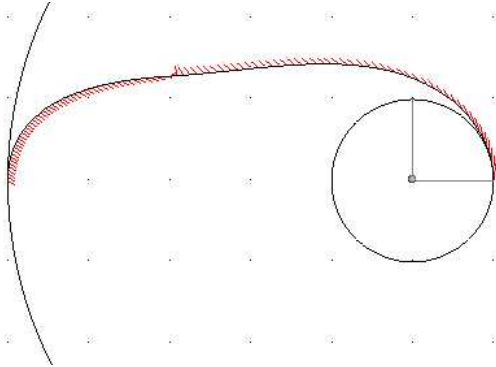


**Figure 8-61:** Transfer Trajectory for VSI type II: Earth to Jupiter without Swing-by.

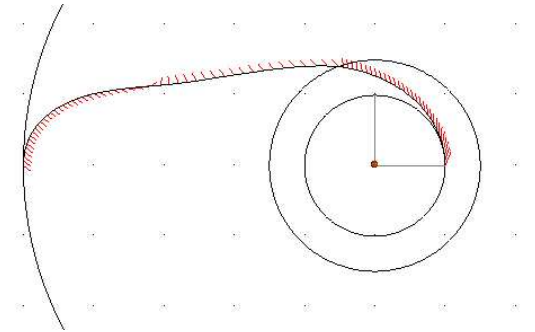


**Figure 8-62:** Transfer Trajectory for VSI type II: Earth to Jupiter with Mars Swing-by.

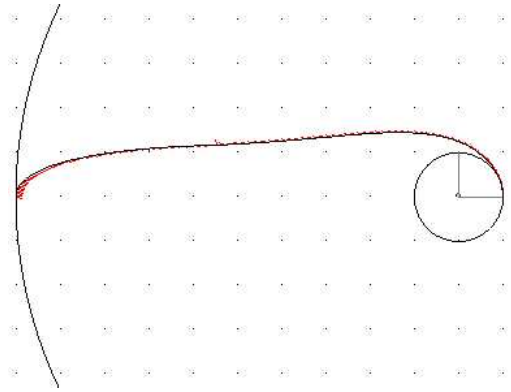


**Figure 8-63:** Transfer Trajectory for VSI type II: Earth to Saturn without Swing-by.

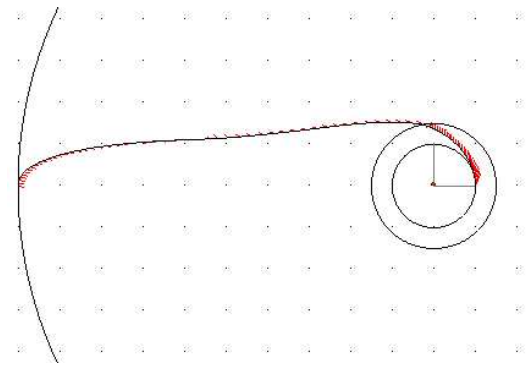


**Figure 8-64:** Transfer Trajectory for VSI type II: Earth to Saturn with Mars Swing-by.

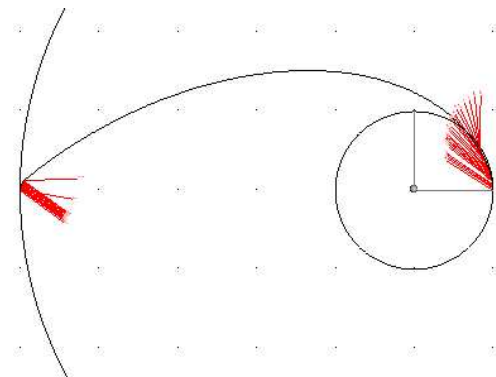


**Figure 8-65:** Transfer Trajectory for CSI type II: Earth to Jupiter without Swing-by.

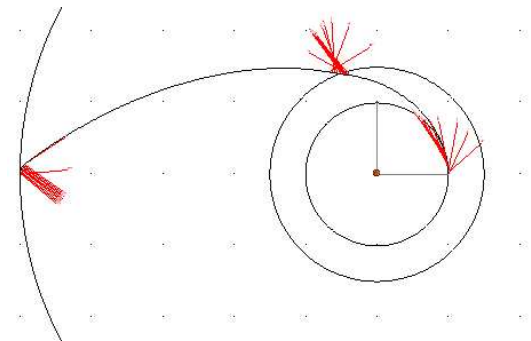


**Figure 8-66:** Transfer Trajectory for CSI type II: Earth to Jupiter with Mars Swing-by.

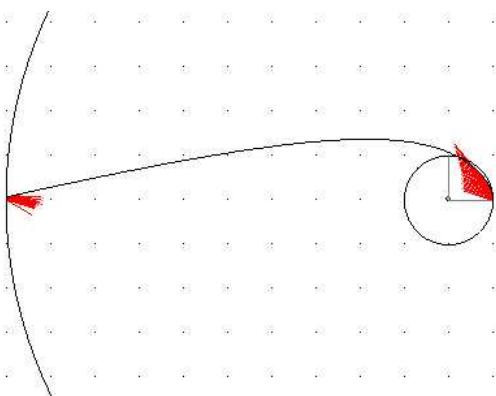


**Figure 8-67:** Transfer Trajectory for CSI type II: Earth to Saturn without Swing-by.

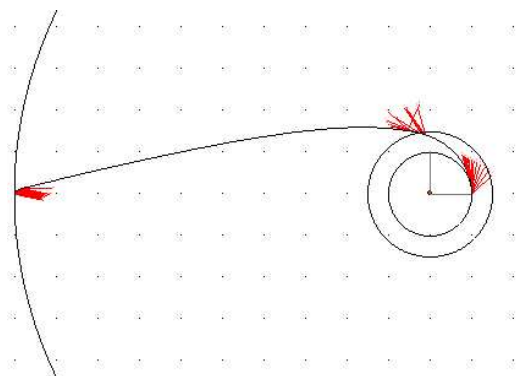


**Figure 8-68:** Transfer Trajectory for CSI type II: Earth to Saturn with Mars Swing-by.

**Table 8-7:** Comparison of Fuel Consumption for VSI type II: from Earth to Jupiter With and Without Mars Swing-by.

Total TOF (TU_Sun)	6	8	10	12	14	16
Without Swing-by	44985.3	21230.1	13524.2	16787.5	19318.7	19572.0
With Swing-by	45086.6	20943.7	13426.2	15525.7	17776.9	20077.1
Savings (%)	-0.225	1.367	0.730	8.127	8.673	-2.516

(Fuel consumption in kg)

**Table 8-8:** Comparison of Fuel Consumption for VSI type II: from Earth to Saturn With and Without Mars Swing-by.

Total TOF (TU_Sun)	10	12	14	16	18	20
Without Swing-by	42785.2	29767.3	22030.1	19808.9	20962.1	23215.9
With Swing-by	41661.8	29411.7	20728.6	19600.0	22265.7	24730.9
Savings (%)	2.696	1.209	6.279	1.066	-5.855	-6.126

(Fuel consumption in kg)

As shown in Tables 8-7 through 8-10, fuel can be saved with swing-by for any type of engines. However, fuel savings for CSI type II are higher than VSI type I and II in general.

Figs. 8-69 and 8-70 show the history of specific energy of a spacecraft going from Earth to Jupiter and Saturn. Before and after swing-by, there is a jump on the specific energy for all engine types. Throughout the mission, high thrust and CSI type II are operated with the minimum specific energy required to reach the target. However, both VSI engines increase their specific energy even after swing-by, and it seems that they waste fuel. VSI type II has a constraint on  $I_{sp}$  and cannot lower the thrust level below its constrained thrust level, so it may be inevitable that a VSI type II engine wastes fuel. But it is interesting that a VSI type I engine, that does not have a constraint on  $I_{sp}$ , also unnecessarily increases its specific energy and wastes fuel. That is the reason that the effect of swing-by maneuvers on VSI engines is smaller compared to high thrust or CSI type II engines. The reason of the increase of the specific energy for VSI engines should be further investigated.



**Table 8-9:** Comparison of Fuel Consumption for CSI type II: from Earth to Jupiter With and Without Mars Swing-by.

Total TOF (TU_Sun)	6	8	10	12	14	16
Without Swing-by	67193.5	46132.9	36772.6	32092.4	35101.1	36104.0
With Swing-by	60913.2	37989.9	31443.7	24703.4	21846.0	24108.8
Savings (%)	10.31	21.43	16.95	29.91	60.68	49.75

(Fuel consumption in kg)

**Table 8-10:** Comparison of Fuel Consumption for CSI type II: from Earth to Saturn With and Without Mars Swing-by.

Total TOF (TU_Sun)	10	12	14	16	18	20
Without Swing-by	68530.7	60173.3	52651.6	48138.6	43625.6	40115.5
With Swing-by	43271.1	44381.0	45490.9	38780.5	37014.2	36762.8
Savings (%)	58.38	35.58	15.74	24.13	17.86	9.12

(Fuel consumption in kg)

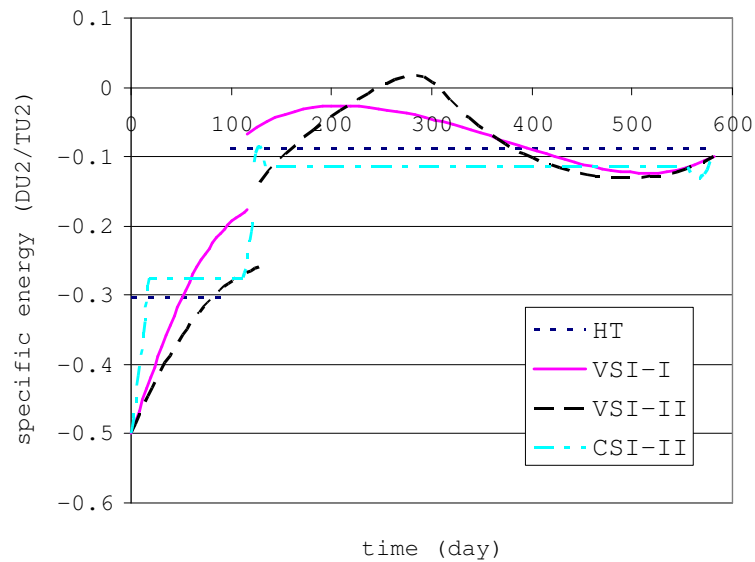


**Figure 8-69:** Specific Energy for Swing-by Trajectory: Earth – Mars – Jupiter.

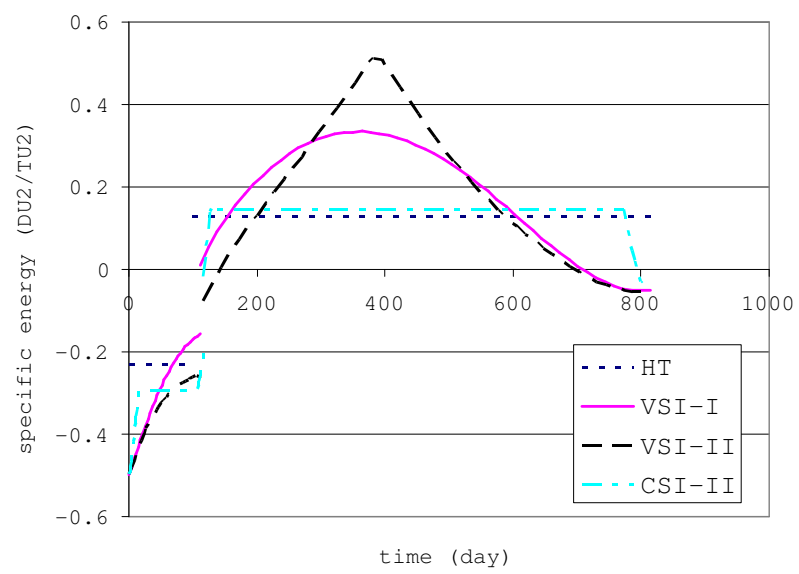


**Figure 8-70:** Specific Energy for Swing-by Trajectory: Earth – Mars – Saturn.

## CHAPTER IX

### CONCLUSIONS AND FUTURE WORK

This paper has presented the methods and results for the comparison of several engine types used for solar system exploration.

Five different engine types have been investigated in this research. They are

1. VSI type I (variable thrust, variable  $I_{sp}$  with no constraint on  $I_{sp}$ ).
2. VSI type II (variable thrust, variable  $I_{sp}$  with upper limit on  $I_{sp}$ ).
3. CSI type I (constant thrust, constant  $I_{sp}$  with continuous thrust).
4. CSI type II (constant thrust, constant  $I_{sp}$  with the capability of switching on/off the engine).
5. High thrust (infinitesimal burn time).

At first, a preliminary study was conducted with simple spiral trajectories, and fuel consumption was calculated for VSI, CSI, and high thrust engines. This preliminary study identified some promise for VSI.

An interplanetary trajectory calculation software application *SAMURAI* was developed to analyze the characteristics of trajectories for these five engines. The results with *SAMURAI* were compared with the results from existing interplanetary trajectory calculation programs such as IPREP and ChebyTOP. The comparison of results with these programs validated the new application *SAMURAI*.

Using *SAMURAI*, many Earth-originating trajectories have been calculated and some relationships among fuel consumption, jet power, and travel distance were established.

Finally, using actual ephemeris of planets, three-dimensional trajectories were calculated to various destination planets to verify the relationships established in the preliminary study.

In this chapter, summary of the results, research accomplishments, and recommended future work are presented.

## ***9.1 Conclusions and Observations***

In the numerical calculations that have been performed up to the last chapter, the following statements were obtained.

- For almost all cases considered in this research (any target condition, jet power, and time of flight), VSI type I is the most efficient. Specifically, a VSI type I engine requires the least amount of fuel among the five engine classes.
- If the transfer time is very long, it sometimes happens that VSI type I needs more fuel than CSI type I. A spacecraft with a CSI type I engine sometimes travels around the Sun for more than one revolution when the time of flight is longer than normally required. This helps to lower the required thrust level drastically, resulting in a lower fuel consumption than VSI type I who travels around the Sun with less than one revolution. However, if a good initial guess of control variables for a VSI type I engine is made, and if a trajectory of a spacecraft with a VSI type I engine that travels around the Sun for more than one revolution is obtained, the fuel consumption of a VSI type I engine is lower than that of a CSI type I engine. This is confirmed by manually selecting the initial guess of the control variables for a VSI type I trajectory and make the trajectory travel around the Sun for more than one revolution. A VSI type I trajectory requires less fuel than a CSI type I trajectory if both trajectories travel around the Sun for more than one revolution.
- When the target planet is close to the Sun, the time of flight that minimizes fuel consumption is almost equal for all engine types. This is because the spacecraft's trajectory is more affected by the gravitational force from the Sun than by the acceleration from the engine. The trajectory for different types of engines look similar for each engine type and therefore the time of flight also becomes almost equal for each engine type.

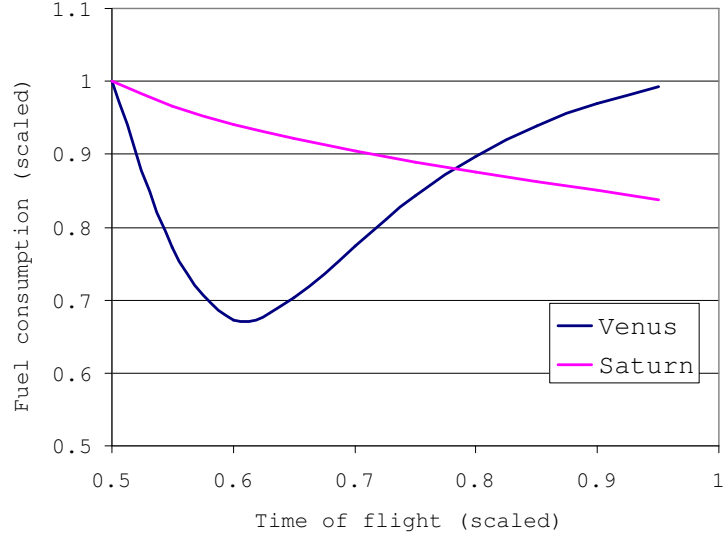


**Figure 9-1:** Example of Fuel vs. Time of Flight for VSI type I.

- If the target is far from the Sun, the above statement does not hold. This is because the gravitational force from the Sun becomes smaller as the spacecraft travels farther from the Sun, and therefore the spacecraft's trajectory is dominated by the force exerted by the engine rather than the gravitational force from the Sun. The spacecraft is allowed more freedom in its movement, and the spacecraft chooses the time of flight that is best for its engine type.
- When the target planet is far from the Sun, the fuel consumption for VSI type I becomes smaller as the time of flight becomes longer. But for a target planet close to the Sun, there is a time of flight that minimizes the fuel consumption, and extending the time of flight does not necessarily decreases the fuel consumption as shown in Fig. 9-1. This can be explained similarly to the previous statement: For a trajectory to a planet far from the Sun, a spacecraft can choose the best time of flight. This is not the case for VSI type II or CSI type I whose  $I_{sp}$  has an upper bound and therefore fuel consumption increases as time of flight increases.
- For VSI type II whose  $I_{sp}$  limit is  $x$  sec, the fuel consumption is always between that of VSI type I and that of CSI type I whose  $I_{sp}$  limit is  $x$  sec. As the time of flight gets

shorter, thrust history for VSI type I and type II becomes more and more similar, and at a certain time of flight, they become identical (constrained arc disappears for VSI type II). On the other hand, as the time of flight gets longer, the thrust history for VSI type II and CSI type I becomes more and more similar, and at a certain time of flight, they become identical: constant thrust and constant  $I_{sp}$  at  $x$  sec.

- For the same initial mass, a spacecraft with a VSI engine with higher jet power is relatively more advantageous than lower jet power. That means the merit of using a VSI engine increases as the jet power increases for a certain mass of spacecraft. This statement can be also rephrased as the following way: for the same jet power, a lighter spacecraft is more advantageous than heavier one. Therefore the merit of using a VSI engine increases as the mass of spacecraft decreases for a certain jet power.
- The merit of using a VSI engine against using a CSI engine may increase or decrease as the travel distance increases. It depends on how the problem is set:
  - If the  $I_{sp}$  of the comparative CSI engine is fixed for any mission profile (time of flight and target conditions), the merit of using a VSI engine increases as the travel distance increases. Therefore, using a VSI engine for a transfer to Pluto is the most effective.
  - If the best  $I_{sp}$  level for the comparative CSI engine is chosen for each mission depending on the mission profile (like CSI type I in the current research), the merit of using a VSI engine decreases as the travel distance increases. Hence, using a VSI engine for a transfer to Mercury is the most effective.
- Fuel can be saved by applying swing-by maneuvers for VSI engines, CSI type II, and high thrust. However, effects of swing-by on VSI engines are smaller than that of high thrust or CSI engines. This is because for VSI engines unnecessary increase of the specific energy is observed after swing-by maneuvers, and therefore more fuel than required is consumed. This is an unnecessary increase of the specific energy that is not observed for high thrust and CSI type II engines.

## 9.2 *Research Accomplishments*

In this section, the accomplishments of research goals and objectives proposed in Chap. 1 are presented.

- The primary goal of this research is to show the advantages and disadvantages of VSI engines over conventional engines such as CSI engines and high thrust engines that are currently used for interplanetary missions. As stated in the previous section, it is concluded that VSI engines are better than CSI engines and high thrust engines when considering propellant consumption as the evaluation metric.
- The objective that supports the primary goal was to establish a generalized rule that
  1. qualitatively states the advantages and disadvantages of VSI engines
  2. quantitatively determines the fuel savings by using VSI engines over CSI or high thrust engines.

As stated in the last section, the 1st rule was established as the relationship between the fuel savings and the jet power, or the relationship between the fuel savings and the travel distance. Establishing the 2nd rule is difficult. The fuel consumption is a function of many parameters such as jet power, time of flight,  $I_{sp}$  constraints, and the configuration of the two planets. Numerically, it is even affected by the number of time steps or the tolerance for the convergence criteria. However, estimating the fuel savings is not impossible. From the parameters such as jet power and configuration of the planets, Tables 7-2 to 7-3 will help roughly estimate the fuel savings.

- To support the above goals, it was also a goal to create an interplanetary trajectory optimization program that can calculate the trajectories for VSI, CSI, and high thrust engines. The software application *SAMURAI* – Simulation and Animation Model Used for Rockets with Adjustable  $I_{sp}$  – was created. This application can calculate trajectories for each of the five propulsion systems. *SAMURAI* also conducts planetary swing-bys if desired, and it has a capability of drawing an animation of the resulted trajectory on a web browser using VRML. Although this application was developed

for the purpose of study of this research, it has a potential to be widely used for any interplanetary mission analyses, and that is the hope of the author.

### ***9.3 Recommended Future Work***

**Multiple Swing-bys** Currently, *SAMURAI* has a capability of calculating a swing-by trajectory with only one planet, but not more than one. This limitation might not be desirable if Mars missions are to be analyzed because previous studies show that some missions to Mars do multiple swing-bys with Venus and Earth before arriving at Mars.

Using *SAMURAI* and an existing interplanetary calculation application IPREP (Interplanetary PREProcessor), several calculations have been performed for high thrust trajectories with and without swing-bys. This is to investigate if more  $\Delta V$  is required for a swing-by trajectory with only one planet than for a trajectory without swing-by. The results showed that the  $\Delta V$  for a trajectory with a single swing-by with Venus is worse than the  $\Delta V$  for a trajectory without swing-by.

Therefore, adding a feature of multiple swing-by may improve the mission analysis and give broader knowledge about VSI engines.

**Mission to the Moon** In this research only trajectories from Earth to other planets were investigated. Although VSI engines may be the best for the fast transfers between two planets, studying a mission to the Moon with VSI engines may give us interesting results. Some minor modifications of *SAMURAI* should make *SAMURAI* suitable for analyzing the Moon missions because the equations of motion are the same for a trajectory around the Sun and a trajectory around the Earth.

**Optimization Methods for Swing-by, Lagrange Multipliers** Currently *SAMURAI* employs Powell's method to find the optimal values for parameters such as conditions at the entry point of the sphere of influence or the Lagrange multipliers for VSI type II and CSI type II. Powell's method works well for most of these problems because in many of the cases the response surface for these parameters should be near-quadratic. However, some problems require long computational time or they do not converge. Exploring other



methods such as sequential quadratic programming and applying it to *SAMURAI* may improve the robustness and computation time.

# APPENDIX A

## RESULTS FROM PRELIMINARY STUDY

**Table A-1:** Transfer Orbit to Venus with 20MW Jet Power.

Venus	Fuel	Consumed (kg)									
Pj	20.000	(MW) nju	60.000 (deg)	r	0.3750	0.6495	V	-1.0000	0.5774		
TOF (TU_Sun)	0.600	0.700	0.800	0.900	1.000	1.100	1.200	1.300	1.400	1.500	1.600
VSI type I	75460.6	55333.1	37883.9	31468.9	33372.4	38092.8	42879.0	46934.2	50183.6	52746.8	54765.5
VSI typeII	75472.9	55374.2	37907.7	31497.4	33441.1	38137.8	42896.0	46939.7	50185.4	52747.3	54765.5
CSI type I	91998.7	70503.4	47570.1	37915.3	39492.3	44013.7	48504.1	52327.1	55439.9	57940.4	59943.2
CSI typeII	100000.0	100000.0	42789.9	36856.1	38444.1	44127.1	48138.6	52150.2	56161.7	58919.7	65522.0
highThrust	99962.2	99517.3	98209.7	97435.0	98007.0	98951.2	99520.5	99780.0	99893.8	99945.5	99970.3
Pj	20.000	(MW) nju	90.000 (deg)	r	-0.0000	0.7500	V	-1.1547	-0.0000		
TOF (TU_Sun)	1.000	1.100	1.200	1.300	1.400	1.500	1.600	1.700	1.800	1.900	2.000
VSI type I	41684.2	24944.3	14710.8	11680.0	13491.7	17538.3	22175.9	26622.2	30587.2	34009.2	36921.2
VSI typeII	41741.4	25096.1	14888.4	11872.7	13746.5	17768.4	22332.1	26728.1	30663.5	34068.8	36971.2
CSI type I	55130.8	34204.4	19806.3	15209.7	17879.9	22580.4	27468.1	31995.3	35991.9	39441.8	42392.2
CSI typeII	50144.4	33095.3	24069.3	23902.2	32761.0	28833.0	33429.6	38360.5	43625.6	47637.2	48472.9
highThrust	99199.9	96601.8	92196.7	90080.6	91669.9	94920.9	97316.9	98602.2	99248.9	99578.9	99753.5
Pj	20.000	(MW) nju	120.000 (deg)	r	-0.3750	0.6495	V	-1.0000	-0.5774		
TOF (TU_Sun)	1.000	1.200	1.400	1.600	1.800	2.000	2.200	2.400	2.600	2.800	3.000
VSI type I	74914.2	49139.3	21413.7	6560.0	5604.9	10843.1	17186.2	22845.2	27463.5	31126.4	34009.9
VSI typeII	74929.3	49187.9	21618.1	7137.3	6362.2	11376.8	17558.6	23143.6	27728.2	31376.8	34256.9
CSI type I	89850.6	62939.8	29707.6	9353.5	8174.9	14876.2	22025.9	28210.4	33208.6	37160.9	40269.3
CSI typeII	100000.0	57164.6	38611.2	17383.4	18052.0	30086.7	33095.3	38109.8	43458.5	49141.5	52651.6
highThrust	99995.2	99784.6	96844.2	83979.1	81463.7	91996.8	97086.1	98835.5	99480.0	99743.9	99863.0
Pj	20.000	(MW) nju	150.000 (deg)	r	-0.6495	0.3750	V	-0.5773	-1.0000		
TOF (TU_Sun)	1.400	1.600	1.800	2.000	2.200	2.400	2.600	2.800	3.000	3.200	3.400
VSI type I	51039.2	28338.6	11307.8	3388.9	2504.3	5208.1	9157.3	13203.8	16893.4	20096.8	22817.9
VSI typeII	51139.3	28554.0	11813.1	4814.9	5107.3	6593.9	10100.9	13989.7	17604.6	20771.4	23476.3
CSI type I	64679.2	38200.1	16350.2	5082.5	3909.4	7884.5	12857.8	17738.0	22090.5	25814.7	28944.2
CSI typeII	60841.9	40115.5	27078.0	18386.3	12870.4	18052.0	28248.0	30420.9	37608.3	42789.9	42622.8
highThrust	99879.8	98789.1	92977.7	76848.6	70563.1	83707.4	92446.6	96349.1	98107.2	98950.3	99382.1
Pj	20.000	(MW) nju	180.000 (deg)	r	-0.7500	-0.0000	V	0.0000	-1.1547		
TOF (TU_Sun)	2.000	2.200	2.400	2.600	2.800	3.000	3.200	3.400	3.600	3.800	4.000
VSI type I	15564.6	6200.8	1951.1	1240.3	2531.4	4761.0	7308.9	9849.4	12229.4	14388.2	16311.5
VSI typeII	16044.3	7236.2	5571.6	6035.9	6500.2	7074.6	8995.4	11302.9	13569.5	15670.7	17568.1
CSI type I	22038.8	9288.4	3034.1	1995.6	4191.4	7303.0	10692.1	13986.5	17016.5	19723.7	22107.0
CSI typeII	31758.1	45965.7	14040.4	10864.6	16380.5	17550.5	24069.3	28415.2	33095.3	34933.9	40115.5
highThrust	96465.2	88436.0	73129.6	64867.6	75219.4	85622.9	91707.3	95046.0	96914.4	97999.5	98654.8

**Table A-2:** Transfer Orbit to Venus with 30MW Jet Power.

Venus	Fuel	Consumed (kg)									
Pj	30.000 (MW)	nju	60.000 (deg)	r	0.3750	0.6495	V	-1.0000	0.5774		
TOF (TU_Sun)	0.600	0.700	0.800	0.900	1.000	1.100	1.200	1.300	1.400	1.500	1.600
VSI type I	67214.1	45231.5	28906.2	23437.7	25032.9	29088.7	33353.1	37092.5	40176.4	42666.2	44663.8
VSI typeII	67246.0	45318.8	28989.0	23545.8	25205.9	29226.5	33435.9	37142.6	40209.8	42690.8	44683.8
CSI type I	83392.5	58208.3	36712.9	28924.4	30603.1	34734.7	38880.4	42468.5	45432.6	47840.3	49788.6
CSI typeII	100000.0	53529.2	37106.9	36104.0	42622.8	45506.1	45130.0	66817.4	56161.7	67695.0	58167.5
highThrust	99962.2	99517.3	98209.7	97435.0	98007.0	98951.2	99520.5	99780.0	99893.8	99945.5	99970.3
Pj	30.000 (MW)	nju	90.000 (deg)	r	-0.0000	0.7500	V	-1.1547	-0.0000		
TOF (TU_Sun)	1.000	1.100	1.200	1.300	1.400	1.500	1.600	1.700	1.800	1.900	2.000
VSI type I	32273.9	18137.6	10312.9	8102.1	9418.0	12418.2	15963.9	19476.5	22706.6	25571.7	28068.5
VSI typeII	32425.2	18474.5	10785.9	8677.7	10062.5	12994.1	16417.3	19835.7	23003.9	25830.4	28303.3
CSI type I	43010.5	24998.0	13960.5	10723.6	12824.1	16505.7	20438.1	24177.5	27555.5	30532.4	33121.5
CSI typeII	43876.4	31716.3	22565.0	21186.0	24570.8	28206.2	32092.4	42622.8	40617.0	45255.3	47637.2
highThrust	99199.9	96601.8	92196.7	90080.6	91669.9	94920.9	97316.9	98602.2	99248.9	99578.9	99753.5
Pj	30.000 (MW)	nju	120.000 (deg)	r	-0.3750	0.6495	V	-1.0000	-0.5774		
TOF (TU_Sun)	1.000	1.200	1.400	1.600	1.800	2.000	2.200	2.400	2.600	2.800	3.000
VSI type I	66566.4	39176.8	15373.1	4471.1	3807.8	7499.8	12153.7	16485.5	20154.0	23153.2	25572.3
VSI typeII	66609.7	39316.7	15867.5	5941.2	6268.1	8872.0	13150.8	17328.0	20928.4	23902.2	26320.2
CSI type I	81045.0	50691.8	21424.4	6384.8	5645.2	10551.8	16021.6	20946.8	25058.7	28393.7	31069.1
CSI typeII	75216.6	51147.3	31591.0	18052.0	20308.5	22565.0	33095.3	36104.0	45631.4	52651.6	75216.6
highThrust	99995.2	99784.6	96844.2	83979.1	81463.7	91996.8	97086.1	98835.5	99480.0	99743.9	99863.0
Pj	30.000 (MW)	nju	150.000 (deg)	r	-0.6495	0.3750	V	-0.5773	-1.0000		
TOF (TU_Sun)	1.400	1.600	1.800	2.000	2.200	2.400	2.600	2.800	3.000	3.200	3.400
VSI type I	41001.9	20863.2	7833.8	2285.1	1683.6	3533.4	6297.0	9207.8	11934.3	14359.8	16464.2
VSI typeII	41233.9	21365.3	9037.3	6964.5	7661.0	8357.4	9053.9	11255.3	13752.9	16080.0	18146.1
CSI type I	52700.8	28396.9	11360.7	3428.3	2652.0	5438.6	9032.2	12673.6	16015.2	18945.8	21459.1
CSI typeII	56161.7	38109.8	24821.5	15043.3	13789.7	18052.0	26075.1	31591.0	33847.5	40115.5	100000.0
highThrust	99879.8	98789.1	92977.7	76848.6	70563.1	83707.4	92446.6	96349.1	98107.2	98950.3	99382.1
Pj	30.000 (MW)	nju	180.000 (deg)	r	-0.7500	-0.0000	V	0.0000	-1.1547		
TOF (TU_Sun)	2.000	2.200	2.400	2.600	2.800	3.000	3.200	3.400	3.600	3.800	4.000
VSI type I	10944.2	4221.1	1309.2	830.3	1701.9	3225.1	4994.3	6789.2	8499.4	10075.3	11499.6
VSI typeII	12085.0	7661.0	8357.4	9053.9	9750.3	10446.8	11143.2	11839.7	12536.1	13606.3	14895.9
CSI type I	15610.6	6335.4	2036.2	1342.6	2847.0	5020.2	7439.8	9844.7	12101.6	14154.7	15990.0
CSI typeII	30086.7	22063.5	15043.3	16296.9	17550.5	45130.0	24069.3	100000.0	100000.0	100000.0	100000.0
highThrust	96465.2	88436.0	73129.6	64867.6	75219.4	85622.9	91707.3	95046.0	96914.4	97999.5	98654.8

**Table A-3:** Transfer Orbit to Mars with 10MW Jet Power.

Mars	Fuel	Consumed (kg)										
Pj	10.000 (MW)	nju	60.000 (deg)	r	0.7500	1.2990	V	-0.7071	0.4082			
TOF (TU_Sun)	1.000	1.200	1.400	1.600	1.800	2.000	2.200	2.400	2.600	2.800	3.000	
VSI type I	79408.5	61606.1	47004.4	41423.9	41965.7	44635.0	47528.4	50048.1	52091.7	53705.2	54964.0	
VSI typeII	79414.2	61614.3	47009.5	41449.5	42047.2	44712.1	47576.1	50077.0	52110.4	53718.3	54974.0	
CSI type I	87181.9	69845.2	57111.4	54419.3	57128.6	60687.3	63716.2	66008.5	67660.3	68807.4	69570.4	
CSI typeII	100000.0	100000.0	100000.0	48807.2	50395.1	53487.4	56997.5	59170.4	67360.7	65522.0	66441.4	
highThrust	99967.2	99643.5	98934.1	98558.6	98794.2	99254.3	99593.6	99781.4	99878.4	99929.2	99956.7	
Pj	10.000 (MW)	nju	90.000 (deg)	r	-0.0000	1.5000	V	-0.8165	-0.0000			
TOF (TU_Sun)	1.600	1.800	2.000	2.200	2.400	2.600	2.800	3.000	3.200	3.400	3.600	
VSI type I	52612.7	34420.2	22335.6	17921.9	18736.4	21928.2	25761.6	29449.8	32714.5	35503.2	37846.4	
VSI typeII	52627.3	34477.5	22396.5	18006.8	18911.1	22160.7	25959.4	29604.2	32838.6	35607.1	37938.0	
CSI type I	58608.9	40521.7	27802.8	24128.0	27162.8	32041.5	36853.9	41065.3	44567.3	47414.9	49702.4	
CSI typeII	56161.7	39112.6	29250.9	26660.1	28080.9	31507.4	36271.1	41369.1	44127.1	48305.8	51147.3	
highThrust	99544.1	97903.7	95112.7	93454.1	93878.0	95641.3	97361.7	98473.3	99104.8	99457.6	99658.9	
Pj	10.000 (MW)	nju	120.000 (deg)	r	-0.7500	1.2990	V	-0.7071	-0.4082			
TOF (TU_Sun)	2.000	2.200	2.400	2.600	2.800	3.000	3.200	3.400	3.600	3.800	4.000	
VSI type I	49261.4	33360.6	20285.3	11933.7	8234.4	7930.3	9621.9	12265.4	15221.2	18145.8	20874.8	
VSI typeII	49278.2	33415.1	20430.7	12185.9	8578.9	8375.6	10127.5	12759.9	15662.1	18538.1	21230.8	
CSI type I	55204.5	39177.4	25461.6	15715.4	11051.3	11872.3	15087.1	18902.7	22736.7	26321.4	29540.5	
CSI typeII	53487.4	38611.2	29083.8	26075.1	18720.6	18804.2	20057.8	26994.4	27078.0	31758.1	35101.1	
highThrust	99644.3	98507.0	95434.2	90129.7	85574.1	84744.6	87331.3	91130.8	94232.7	96288.8	97575.1	
Pj	10.000 (MW)	nju	150.000 (deg)	r	-1.2990	0.7500	V	-0.4082	-0.7071			
TOF (TU_Sun)	3.000	3.200	3.400	3.600	3.800	4.000	4.200	4.400	4.600	4.800	5.000	
VSI type I	12905.5	7430.8	4572.3	3700.7	4175.4	5473.8	7219.5	9162.5	11147.5	13081.4	14914.5	
VSI typeII	13203.7	7934.8	5356.1	4753.6	5397.9	6588.9	8188.1	10019.7	11933.4	13818.8	15617.8	
CSI type I	17181.4	10394.2	6346.7	5428.2	6904.0	9151.1	11765.3	14462.9	16993.3	19474.7	21775.7	
CSI typeII	26325.8	20057.8	14207.6	15043.3	14291.2	16714.8	21060.7	22063.5	26910.8	30086.7	33429.6	
highThrust	93009.0	86705.5	79495.9	75314.1	76448.8	81046.5	86048.4	90035.3	92892.5	94876.2	96249.8	
Pj	10.000 (MW)	nju	180.000 (deg)	r	-1.5000	-0.0000	V	0.0000	-0.8165			
TOF (TU_Sun)	3.000	3.200	3.400	3.600	3.800	4.000	4.200	4.400	4.600	4.800	5.000	
VSI type I	29615.1	20793.0	13728.2	8527.5	5049.8	3014.4	2100.0	2005.5	2480.1	3328.2	4405.8	
VSI typeII	29768.1	21023.1	14075.4	9059.4	5913.8	4643.0	4875.2	5107.3	5339.5	5659.8	7784.6	
CSI type I	36181.1	26430.4	18252.6	11895.2	7352.7	4422.1	2962.3	3385.1	6057.8	9658.5	9158.2	
CSI typeII	38861.9	36104.0	29835.9	24069.3	17467.0	15043.3	12285.4	12870.4	13455.4	22063.5	16714.8	
highThrust	98824.9	97418.4	94892.9	90837.7	85117.1	78401.6	72711.3	70651.6	72753.6	77052.0	81602.4	

**Table A-4:** Transfer Orbit to Mars with 20MW Jet Power.

Mars	Fuel	Consumed (kg)										
Pj	20.000 (MW)	nju	60.000 (deg)	r	0.7500	1.2990	V	-0.7071	0.4082			
TOF (TU_Sun)	1.000	1.200	1.400	1.600	1.800	2.000	2.200	2.400	2.600	2.800	3.000	
VSI type I	65849.9	44515.0	30722.7	26122.7	26555.2	28729.5	31172.0	33376.3	35219.5	36710.9	37897.2	
VSI typeII	65876.5	44570.0	30803.1	26302.2	26864.3	29053.7	31453.6	33617.8	35433.3	36908.0	38085.8	
CSI type I	73308.0	51853.8	38181.0	34785.1	36617.2	39583.9	42341.3	44580.5	46299.1	47573.3	48487.3	
CSI typeII	71037.9	52150.2	40951.3	37441.2	39112.6	43458.5	49643.0	50144.4	52150.2	60841.9	57666.1	
highThrust	99967.2	99643.5	98934.1	98558.6	98794.2	99254.3	99593.6	99781.4	99878.4	99929.2	99956.7	
Pj	20.000 (MW)	nju	90.000 (deg)	r	-0.0000	1.5000	V	-0.8165	-0.0000			
TOF (TU_Sun)	1.600	1.800	2.000	2.200	2.400	2.600	2.800	3.000	3.200	3.400	3.600	
VSI type I	35696.9	20787.7	12571.8	9842.9	10336.5	12314.2	14785.2	17267.5	19556.5	21583.1	23339.7	
VSI typeII	35801.6	21060.4	13005.6	10476.9	11177.9	13230.7	15645.1	18052.8	20281.2	22266.4	23998.0	
CSI type I	41605.8	25802.7	16198.6	13393.0	15069.8	18116.1	21323.7	24302.1	26918.2	29148.7	31020.4	
CSI typeII	45464.3	34599.6	26743.7	25740.8	26075.1	28248.0	35101.1	37608.3	40115.5	45464.3	45130.0	
highThrust	99544.1	97903.7	95112.7	93454.1	93878.0	95641.3	97361.7	98473.3	99104.8	99457.6	99658.9	
Pj	20.000 (MW)	nju	120.000 (deg)	r	-0.7500	1.2990	V	-0.7071	-0.4082			
TOF (TU_Sun)	2.000	2.200	2.400	2.600	2.800	3.000	3.200	3.400	3.600	3.800	4.000	
VSI type I	32679.9	20019.6	11287.5	6345.5	4294.0	4128.9	5054.1	6533.3	8237.5	9978.3	11654.1	
VSI typeII	32826.0	20353.8	11965.7	7541.6	6500.2	6964.5	7609.8	8809.3	10228.2	11769.6	13325.0	
CSI type I	38420.8	24897.0	14927.2	8656.4	5835.9	6195.6	7947.9	10115.5	12384.6	14595.5	16662.2	
CSI typeII	45130.0	34933.9	26075.1	20280.6	17160.5	17550.5	18720.6	24626.5	25072.2	28582.3	32315.3	
highThrust	99644.3	98507.0	95434.2	90129.7	85574.1	84744.6	87331.3	91130.8	94232.7	96288.8	97575.1	
Pj	20.000 (MW)	nju	150.000 (deg)	r	-1.2990	0.7500	V	-0.4082	-0.7071			
TOF (TU_Sun)	3.000	3.200	3.400	3.600	3.800	4.000	4.200	4.400	4.600	4.800	5.000	
VSI type I	6897.9	3858.8	2339.6	1885.3	2132.2	2813.9	3744.9	4801.4	5902.9	6998.4	8057.9	
VSI typeII	8341.4	7428.8	7893.1	8357.4	8821.7	9286.0	9750.3	10214.6	10678.9	11143.2	11704.0	
CSI type I	9585.5	5559.6	3297.9	2771.4	3529.0	4714.7	6158.8	7575.7	9084.9	10518.6	11901.8	
CSI typeII	23400.7	17829.1	15154.8	13037.5	13761.9	15600.5	17550.5	20837.8	23066.4	26743.7	27858.0	
highThrust	93009.0	86705.5	79495.9	75314.1	76448.8	81046.5	86048.4	90035.3	92892.5	94876.2	96249.8	
Pj	20.000 (MW)	nju	180.000 (deg)	r	-1.5000	-0.0000	V	0.0000	-0.8165			
TOF (TU_Sun)	3.000	3.200	3.400	3.600	3.800	4.000	4.200	4.400	4.600	4.800	5.000	
VSI type I	17381.3	11603.0	7370.0	4453.6	2590.3	1530.3	1061.1	1012.9	1255.6	1692.3	2252.5	
VSI typeII	18085.3	12667.3	9093.3	8357.4	8821.7	9286.0	9750.3	10214.6	10678.9	11143.2	11607.5	
CSI type I	22434.7	15514.7	10225.1	6419.0	3858.6	2276.3	1504.0	1712.3	3616.8	4837.7	5282.8	
CSI typeII	35936.8	30309.5	24626.5	21060.7	16937.7	14486.2	11700.4	12257.5	12814.7	13371.8	16714.8	
highThrust	98824.9	97418.4	94892.9	90837.7	85117.1	78401.6	72711.3	70651.6	72753.6	77052.0	81602.4	

**Table A-5:** Transfer Orbit to Mars with 30MW Jet Power.

Mars	Fuel	Consumed (kg)										
Pj	30.000	(MW) nju	60.000 (deg)	r	0.7500	1.2990	V	-0.7071	0.4082			
TOF (TU_Sun)	1.000	1.200	1.400	1.600	1.800	2.000	2.200	2.400	2.600	2.800	3.000	
VSI type I	56245.6	34847.5	22818.6	19076.2	19422.7	21181.5	23191.1	25036.3	26602.8	27886.4	28918.1	
VSI typeII	56312.3	34999.4	23081.5	19556.1	20113.3	21928.9	23913.2	25723.7	27266.8	28541.3	29576.4	
CSI type I	63479.1	41490.0	28785.3	25591.4	26938.8	29346.5	31669.5	33613.7	35146.0	36311.8	37172.4	
CSI typeII	61426.9	45631.4	37441.2	35435.4	36856.1	40115.5	43207.8	47135.8	49977.3	53821.7	55158.9	
highThrust	99967.2	99643.5	98934.1	98558.6	98794.2	99254.3	99593.6	99781.4	99878.4	99929.2	99956.7	
Pj	30.000	(MW) nju	90.000 (deg)	r	-0.0000	1.5000	V	-0.8165	-0.0000			
TOF (TU_Sun)	1.600	1.800	2.000	2.200	2.400	2.600	2.800	3.000	3.200	3.400	3.600	
VSI type I	27012.1	14890.2	8747.8	6784.6	7136.9	8560.9	10367.7	12214.7	13946.9	15504.2	16872.9	
VSI typeII	27303.7	15555.1	9890.1	8497.3	9301.1	10776.3	12464.3	14187.5	15830.9	17335.4	18680.9	
CSI type I	32452.6	19001.4	11450.4	9275.4	10428.6	12626.6	14999.1	17253.7	19277.9	21039.8	22545.1	
CSI typeII	42121.3	32343.1	25907.9	23902.2	54156.0	27161.6	30420.9	35101.1	38778.3	41202.0	45130.0	
highThrust	99544.1	97903.7	95112.7	93454.1	93878.0	95641.3	97361.7	98473.3	99104.8	99457.6	99658.9	
Pj	30.000	(MW) nju	120.000 (deg)	r	-0.7500	1.2990	V	-0.7071	-0.4082			
TOF (TU_Sun)	2.000	2.200	2.400	2.600	2.800	3.000	3.200	3.400	3.600	3.800	4.000	
VSI type I	24450.0	14300.7	7819.2	4321.7	2904.2	2791.0	3427.1	4452.5	5646.8	6881.0	8083.4	
VSI typeII	24877.1	15174.1	9561.4	9053.9	9750.3	10446.8	11143.2	11839.7	12536.1	13232.6	13929.0	
CSI type I	29628.8	18313.6	10578.6	5977.9	3965.9	4191.8	5394.9	6904.9	8509.1	10096.6	11603.0	
CSI typeII	43458.5	34014.6	26075.1	20642.8	17550.5	17550.5	18720.6	21311.4	25573.7	28582.3	31758.1	
highThrust	99644.3	98507.0	95434.2	90129.7	85574.1	84744.6	87331.3	91130.8	94232.7	96288.8	97575.1	
Pj	30.000	(MW) nju	150.000 (deg)	r	-1.2990	0.7500	V	-0.4082	-0.7071			
TOF (TU_Sun)	3.000	3.200	3.400	3.600	3.800	4.000	4.200	4.400	4.600	4.800	5.000	
VSI type I	4706.8	2606.0	1572.0	1264.8	1431.6	1893.7	2528.2	3253.0	4014.2	4777.2	5520.5	
VSI typeII	10446.8	11143.2	11839.7	12536.1	13232.6	13929.0	14625.5	15321.9	16018.4	16714.8	17411.3	
CSI type I	6653.0	3796.1	2228.1	1860.7	2370.3	3175.3	4447.3	5162.0	6181.7	7204.9	8188.8	
CSI typeII	23818.6	18720.6	14207.6	13539.0	14291.2	15043.3	17550.5	22063.5	23066.4	28080.9	29250.9	
highThrust	93009.0	86705.5	79495.9	75314.1	76448.8	81046.5	86048.4	90035.3	92892.5	94876.2	96249.8	
Pj	30.000	(MW) nju	180.000 (deg)	r	-1.5000	-0.0000	V	0.0000	-0.8165			
TOF (TU_Sun)	3.000	3.200	3.400	3.600	3.800	4.000	4.200	4.400	4.600	4.800	5.000	
VSI type I	12300.2	8046.5	5037.1	3013.8	1741.9	1025.4	709.9	677.5	840.6	1134.6	1513.0	
VSI typeII	14082.7	11143.2	11839.7	12536.1	13232.6	13929.0	14625.5	15321.9	16018.4	16714.8	17411.3	
CSI type I	16302.1	10998.6	7108.1	4397.4	2616.1	1532.8	1007.9	1294.2	2279.5	2972.4	3427.4	
CSI typeII	35101.1	30755.2	25573.7	21060.7	17467.0	15043.3	12285.4	12870.4	13455.4	14040.4	16714.8	
highThrust	98824.9	97418.4	94892.9	90837.7	85117.1	78401.6	72711.3	70651.6	72753.6	77052.0	81602.4	

**Table A-6:** Transfer Orbit to Asteroids with 10MW Jet Power.

Asteroids	Fuel	Consumed (kg)									
Pj	10.000 (MW)	nju	60.000 (deg)	r	1.5000	2.5981	V	-0.5000	0.2887		
TOF (TU_Sun)	4.000	4.500	5.000	5.500	6.000	6.500	7.000	7.500	8.000	8.500	9.000
VSI type I	54518.7	52226.3	50615.2	49368.2	48314.9	47365.1	46470.9	45606.4	44758.8	43921.9	43092.3
VSI typeII	54754.2	52565.3	51006.8	49775.2	48720.7	47762.5	46857.6	46278.5	45125.8	44280.8	43445.2
CSI type I	76035.4	73914.0	70945.9	63355.0	42451.6	36651.8	26349.2	21317.1	17312.0	14098.9	11527.3
CSI typeII	67416.4	65814.5	65466.3	65884.2	66023.5	66093.1	66302.1	66859.2	66859.2	68670.0	67695.0
highThrust	99967.1	99964.3	99966.5	99971.5	99977.0	99982.0	99985.9	99989.0	99991.3	99993.0	99994.4
Pj	10.000 (MW)	nju	90.000 (deg)	r	-0.0000	3.0000	V	-0.5774	-0.0000		
TOF (TU_Sun)	4.000	4.500	5.000	5.500	6.000	6.500	7.000	7.500	8.000	8.500	9.000
VSI type I	39105.7	35795.5	34350.4	33820.1	33688.6	33699.6	33731.2	33731.6	33679.6	33571.4	33409.0
VSI typeII	39220.8	36035.8	34764.0	34395.4	40277.9	34434.1	34484.2	34489.5	34438.3	34330.3	34169.7
CSI type I	54883.4	53077.3	52192.0	51548.0	50910.3	44763.1	36283.3	28483.0	21993.8	16969.2	13705.8
CSI typeII	51815.9	50144.4	50144.4	50562.3	50980.2	52512.3	54601.7	54323.1	55716.0	58014.3	58919.7
highThrust	99770.3	99684.1	99646.4	99657.2	99701.0	99757.3	99811.1	99855.5	99889.7	99915.3	99934.2
Pj	10.000 (MW)	nju	120.000 (deg)	r	-1.5000	2.5981	V	-0.5000	-0.2887		
TOF (TU_Sun)	4.000	4.500	5.000	5.500	6.000	6.500	7.000	7.500	8.000	8.500	9.000
VSI type I	34246.8	26058.3	21775.9	19995.2	19588.6	19854.0	20401.3	21028.4	21635.6	22178.4	22640.2
VSI typeII	34438.6	26340.3	22190.0	20605.1	20428.4	20898.6	21595.1	22778.9	22973.9	23548.2	24033.8
CSI type I	41599.0	34564.4	32124.3	31954.9	32561.5	41801.1	39133.9	36625.4	31467.4	23235.1	17779.9
CSI typeII	45687.1	41369.1	42483.5	42135.2	40951.3	40742.3	40951.3	40742.3	43458.5	43806.7	45130.0
highThrust	99699.9	99248.7	98737.2	98367.9	98225.4	98293.0	98500.5	98763.9	99019.3	99235.7	99406.6
Pj	10.000 (MW)	nju	150.000 (deg)	r	-2.5981	1.5000	V	-0.2887	-0.5000		
TOF (TU_Sun)	4.000	4.500	5.000	5.500	6.000	6.500	7.000	7.500	8.000	8.500	9.000
VSI type I	42016.8	29363.1	20474.1	15067.3	12223.5	11029.3	10805.5	11110.7	11677.2	12349.2	13039.8
VSI typeII	42139.6	29628.2	20956.5	15827.0	13315.9	12496.8	12658.0	13275.0	14032.2	20960.3	22061.4
CSI type I	47717.3	34972.2	25591.8	20142.3	18415.6	18645.2	19515.8	20531.3	21505.1	30516.8	25984.2
CSI typeII	52930.2	45756.8	39001.2	34474.3	33429.6	35310.0	36076.1	42831.7	49030.1	41438.8	73963.0
highThrust	99935.6	99722.7	99178.8	98208.4	96978.2	95875.5	95233.5	95146.7	95498.8	96086.1	96730.5
Pj	10.000 (MW)	nju	180.000 (deg)	r	-3.0000	-0.0000	V	0.0000	-0.5774		
TOF (TU_Sun)	6.000	6.500	7.000	7.500	8.000	8.500	9.000	9.500	10.000	10.500	11.000
VSI type I	12882.8	9386.3	7424.0	6488.3	6207.2	6325.3	6674.7	7147.9	7676.9	8220.0	8752.4
VSI typeII	13768.9	10752.3	9424.0	9465.2	10009.2	10646.2	11305.7	15828.4	18178.6	20929.8	16629.2
CSI type I	16573.3	12515.7	11336.8	11172.2	11871.1	12755.2	17090.6	21167.9	24284.7	15357.2	12501.8
CSI typeII	33429.6	31688.5	29250.9	31340.3	32315.3	28415.2	31340.3	42344.2	40394.1	38026.2	42901.3
highThrust	98779.1	97738.9	96399.6	94991.9	93826.3	93143.5	93003.4	93300.4	93862.1	94534.8	95215.6

**Table A-7:** Transfer Orbit to Asteroids with 20MW Jet Power.

Asteroids	Fuel	Consumed (kg)									
Pj	20.000 (MW)	nju	60.000 (deg)	r	1.5000	2.5981	V	-0.5000	0.2887		
TOF (TU_Sun)	4.000	4.500	5.000	5.500	6.000	6.500	7.000	7.500	8.000	8.500	9.000
VSI type I	37474.8	35342.1	33882.3	32774.1	31852.3	31031.7	30268.6	29539.2	28831.9	28141.0	27463.6
VSI typeII	38357.0	36513.3	35279.1	34327.7	33543.6	32847.1	16250.5	17411.3	18572.0	19732.8	20893.5
CSI type I	53561.8	50857.4	48572.6	35822.5	29394.4	25010.2	19683.8	11927.9	9480.0	7590.7	6122.3
CSI typeII	60173.3	58919.7	58501.8	59755.4	96945.9	61566.2	62401.9	62680.5	64630.6	63934.1	100000.0
highThrust	99967.1	99964.3	99966.5	99971.5	99977.0	99982.0	99985.9	99989.0	99991.3	99993.0	99994.4
Pj	20.000 (MW)	nju	90.000 (deg)	r	-0.0000	3.0000	V	-0.5774	-0.0000		
TOF (TU_Sun)	4.000	4.500	5.000	5.500	6.000	6.500	7.000	7.500	8.000	8.500	9.000
VSI type I	24305.2	21799.1	20736.7	20351.3	20256.2	20264.2	20287.2	20287.5	20249.9	20171.7	20054.6
VSI typeII	25174.0	23161.2	22608.8	22657.8	22900.8	23174.7	23428.9	23648.7	23835.4	19732.8	20893.5
CSI type I	34499.9	32746.4	31994.2	32579.7	31122.0	30678.8	27221.8	17613.4	12321.4	9382.4	7374.8
CSI typeII	50144.4	52651.6	57108.9	45965.7	83574.0	47080.0	50701.6	52233.8	53487.4	54462.4	72709.4
highThrust	99770.3	99684.1	99646.4	99657.2	99701.0	99757.3	99811.1	99855.5	99889.7	99915.3	99934.2
Pj	20.000 (MW)	nju	120.000 (deg)	r	-1.5000	2.5981	V	-0.5000	-0.2887		
TOF (TU_Sun)	4.000	4.500	5.000	5.500	6.000	6.500	7.000	7.500	8.000	8.500	9.000
VSI type I	20661.2	14980.9	12218.4	11108.2	10857.6	11021.1	11359.5	11749.5	12130.1	12472.3	12765.1
VSI typeII	21632.0	16577.5	14665.6	14693.7	15408.9	20792.4	17147.7	22416.2	18572.0	19732.8	20893.5
CSI type I	26006.4	20212.3	18154.4	17877.9	18196.3	21482.9	21256.1	20641.9	20067.3	13979.6	10060.4
CSI typeII	43458.5	38861.9	39001.2	38304.8	35101.1	38026.2	39001.2	41787.0	42344.2	44990.7	47637.2
highThrust	99699.9	99248.7	98737.2	98367.9	98225.4	98293.0	98500.5	98763.9	99019.3	99235.7	99406.6
Pj	20.000 (MW)	nju	150.000 (deg)	r	-2.5981	1.5000	V	-0.2887	-0.5000		
TOF (TU_Sun)	4.000	4.500	5.000	5.500	6.000	6.500	7.000	7.500	8.000	8.500	9.000
VSI type I	26595.7	17207.8	11404.8	8147.4	6509.6	5836.4	5711.2	5882.2	6200.6	6580.9	6974.6
VSI typeII	27258.9	18476.5	13622.1	12768.3	13929.0	15089.8	16250.5	17411.3	18572.5	19732.8	22667.5
CSI type I	31832.7	21580.3	14811.6	11085.3	9851.1	9897.7	10367.5	10945.5	12828.6	18107.3	14175.7
CSI typeII	54601.7	45130.0	40394.1	32176.0	35101.1	36215.4	35101.1	33429.6	35658.3	33151.0	35101.1
highThrust	99935.6	99722.7	99178.8	98208.4	96978.2	95875.5	95233.5	95146.7	95498.8	96086.1	96730.5
Pj	20.000 (MW)	nju	180.000 (deg)	r	-3.0000	-0.0000	V	0.0000	-0.5774		
TOF (TU_Sun)	6.000	6.500	7.000	7.500	8.000	8.500	9.000	9.500	10.000	10.500	11.000
VSI type I	6885.3	4924.3	3855.0	3353.0	3203.0	3265.9	3452.6	3706.3	3991.7	4286.2	4576.5
VSI typeII	13929.0	15089.8	16250.5	17411.3	18572.2	19732.8	20903.7	22054.3	23215.0	24375.8	25536.5
CSI type I	9148.9	6677.1	5744.1	5847.3	6138.1	6599.7	7813.8	12453.8	11089.7	9988.9	6734.1
CSI typeII	35101.1	34404.6	29250.9	27161.6	26743.7	30783.1	30086.7	26465.1	36215.4	35101.1	39837.0
highThrust	98779.1	97738.9	96399.6	94991.9	93826.3	93143.5	93003.4	93300.4	93862.1	94534.8	95215.6



**Table A-8:** Transfer Orbit to Asteroids with 30MW Jet Power.

Asteroids	Fuel	Consumed (kg)										
Pj	30.000	(MW) nju	60.000 (deg)	r	1.5000	2.5981	V	-0.5000	0.2887			
TOF (TU_Sun)	4.000	4.500	5.000	5.500	6.000	6.500	7.000	7.500	8.000	8.500	9.000	
VSI type I	28549.5	26707.8	25464.1	24529.1	23757.3	23074.7	22443.5	21843.6	21265.0	20702.6	20154.1	
VSI typeII	30524.2	31094.3	28547.8	28093.0	20893.5	22634.6	24375.8	31791.4	27858.0	29599.1	31340.3	
CSI type I	41167.5	38762.4	36798.1	25440.6	21356.4	14955.0	10917.0	8285.2	6530.5	5194.9	4168.8	
CSI typeII	58501.8	56412.5	56412.5	57457.1	60173.3	62471.6	64352.0	65814.5	70202.2	68670.0	63934.1	
highThrust	99967.1	99964.3	99966.5	99971.5	99977.0	99982.0	99985.9	99989.0	99991.3	99993.0	99994.4	
Pj	30.000	(MW) nju	90.000 (deg)	r	-0.0000	3.0000	V	-0.5774	-0.0000			
TOF (TU_Sun)	4.000	4.500	5.000	5.500	6.000	6.500	7.000	7.500	8.000	8.500	9.000	
VSI type I	17632.0	15671.5	14851.0	14554.9	14482.0	14488.1	14505.7	28947.3	14477.1	14417.1	14327.5	
VSI typeII	20021.8	19296.6	19719.1	25341.5	21401.4	22674.2	24375.8	26116.9	27858.0	29599.1	31340.3	
CSI type I	25172.7	23661.1	23038.6	23793.8	22636.6	21852.3	16365.8	12409.7	12174.9	6531.0	7281.4	
CSI typeII	50144.4	43249.6	43876.4	43667.4	47637.2	46174.7	49726.5	50144.4	53487.4	92349.3	56412.5	
highThrust	99770.3	99684.1	99646.4	99657.2	99701.0	99757.3	99811.1	99855.5	99889.7	99915.3	99934.2	
Pj	30.000	(MW) nju	120.000 (deg)	r	-1.5000	2.5981	V	-0.5000	-0.2887			
TOF (TU_Sun)	4.000	4.500	5.000	5.500	6.000	6.500	7.000	7.500	8.000	8.500	9.000	
VSI type I	14793.0	10512.2	8491.4	7690.1	7510.2	7627.5	7871.0	8152.3	8427.5	8675.6	8888.2	
VSI typeII	17240.3	15670.1	17411.3	19152.4	23588.5	24949.4	24375.8	26126.8	27858.0	29599.1	31340.3	
CSI type I	18997.5	14314.4	12660.6	12409.7	12626.4	15152.1	15818.5	14643.3	14768.3	10464.4	7050.9	
CSI typeII	46801.5	41369.1	41787.0	34474.3	37608.3	40742.3	38026.2	43876.4	40115.5	42622.8	63934.1	
highThrust	99699.9	99248.7	98737.2	98367.9	98225.4	98293.0	98500.5	98763.9	99019.3	99235.7	99406.6	
Pj	30.000	(MW) nju	150.000 (deg)	r	-2.5981	1.5000	V	-0.2887	-0.5000			
TOF (TU_Sun)	4.000	4.500	5.000	5.500	6.000	6.500	7.000	7.500	8.000	8.500	9.000	
VSI type I	19455.2	12170.0	7903.3	5583.2	4435.9	3968.1	3881.4	3999.9	4220.9	4485.7	4760.4	
VSI typeII	21168.6	15670.1	17411.3	19152.4	20893.5	22634.6	24375.8	26116.9	27858.0	29599.1	31340.3	
CSI type I	24010.2	15658.2	10443.3	7656.3	6726.8	6737.3	7057.8	7461.4	7875.6	8447.2	8619.2	
CSI typeII	50144.4	43249.6	37608.3	34474.3	30086.7	27161.6	32176.0	34474.3	30086.7	35519.0	41369.1	
highThrust	99935.6	99722.7	99178.8	98208.4	96978.2	95875.5	95233.5	95146.7	95498.8	96086.1	96730.5	
Pj	30.000	(MW) nju	180.000 (deg)	r	-3.0000	-0.0000	V	0.0000	-0.5774			
TOF (TU_Sun)	6.000	6.500	7.000	7.500	8.000	8.500	9.000	9.500	10.000	10.500	11.000	
VSI type I	4698.0	3337.6	2603.4	2260.6	2158.4	2201.3	2328.5	2501.8	2697.0	2898.9	3098.2	
VSI typeII	20893.5	22634.6	24375.8	26116.9	27858.0	29599.1	31340.3	33081.4	34822.5	36563.6	38304.8	
CSI type I	6324.2	4555.7	4248.1	3896.6	4139.1	4456.8	4793.7	10159.3	7011.9	5746.0	5028.4	
CSI typeII	35101.1	32593.9	29250.9	28206.2	26743.7	28415.2	33847.5	31758.1	37608.3	35101.1	32176.0	
highThrust	98779.1	97738.9	96399.6	94991.9	93826.3	93143.5	93003.4	93300.4	93862.1	94534.8	95215.6	

**Table A-9:** Transfer Orbit to Jupiter with 10MW Jet Power.

Jupiter	Fuel	Consumed (kg)									
Pj	10.000	(MW) nju	90.000 (deg)	r	-0.0000	5.0000	V	-0.4472	-0.0000		
TOF (TU_Sun)	4.000	5.000	6.000	7.000	8.000	9.000	10.000	11.000	12.000	13.000	14.000
VSI type I	68922.4	54109.3	44194.4	38342.0	34862.0	32617.2	31001.3	29711.2	28597.2	27584.5	26636.6
VSI typeII	68994.4	54235.7	44452.2	38861.4	35744.8	33874.4	42448.3	35060.1	31855.4	29766.1	28967.9
CSI type I	82191.1	70667.9	63066.3	58046.7	49407.1	38829.4	29936.5	24986.9	18634.6	14575.0	11552.9
CSI typeII	77222.4	67277.1	61677.6	57916.8	58836.1	60173.3	61009.0	62513.4	67193.5	79311.8	57331.8
highThrust	99999.3	99991.5	99968.0	99934.9	99904.4	99884.1	99876.3	99879.4	99889.8	99903.5	99917.6
Pj	10.000	(MW) nju	120.000 (deg)	r	-2.5000	4.3301	V	-0.3873	-0.2236		
TOF (TU_Sun)	6.000	7.000	8.000	9.000	10.000	11.000	12.000	13.000	14.000	15.000	16.000
VSI type I	37660.5	28892.2	24224.3	21840.1	20604.3	19918.3	19484.3	19157.5	18868.9	18587.5	18299.6
VSI typeII	38009.0	29494.7	25216.5	23351.1	22668.8	34509.0	34375.4	28261.1	22531.8	17411.3	18572.0
CSI type I	48876.4	42256.6	43059.1	41097.5	34475.0	29231.0	21202.5	17776.4	13827.0	13661.1	8826.7
CSI typeII	57164.6	57331.8	52150.2	50395.1	51815.9	49643.0	49141.5	51063.7	46801.5	50144.4	49475.8
highThrust	99946.8	99813.8	99619.5	99436.2	99312.6	99261.3	99273.4	99329.6	99408.4	99492.6	99571.5
Pj	10.000	(MW) nju	150.000 (deg)	r	-4.3301	2.5000	V	-0.2236	-0.3873		
TOF (TU_Sun)	10.000	12.000	14.000	16.000	18.000	20.000	22.000	24.000	26.000	28.000	30.000
VSI type I	13407.1	12157.1	12101.6	12246.5	12339.9	12336.6	12246.3	12089.1	11884.3	11647.6	11390.4
VSI typeII	16253.2	17015.2	22551.5	18606.6	28072.7	23215.0	25536.5	27858.0	30179.5	32501.0	34822.5
CSI type I	28756.7	26063.8	15761.6	10220.8	7105.5	6209.5	21280.2	11927.6	5652.2	5674.7	7850.5
CSI typeII	35101.1	43124.2	38611.2	42789.9	43625.6	41787.0	44127.1	48138.6	49977.3	49141.5	50144.4
highThrust	98608.4	97673.4	97543.9	97947.1	98444.9	98849.6	99140.9	99344.5	99487.6	99589.9	99664.7
Pj	10.000	(MW) nju	180.000 (deg)	r	-5.0000	-0.0000	V	0.0000	-0.4472		
TOF (TU_Sun)	10.000	12.000	14.000	16.000	18.000	20.000	22.000	24.000	26.000	28.000	30.000
VSI type I	10675.1	7920.0	7466.6	7680.3	8025.5	8336.4	8571.0	8727.8	8817.4	8852.4	8844.4
VSI typeII	13524.2	16787.5	18806.3	18572.0	20893.5	26293.5	25536.6	27887.6	30179.5	32501.0	34823.0
CSI type I	16642.0	17461.6	18871.0	11500.2	8246.9	6347.1	19293.9	6052.0	13178.8	8717.2	15118.9
CSI typeII	41787.0	41118.4	40951.3	40115.5	43625.6	45130.0	44127.1	44127.1	45631.4	42121.3	47637.2
highThrust	99304.7	97994.9	96654.4	96089.4	96281.1	96800.9	97354.6	97832.8	98216.6	98517.3	98751.9

**Table A-10:** Transfer Orbit to Jupiter with 20MW Jet Power.

Jupiter	Fuel	Consumed (kg)									
Pj	20.000	(MW) nju	90.000 (deg)	r	-0.0000	5.0000	V	-0.4472	-0.0000		
TOF (TU_Sun)	4.000	5.000	6.000	7.000	8.000	9.000	10.000	11.000	12.000	13.000	14.000
VSI type I	52581.6	37089.1	28365.3	23718.1	21110.8	31141.2	18344.1	17447.5	16684.2	15998.9	15364.6
VSI typeII	52937.9	37889.5	29967.7	26490.1	36188.2	28647.2	23229.7	31611.1	27858.0	30179.5	32501.0
CSI type I	63502.3	49153.3	41155.2	36602.8	33208.0	26847.3	17842.6	14434.4	10322.3	7957.7	6132.9
CSI typeII	70870.8	61844.8	57164.6	53821.7	54824.6	52651.6	53487.4	53320.2	54156.0	69533.6	65522.0
highThrust	99999.3	99991.5	99968.0	99934.9	99904.4	99884.1	99876.3	99879.4	99889.8	99903.5	99917.6
Pj	20.000	(MW) nju	120.000 (deg)	r	-2.5000	4.3301	V	-0.3873	-0.2236		
TOF (TU_Sun)	6.000	7.000	8.000	9.000	10.000	11.000	12.000	13.000	14.000	15.000	16.000
VSI type I	23198.5	16885.2	13781.4	12258.5	11485.4	11060.7	10793.7	10593.5	10417.3	10246.0	10071.3
VSI typeII	24994.9	20248.7	19819.7	20967.6	23215.1	25536.5	27858.0	30179.5	32501.0	34822.5	37144.0
CSI type I	30675.8	24971.0	23126.5	21236.8	25901.9	15797.8	11853.5	9884.1	7322.0	5771.5	5353.4
CSI typeII	54156.0	53821.7	45464.3	54156.0	48472.9	49643.0	50144.4	49977.3	46801.5	47637.2	50813.0
highThrust	99946.8	99813.8	99619.5	99436.2	99312.6	99261.3	99273.4	99329.6	99408.4	99492.6	99571.5
Pj	20.000	(MW) nju	150.000 (deg)	r	-4.3301	2.5000	V	-0.2236	-0.3873		
TOF (TU_Sun)	10.000	12.000	14.000	16.000	18.000	20.000	22.000	24.000	26.000	28.000	30.000
VSI type I	7098.0	6472.0	6440.5	6522.6	6575.7	6573.9	6522.5	6433.4	6317.6	6184.0	6039.1
VSI typeII	23215.0	27862.0	32501.0	37144.0	41787.0	46458.9	51073.0	55716.0	60360.2	65002.0	69645.0
CSI type I	17436.4	13174.4	9938.4	5600.6	4820.0	3374.2	5554.5	3521.5	5170.9	3058.3	6698.7
CSI typeII	43458.5	44127.1	42121.3	42789.9	45130.0	50144.4	47804.3	48138.6	52150.2	56161.7	55158.9
highThrust	98608.4	97673.4	97543.9	97947.1	98444.9	98849.6	99140.9	99344.5	99487.6	99589.9	99664.7
Pj	20.000	(MW) nju	180.000 (deg)	r	-5.0000	-0.0000	V	0.0000	-0.4472		
TOF (TU_Sun)	10.000	12.000	14.000	16.000	18.000	20.000	22.000	24.000	26.000	28.000	30.000
VSI type I	5638.6	4123.3	3878.1	3993.5	4180.5	4349.5	4477.4	4563.0	4612.0	4631.2	4626.8
VSI typeII	23239.4	27858.0	32501.0	37144.0	41787.0	46430.0	51073.0	55716.0	60359.0	65002.0	69645.0
CSI type I	8774.6	8848.1	8885.8	6560.6	3849.7	3178.0	2092.9	11401.3	5475.0	3433.9	8291.4
CSI typeII	40115.5	50144.4	35101.1	40115.5	42121.3	36772.6	44127.1	40115.5	47804.3	46801.5	45130.0
highThrust	99304.7	97994.9	96654.4	96089.4	96281.1	96800.9	97354.6	97832.8	98216.6	98517.3	98751.9

**Table A-11:** Transfer Orbit to Jupiter with 30MW Jet Power.

Jupiter Pj	Fuel 30.000	Consumed (kg) (MW) nju	90.000 (deg)	r	-0.0000	5.0000	V	-0.4472	-0.0000		
TOF (TU_Sun)	4.000	5.000	6.000	7.000	8.000	9.000	10.000	11.000	12.000	13.000	14.000
VSI type I	42504.2	28214.2	20884.8	17169.5	15139.3	13893.7	13025.9	12350.0	11777.9	11266.8	10796.0
VSI typeII	43413.9	30371.8	25314.0	25137.0	27892.8	31340.3	34853.6	38304.8	41787.0	45269.3	48751.5
CSI type I	51958.1	37767.8	30533.8	26691.7	24249.9	17712.6	12499.8	10019.3	7146.5	5419.6	4245.6
CSI typeII	69199.3	60173.3	60173.3	59671.9	54156.0	56412.5	55158.9	63432.7	54156.0	61928.4	59671.9
highThrust	99999.3	99991.5	99968.0	99934.9	99904.4	99884.1	99876.3	99879.4	99889.8	99903.5	99917.6
Pj	30.000 (MW)	nju	120.000 (deg)	r	-2.5000	4.3301	V	-0.3873	-0.2236		
TOF (TU_Sun)	6.000	7.000	8.000	9.000	10.000	11.000	12.000	13.000	14.000	15.000	16.000
VSI type I	16761.8	11928.5	9630.0	8520.5	7961.8	7656.1	7464.4	7320.8	7194.7	7072.2	6947.4
VSI typeII	21596.9	24375.8	27858.0	31340.3	34822.5	38304.8	41787.0	45269.3	48751.5	52233.8	55716.0
CSI type I	22437.8	17741.4	15924.6	16518.3	14814.4	11065.7	8743.5	6794.0	5039.1	3848.4	3207.5
CSI typeII	52651.6	49141.5	54156.0	49643.0	45130.0	46885.0	48138.6	52150.2	49141.5	45130.0	52150.2
highThrust	99946.8	99813.8	99619.5	99436.2	99312.6	99261.3	99273.4	99329.6	99408.4	99492.6	99571.5
Pj	30.000 (MW)	nju	150.000 (deg)	r	-4.3301	2.5000	V	-0.2236	-0.3873		
TOF (TU_Sun)	10.000	12.000	14.000	16.000	18.000	20.000	22.000	24.000	26.000	28.000	30.000
VSI type I	4907.7	4409.8	4387.8	4445.0	4482.0	4480.8	4445.0	4382.9	4302.3	4209.4	4108.8
VSI typeII	34822.5	41787.0	48751.5	55716.0	62683.3	69645.0	76609.5	83574.0	90538.5	97503.0	100000.0
CSI type I	10639.5	9546.6	5718.2	3599.7	2652.7	3372.8	2044.2	2413.2	3540.2	3420.7	5788.7
CSI typeII	40115.5	45130.0	35101.1	48138.6	40617.0	50144.4	49643.0	54156.0	52150.2	49141.5	60173.3
highThrust	98608.4	97673.4	97543.9	97947.1	98444.9	98849.6	99140.9	99344.5	99487.6	99589.9	99664.7
Pj	30.000 (MW)	nju	180.000 (deg)	r	-5.0000	-0.0000	V	0.0000	-0.4472		
TOF (TU_Sun)	10.000	12.000	14.000	16.000	18.000	20.000	22.000	24.000	26.000	28.000	30.000
VSI type I	3831.0	2787.2	2619.2	2698.3	2826.4	2942.3	3030.1	3089.0	3122.7	474.5	3132.8
VSI typeII	34822.5	41787.0	48751.5	55716.0	62680.5	69645.0	76609.5	83574.0	90538.5	97503.0	100000.0
CSI type I	5931.2	6264.0	6552.7	4354.4	2711.1	2168.6	1695.4	3563.3	6223.1	3101.7	2383.5
CSI typeII	37608.3	39112.6	35101.1	32092.4	36104.0	40115.5	38611.2	48138.6	45631.4	49141.5	45130.0
highThrust	99304.7	97994.9	96654.4	96089.4	96281.1	96800.9	97354.6	97832.8	98216.6	98517.3	98751.9

**Table A-12:** Transfer Orbit to Saturn with 10MW Jet Power.

Saturn Pj	Fuel 10.000	Consumed (kg) (MW) nju	120.000 (deg)	r	-5.0000	8.6603	V	-0.2739	-0.1581		
TOF (TU_Sun)	20.000	22.000	24.000	26.000	28.000	30.000	32.000	34.000	36.000	38.000	40.000
VSI type I	17892.9	16648.4	15629.8	14756.3	13982.6	13282.7	12640.5	12045.9	100000.0	100000.0	100000.0
VSI typeII	31027.5	25536.5	27858.0	30179.5	32501.0	34822.5	37144.0	39465.5	41787.0	44108.5	100000.0
CSI type I	17555.4	16238.1	11293.8	9867.6	8706.0	7882.0	11860.0	8928.3	100000.0	100000.0	100000.0
CSI typeII	56830.3	51481.6	52150.2	56496.0	56161.7	55158.9	56161.7	100000.0	100000.0	100000.0	100000.0
highThrust	99698.5	99640.2	99600.0	99577.6	99570.8	99576.6	99591.8	99613.1	99637.9	99664.0	99689.9
Pj	10.000 (MW)	nju	150.000 (deg)	r	-8.6603	5.0000	V	-0.1581	-0.2739		
TOF (TU_Sun)	20.000	22.000	24.000	26.000	28.000	30.000	32.000	34.000	36.000	38.000	40.000
VSI type I	12681.2	11765.2	11117.8	10622.6	10216.5	9864.9	9548.3	9255.6	8980.4	8718.8	8468.7
VSI typeII	28541.7	25536.5	27858.0	30179.5	32501.0	34822.5	40193.6	39465.5	41787.0	44108.5	46430.0
CSI type I	15820.9	13901.6	13730.3	17862.9	9131.8	11561.2	6443.6	6717.2	18626.9	15607.2	7536.4
CSI typeII	56830.3	45965.7	52150.2	52150.2	53821.7	49643.0	45464.3	51147.3	48138.6	47637.2	56830.3
highThrust	99369.4	99086.7	98824.4	98611.2	98460.4	98373.1	98342.9	98358.7	98408.6	98480.9	98566.1
Pj	10.000 (MW)	nju	180.000 (deg)	r	-10.0000	-0.0000	V	0.0000	-0.3162		
TOF (TU_Sun)	24.000	26.000	28.000	30.000	32.000	34.000	36.000	38.000	40.000	42.000	44.000
VSI type I	7941.0	7556.6	7296.5	7107.7	6960.2	6836.2	6725.6	6622.4	6523.2	6426.2	6330.2
VSI typeII	27858.0	30179.9	32501.0	37501.6	37144.0	39465.5	41788.3	44108.5	46430.0	48751.5	52091.9
CSI type I	11227.4	15076.9	10948.9	10200.1	16081.4	6412.9	11603.6	31218.0	6418.6	8654.8	21503.5
CSI typeII	46132.9	43458.5	49141.5	37608.3	48138.6	53988.8	45130.0	47637.2	43458.5	49141.5	55158.9
highThrust	99108.2	98745.0	98372.4	98023.9	97725.5	97493.0	97331.2	97236.4	97199.5	97209.0	97253.4

**Table A-13:** Transfer Orbit to Saturn with 20MW Jet Power.

Saturn	Fuel	Consumed (kg)										
Pj	20.000 (MW)	nju	120.000 (deg)	r	-5.0000	8.6603	V	-0.2739	-0.1581			
TOF (TU_Sun)	20.000	22.000	24.000	26.000	28.000	30.000	32.000	34.000	36.000	38.000	40.000	
VSI type I	9825.5	9080.1	8477.4	7965.9	7516.9	7113.8	6746.7	6409.0	6096.3	5805.5	5534.3	
VSI typeII	46430.0	51073.0	55716.0	60359.0	65002.0	69645.0	74288.0	78931.0	83574.0	88217.0	92860.0	
CSI type I	9779.7	9039.5	5992.4	5871.0	4476.6	3722.0	6801.8	6352.7	7364.0	5902.9	5045.8	
CSI typeII	53487.4	58836.1	48138.6	52150.2	46801.5	50144.4	64184.9	56830.3	60173.3	57164.6	66859.2	
highThrust	99698.5	99640.2	99600.0	99577.6	99570.8	99576.6	99591.8	99613.1	99637.9	99664.0	99689.9	
Pj	20.000 (MW)	nju	150.000 (deg)	r	-8.6603	5.0000	V	-0.1581	-0.2739			
TOF (TU_Sun)	20.000	22.000	24.000	26.000	28.000	30.000	32.000	34.000	36.000	38.000	40.000	
VSI type I	6769.8	6250.3	5886.1	5609.2	5383.2	5188.4	5013.5	4852.4	4701.3	4558.1	4421.6	
VSI typeII	46430.0	51073.0	55716.0	60359.0	65002.0	69645.0	74288.0	78940.0	83574.0	88218.2	92860.0	
CSI type I	8590.8	8695.6	7164.5	5747.0	4666.1	11097.7	3193.3	10011.6	10042.6	5252.3	5206.6	
CSI typeII	50144.4	47804.3	44127.1	43458.5	46801.5	50144.4	48138.6	51147.3	42121.3	57164.6	46801.5	
highThrust	99369.4	99086.7	98824.4	98611.2	98460.4	98373.1	98342.9	98358.7	98408.6	98480.9	98566.1	
Pj	20.000 (MW)	nju	180.000 (deg)	r	-10.0000	-0.0000	V	0.0000	-0.3162			
TOF (TU_Sun)	24.000	26.000	28.000	30.000	32.000	34.000	36.000	38.000	40.000	42.000	44.000	
VSI type I	4134.6	3926.7	3786.4	3684.8	3605.6	3539.1	3479.8	3424.6	3371.6	3319.8	3268.6	
VSI typeII	55716.0	60359.0	65002.0	69645.0	74288.0	78931.0	83574.0	88217.0	92860.0	97503.0	100000.0	
CSI type I	6147.8	5294.3	4591.6	5177.3	3396.0	4198.0	7280.2	24282.9	3362.5	4542.5	6376.2	
CSI typeII	48138.6	43458.5	42121.3	50144.4	42789.9	34098.2	42121.3	44461.4	46801.5	42121.3	66190.6	
highThrust	99108.2	98745.0	98372.4	98023.9	97725.5	97493.0	97331.2	97236.4	97199.5	97209.0	97253.4	

## APPENDIX B

### EQUATIONS USED IN THE PROGRAM *SAMURAI*

#### ***B.1 1st-order Gradient Method***

For the problems in this research, the Lagrangian  $L$  in Eqn. C-2 and its derivatives are zero, so  $\partial L/\partial x$  in Eqn. C-4 and  $\partial L/\partial u$  in Eqns. C-7 and C-8 are zero. The matrix  $W$  is set to be an identity matrix of size  $m \times m$ , where  $m$  is the number of control variables. So we need the expressions for  $\partial f/\partial x$  and  $\partial f/\partial u$ .

##### **B.1.1 VSI – Unconstrained $I_{sp}$**

The equations of motion and control variables are expressed as Eqns. 5-16 and 5-15. If we change the notation as

$$\vec{x} = \begin{bmatrix} x & y & z & u & v & w & m \end{bmatrix}^T = \begin{bmatrix} x_0 & x_1 & x_2 & x_3 & x_4 & x_5 & x_6 \end{bmatrix}^T \quad (\text{B-1})$$

$$\vec{u} = \begin{bmatrix} T_x & T_y & T_z \end{bmatrix}^T = \begin{bmatrix} u_0 & u_1 & u_2 \end{bmatrix}^T, \quad (\text{B-2})$$

Eqn. 5-16 becomes

$$f = \begin{bmatrix} \dot{x}_0 \\ \dot{x}_1 \\ \dot{x}_2 \\ \dot{x}_3 \\ \dot{x}_4 \\ \dot{x}_5 \\ \dot{x}_6 \end{bmatrix} = \begin{bmatrix} x_3 \\ x_4 \\ x_5 \\ -\mu x_0/r^3 + u_0/x_6 \\ -\mu x_1/r^3 + u_1/x_6 \\ -\mu x_2/r^3 + u_2/x_6 \\ -(u_0^2 + u_1^2 + u_2^2)/2P_J \end{bmatrix} = \begin{bmatrix} x_3 \\ x_4 \\ x_5 \\ a_{A_0} + u_0/x_6 \\ a_{A_1} + u_1/x_6 \\ a_{A_2} + u_2/x_6 \\ -(u_0^2 + u_1^2 + u_2^2)/2P_J \end{bmatrix} \quad (\text{B-3})$$

where  $\vec{a}_A$  is an acceleration vector from an attracting body

$$\vec{a}_A = \begin{bmatrix} -\mu x_0/r^3 \\ -\mu x_1/r^3 \\ -\mu x_2/r^3 \end{bmatrix} \quad (\text{B-4})$$

The derivative of this vector with respect to  $x_j$  is a  $3 \times 7$  matrix:

$$\frac{\partial \vec{a}_A}{\partial \vec{x}} = \frac{1}{r^5} \begin{bmatrix} 3\mu x_0 x_0 - \mu r^2 & 3\mu x_0 x_1 & 3\mu x_0 x_2 \\ 3\mu x_1 x_0 & 3\mu x_1 x_1 - \mu r^2 & 3\mu x_1 x_2 \\ 3\mu x_2 x_0 & 3\mu x_2 x_1 & 3\mu x_2 x_2 - \mu r^2 \end{bmatrix} \quad 0_{3 \times 4}. \quad (\text{B-5})$$

Then  $\partial f / \partial x$  ( $7 \times 7$  matrix) and  $\partial f / \partial u$  ( $7 \times 3$  matrix) become

$$\frac{\partial \vec{f}}{\partial \vec{x}} = \begin{bmatrix} O_{3 \times 3} & I_{3 \times 3} & O_{3 \times 1} \\ \frac{\partial a_A}{\partial x} \quad 3 \times 3 & O_{3 \times 3} & -u_i / x_6^2 \\ O_{1 \times 7} \end{bmatrix}, \quad i = 0, 1, 2. \quad (\text{B-6})$$

$$\frac{\partial \vec{f}}{\partial \vec{u}} = \begin{bmatrix} O_{3 \times 3} \\ 1/x_6 & 0 & 0 \\ 0 & 1/x_6 & 0 \\ 0 & 0 & 1/x_6 \\ -u_0/P_J & -u_1/P_J & -u_2/P_J \end{bmatrix}. \quad (\text{B-7})$$

### B.1.2 VSI – Constrained $I_{sp}$

The equations of motion and control variables are expressed as Eqns. 5-18 and 5-17. If we again use Eqn. B-1 and

$$\vec{u} = \begin{bmatrix} l_x & l_y & l_z & T \end{bmatrix}^T = \begin{bmatrix} u_0 & u_1 & u_2 & u_2 \end{bmatrix}^T, \quad (\text{B-8})$$

Eqn. 5-16 becomes

$$f = \begin{bmatrix} \dot{x}_0 \\ \dot{x}_1 \\ \dot{x}_2 \\ \dot{x}_3 \\ \dot{x}_4 \\ \dot{x}_5 \\ \dot{x}_6 \end{bmatrix} = \begin{bmatrix} x_3 \\ x_4 \\ x_5 \\ -\mu x_0 / r^3 + u_0 u_3 / x_6 \\ -\mu x_1 / r^3 + u_1 u_3 / x_6 \\ -\mu x_2 / r^3 + u_2 u_3 / x_6 \\ -u_3^2 / 2P_J \end{bmatrix} = \begin{bmatrix} x_3 \\ x_4 \\ x_5 \\ a_{A_0} + u_0 u_3 / x_6 \\ a_{A_1} + u_1 u_3 / x_6 \\ a_{A_2} + u_2 u_3 / x_6 \\ -u_3^2 / 2P_J \end{bmatrix} \quad (\text{B-9})$$

The derivative of this vector with respect to  $\vec{x}$  is

$$\frac{\partial \vec{a}_A}{\partial \vec{x}} = \frac{1}{r^5} \begin{bmatrix} 3\mu x_0 x_0 - \mu r^2 & 3\mu x_0 x_1 & 3\mu x_0 x_2 & \\ 3\mu x_1 x_0 & 3\mu x_1 x_1 - \mu r^2 & 3\mu x_1 x_2 & 0_{3 \times 4} \\ 3\mu x_2 x_0 & 3\mu x_2 x_1 & 3\mu x_2 x_2 - \mu r^2 & \end{bmatrix}. \quad (\text{B-10})$$

Then  $\partial f / \partial x$  and  $\partial f / \partial u$  ( $7 \times 4$ ) become

$$\frac{\partial \vec{f}}{\partial \vec{x}} = \begin{bmatrix} O_{3 \times 3} & I_{3 \times 3} & O_{3 \times 1} \\ \frac{\partial a_A}{\partial x} \text{ }_{3 \times 3} & O_{3 \times 3} & -u_i u_3 / x_6^2 \\ & O_{1 \times 7} & \end{bmatrix}, \quad i = 0, 1, 2. \quad (\text{B-11})$$

$$\frac{\partial \vec{f}}{\partial \vec{u}} = \begin{bmatrix} & O_{3 \times 4} & \\ u_3 / x_6 & 0 & 0 & u_0 / x_6 \\ 0 & u_3 / x_6 & 0 & u_1 / x_6 \\ 0 & 0 & u_3 / x_6 & u_2 / x_6 \\ 0 & 0 & 0 & -u_3 / P_J \end{bmatrix}. \quad (\text{B-12})$$

### B.1.3 CSI – Continuous Thrust

The equations of motion and control variables are expressed as Eqns. 5-26 and 5-25. If we use the following expression

$$\vec{u} = \begin{bmatrix} \theta & \phi \end{bmatrix}^T = \begin{bmatrix} u_0 & u_1 \end{bmatrix}^T, \quad (\text{B-13})$$

Eqn. 5-26 becomes

$$f = \begin{bmatrix} \dot{x}_0 \\ \dot{x}_1 \\ \dot{x}_2 \\ \dot{x}_3 \\ \dot{x}_4 \\ \dot{x}_5 \\ \dot{x}_6 \end{bmatrix} = \begin{bmatrix} x_3 \\ x_4 \\ x_5 \\ -\mu x_0 / r^3 + T \cos \theta \cos \phi / x_6 \\ -\mu x_1 / r^3 + T \sin \theta \cos \phi / x_6 \\ -\mu x_2 / r^3 + T \sin \phi / x_6 \\ -T^2 / 2P_J \end{bmatrix} = \begin{bmatrix} x_3 \\ x_4 \\ x_5 \\ a_{A_0} + T \cos u_0 \cos u_1 / x_6 \\ a_{A_1} + T \sin u_0 \cos u_1 / x_6 \\ a_{A_2} + T \sin u_1 / x_6 \\ -(u_0^2 + u_1^2 + u_2^2) / 2P_J \end{bmatrix}. \quad (\text{B-14})$$

Then  $\partial f/\partial x$  and  $\partial f/\partial u$  ( $7 \times 2$ ) become

$$\frac{\partial \vec{f}}{\partial \vec{x}} = \begin{bmatrix} O_{3 \times 3} & I_{3 \times 3} & O_{3 \times 1} \\ & & -T \cos u_0 \cos u_1 / x_6^2 \\ \frac{\partial a_A}{\partial x} \quad 3 \times 3 & O_{3 \times 3} & -T \sin u_0 \cos u_1 / x_6^2 \\ & & -T \sin u_1 / x_6^2 \\ & O_{1 \times 7} & \end{bmatrix} \quad (\text{B-15})$$

$$\frac{\partial \vec{f}}{\partial \vec{u}} = \begin{bmatrix} O_{3 \times 2} \\ -T \sin u_0 \cos u_1 / x_6 & -T \cos u_0 \sin u_1 / x_6 \\ T \cos u_0 \cos u_1 / x_6 & -T \sin u_0 \sin u_1 / x_6 \\ 0 & T \cos u_1 / x_6 \\ 0 & 0 \end{bmatrix}. \quad (\text{B-16})$$

#### B.1.4 CSI – Bang-Off-bang Control

Equations are the same as VSI – Constrained  $I_{sp}$  case.



## APPENDIX C

### NUMERICAL TECHNIQUES

In this chapter, numerical techniques that are used to create an interplanetary trajectory optimization program are introduced. These techniques are used to implement the methods described in the last chapter into the program and they are as follows:

- A first-order gradient algorithm based on the optimal control technique is used to compute the optimal control history of the thrust.
- Runge-Kutta integrates the equations of motion with a given initial condition. This is used along with the first-order gradient algorithm.
- A line search is used with Powell's method. Three-point quadratic polynomial approximations are used in this research.
- Powell's method is a zero-order method that finds the minimum point. This is used for several purposes:
  - to find the best directions of motion of the spacecraft at departure and at arrival.
  - to find the best entry velocity and the impact parameter for a swing-by trajectory.
  - to find the initial values of the Lagrange multipliers that satisfy the target conditions.
- Among several methods available to solve the Gauss problem that calculate a high thrust trajectory, the direct  $p$ -iteration method is chosen. The procedure and equations for this method are introduced.
- Penalty functions are used for the trajectory inside the SOI for swing-by cases to restrict the minimum approaching distance. As the spacecraft approaches the swing-by planet, the spacecraft must not hit the planet or fly above the planet's atmosphere

if there is an atmosphere.

This chapter also includes the brief explanation of VRML (Virtual Reality Modeling Language).

### ***C.1 Calculus of Variations: First-order Gradient Algorithm***

Suppose that we would like to find the control variables  $u(t)$  on the time interval  $[t_i, t_f]$  that drive the plant

$$\dot{x} = f[x(t), u(t), t], \quad x(t_i) \text{ given}, \quad t_i \leq t \leq t_f, \quad (\text{C-1})$$

along a trajectory  $x(t)$ .  $x(t)$ , an  $n$ -vector function, is determined by  $u(t)$ , an  $m$ -vector function. The control history will be chosen such that the performance index,  $J$ , is minimized:

$$J = \phi[x(t_f), t_f] + \int_{t_i}^{t_f} L[x(t), u(t), t] dt \quad (\text{C-2})$$

$\phi[x(t_f), t_f] \quad :$  the final weighting function  
 $L[x(t), u(t), t] \quad :$  the Lagrangian

and such that the  $q$ -vector ( $q \leq n - 1$  if  $L = 0$ ,  $q \leq n$  if  $L \neq 0$ ) side constraints  $\psi[x(t_f), t_f]$  satisfy

$$\psi[x(t_f), t_f] = 0 \quad (q \text{ equations}). \quad (\text{C-3})$$

The computation method to obtain the histories of the control variables for the above problem is presented below. This method is called the first-order gradient algorithm[17].

1. Estimate a set of control variable histories,  $u(t)$ .
2. Integrate the system equations  $\dot{x} = f(x, u, t)$  forward with the specified initial conditions  $x(t_i)$  and the control variable histories from Step 1. Record  $x(t)$ ,  $u(t)$ , and  $\psi[x(t_f)]$ .
3. Determine an  $n$ -vector of influence functions  $p(t)$ , and an  $(n \times q)$  matrix of influence functions,  $R(t)$ , by backward integration of the influence equations, using  $x(t_f)$

obtained in Step 2 to determine the boundary conditions.

$$\dot{p} = -\left(\frac{\partial f}{\partial x}\right)^T p - \left(\frac{\partial L}{\partial x}\right)^T; p_i(t_f) = \begin{cases} 0 & i = 1, \dots, q, \\ (\partial\phi/\partial x_i)_{t=t_f} & i = q+1, \dots, n, \end{cases} \quad (C-4)$$

$$\dot{R} = -\left(\frac{\partial f}{\partial x}\right)^T R; R_{ij}(t_f) = \begin{cases} 1, & i = j, \quad i = 1, \dots, n, \\ 0, & i \neq j, \quad j = 1, \dots, q. \end{cases} \quad (C-5)$$

4. Simultaneously with Step 3, compute the following integrals:

$$I_{\psi\psi} = \int_{t_i}^{t_f} R^T \frac{\partial f}{\partial u} W^{-1} \left(\frac{\partial f}{\partial u}\right)^T R dt \quad [(q \times q)\text{-matrix}] \quad (C-6)$$

$$I_{J\psi} = I_{\psi J}^T = \int_{t_i}^{t_f} \left(p^T \frac{\partial f}{\partial u} + \frac{\partial L}{\partial u}\right) W^{-1} \left(\frac{\partial f}{\partial u}\right)^T R dt \quad [q\text{-row vector}] \quad (C-7)$$

$$I_{JJ} = \int_{t_i}^{t_f} \left(p^T \frac{\partial f}{\partial u} + \frac{\partial L}{\partial u}\right) W^{-1} \left[ \left(\frac{\partial f}{\partial u}\right)^T p + \left(\frac{\partial L}{\partial u}\right)^T \right] dt \quad (C-8)$$

where  $W$  is an  $(m \times m)$  positive-definite matrix and  $I_{JJ}$  is a scalar.

5. Choose values of  $\delta\psi$  such that the next nominal solution is closer to the desired values  $\psi[x(t_f)] = 0$ . For example, one might choose  $\delta\psi = -\epsilon\psi[x(t_f)]$ ,  $0 < \epsilon \leq 1$ . Then determine  $\nu$  from  $\nu = -[I_{\psi\psi}]^{-1}(\delta\psi + I_{\psi J})$ .

6. Repeat Steps 1 through 6, using an improved estimate of  $u(t)$ , where

$$\delta u(t) = -[W(t)]^{-1} \left[ \frac{\partial L}{\partial u} + [p(t) + R(t)\nu]^T \frac{\partial f}{\partial u} \right]^T. \quad (C-9)$$

Stop when  $\psi[x(t_f)] = 0$  and  $I_{JJ} - I_{J\psi} I_{\psi\psi}^{-1} I_{\psi J} = 0$  to the desired degree of accuracy.

The explicit forms of the derivatives  $(\partial f/\partial x)$ ,  $(\partial L/\partial x)$ ,  $(\partial L/\partial x)$ ,  $(\partial L/\partial u)$  are in Appendix B.1.

## C.2 Numerical Integration: Runge-Kutta

The Runge-Kutta algorithm lets us solve a differential equation numerically. Consider a single variable problem

$$y' = f(x, y) \quad (C-10)$$

with initial condition  $y(0) = y_0$ . Suppose that  $y_n$  is the value of the variable at  $x_n$ . The Runge-Kutta formula takes  $y_n$  and  $x_n$  and calculates an approximation for  $y_{n+1}$  at  $x_{n+1}(=x_n + h)$ , where  $h$  is assumed to be small).

For a second-order Runge-Kutta[11],

$$y_{n+1} = y_n + \frac{h}{2}[f(x_n, y_n) + f(x_{n+1}, y_n + hf(x_n, y_n))] \quad (\text{C-11})$$

or

$$y_{n+1} = y_n + \frac{h}{2}[F_1 + F_2] \quad (\text{C-12})$$

$$F_1 = hf(x_n, y_n) \quad (\text{C-13})$$

$$F_2 = hf(x_{n+1}, y_n + hf(x_n, y_n)) \quad (\text{C-14})$$

For a fourth-order Runge-Kutta,

$$y_{n+1} = y_n + \frac{h}{6}[F_1 + 2F_2 + 2F_3 + F_4] \quad (\text{C-15})$$

$$F_1 = f(x_n, y_n) \quad (\text{C-16})$$

$$F_2 = f\left(x_n + \frac{1}{2}h, y_n + \frac{1}{2}hF_1\right) \quad (\text{C-17})$$

$$F_3 = f\left(x_n + \frac{1}{2}h, y_n + \frac{1}{2}hF_2\right) \quad (\text{C-18})$$

$$F_4 = f(x_n + h, y_n + hF_3) \quad (\text{C-19})$$

### ***C.3 Line Search: Three-point Polynomial Approximations***

There are several line search methods. Golden Section Method[78] converges rapidly, but a disadvantage is that the region where the minimum point lies should be known beforehand. Most of the problems dealt with in this paper cannot use this method because there is little information on the minimum points in these problems. In this research, three-point polynomial approximations are used. This method can easily change the range and the direction of the search vector. Therefore, this method is appropriate to the problems dealt with in this research.

The second-order approximating polynomial is[78]

$$F = a_0 + a_1X + a_2X^2 \quad (\text{C-20})$$

For a three-point quadratic approximation, there are three known points:  $(X_1, F_1)$ ,  $(X_2, F_2)$ , and  $(X_3, F_3)$ . From these points and Eqn. C-20, coefficients  $a_0, a_1, a_2$  are obtained:

$$a_0 = F_1 - a_1 X_1 - a_2 X_1^2 \quad (\text{C-21})$$

$$a_1 = \frac{F_2 - F_1}{X_2 - X_1} - a_2(X_1 + X_2) \quad (\text{C-22})$$

$$a_2 = \frac{(F_3 - F_1)/(X_3 - X_1) - (F_2 - F_1)/(X_2 - X_1)}{X_3 - X_2}. \quad (\text{C-23})$$

Assuming that the distance between  $X_1$  and  $X_2$  and between  $X_2$  and  $X_3$  are the same and is expressed as  $dX$ , the value of  $X$  that minimizes the value of this polynomial is

$$X^* = -\frac{a_1}{2a_2} = \frac{4F_2 - 3F_1 - F_3}{4F_2 - 2F_3 - 2F_1} dX. \quad (\text{C-24})$$

In the case where  $F_1 > F_2 > F_3$  or  $F_1 < F_2 < F_3$ , that is, if the minimum does not lie between  $X_1$  and  $X_3$ , the accuracy of this polynomial approximation is questionable. In such cases we can find a region where  $F_2$  is smaller than both  $F_1$  and  $F_3$  by either increasing or decreasing the value of  $dX$ .

If the minimum does not exist between  $X_1$  and  $X_3$ , the following steps are taken.

- If  $F_1 > F_2 > F_3$ , it is likely that the minimum should lie a point beyond  $X_3$ . By doubling  $dX$ , the same search described above is repeated.
- If  $F_1 < F_2 < F_3$ , the minimum is in the opposite direction. Change the search direction by multiplying  $dX$  by -1, then repeat the same search.

#### ***C.4 Numerical Optimization: Powell's Method***

There are several types of methods for finding the minimum point of unconstrained problems. For example, first-order methods for finding the minimum utilize gradient information. Examples of these methods are the steepest-decent method and Fletcher-Reeves method. Second-order methods, such as Newton's method, use gradients and the Hessian matrix and usually converge faster than first-order methods. These gradient-based methods require the calculation of the gradient of functions, but sometimes computing gradients is extremely difficult or time-consuming, especially if the functions are complicated. Compared to these

methods, zero-order methods do not require tedious computation or complicated programming, although thousands of function calls may be required. In this research Powell's method, one of the most efficient and reliable zero-order methods, is applied.

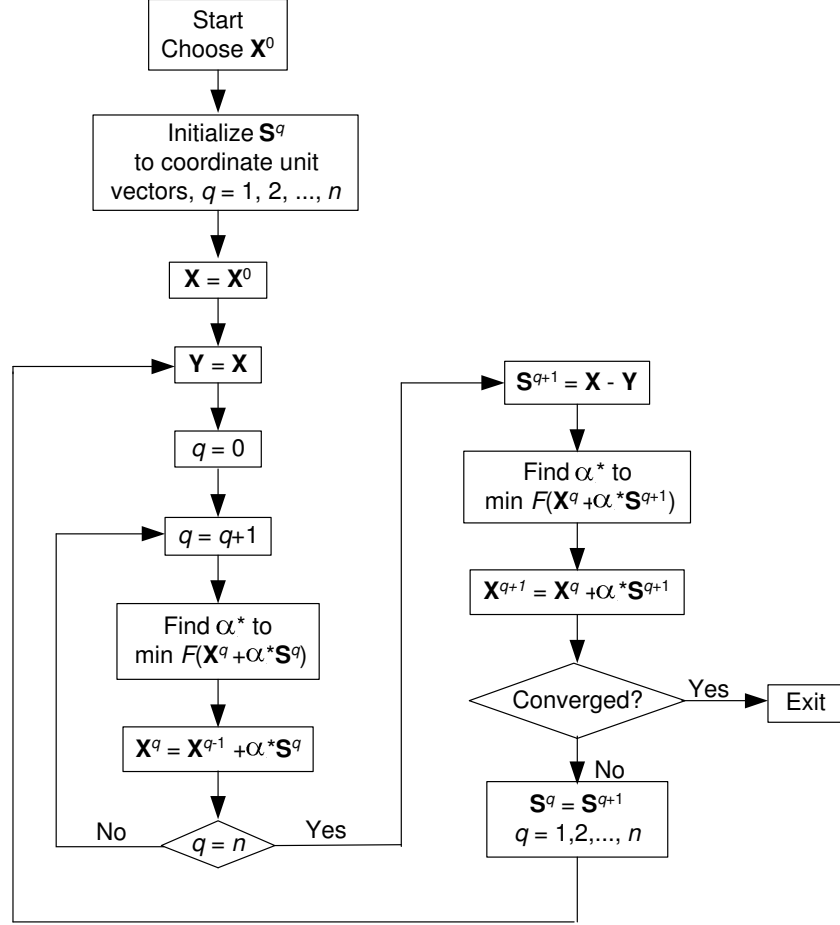


**Figure C-1:** Flowchart of Powell's method[78].

The flow of Powell's method is shown in Fig. C-1. The basic concept of Powell's method is to first search in  $n$ -orthogonal directions, where  $\mathbf{S}^i, i = 1, \dots, n$ , are the coordinate directions and each search consists of updating of the  $\mathbf{X}$  vector. The starting point of  $i$ -th iteration,  $\mathbf{X}^i$ , can be calculated by  $\mathbf{X}^i = \mathbf{X}^{i-1} + \alpha_i^* \mathbf{S}^i$  where  $\alpha_i^*$  is a scalar multiplier determining the amount of change in  $\mathbf{X}$  for this iteration. These directions are not usually conjugate but provide a starting point from which conjugate directions are built. Having completed the  $n$  unidirectional searches, a new search direction is created by connecting the first and last design points. This becomes the  $n + 1$  search direction. At the end of the

$n$ -th iteration, the  $n + 1$ -th search direction  $\mathbf{S}^{n+1}$  is found by connecting all the points from  $\mathbf{X}^0$  through the point  $\mathbf{X}^n$ .

$$\mathbf{S}^{n+1} = \sum_{i=1}^n \alpha_i^* \mathbf{S}^i \quad (\text{C-25})$$

It is convenient to store the search information in an  $n \times n$  array  $\mathbf{H}$ . Initially, the identity matrix is used for this array. The columns of  $\mathbf{H}$  correspond to the unidirectional search vectors  $\mathbf{S}^i, i = 1 \cdots n$ . After finding the minimum in each direction, we replace  $\mathbf{S}^i$  in matrix  $\mathbf{H}$  by  $\alpha_i^* \mathbf{S}^i$ .

$$\mathbf{H} = [\alpha_1^* \mathbf{S}^1 \quad \alpha_2^* \mathbf{S}^2 \quad \cdots \quad \alpha_n^* \mathbf{S}^n] \quad (\text{C-26})$$

For the  $n + 1$ -th search, we create a conjugate direction using Eqn. C-25. With this search vector the minimum point is calculated to determine the parameter  $\alpha_{i+1}^*$ . Now each column of the  $\mathbf{H}$  matrix is shifted by one to the left, eliminating the  $\alpha_1^* \mathbf{S}^1$  entry, and storing  $\alpha_{n+1}^* \mathbf{S}^{n+1}$  in  $n$ -th column. This provides a new  $\mathbf{H}$  matrix containing  $n$  search directions to start the entire search process over. Therefore for this new search, the first search direction is  $\alpha_2^* \mathbf{S}^2$ .

Note that as the search goes on, the search directions may gradually become parallel. To avoid the searches becoming stuck in the same direction, the  $\mathbf{H}$  matrix should be periodically reset to the identity matrix, in this case every  $2n + 1$  iterations.

## ***C.5 Solving High Thrust Problems: Gauss Problem***

In this section, numerical method for solving Gauss problem is presented. The method used in this research is “Solution via universal variables” explained in Sec. 5.3

### **C.5.1 Solution via Universal Variables**

As explained above, this method requires the “direction of motion” to obtain  $\Delta V$ . Following this procedure:

1. From  $\vec{r}_1$  and  $\vec{r}_2$  and the “direction of motion,” evaluate the constant,  $A$ , using

$$A = \frac{\sqrt{r_1 r_2} \sin \Delta \nu}{\sqrt{1 - \cos \Delta \nu}} \quad (\text{C-27})$$

where  $\Delta\nu$  is obtained from

$$\Delta\nu = \arccos\left(\frac{\vec{r}_1 \cdot \vec{r}_2}{|\vec{r}_1||\vec{r}_2|}\right). \quad (\text{C-28})$$

2. Pick a trial value for  $z$ . Since  $z = \Delta E^2$  and  $-z = \Delta F^2$ , this amounts to guessing the change in the eccentric anomaly. The usual range for  $z$  is from negative values to  $(2\pi)^2$ . Values of  $z$  greater than  $(2\pi)^2$  correspond to a change in the eccentric anomaly of more than  $2\pi$  and can occur only if the satellite passes back through  $\vec{r}_1$  enroute to  $\vec{r}_2$ .
3. Evaluate the functions  $S$  and  $C$  for the selected trial value of  $z$  using the following equations.

$$\begin{aligned} C(z) &\equiv \frac{1 - \cos \sqrt{z}}{z} = \frac{1 - \cosh \sqrt{-z}}{z} = \frac{1}{2!} - \frac{z}{4!} + \frac{z^2}{6!} - \frac{z^3}{8!} + \dots \\ &= \sum_{k=0}^{\infty} \frac{(-z)^k}{(2k+2)!} \end{aligned} \quad (\text{C-29})$$

$$\begin{aligned} S(z) &\equiv \frac{\sqrt{z} - \sin \sqrt{z}}{\sqrt{z^3}} = \frac{\sinh \sqrt{-z} - \sqrt{-z}}{\sqrt{(-z)^3}} = \frac{1}{3!} - \frac{z}{5!} + \frac{z^2}{7!} - \frac{z^3}{9!} + \dots \\ &= \sum_{k=0}^{\infty} \frac{(-z)^k}{(2k+3)!}. \end{aligned} \quad (\text{C-30})$$

4. Determine the auxiliary variable,  $y$ , from

$$y = r_1 + r_2 - A \frac{(1 - zS)}{\sqrt{C}}. \quad (\text{C-31})$$

5. Determine  $x$  from

$$x = \sqrt{\frac{y}{C}}. \quad (\text{C-32})$$

6. Check the trial value of  $z$  by computing  $t$  from the equation

$$\sqrt{\mu}t = x^3 S + A\sqrt{y} \quad (\text{C-33})$$

and compare it with the desired time of flight. If the two values are not nearly equal, adjust the trial value of  $z$  and repeat the procedure until the desired value of  $t$  is obtained. A Newton iteration is typically used to calculate next value of  $z$ .

$$z_{n+1} = z_n + \frac{t - t_n}{dt/dz|_{z=z_n}} \quad (\text{C-34})$$



where

$$\sqrt{\mu} \frac{dt}{dz} = x^3 \left( S' - \frac{3SC'}{2C} \right) + \frac{A}{8} \left( \frac{3S\sqrt{y}}{C} + \frac{A}{x} \right). \quad (\text{C-35})$$

$S'$  and  $C'$  are the derivatives of  $S$  and  $C$  with respect to  $z$ . These derivatives may be evaluated from these equations except when  $z$  is nearly zero (near-parabolic orbit).

$$\frac{dS}{dz} = \frac{1}{2z}(C - 3S) \quad (\text{C-36})$$

$$\frac{dC}{dz} = \frac{1}{2z}(1 - zS - 2C). \quad (\text{C-37})$$

If  $z$  is near zero, these equations may be used.

$$C' = -\frac{1}{4!} + \frac{2z}{6!} - \frac{3z^2}{8!} + \frac{4z^3}{10!} - \dots \quad (\text{C-38})$$

$$S' = -\frac{1}{5!} + \frac{2z}{7!} - \frac{3z^2}{9!} + \frac{4z^3}{11!} - \dots \quad (\text{C-39})$$

7. When the method has converged to a solution, evaluate  $f$ ,  $g$ , and  $\dot{g}$  from Eqns. 5-34, 5-35, and 5-37, then compute  $\vec{v}_1$  and  $\vec{v}_2$  from

$$\vec{v}_1 = \frac{\vec{r}_2 - f\vec{r}_1}{g} \quad (\text{C-40})$$

$$\vec{v}_2 = \frac{\dot{g}\vec{r}_2 - \vec{r}_1}{g}. \quad (\text{C-41})$$

When  $\Delta\nu = \pi$ , the Gauss problem cannot be solved because two collinear vectors cannot determine a unique orbital plane and therefore a unique solution for  $\vec{v}_1$  and  $\vec{v}_2$  is not possible. In such a case,  $\Delta V$  is calculated in the same way as the  $\Delta V$  for a Hohmann transfer.

The semi-major axis of the transfer orbit is  $a = (r_1 + r_2)/2$ , and the specific energy is  $E = -\mu/(2a)$ . The speeds at  $r_1$  and  $r_2$  are

$$V_1 = \sqrt{2 \left( E + \frac{\mu}{r_1} \right)} \quad (\text{C-42})$$

$$V_2 = \sqrt{2 \left( E + \frac{\mu}{r_2} \right)} \quad (\text{C-43})$$

Although the magnitude of the velocity is defined by the above equations, the velocity of the spacecraft can be freely chosen. *SAMURAI* calculates the departure and arrival velocities

so that the total  $\Delta V$  is minimized. The components of these velocities are adjusted with Powell's method until the following value is minimized:

$$\begin{aligned} \text{total } \Delta V &= \sqrt{(u(t_i) - u_{initial})^2 + (v(t_i) - v_{initial})^2 + (w(t_i) - w_{initial})^2} \\ &+ \sqrt{(u(t_f) - u_{target})^2 + (v(t_f) - v_{target})^2 + (w(t_f) - w_{target})^2} \quad (\text{C-44}) \end{aligned}$$

where  $u_{initial}$ ,  $v_{initial}$ ,  $w_{initial}$  are the velocity components of the departure planet, and  $u_{target}$ ,  $v_{target}$ , and  $w_{target}$  are the velocity components of the arrival planet.

## C.6 Solving Swing-by Problems

A trajectory with a swing-by is solved based on the method shown previously (Sec.5.4).

Assume that we know the following numbers from the inputs: initial position and velocity of the spacecraft, position of the swing-by planet, target position and velocity of the spacecraft, times of flight for two phases (initial planet to swing-by planet, swing-by planet to target planet). We would like to find the best thrust history that minimizes the fuel consumption over an entire trajectory. Then we need to find the best velocity vector of the spacecraft at the entrance of the SOI of the swing-by planet that minimizes the fuel consumption. Once we set this velocity, fuel consumption for each phase can be solved.

Therefore, the velocity components are the parameters that we need to optimize. In addition, the impact parameter  $\beta$  determines the trajectory's characteristics. Powell's method is used for the optimization to minimize the fuel consumption by changing these four parameters:  $u, v, w$ , and  $\beta$ .

Intuitively, Powell's method is appropriate for this type of problem because there is only one possible solution for the combination of  $u, v, w$ , and  $\beta$ . However, Powell's method is valid only for an unconstrained problem. As shown in Eqn. 5-65, there is a restriction on  $\beta$  such that the spacecraft will not be decelerated by the atmosphere of the swing-by planet.

To deal with a constrained problem, while still using Powell's method, a method of penalty function is used.

### C.6.1 Penalty Functions

The general approach for constrained minimization problems is to minimize the objective function as an unconstrained function but to add some penalty to limit constraint violations[78]. The common approach is to create a pseudo-objective function of the form

$$\Phi(\mathbf{X}, k) = F(\mathbf{X}) + kP(\mathbf{X}) \quad (\text{C-45})$$

where  $F(\mathbf{X})$  is the original objective function and  $P(\mathbf{X})$  is an imposed penalty function. The scalar  $k$  is a multiplier which determines the magnitude of the penalty, and  $k$  is held constant for a complete unconstrained minimization. There are several types of penalty functions[78].

#### C.6.1.1 Exterior Penalty Functions

This type of penalty function is the easiest to incorporate into the optimization process. The exterior penalty function  $P(\mathbf{X})$  is given by

$$P(\mathbf{X}) = \sum_{i=1}^m \max[0, g_i(\mathbf{X})]^2 + \sum_{k=1}^l [h_k(\mathbf{X})]^2 \quad (\text{C-46})$$

This means that no penalty is imposed if all constraints are satisfied (all  $g_i(\mathbf{X}) \leq 0$  and all  $h_k(\mathbf{X}) = 0$ ), but whenever one or more constraints are violated, the square of this constraint is included in the penalty function.

We usually start with a small  $k$  and minimize  $\Phi(\mathbf{X}, k)$ . Then increase  $k$  by a factor of  $\gamma$ , for example  $\gamma = 3$ , and minimize  $\Phi$  again. This process continues until a satisfactory result is obtained.

The disadvantage of the exterior penalty function is that it begins from an infeasible region, and the solution becomes feasible only in the limit as  $k \rightarrow \infty$ . Therefore, if the optimization process is stopped prematurely, the result is unusable.

#### C.6.1.2 Interior Penalty Functions

Unlike exterior penalty functions, interior penalty functions start within the feasible region, and even if the optimization is prematurely stopped, the design will at least be feasible, even though it may not be optimum.

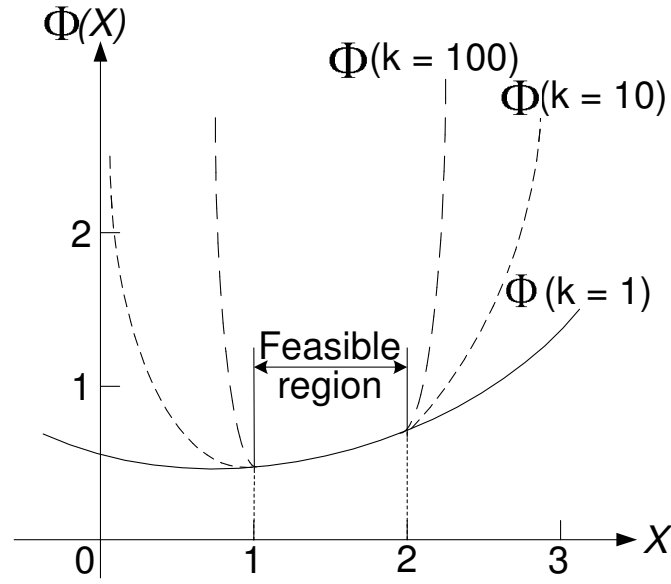


**Figure C-2:** Example of Exterior Penalty Function [78].

A common form of this type of penalty function is

$$P(\mathbf{X}) = \sum_{j=1}^m \frac{-1}{g_j(\mathbf{X})} \quad (\text{C-47})$$

Using this equation and including equality constraints via the exterior penalty function of Eqn. C-46,

$$\Phi(\mathbf{X}, k', k) = F(\mathbf{X}) + k' \sum_{j=1}^m \frac{-1}{g_j(\mathbf{X})} + k \sum_{k=1}^l [h_k(\mathbf{X})]^2 \quad (\text{C-48})$$

The reason we use the exterior penalty function for  $h_k$  is that we wish to drive  $h_k$  to zero.

The penalty parameter  $k'$  for the interior penalty function begins as a large positive number and decreases as the iterations progress, while  $k$  for the exterior penalty function begins as a small positive number and increases.

With this method, the function is discontinuous at the boundaries  $g_j(\mathbf{X}) = 0$ . Therefore extreme caution must be used in developing a line search algorithm.

#### C.6.1.3 Linear Extended Penalty Functions

This approach attempts to incorporate the best features of the interior and exterior methods for inequality constraints. For equality constraints, the exterior penalty can still be used.

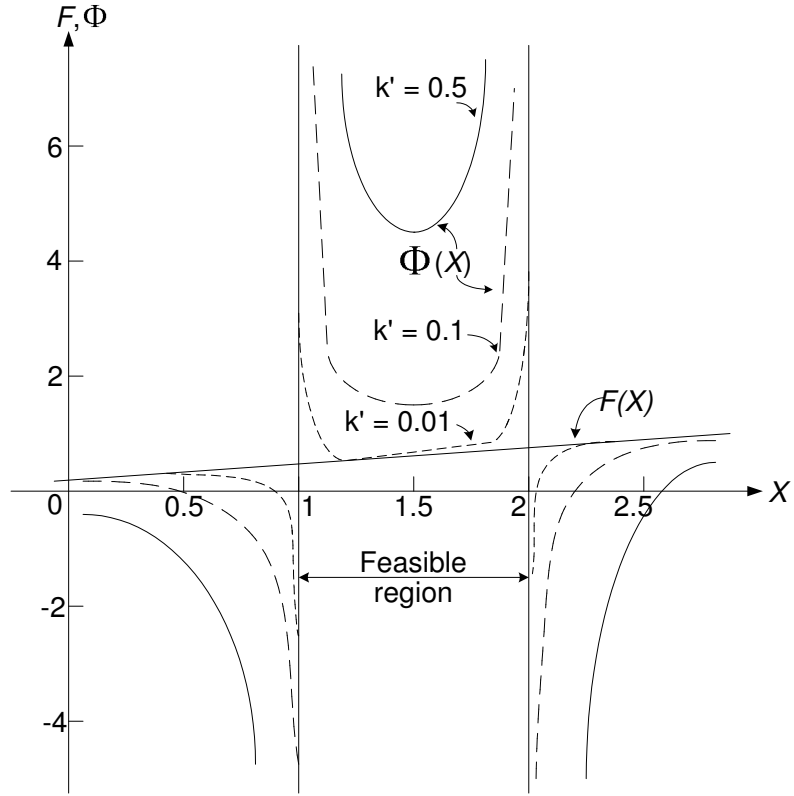


**Figure C-3:** Example of Interior Penalty Function [78].

The linear extended penalty function has the following form:

$$P(\mathbf{X}) = \sum_{i=1}^m \tilde{g}_j(\mathbf{X}) \quad (\text{C-49})$$

$$\text{where } \tilde{g}_j = -\frac{1}{g_j(\mathbf{X})} \quad \text{if } g_j(\mathbf{X}) \leq \epsilon \quad (\text{C-50})$$

$$\tilde{g}_j = -\frac{2\epsilon - g_j(\mathbf{X})}{\epsilon^2} \quad \text{if } g_j(\mathbf{X}) > \epsilon \quad (\text{C-51})$$

The parameter  $\epsilon$  is a small negative number which marks the transition from the interior penalty given by Eqn. C-50 to the extended penalty given by Eqn. C-51, and the value of  $\epsilon$  is recommended as

$$\epsilon = -C(k')^a \quad \frac{1}{3} \leq a \leq \frac{1}{2} \quad (\text{C-52})$$

where  $C$  and  $a$  are constants and  $C \approx 0.15$  and  $a \approx 0.50$  are typically used.

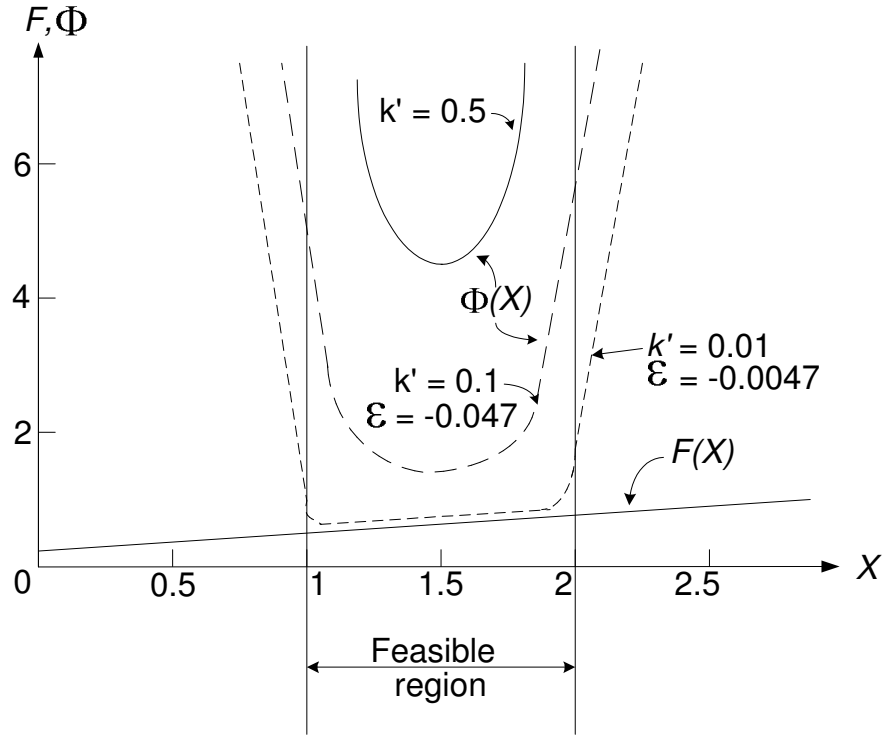


**Figure C-4:** Example of Extended Penalty Function [78].

#### C.6.1.4 Application to Swing-by problems

Among the penalty functions explained above, the method of extended penalty functions seems to be the most reliable. Therefore, in this research, extended penalty functions are applied.

The parameter to be restricted is the distance of closest approach between the spacecraft and the center of the swing-by planet,  $r_p$ . This parameter is bounded with lower limit ( $r_{p_{min}}$ ) and upper limit ( $r_{p_{max}}$ ). Then  $g$  and  $k'$  can be defined as

$$\begin{aligned} g_1 &= r_{p_{min}} - r_p \\ g_2 &= r_p - r_{p_{max}} \\ k' &= 1.0/(\text{number of iterations}) \end{aligned}$$

## C.7 Trajectory Visualization with VRML

### C.7.1 Virtual Reality Modeling Language

VRML is an acronym for the Virtual Reality Modeling Language[10]. Using VRML one

can craft three-dimensional virtual worlds on the internet. With a text file as an input file, VRML draws many types of objects as well as animations.

In this research, the trajectory is drawn with VRML for easy visualization. *SAMURAI* outputs a file that is used as a VRML input file. A three dimensional trajectory is drawn on a web browser with the thrust direction vectors shown at several points along the trajectory.

It is sometimes difficult to choose the departure date or time of flight. If a user chooses a bad combination of these two values, the calculation will not converge. Because this drawing displays the positions of departure and arrival planets, it is helpful to determine when to depart and what time of flight to choose.

### C.7.2 Input and Output in General

Several simple examples shown introduce how VRML works.

A VRML input file must start with the line

```
#VRML V2.0 utf8
```

The following very simple file `sphere.wrl` draws a sphere with a radius of 1.0 with its center at the origin.

```
#VRML V2.0 utf8 Sphere{}
```

A red cone with a bottom radius of 2.0 and a height of 3.0 is:

```
#VRML V2.0 utf8 Shape {
  appearance Appearance {
    material Material {
      emissiveColor 1 0 0 # red=1 green=0 blue=0
    }
  }
  geometry Cone{
    bottomRadius 2.0
    height 3.0
  }
}
```

Comment lines can be written beginning with “#” except for the first line. By grouping a cone and a cylinder, we can make a simple house as shown in Fig. C-5. We need to move either a cone or a cylinder with the `translation` command because all of the shapes are drawn with its center at the origin unless otherwise specified.

```
#VRML V2.0 utf8 Group {
  children [
    Shape {
      appearance Appearance {
        material Material {
          emissiveColor 0 0 1 # blue
        }
      }
    }
  ]
}
```

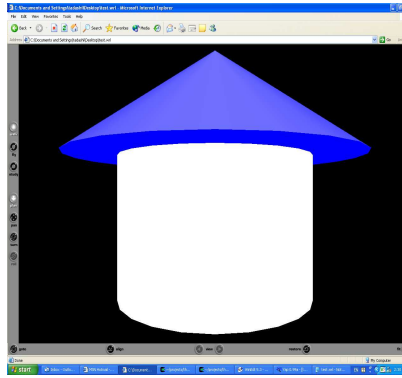


**Figure C-5:** VRML Example – Simple House.

```

    }
  }
  geometry Cone{
    bottomRadius 3.0
    height 2.0
  }
}
Transform {
  translation 0 -2 0 # move -2 in y-direction
  children Shape {
    appearance Appearance {
      material Material {
        emissiveColor 1 1 1 # white
      }
    }
    geometry Cylinder{
      radius 2.0
      height 3.0
    }
  }
}
}
]
}

```

By combining different types of shapes, we can draw any complicated objects.

### C.7.3 Making an Animation

VRML provides animation for position, orientation, and scale. In this research, we would like to check the movement of the spacecraft and planets, so position animation is mostly used. The following simple example is an animation of a planet's movement. A path of the planet is drawn, with a sphere following the path.

```

#VRML V2.0 utf8 Group {
  children [
    #== Clock ==
    DEF Clock TimeSensor { # Define a clock.
      cycleInterval 2.0 # Two seconds per cycle.
      loop TRUE # Loop the animation.
    }
  ]
}

```



```

#== Planet ==
DEF Planet Transform { # A sphere that moves.
  children [
    Shape {
      appearance Appearance {
        material Material {
          emissiveColor 1 1 1
        }
      }
      geometry Sphere { radius 0.05 }
    }
  ]
}

#== Trajectory ==
Shape {
  appearance Appearance {
    material Material {
      emissiveColor 1 1 1 # Color of path
    }
  }
  geometry IndexedLineSet { # Draws a line connecting
    coord Coordinate { # the following points.
      point [
        1.000 0.000 0.000 # 0
        0.951 0.309 0.000 # 1
        0.809 0.588 0.000 # 2
        0.588 0.809 0.000 # 3
        0.309 0.951 0.000 # 4
        -0.000 1.000 0.000 # 5
        -0.309 0.951 0.000 # 6
        -0.588 0.809 0.000 # 7
        -0.809 0.588 0.000 # 8
        -0.951 0.309 0.000 # 9
        -1.000 0.000 0.000 # 10
      ]
    }
    coordIndex [ # connect points 0 - 10, end with -1
      0 1 2 3 4 5 6 7 8 9 10 -1
    ]
  }
}

#== Planet's position ==
DEF Path PositionInterpolator { # Animate position
  key [ # Scaled time to draw points, end with 1.0
    0.0 0.1 0.2 0.3 0.4 0.5 0.6 0.7 0.8 0.9 1.0
  ]
  keyValue [ # Points to be animated
    1.000 0.000 0.000 # 0
    0.951 0.309 0.000 # 1
    0.809 0.588 0.000 # 2
    0.588 0.809 0.000 # 3
    0.309 0.951 0.000 # 4
    -0.000 1.000 0.000 # 5
    -0.309 0.951 0.000 # 6
    -0.588 0.809 0.000 # 7
    -0.809 0.588 0.000 # 8
    -0.951 0.309 0.000 # 9
    -1.000 0.000 0.000 # 10
  ]
}

}

ROUTE Clock.fraction_changed TO Path.set_fraction # Line 1
ROUTE Path.value_changed TO Planet.set_translation # Line 2

```

The last two lines (Line 1 and Line 2) make the animation work. VRML checks the clock of the computer, and the clock information is brought to **TimeSensor** that induces the change of **fraction** of **Clock**. The change of **fraction** (**Clock.fraction\_changed** in Line 1) is routed to **PositionInterpolator**, which is defined as **Path**, and sets the fraction of **Path**. Setting the fraction is notified to Line 2 as the change of value in **Path**, and this information is routed to **Planet**. **Planet** then draws a sphere to the coordinates (or **keyValue**) specified by **Path**. These two lines are looped and a sphere is drawn according to the coordinates specified at **keyValue**, resulting in an animation of a moving sphere.

## APPENDIX D

### “SAMURAI” CODE MANUAL

#### *D.1 Input data*

##### Mandatory Inputs

Variable	Type	Default	Description
<b>option</b>	integer	–	= 1, VSI type I(unlimited $I_{sp}$ ), no swing-by = 2, VSI type II(bounded $I_{sp}$ ), no swing-by = 3, CSI type I(continuous thrust), no swing-by = 4, CSI type II(bang-off-bang), no swing-by = 5, High thrust, no swing by = 6, VSI type I(unlimited $I_{sp}$ ), swing-by = 7, VSI type II(bounded $I_{sp}$ ), swing-by = 8, CSI type I(continuous thrust), swing-by = 9, CSI type II(bang-off-bang), swing-by = 10, High thrust, swing by
<b>jetPower</b>	real	–	Jet power(W) (for options 1 – 4, 6 – 9)
<b>initialMass</b>	real	–	Initial mass(kg)
<b>tof</b>	1 or 2 real	–	Time of flight(day) (one value for options 1 – 5, two values for options 6 – 10)

Input either one of the following sets to locate the planets

(1) For actual ephemeris data

<b>date</b>	6 integer	–	Calender date of epoch ( <i>yyyy, mm, dd, hr, min, sec</i> )
<b>depPlanet</b>	integer	–	Departure planet index
<b>arrPlanet</b>	integer	–	Arrival planet index
<b>sbyPlanet</b>	integer	–	Swing-by planet index(for options 6 – 10)

- = 1, Mercury
- = 2, Venus
- = 3, Earth
- = 4, Mars
- = 5, Jupiter
- = 6, Saturn
- = 7, Uranus
- = 8, Neptune
- = 9, Pluto/Caron

(2) For user-defined planets

- initial**      6 real    –    Position( $x, y, z$ ) and velocity( $u, v, w$ ) of departure planet
- target**       6 real    –    Position( $x, y, z$ ) and velocity( $u, v, w$ ) of arrival planet
- swingby**      6 real    –    Position( $x, y, z$ ) and velocity( $u, v, w$ ) of swing-by planet(for options 6 – 10)

The following inputs are required for grid search.

- depRange**    3 real    –    Days from epoch for departure date (starting, ending, increment) (day)
- tofRange**    3 real    –    Time of flight (starting, ending, increment) (day)
- tofRange2**   3 real    –    **tofRange** for the 2nd phase (for options 6 – 10)

### Additional Inputs

Variable	Type	Default	Description
<b>Isp</b>	real	30,000	Specific impulse (sec)  For options 2, 3, 7, 8: maximum allowable $I_{sp}$  For options 4, 9: $I_{sp}$ value when the engine is on  For options 5, 10: $I_{sp}$ value for high thrust
<b>maxC3</b>	2 real	0, 0	Maximum $C_3$ values at departure planet and arrival planet( $\text{km}^2/\text{s}^2$ )
<b>rp_min</b>	real	*	Minimum allowable distance of periapsis at swing-by planet (radii of swing-by planet)(for options 6 – 10)

<code>rp_max</code>	real	*	Maximum allowable distance of periapsis at swing-by planet (radii of swing-by planet)(for options 6 – 10)
<code>rSOI_sby</code>	real	9.245E+05	SOI radius of swing-by planet (km) (for options 6 – 10)
<code>TU_sby</code>	real	806.812	Time unit of swing-by planet (sec) (for options 6 – 10)
<code>DU_sby</code>	real	6378.145	Distance unit of swing-by planet (km) (for options 6 – 10)

### Optional Inputs

Variable	Type	Default	Description
<code>timeSteps</code>	1 or 2 integer	100, 100	Number of time steps for each leg (one value for options 1 – 5, two values for options 6 – 10)
<code>max_ite</code>	integer	300	Maximum number of iterations for optimal control process

## D.2 Executing “SAMURAI”

*SAMURAI* reads an input data file (e.g. `INPUT.txt`) and the results are written to an output data file (e.g. `OUTPUT.txt`). A VRML file (e.g. `VRML.wrl`) is also created. Users must specify these three files from the command line.

```
> samurai INPUT.txt OUTPUT.txt VRML.wrl
```

The computation time strongly depends on the option (`option`) and the number of time steps (`timeSteps`). If the number of time steps is 300, approximate computation time with Pentium 4, 1.9GHz for each option is: less than 10 sec for option 1, less than a few minutes for option 2, less than 10 minutes for option 3 and 4, and less than 1 sec for option 5.

It is not recommended to conduct a grid search for swing-by trajectories with CSI engines with a wide search range because it may take very long time to complete.

## REFERENCES

- [1] “A Crewed Mission to Mars....”  
<http://nssdc.gsfc.nasa.gov/planetary/mars/marswhy.html>.
- [2] “EICR Plasma Propulsion Systems at Kyushu University, Japan.”  
<http://art.aees.kyushu-u.ac.jp/members/yositaka/study/doc/japanese/research-j.html>.
- [3] “Jupiter Icy Moons Orbiter.” <http://www.jpl.nasa.gov/jimo/index.cfm>.
- [4] “Spacecraft Propulsion – Wikipedia, the free encyclopedia.”  
[http://en.wikipedia.org/wiki/Spacecraft\\_propulsion](http://en.wikipedia.org/wiki/Spacecraft_propulsion).
- [5] “Superfast VASIMR Rocket in Funding Limbo.”  
[http://www.space.com/business/technology/technology/vasimr\\_rocket\\_020807-1.html](http://www.space.com/business/technology/technology/vasimr_rocket_020807-1.html).
- [6] “The Exploration of Jupiter in the 21st Century.”  
[http://www.vectorsite.net/taxpl\\_b.htm](http://www.vectorsite.net/taxpl_b.htm).
- [7] “Variable-Specific-Impulse Magnetoplasma Rocket.”  
<http://www.nasatech.com/Briefs/Sep01/MS23041.html>.
- [8] AKULENKO, L. D., *Problems and Methods of Optimal Control*, vol. 286 of *Mathematics and Its Applications*. Dordrecht, The Netherlands: Kluwer Academic Publishers, 2003.
- [9] ALPERIN, M. and GREGORY, H. F., *Vistas in Astronautics*, vol. 2. New York: Pergamon Press, 1959.
- [10] AMES, A. L., NADEAU, D. R., and MORELAND, J. L., *VRML 2.0 Sourcebook Second Edition*. New York, NY: John Wiley & Sons, Inc., 1997.
- [11] ATKINSON, K. E., *An Introduction to Numerical Analysis, Second Edition*. New York, NY: John Wiley & Son, 1989.
- [12] BATE, R. R., MUELLER, D. D., and E. WHITE, J., *Fundamentals of Astrodynamics*. New York, NY: Dover Publications, Inc., 1971.
- [13] BATTIN, R. H., *An Introduction to the Mathematics and Methods of Astrodynamics, Revised Edition*. AIAA Education Series, Reston, VA: American Institute of Aeronautics and Astronautics, Inc., 1999.
- [14] BROUCKE, R. A. and PRADO, A. F. B. A., “Optimal N-Impulse Transfer Between Coplanar Orbits,” *Advances in the Astronautical Sciences, Astrodynamics 1993*, vol. 85, pp. 483–502, 1993. AAS93-660.
- [15] BRYSON, JR., A., DENHAM, W., and DREYFUS, S., “Optimal Programming Problems with Inequality Constraints I: Necessary Conditions for Extremal Solutions,” *AIAA Journal*, vol. 1, pp. 2544 – 2550, Nov. 1963.

- [16] BRYSON, JR., A., DENHAM, W., and DREYFUS, S., "Optimal Programming Problems with Inequality Constraints II: Solution by Steepest-Ascent," *AIAA Journal*, vol. 2, pp. 25 – 34, Jan. 1964.
- [17] BRYSON, JR., A. E. and HO, Y.-C., *Applied Optimal Control*. Bristol, PA: Taylor & Francis, 1975.
- [18] CAREY, R. and BELL, G., *The Annotated VRML 2.0 Reference Manual*. Boston, MA: Addison-Wesley, 1997.
- [19] CASALINO, L., COLASURDO, G., and PASTRONE, D., "Optimization of  $\Delta V$  Earth-Gravity-Assist Trajectories," *Journal of Guidance, Control, and Dynamics*, vol. 21, no. 6, pp. 991–995, 1998.
- [20] CASALINO, L., COLASURDO, G., and PASTRONE, D., "Optimal Low-Thrust Escape Trajectories Using Gravity Assist," *Journal of Guidance, Control, and Dynamics*, vol. 22, no. 5, pp. 638–642, 1999.
- [21] CASALINO, L., COLASURDO, G., and PASTRONE, D., "Simple Strategy for Powered Swingby," *Journal of Guidance, Control, and Dynamics*, vol. 22, no. 1, pp. 156–159, 1999.
- [22] CHANG-DIAZ, F. R., "An Overview of the VASIMR Engine: High Power Space Propulsion with RF Plasma Generation and Heating." 14th Topical Conference on Radio Frequency Power in Plasmas, Oxnard, California, May 7-9, 2001.
- [23] CHANG-DIAZ, F. R., "The VASIMR Rocket," *Scientific American*, pp. 91–97, Nov. 2000.
- [24] CHANG-DIAZ, F. R., BENGSTON, R. D., BREIZMAN, B. N., and BAITY, F. W., "The physics and Engineering of the VASIMR Engine." 36th AIAA/ASME/SAE/ASEE Joint Propulsion Conference Huntsville, Alabama, July 17-19 2000.
- [25] CHANG-DIAZ, F. R., HSU, M. M., BRADEN, E., JOHNSON, I., and YANG, T. F., "Rapid Mars Transits With Exhaust-Modulated Plasma Propulsion," NASA Technical Paper 3539, NASA, 1995.
- [26] CHANG-DIAZ, F. R., SQUIRE, J. P., ILIN, A., NGUYEN, T., WINER, D., PETRO, A., GOEBEL, G., CASSADY, L., STOKKE, K., DEXTER, C., GRAVES, T., JR., L. A., and GEORGE, J., "The Development of the VASIMR Engine."
- [27] CHOBOTOV, V. A., *Orbital Mechanics Second Edition*. AIAA Education Series, Reston, VA: American Institute of Aeronautics and Astronautics, Inc., 1996.
- [28] DE ALMEIDA PRADO, A. F. B., "Powered Swingby," *Journal of Guidance, Control, and Dynamics*, vol. 19, no. 5, pp. 1142–1147, 1996.
- [29] DICKEY, B., "Star Power," *Air & Space*, pp. 64–67, 2004.
- [30] E.A.BERING, I., BRUKARDT, M., CHANG-DIAZ, F. R., SQUIRE, J., JACOBSON, V., BENGSTON, R. D., J.N.GIBSON, and T.W.GLOVER, "Experimental Studies of the Exhaust Plasma of The VASIMR Engine." 40th AIAA Aerospace Sciences Meeting & Exhibit, Reno, NV, January 14-17 2002. AIAA2002-0345.

- [31] ESCOBAL, P. R., *Methods of Orbit Determination*. New York: John Wiley & Sons, Inc., 1965.
- [32] ESCOBAL, P. R., *Methods of Astrodynamics*. New York: John Wiley and& Sons, Inc., 1968.
- [33] GOODSON, T., *Fuel-Optimal Control and Guidance for Low- and Medium-Thrust Orbit Transfer*. PhD dissertation, Georgia Institute of Technology, School of Aerospace Engineering, Aug. 1995.
- [34] GRIFFIN, M. D. and FRENCH, J. R., *Space Vehicle Design*. AIAA Education Series, Washington, DC: American Institute of Aeronautics and Astronautics, Inc., 1991.
- [35] HACK, K. J., GEORGE, J. A., and DUDZINSKI, L. A., "Nuclear Electric Propulsion Mission Performance for Fast Piloted Mars Missions," AIAA Paper 91-3488, AIAA, Sept. 1991.
- [36] HACK, K. J., GEORGE, J., RIEHL, J., and GILLAND, J. H., "Evolutionary Use of Nuclear Electric Propulsion," AIAA Paper 90-3821, AIAA, Sept. 1990.
- [37] HALE, F. J., *Introduction to Space Flight*. Englewood Cliffs, NJ: Prentice-Hall, Inc., 1994.
- [38] HILL, P. and PETERSON, C., *Mechanics and Thermodynamics of Propulsion Second Edition*. Reading, MA: Addison-Wesley Publishing Company, 1992.
- [39] HOLZNER, S., *Perl Core Language*. Little Black Book, Scottsdale, AZ: Coriolis Technology Press, 1999.
- [40] HONG, P., KENT, P., OLSON, D., and VALLADO, C., "Interplanetary Program To Optimize Simulated Trajectories (IPOST) User's Guide," Oct. 1992. NAS1-18230.
- [41] HULL, D. G., *Optimal Control Theory for Applications*. Mechanical Engineering Series, New York, NY: Springer, 2003.
- [42] HUMBLE, R. W., HENRY, G. N., and LARSON, W. J., *Space Propulsion Analysis and Design*. Space Technology Series, New York, NY: The MacGraw-Hill Companies, Inc., 1995.
- [43] ILIN, A., CHANG-DIAZ, F. R., SQUIRE, J., BREIZMAN, B., and CARTER, M., "Particle Simulations of Plasma Heating in VASIMR." 36th AIAA/ASME/SAE/ASEE Joint Propulsion Conference Huntsville, Alabama, July 17-19 2000. AIAA2000-3753.
- [44] ILIN, A., CHANG-DIAZ, F. R., SQUIRE, J., TARDITI, A., B.N.BREIZMAN, and M.D.CARTER, "Simulations of Plasma Detachment in VASIMR." 40th AIAA Aerospace Sciences Meeting & Exhibit, Reno, NV, January 14-17 2002. AIAA2002-0346.
- [45] JACOBSON, V. T., DIAZ, F. R. C., SQUIRE, J. P., MCCASKILL, G. E., MCCOY, J. E., PETRO, A. J., WINTER, D. S., and JAMISON, H. M., "Development of VASIMR Helicon Source." 43rd Annual Meeting of the APS Division of Plasma Physics Mini-Conference on Helicon Sources, Long Beach, California.



- [46] KAHLER, S., LU, P., and HANSON, J., “Optimal Interplanetary Trajectories Using an Advanced Pulsed Fusion Propulsion System.” AAS03-571, AAS/AIAA Astrodynamics specialists Conference, Big Sky Resort, Big Sky, Montana, August 3–7, 2003.
- [47] KECHICHIAN, J. A., “Trajectory Optimization Using Eccentric Longitude Formulation,” *Advances in the Astronautical Sciences, Astrodynamics 1993*, vol. 85, pp. 543–562, 1993. AAS93-664.
- [48] KECHICHIAN, J. A., “Mechanics of Trajectory Optimization Using Nonsingular Variational Equations in Polar Coordinates,” *Advances in the Astronautical Sciences, Spaceflight Mechanics 1995*, vol. 89, pp. 937–958, 1995. AAS95-121.
- [49] KECHICHIAN, J. A., “Optimal Low-Thrust Transfer Using Variable Bounded Thrust,” *Acta Astronautica*, vol. 36, no. 7, pp. 357–365, 1995.
- [50] KECHICHIAN, J. A., “Trajectory Optimization Using Nonsingular Orbital Elements and True Longitude,” *Advances in the Astronautical Sciences, Astrodynamics 1995*, vol. 90, pp. 1793–1814, 1995. AAS95-422.
- [51] KLUEVER, C. A. and PIERSON, B. L., “Optimal low-thrust three-dimensional earth-moon trajectories,”
- [52] KLUEVER, C. A. and PIERSON, B. L., “Optimal Earth-Moon Trajectories Using Nuclear Electric Propulsion,” *Advances in the Astronautical Sciences, Astrodynamics 1995*, vol. 90, pp. 1623–1638, 1995.
- [53] LABUNSKY, A. V., PAPKOV, O. V., and SUKHANOV, K. G., *Multiple Gravity Assist Interplanetary Trajectories*, vol. 3 of *Earth Space Institute Book Series*. Amsterdam, The Netherlands: Gordon and Breach Science Publishers, 1998.
- [54] LAWDEN, D. F., *Optimal Trajectories for Space Navigation*. London: Butterworths, 1963.
- [55] LEDSINGER, L. A., *Solutions to Decomposed Branching Trajectories with Powered Flyback Using Multidisciplinary Design Optimization*. PhD dissertation, Georgia Institute of Technology, School of Aerospace Engineering, July 2000.
- [56] LEITMANN, G., *The Calculus of Variations and Optimal Control*, vol. 24 of *Mathematical Concepts and Methods in Science and Engineering*. New York, NY: Plenum Press, 1981.
- [57] LEWIS, F. L., *Optimal Control*. New York, NY: John Wiley & Sons, Inc., 1986.
- [58] MARC R. ILGEN, “Low Thrust OTV Guidance Using Lyapunov Optimal Feedback Control,” *Advances in the Astronautical Sciences, Astrodynamics 1993*, vol. 85, pp. 1527–1545, 1993. AAS93-680.
- [59] MAREC, J.-P., *Optimal Space Trajectories*, vol. 1 of *Studies in Astronautics*. Amsterdam, The Netherlands: Elsevier Scientific Publishing Company, 1979.
- [60] MIELE, A., WANG, T., and MANCUSO, S., “Optimal Free-Return Trajectories for Moon Missions and Mars Missions,” *Advances in the Astronautical Sciences, The Richard H. Battin Astrodynamics Symposium 2000*, vol. 106, pp. 93–115, 2000. AAS00-254.

- [61] NAH, R. and VADALI, S., “Fuel-Optimal, Low-Thrust Three-Dimensional Earth-Mars Trajectories,” *Journal of Guidance, Control, and Dynamics*, vol. 24, no. 6, pp. 1100–1107, 2001.
- [62] OCAMPO, C. A., “Trajectory Optimization with Dual Thrust Limited Propulsion Systems,” *Advances in the Astronautical Sciences, Astrodynamics 2001*, vol. 109, pp. 2015–2032, 2001. AAS01-443.
- [63] OCAMPO, C. A. and ROSBOROUGH, G. W., “Optimal Low-Thrust Transfers Between a Class of Restricted Three-Body Trajectories,” *Advances in the Astronautical Sciences, Astrodynamics 1993*, vol. 85, pp. 1547–1566, 1993. AAS93-681.
- [64] PASTRONE, D., CASALINO, L., and COLASURDO, G., “Indirect Optimization Method for Round-Trip Mars Trajectories,” *Advances in the Astronautical Sciences, Astrodynamics 1995*, vol. 90, pp. 85–99, 1995. AAS95-305.
- [65] PETRO, A., CHANG-DIAZ, F. R., CARTER, M. D., SCHWENTERLY, S., HITT, M., and LEPORE, J., “A Flight Demonstration of Plasma Rocket Propulsion.” 36th AIAA/ASME/SAE/ASEE Joint Propulsion Conference Huntsville, Alabama, July 17-19 2000. AIAA2000-3751.
- [66] PETRO, A., CHANG-DIAZ, F. R., ILIN, A., and SQUIRE, J., “Development of a Space Station-Based Flight Experiment for the VASIMR Magneto-Plasma Rocket.” 40th AIAA Aerospace Sciences Meeting & Exhibit, Reno, NV, January 14-17 2002. AIAA2002-0344.
- [67] PIERSON, B. L. and KLUEVER, C. A., “A Three-Stage Approach to Optimal Low-Thrust Earth-Moon Trajectories,” *Advances in the Astronautical Sciences, Astrodynamics 1993*, vol. 85, pp. 563–582, 1993.
- [68] PRESS, W. H., TEUKOLSKY, S. A., VETTERLING, W. T., and FLANNERY, B. P., *Numerical Recipes in C – The Art of Scientific Computing – Second Edition*. Cambridge: Cambridge University Press, 1988.
- [69] RANIERI, C. L. and OCAMPO, C. A., “Optimization of Roundtrip, Time-Constrained, Finite Burn Trajectories Via an Indirect Method.” AAS03-572, AAS/AIAA Astrodynamics specialists Conference, Big Sky Resort, Big Sky, Montana, August 3–7, 2003.
- [70] SAKAI, T. and OLDS, J. R., “Development of a Multipurpose Low Thrust Interplanetary Trajectory Calculation Code.” AAS03-667, AAS/AIAA Astrodynamics specialists Conference, Big Sky Resort, Big Sky, Montana, August 3–7, 2003.
- [71] SCARBERRY, D. P. and PERNICKA, H. J., “Low  $\Delta V$  Earth-to-Moon Trajectories,” *Advances in the Astronautical Sciences, Astrodynamics 1995*, vol. 90, pp. 1639–1653, 1995. AAS95-400.
- [72] SEYWALD, H., ROITHMAYR, C. M., and TROUTMAN, P. A., “Fuel-Optimal Orbital Transfers for Variable Specific Impulse Powered Spacecraft,” *Advances in the Astronautical Sciences, Spaceflight Mechanics 2003*, vol. 114, pp. 347–364, 2003.
- [73] SPENCER, D. B. and CULP, R. D., “An Analytical Solution Method for Near-Optimal, Continuous-Thrust Orbit Transfers,” *Advances in the Astronautical Sciences, Astrodynamics 1993*, vol. 85, pp. 523–539, 1993. AAS93-663.

- [74] SQUIRE, J., CHANG-DIAZ, F. R., JACOBSON, V., MCCASKILL, G., and BENGSTON, R., "Helicon Plasma Injector and Ion Cyclotron Acceleration Development in the VASIMR Experiment." 36th AIAA/ASME/SAE/ASEE Joint Propulsion Conference Huntsville, Alabama, July 17-19 2000. AIAA2000-3752.
- [75] STENGEL, R. F., *Optimal Control and Estimation*. New York, NY: Dover Publications, Inc., 1994.
- [76] VADALI, S. R., NAH, R., BRADEN, E., and I. L. JOHNSON, J., "Fuel-Optimal Planar Interplanetary Trajectories Using Low-Thrust Exhaust-Modulated Propulsion," *Advances in the Astronautical Sciences, Spaceflight Mechanics 1999*, vol. 102, pp. 431–448, 1993.
- [77] VALLADO, D. A., *Fundamentals of Astrodynamics and Applications*, vol. 12 of *Space Technology Library*. El Segundo, CA: Microcosm Press, 2001.
- [78] VANDERPLAATS, G. N., *Numerical Optimization Techniques for Engineering Design: With Applications*. Colorado Springs, CO: Vanderplaats Research & Development, Inc., 1998.
- [79] VINH, N. X., *Optimal Trajectories in Atmospheric Flight*. New York, NY: Elsevier Scientific Publishing Company, 1981.
- [80] WAY, D. W., *Uncertainty Optimization Applied to the Monte Carlo Analysis of Planetary Entry Trajectories*. PhD dissertation, Georgia Institute of Technology, School of Aerospace Engineering, July 2001.
- [81] YAMAKAWA, H., KAWAGUCHI, J., ISHII, N., and MATSUO, H., "On Earth-Moon Transfer Trajectory with Gravitational Capture," *Advances in the Astronautical Sciences, Astrodynamics 1993*, vol. 85, pp. 397–416, 1993. AAS93-663.
- [82] YANG, D., *C++ and Object-Oriented Numeric Computing for Scientists and Engineers*. New York, NY: Springer, 2001.

## VITA

Tadashi Sakai was born on October 27, 1970 and grew up in Ichinomiya, Aichi, Japan. He attended Kyoto University, Kyoto, Japan, and earned his Bachelor of Engineering in nuclear engineering in 1993, and Master of Engineering in nuclear engineering in 1995. Then he joined the Nuclear Fuel Industries, Ltd. in Osaka, Japan, and worked for three years. He then entered the graduate program of the Georgia Institute of Technology, completing his Master of Science in Aerospace Engineering during the spring of 2000.